20113-FR1

FINAL REPORT
For Period 1 August 1964 to 31 March 1965

STUDY OF AN ATTITUDE REFERENCE SYSTEM UTILIZING AN ELECTRICALLY SUSPENDED GYRO

Jet Propulsion Laboratory
Contract No. 950915

31 March 1965

20113-FR1 31 March 1965

FINAL REPORT
For Period 1 August 1964 to 31 March 1965

STUDY OF AN ATTITUDE REFERENCE SYSTEM UTILIZING AN ELECTRICALLY SUSPENDED GYRO

Jet Propulsion Laboratory
Contract No. 950915

This work was performed for the Jet Propulsion Laboratory, California Institute of Technology, sponsored by the National Aeronautics and Space Administration under Contract NAS7-100.

Approved by:

R. E. Dobrzynski
Project Engineer

J. K. Olson
Section Head

R. C. Amos
Program Administrator

Honeywell Inc.
Aeronautical Division
Minneapolis, Minnesota

CONTENTS

ILLUSTRATIONS

TABLES

SECTION I
GENERAL

This is the final report submitted in accordance with the Statement of Work at Jet Propulsion Laboratory Contract No. 950915. It covers work performed during the period 1 August 1964 through 31 March 1965.

SECTION II
OBJECTIVES AND CONCLUSIONS

OBJECTIVES

The goal of this study program is to establish on a factual basis the feasibility of using miniature electro-static gyros (MEG) in a spacecraft attitude reference system. In order to accomplish this goal the program was divided into two tasks. Task I was a study to establish the relationships between major system parameters, and Task II was the preliminary design of a strapped down MEG attitude reference system for a specific application - a landing capsule. Table 2-1 shows the breakdown of the two major tasks into subtasks for the purpose of carrying out the program. Figure 2-1 shows the schedule used in performing the study.

Since a parameter study such as selected for Task I can have almost any desired magnitude, it was necessary to constrain the study to contain it within the available time and funds. Also constraints were necessary to ensure that the study results would be within the category of JPL's interest.

Following are the constraints or ground rules used during the course of the Task I parameter study:

- The Attitude Reference System (ARS) will be all attitude
- The system will be instrumented with strapped down MEG's
- The attitude reference system will output to the attitude control system only
- The attitude reference system will provide outputs for three axis attitude control of the vehicle

Table 2-1. Definition of Study Tasks

Task I	Definition
IA	Select the parameters and the range and manner of variation for a parametric study of the SDMEG-ARS.
IB	Discuss factors affecting system design.
IC	System definition (1) Derive block diagrams and system equations to cover the range of parameters selected in Task IA (2) Produce preliminary design of logic for gyro computer interface (3) Produce preliminary designs of computers for systems defined in (1). Design to the level of block diagrams and size, weight, power and reliability estimates. (4) Produce preliminary design of system other than computer for systems in (1). Design to level of system detail block diagram and size, weight, power and reliability estimates. (5) Conduct a performance analysis to estimate the accuracy of each of the systems derived in (1). (6) Tabulate size, weight, power, reliability, and accuracy for all systems investigated.
ID	Discuss system additions and/or alterations required to utilize a SDMEG caging capability.
IE	Investigate and discuss the advantages of SDMEG modifications other than caging and torquing.
Task II	
IIA	Define functional requirements of an ARS for a capsule lander. List or tabulate ARS requirements.
IIB	Select a system configuration to meet requirements defined in IIA. Write a description of the system and its operation.
IIC	Make detail block diagrams of the system selected in IIB.
IID	Determine characteristics of selected system (1) Estimate size, weight, and power. Tabulate and discuss basis for estimates. (2) Estimate system reliability. Tabulate estimates for subsystems and discuss basis of estimates. (3) Estimate system accuracy. Discuss basis for estimates and present results. (4) Make a summary tabulation of IID(1), (2), and (3).
IIE	Discuss any modifications that may be necessary in the SDMEG for the system selected in Task II.

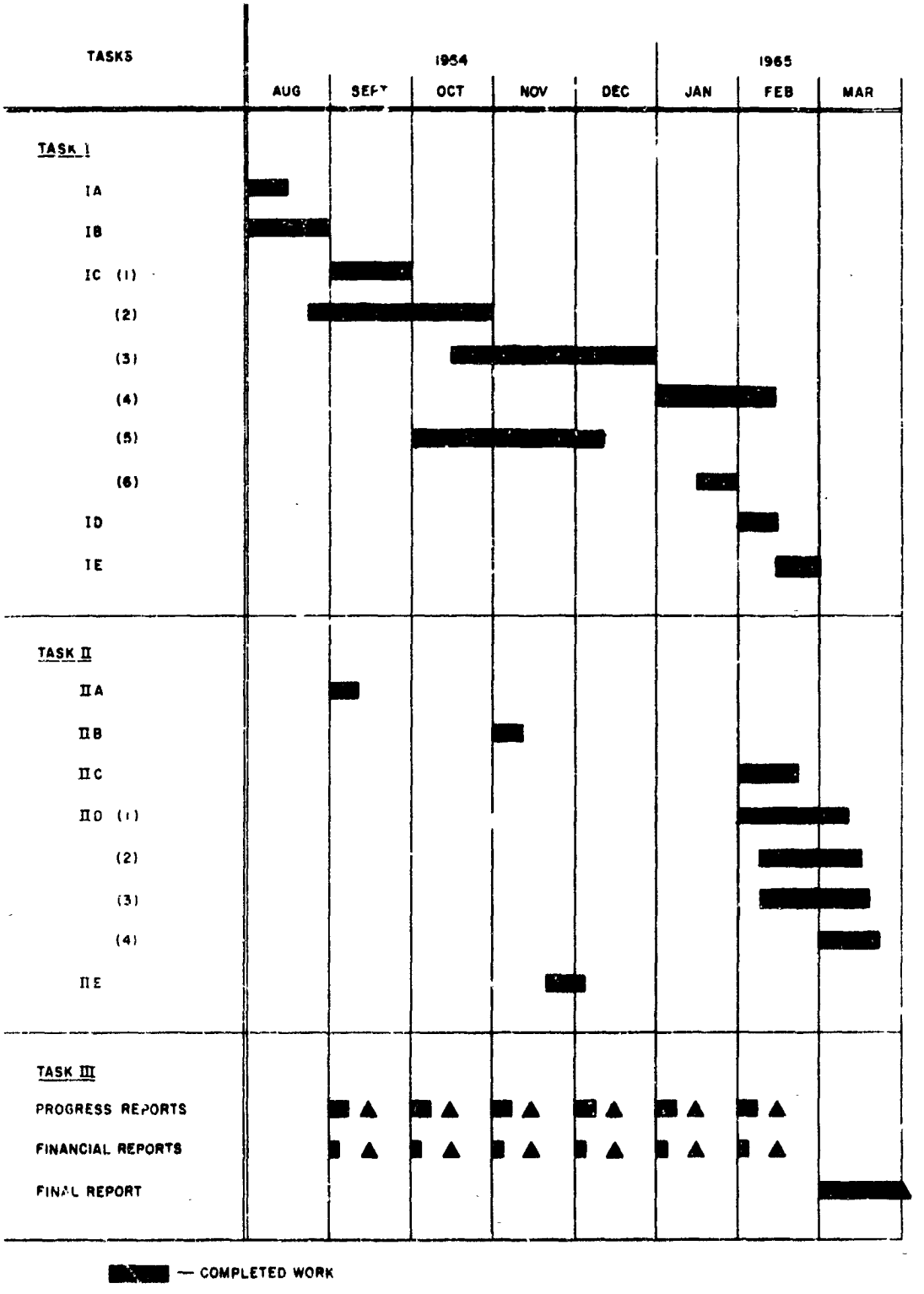

Figure 2-1. Program Schedule

- The attitude reference system will accept commands to change attitude
- Optical sensors will provide the information for initial alignment of the ARS
- Initial vehicle tumbling will be arrested by a means separate from the ARS
- The gyros will not be operating during launch but will be started and put in operation in space following launch.

The application selected for the preliminary design to be performed in Task II of the program is an attitude reference system for a landing capsule. The mission for the landing capsule assumes it is separated from a parent space vehicle in transit to, or while orbiting a target planet. After separation, the capsule is two-axis attitude stabilized in pitch and yaw, and roll-rate stabilized during retrofire and free-fall entry into the planet's atmosphere,if any. Once into the planet's atmosphere the aerodynamic forces will overpower the reaction jet system and the capsule will reorient as dictated by physical shape, and fall to the planet's surface.

The attitude reference system's function is to provide two-axis attitude hold and three-axis rate stabilization signals to the capsule autopilot or stabilization and control system. Events during the mission are assumed to be as follows:

- The orbiter attitude will be oriented to give the landing capsule the desired attitude
- The landing capsule gyro will be started and oriented to the capsule body axes
- The landing capsule will be separated from the orbiter and the ARS will maintain the attitude established by the orbiter
- The ARS will hold the attitude established before separation while the retro rockets are fired to decelerate the capsule

- The ARS will maintain the same attitude as the capsule falls to the surface.

CONCLUSIONS

In addition to a better general understanding and appreciation of the requirements that must be satisfied by the instrumentation of a spacecraft strapped down ESG attitude reference system, the study produced five rather specific conclusions.

1) The parameter study produced results showing that the ARS configurations selected for the study can be built for a system pointing accuracy in the range 0.04 to 0.07 degree within a volume of 0.5 cubic feet, a weight of 45 pounds and a maximum power consumption of 140 watts.

2) The parameter study results showed that the system size, weight, power and reliability was increased by less than 10 percent when the ARS was changed from an output of attitude error only to an output of attitude error and body rate.

3) The investigation of possible uses for a caging and torquing capability in the gyro showed that caging capability beyond that available in the current gyro design would not simplify or reduce the size of the system configuration considered in the parameter study. The investigation covered possible use of caging and torquing to simplify initial conditions and the possible use of torquing to assist in obtaining a less noisy vehicle body rate signal.

4) The results of the preliminary design performed in Task II show that, except for the rate stabilization signals, the performance

requirements of the attitude reference system for the landing capsule can be satisfied by a system instrumented with a single electro-static gyro.

5) Results from both the performance analyses performed for the parameter study of Task I and the preliminary design of Task II revealed that the quality and usefulness of the ARS rate outputs were limited by the level of noise on the gyro readout.

The investigations conducted in the course of performing Tasks I and II also produced some "by product" type results.

1) In order to provide output information at a rate of 100 iterations per second it will be necessary to supply each gyro pickoff with it's own set of shaping electronics rather than attempt to time share two sets of electronics between three pickoffs.

2) In the course of the parameter study it was necessary to establish the characteristics of a digital computer which would be suitable for the selected ARS concept. It was concluded that the computer will be a general purpose, serial/parallel machine with a 12-to-16-bit word length. The arithmetic would be done with 4 bits per bite at a bit rate of 1.5 megacycles per second. The memory would have a capacity of 512 to 1024 words. The smaller memory will be used in the ARS system that provides only attitude error output.

SECTION III
SDMEG-ARS PARAMETER STUDY

INTRODUCTION

The objective of a parameter study for an SDMEG-ARS or any other system is to establish in some way the relationships between the various system parameters or characteristics. Since even a modest system may have many parameters, attention must be focused on the most prominent ones to keep the study within manageable proportions. In the parameter study of the SDMEG-ARS three independent parameters and four dependent parameters were selected for investigation.

INDEPENDENT PARAMETERS

The independent parameters were the gyro configuration, the system accuracy and the form of the system output. The dependent parameters were system size, weight, power consumption and reliability. Since the selected independent parameters are not continuous throughout their range and since it was impractical within the scope of the study to investigate a large number of parameter values, the study considered the following discrete values of the independent parameters.

A. Gyro Configuration

A(1) Gyro developed under Contract No. 950607
A(2) Gyro with Caging Capability
A(3) Gyro with Torquing Capability

B. System Outputs

B(1) Three Axes Attitude Error and Body Rate
B(2) Three Axes Attitude Error

C. System Accuracy

C(1) High Accuracy System
C(2) Low Accuracy System

GYRO CONFIGURATIONS

The gyro developed under JPL Contract No. 950607 was not designed to provide caging or torquing as such. However, the gyro was designed with the customary damping coils which cause the gyro to spin in a stable manner about its preferred axis. In addition to this function the damping coils provide a limited caging capability as a by product. In reducing "wobble" in the rotor motion the damping coils tend to align the gyro spin vector along the magnetic axis of the damping coils.

For the purposes of this parameter study a gyro with a caging capability has as part of its design the ability to precisely align the gyro spin axis with a fixed line in the gyro case. With the gyro having this capability it will be possible to return the gyro spin axis to a known orientation relative to the gyro case. It is anticipated that caging capability will be mechanized with coils similar to the damping coils. However, the coils will be precisely made and mounted to the gyro case so that the coil magnetic axis can be properly aligned with the desired caging orientation.

A torquing capability in the strapped down miniature electrostatic gyro is defined as the ability to orient the gyro spin vector in any selected direction relative to the gyro case. It is anticipated that this capability will be instrumented with three sets of coils similar to the damping coils. The coils would be mounted to the gyro with their magnetic axes forming an orthogonal triad. Thus, the current in the coils could be adjusted to produce a resulting magnetic force vector that could have any orientation relative to the gyro case. Since the torques on the gyro rotor (caused by the magnetic force vector) are such as to align the spin vector along the magnetic vector, the desired torquing action results.

It was felt that these three levels of gyro complexity would provide useful information for making future gyro development decisions. Also, it would provide generally useful trade-off information between gyro caging and torquing capability and system complexity.

SYSTEM OUTPUTS

System output was selected as a parameter to be varied since not all spacecraft applications are likely to need both attitude error signal and a signal proportional body rate. It was therefore desirable to determine how omitting the body rate output signal would affect system size and power. Also, this information could be combined with information on the size, weight, etc., to obtain body rate from another source, such as a rate gyro, and determined which source of rate signal best suits the considered application.

SYSTEM ACCURACY

System output accuracy is important in selecting an attitude reference system for a spacecraft application. The required accuracy may range from two or three seconds of arc, as required for the AOSO program, to two or three degrees, as required for the Mercury spacecraft.

Therefore, the information resulting from a study of the trade-off between system accuracy and size, weight, power and reliability, will be useful in future decisions regarding the use of the strapped down electrostatic gyro attitude reference.

Two levels of accuracy, labeled "high" and "low", were selected for investigation in the parameter study. It was assumed the "high" level system would include mathematical compensation for misalignments in

the gyro pickoffs and mountings aboard the spacecraft, as well as any non-orthogonality of the spin vectors. The system with the "low" level accuracy would neglect these corrections. Also, it was assumed the "high" accuracy system would have an accuracy in the computer or data processor equivalent to 0.01 degrees error in the attitude output. And it would be capable of processing data fast enough as to provide the attitude information 10 times per second and the body rate information 100 times per second. The "low" accuracy system was assumed to have a computing accuracy equivalent to 0.1 degrees error in attitude output and iteration rates on the outputs of one per second for attitude and 10 per second for body rate.

PARAMETER COMBINATIONS

If all combinations of the independent parameters are used to define attitude reference systems, there are 12 systems which can be studied. With the symbols previously used to indicate the variations of the independent parameters the systems are:

ARS No. 1 = A(1) B(1) C(1)
ARS No. 2 = A(1) B(1) C(2)
ARS No. 3 = A(1) B(2) C(1)
ARS No. 4 = A(1) B(2) C(2)
ARS No. 5 = A(2) B(1) C(1)
ARS No. 6 = A(2) B(1) C(2)
ARS No. 7 = A(2) B(2) C(1)
ARS No. 8 = A(2) B(2) C(2)
ARS No. 9 = A(3) B(1) C(1)
ARS No. 10 = A(3) B(1) C(2)
ARS No. 11 = A(3) B(2) C(1)
ARS No. 12 = A(3) B(2) C(2)

Although there are 12 combinations of the independent parameters defining 12 attitude reference systems, this does not necessarily mean that 12 distinct sets of hardware will be required to satisfy the 12 system requirements.

SUMMARY OF RESULTS

The parameter study's objective was to establish the relationships between the independent and dependent parameters. These parameters were defined and discussed in the preceding introduction. Counting all combinations of the independent parameters there were 12 attitude reference systems to be considered in the study. It was determined that three distinct sets of system hardware would satisfy the requirements of all 12 systems.

HARDWARE CONFIGURATIONS

Although it was originally thought that gyro caging and torquing would significantly simplify system mechanization, the investigation did not support such a conclusion. It was therefore concluded that the systems would all be instrumented with the same type gyros, without caging or torquing. Therefore, for hardware and instrumentation the original 12 systems were reduced to four. The study and preliminary design of the data processor required by the strapped down ESG attitude reference system revealed that the requirements of the remaining four systems could be satisfied with three different designs of the data processor. As a result, the requirements of the original 12 combinations of independent parameters can be satisfied by three distinct sets of hardware. These sets of hardware were labeled systems A, B and C. Table 3-1 shows the values of the dependent parameters of size, weight, power and reliability for each of the three systems of hardware.

Table 3-1. System Sizing Estimates

	Size (in.^{3})	Weight (pounds)	Input Power (watts)			Failure Rate (%/1000 hours)
			Min.	Standby	Maximum	
System A	898	46.7	7.2	62	137	10.4202
System B	765	43.5	7.2	43	118	8.9102
System C	833	45.0	7.2	56	121	9.4720

INDEPENDENT PARAMETERS FOR HARDWARE CONFIGURATIONS

The independent parameters associated with each of the systems of Table 3-1 are: System A is a high accuracy system that provides both attitude error and body rate outputs; System B is a low accuracy system that provides both attitude error and body rate outputs; and System C is a high accuracy system that provides attitude error output only. The parameter combination of low accuracy and attitude error output did not result in system hardware distinctly different from system B.

Table 3-1 indicates three levels of power input to the systems. The maximum power assumes everything operating with the gyros in the high "g" mode. The standby power assumes the computer "on" but not operating and the gyro in the low "g" mode and pickoffs turned off. Minimum power assumes everything "off" except the gyro low "g" suspension.

Table 3-2 indicates the relationship between the originally defined 12 attitude references systems and the three sets of system hardware listed in Table 3-1.

Table 3-2. Hardware for Original 12 ARS

System	Hardware
ARS No. 1	A
ARS No. 2	B
ARS No. 3	C
ARS No. 4	B
ARS No. 5	A
ARS No. 6	B
ARS No. 7	C
ARS No. 8	B
ARS No. 9	A
ARS No. 10	B
ARS No. 11	C
ARS No. 12	B

ACCURACY VERSUS DEPENDENT PARAMETERS

Figure 3-1 is a plot showing the relationship between the independent parameter accuracy and the dependent parameters of system size, weight, power and reliability. The information presented in this plot is limited since, due to practical considerations, the parameter study was restricted to two values of system accuracy. The performance analysis conducted during the parameter study showed these two accuracies to be 0.036 and 0.066 degrees for the high and low accuracy systems, respectively. These are one sigma errors in the accuracy with which a given axis of the space vehicle can be pointed in a commanded direction.

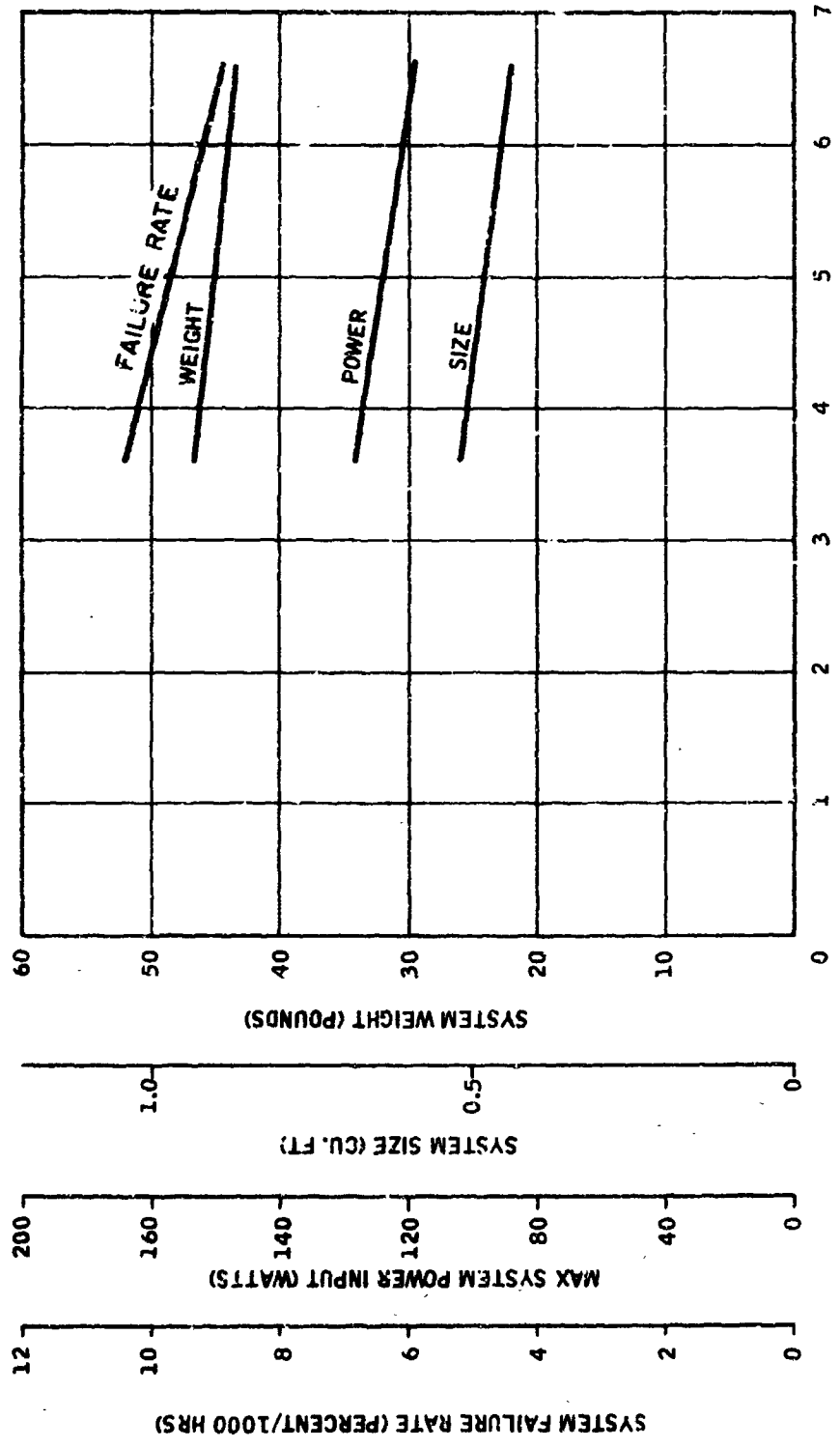

Figure 3-1. System Accuracy Versus System Sizing

BY-PRODUCT RESULTS

In addition to the parameter study's main objective of establishing the relationship between the independent and dependent parameters the study had several other by-product results. One of these was the discovery that the noise level on the gyro readout was the limiting factor in the usefulness of the body rate signal derived from the gyro readout. The performance analysis indicated the error in the body rate signal to have a one sigma value of 1.4 deg/sec. The readout noise contributed 70 times as much to this error as the RSS of all other sources of errors.

It was also discovered that in order to read the gyro 100 times a second each gyro pickoff must be equipped with its own set of shaping electronics, rather than to time share two sets of electronics between three pickoffs as originally planned.

Also, since it was necessary to carry out a preliminary design of the data processor to establish its size, weight, power and reliability, the other characteristic determined in the process is useful by-products. For example, it was concluded that the most accurate data processor would be instrumented with a 16-bit word, and would be a serial parallel machine operating with four bits per bite at a bit rate of 1.5 megacycles.

SELECTION OF THE ARS CONFIGURATION

INTRODUCTION

It has been assumed the SDMEG-ARS is capable of accepting commands in a digital form from the Central Control and Sequencer (CC&S) or an equivalent subsystem and provide torque command outputs to a Stabilization and Control Subsystem (SCS) which will affect the required attitude change of the vehicle. Conceivably, the CC&S can output several types of command signals which all uniquely define a given attitude change of the vehicle. The ARS design will change in complexity depending on the selected type of input from the CC&S. Therefore, the purpose of this discussion is to systematically consider reasonable inputs from the CC&S and determine the corresponding necessary design changes in the ARS.

The type of attitude command signals which are considered in this discussion are:

- Three-Euler angles
- Three sines and three cosines of Euler angles
- Six direction cosines of the gyro spin axes in body axes
- A complete 3 by 3 matrix which can be used to transform vectors from the vehicle reference frame to the frame oriented to the desired attitude of the vehicle.

The following discussion is arranged from the point of view of the ARS design with the following approaches:

- Euler angle approach I
- Euler angle approach II
- Gyro spin axis commands
- Vehicle steering in the gyro frame

The use of the four types of CC&S commands with each of the above four ARS design approaches will be pointed out at appropriate places in the discussion.

COORDINATE FRAMES

Four different frames of reference are used in the discussion of the ARS design approaches. These frames will carry the subscript: o, f, g, b.

o-frame - is the basic reference frame and, in this discussion will also be used as a navigational frame. It is assumed that this frame is established by optical sensors on board the vehicle independently of the gyro readout. For instance, the o-frame could be the sun-canopus frame.

f-frame - defines the vehicle's desired attitude. The orientation of the f-frame is defined by the guidance subsystem relative to the o-frame. By the assumptions of o-frame the definition of this frame is independent of the gyro readout. Let the relative attitudes of the f and o-frame be defined by the transformation T_{o2f} (transformation from o to f-frame). The transformation T_{o2f} consists of nine direction cosines; however, it requires only three Euler angles to define the nine direction cosines.

g-frame - is the inertial reference frame whose two axes are along the two gyro spin axes; the third is along a vector which is perpendicular to the two gyro spin axes.

The orientation of this frame is defined by the transformation (T_{b2g}) relative to the vehicle body axes. The elements of the T_{b2g} are determined in the ARS computer from the gyro readout information.

b-frame - is the vehicle body frame whose axes are the roll, pitch and yaw axes.

The transformations between the four frames contain the necessary information for the vehicle attitude control. This information is summarized below.

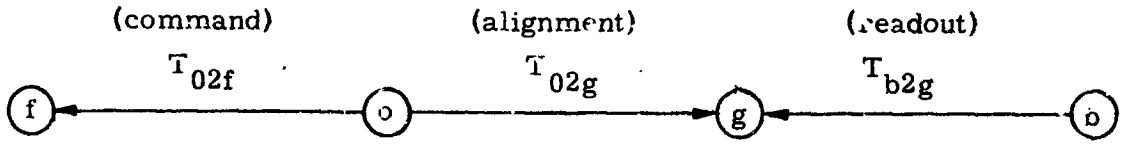

T_{02f} - Defined by a guidance subsystem

T_{02g} - Defined by the initial alignment of the ARS

T_{b2g} - Defined by the gyro readout

EULER ANGLE APPROACH I

Concept

The Euler Angle Approach I is identical in concept to the control system mechanization using a four-gimbal platform for attitude reference. The similarity in mechanizations is depicted in Figures 3-2 and 3-3.

The basic difference between the two mechanizations in Figures 3-2 and Figure 3-3 is that the four-gimbal platform in Figure 3-2 is replaced by the two SDMEG's and the digital computer in Figure 3-3.

In this discussion it is not the intent to arrive at the trade-offs of the two mechanizations. The four-gimbal mechanization is introduced to aid the understanding of the SDMEG-ARS mechanization using the Euler Angle Approach I.

Conceivably, the mechanization in Figure 3-3 can be a hybrid system (analog) and digital) where the digital computer outputs are the three Euler angles. The comparison of commanded Euler Angles to measured Euler angles and the transformation to body axes can conceivably be an electromechanical

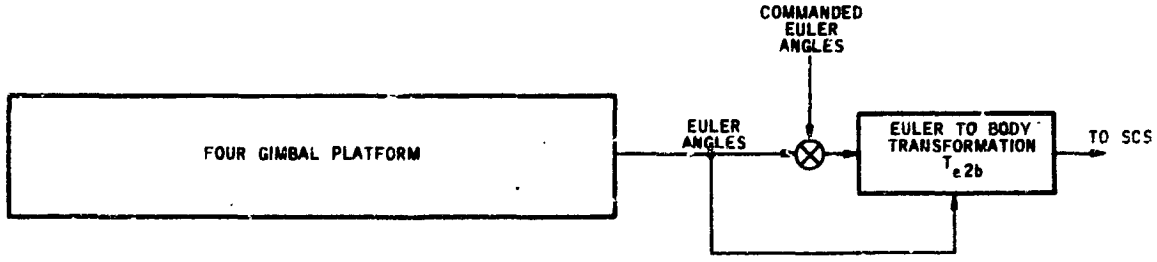

Figure 3-2. Platform Mechanization

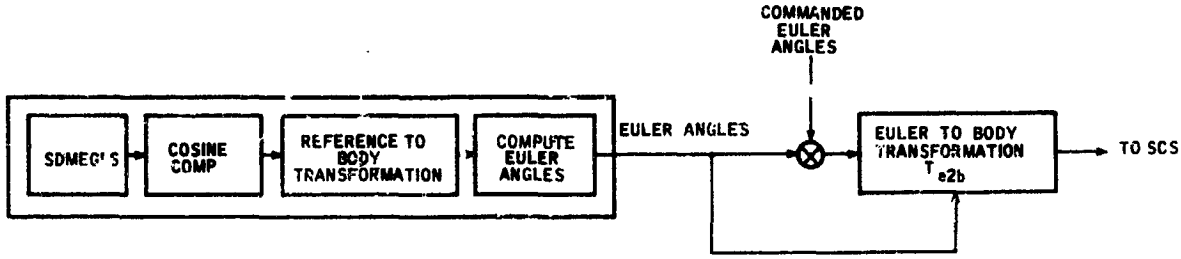

Figure 3-3. SDMEG-ARS Mechanization

analog system. However, in the present discussion all mechanizations will be assumed to be of digital type to arrive at the intended trade-offs among the different approaches of mechanizing the SDMEG-ARS system.

Computational Requirements

To mechanize the ARS concept shown in Figure 3-3 the following computations must be performed by the digital computer.

(1) Compute six direction cosines.

(2) Perform a vector cross-product; hence, complete the definition of the body-to-gyro transformation (T_{b2g}). This transformation also defines the T_{02g} ARS alignment matrix when the vehicle is held to the basic reference attitude by optical sensors.

(3) Invert matrix T_{02g} and obtain T_{g2o}. This is a comparatively trivial computation if the gyro spin axes are orthogonal.

(4) Multiply two 3 by 3 matrixes and obtain body-to-reference transformation

$$T_{b2o} = T_{g2o}\, T_{b2g}$$

(5) The elements of the T_{b2o} transformation are functions of the desired Euler Angles. And, in particular, three elements (a_{21}, a_{31}, a_{32}) of the transformation will be

$$\text{Sin } \theta = -a_{31}$$

$$\text{Sin } \phi \cos \theta = a_{32}$$

$$\text{Sin } \psi \cos \theta = a_{21}$$

Use the "method of least work" in Appendix C to verify the above relationship. Therefore, compute the Euler angles as follows:

(5.1) $\theta = -\sin^{-1} a_{31}$

(5.2) $\cos\theta = \cos(-\sin^{-1} a_{31})$

(5.3) $\phi = \sin^{-1}(a_{32}/\cos\theta)$

(5.4) $\psi = \sin^{-1}(a_{21}/\cos\theta)$

(6) Compute Euler Transformation T_{e2b}

To compute this transformation it is required to determine

(6.1) $\sin\theta$

(6.2) $\sin\phi\cos\theta$

(*6.3) $\cos\theta\cos\phi$

(6.4) $\sin\phi$

(*6.5) $\cos\phi$

(7) Compute the difference ($\Delta\phi$, $\Delta\theta$, $\Delta\psi$) between the commanded and computed Euler angles.

(8) Transform $\Delta\phi$, $\Delta\theta$, $\Delta\psi$ to body axes to be used by the SCS as the vehicle rate commands

$$\begin{bmatrix} \omega_{xc} \\ \omega_{yc} \\ \omega_{zc} \end{bmatrix} = T_{e2b} \begin{bmatrix} \Delta\phi \\ \Delta\theta \\ \Delta\psi \end{bmatrix}$$

The ω_{xc}, ω_{yc} and ω_{zc} are the rate commands to the autopilot.

*Quantities to be computed in Step (6); the other quantities were already computed in Step (5).

All of the computation steps, except for Step (3), must be done at a computation rate which is consistent with the autopilot bandwidths requirements.

Step (4) does not have to be completely carried out since only three elements (a_{21}, a_{31}, a_{32}) are required for the Euler angle computation.

Table 3-3 does not include operations in the cosine computer (Step 1 above).

Table 3-3. Summary of Major Arithmetic Operations if Guidance Provides Three Euler Angles

High Speed Computations (Computations During Maneuver)	Low Speed Computations (Calculations Prior to a Maneuver)
Multiplications = 25	(None Required)
Divisions = 2	
ARC sine = 3	
Cos = 2	

Interface with Guidance Subsystem

Guidance Subsystem sends three numbers (Euler angles) to the SDMEG-ARS for the re-orientation maneuver.

ARS initial alignment procedure will require that the guidance subsystem:

- Command vehicle hold attitude using optical sensors with vehicle body axes along the body reference attitude (body axes along o-frame).
- Instruct the ARS that it is in the alignment mode.

EULER ANGLE APPROACH II

Concept

In this concept, the Euler angle error signals are computed without the explicit computation of the Euler angles and comparing to the commanded angles. Examination of the computation of the torque command signals (attitude error in body axis) shows that the Euler angle transformation (T_{e2b}) is not required.

The concept is explained using the pictorial representation of the coordinate rotations in Figure 3-4.

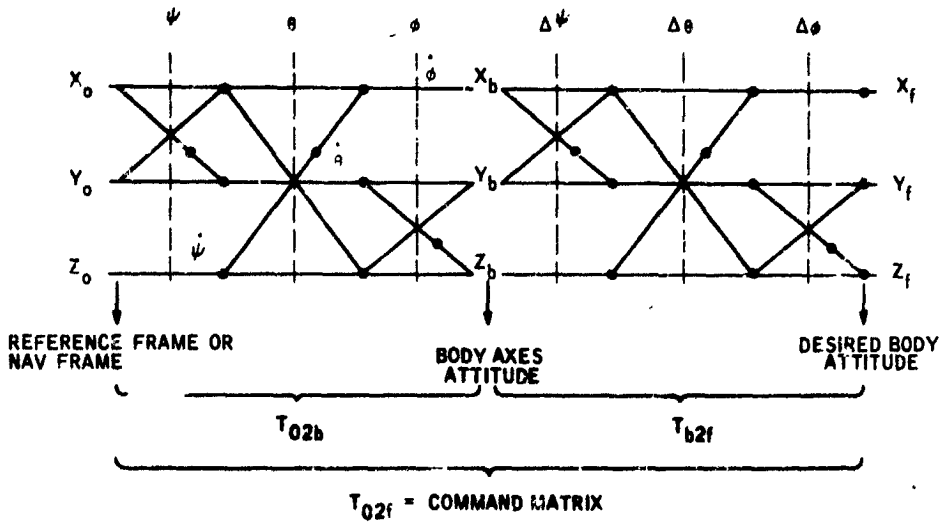

Figure 3-4. Graphic Coordinate Transformation

The method used in Figure 3-4 to describe the coordinate rotation is explained in Appendix C. However, at this point it will suffice to say that this figure is analogous to resolver mechanization of the transformations, namely

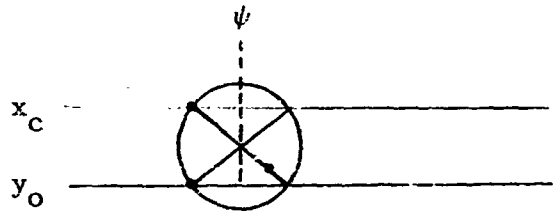

$$x_1 = x_o \cos\psi + y_o \sin\psi$$

$$y_1 = -x_o \sin\psi + y_o \cos\psi$$

$$z_1 = z_o$$

Following a signal through the resolver in a diagonal direction gives a sine function. A dot can indicate which function requires the negative sign. A signal going straight across is multiplied by the cosine.

In Figure 3-4 the transformation T_{02f} is the guidance subsystem command matrix and is always uniquely defined by a consistent set of command signals.

The transformation T_{02b} is computed in the ARS computer using gyro read-out and ARS alignment data.

The body axes (x_b, y_b, z_b) attitude at any time during the maneuver is known both in the o and f frames and the autopilot has to torque the vehicle such as to drive the Euler angle errors $\Delta\psi$, $\Delta\theta$ and $\Delta\phi$ to zero or drive the transformation T_{b2f} to a unit matrix.

The concept of the Euler angle Approach II then involves the computation of the transformation T_{b2f} and computation of the steering commands which will drive the T_{b2f} to unit matrix.

Computational Requirements

The mechanization of the ARS using the Euler Angle Approach II requires the following computations in the ARS digital computer.

(1) Compute six direction cosines.

(2) Perform a vector cross product, hence, define the body-to-gyro transformation (T_{b2g}). This transformation also defines the T_{o2g} ARS alignment matrix when the vehicle is held to the basic reference attitude by optical sensors.

(3) Invert matrix T_{o2g} and obtain T_{g2o}. This is a comparatively trivial computation if the gyro spin axes are orthogonal. The orthogonality of the spin axes can be assured if the gyros have caging or torquing capability. This computation can be done prior to a re-orientation maneuver.

(4) Multiply two 3 by 3 matrixes and obtain body-to-reference transformation.

$$T_{b2o} = T_{g2o} \quad T_{b2g}$$

(5) Establish the command matrix T_{o2f}.

Depending on the form of the guidance command signals, the ARS computer will be required to perform different amounts of computations. However, these computations do not have to be done simultaneously with the computations which enter into real time vehicle control. In other words, the T_{o2f} can be precomputed by the ARS GP computer prior to a maneuver when the computer is not used for the vehicle control purposes.

If ψ_c, θ_c, ϕ_c are the commanded Euler angles, then

$$T_{o2f} = \begin{bmatrix} (c\psi_c\, c\theta_c) & (s\psi_c\, c\theta_c) & (-s\theta_c) \\ (-s\psi_c\, c\theta_c + c\psi_c\, s\theta_c) & (s\psi_c\, s\theta_c\, s\phi_c + c\psi_c\, c\phi_c) & (c\theta_c\, s\phi_c) \\ (s\psi_c\, s\phi_c + c\psi_c\, c\phi_c) & (s\psi_c\, s\theta_c\, c\phi_c - c\psi_c\, s\phi_c) & (c\theta_c\, c\phi_c) \end{bmatrix}$$

Use the "Method of Least Work" in Appendix C to verify the above transformation.

Note that in order to evaluate the T_{o2f} matrix the computer must have in its memory the sine subroutine which is the new addition to the functions the computer must perform in its primary mode of operation (vehicle control mode).

In order to eliminate the storage of sine subroutine the guidance system command signals must have one of the following forms:

$$\sin \psi_c, \cos \psi_c, \sin \theta_c, \cos \theta_c, \sin \phi_c, \cos \phi_c$$

$$\sin \psi_c, \sin \theta_c, \sin \phi_c \text{ and}$$

$$\begin{aligned} &\text{sign of} \quad \cos \psi_c \\ &\text{sign of} \quad \cos \theta_c \\ &\text{sign of} \quad \cos \phi_c \end{aligned}$$

Guidance provides the nine elements of the T_{o2f} transformation.

(6) Compute T_{b2f} transformation.

$$T_{b2f} = T_{o2f} \quad T_{b2o}$$

The matrix T_{b2f} is a 3 by 3 matrix and consists of nine elements, namely

$$T_{b2f} = \begin{bmatrix} \epsilon_{11} & \epsilon_{12} & \epsilon_{13} \\ \epsilon_{21} & \epsilon_{22} & \epsilon_{23} \\ \epsilon_{31} & \epsilon_{32} & \epsilon_{33} \end{bmatrix}$$

From Figure 3-4 the T_{b2f} matrix can be written as follows

$$T_{b2f} = \begin{bmatrix} (c\Delta\psi\, c\Delta\phi) & (s\Delta\psi\, c\Delta\theta) & (-s\Delta\theta) \\ (-c\Delta\phi\, s\Delta\psi + s\Delta\phi\, s\Delta\theta\, c\Delta\psi) & (c\Delta\phi\, c\Delta\psi + s\Delta\phi\, s\Delta\theta\, s\Delta\psi) & (s\Delta\phi\, c\Delta\theta) \\ (c\Delta\phi\, s\Delta\theta\, c\Delta\psi + s\Delta\phi\, s\Delta\psi) & (c\Delta\phi\, s\Delta\theta\, s\Delta\psi - s\Delta\phi\, c\Delta\psi) & (c\Delta\phi\, c\Delta\theta) \end{bmatrix}$$

The ϵ's are the computed elements of the T_{b2f} transformation and comparing term by term with T_{b2f} transformation expressed in terms of the Euler angle errors it can be seen that

$$\left.\begin{aligned} \epsilon_{12} &= \sin\Delta\psi\cos\Delta\theta \simeq \Delta\psi \\ \epsilon_{13} &= -\sin\Delta\theta \simeq -\Delta\theta \\ \epsilon_{23} &= \sin\Delta\phi\cos\Delta\theta \simeq \Delta\phi \end{aligned}\right\} \text{Approximation for small errors}$$

(7) Determine vehicle steering law which will drive ϵ_{12}, ϵ_{13} and ϵ_{23} terms to zero and thus align the vehicle to the desired attitude.

It is shown below that no further calculations are required to derive vehicle rate command signals in order to null the ϵ_{12}, ϵ_{13} and ϵ_{23} terms. And, in fact,

$\omega_{xc} = -\epsilon_{23}$ → X axis attitude error in body axis

$\omega_{yc} = +\epsilon_{13}$ → Y axis attitude error in body axis

$\omega_{zc} = -\epsilon_{12}$ → Z axis attitude error in body axis

PROOF

Write

$$\begin{bmatrix} \hat{X}_f \\ \hat{Y}_f \\ \hat{Z}_f \end{bmatrix} = \begin{bmatrix} \epsilon_{11} & \epsilon_{12} & \epsilon_{13} \\ \epsilon_{21} & \epsilon_{22} & \epsilon_{23} \\ \epsilon_{31} & \epsilon_{32} & \epsilon_{33} \end{bmatrix} \begin{bmatrix} \hat{X}_b \\ \hat{Y}_b \\ \hat{Z}_b \end{bmatrix}$$

Where

$\hat{X}_f \ \hat{Y}_f \ \hat{Z}_f$	Are unit vectors along f frame
$\hat{X}_b \ \hat{Y}_b \ \hat{Z}_b$	Are unit vectors along b frame

It is desired to align $\hat{X}_f$ with $\hat{X}_b$, $\hat{Y}_f$ with $\hat{Y}_b$ and $\hat{Z}_f$ with $\hat{Z}_b$. To accomplish this maneuver two axes must be aligned and the third axis represents the redundant information. For this derivation assume that the X's and Y's are aligned.

To align X's it is sufficient to rotate the vehicle about the vector $\hat{X}_f \times \hat{X}_b$ until the magnitude of $\hat{X}_f \times \hat{X}_b$ assumes the zero value.

Similarily for Y's rotate the vehicle about the $\hat{Y}_f \times \hat{Y}_b$ vector until its magnitude is zero.

Since the relative attitude of f and the b frame is defined by the T_{b2f} transformation the vector cross products can be evaluated as follows:

$$\hat{X}_f \times \hat{X}_b = (\epsilon_{11} \hat{X}_b + \epsilon_{12} \hat{Y}_b + \epsilon_{13} \hat{Z}_b) \times \hat{X}_b$$

$$= - \epsilon_{12} \hat{Z}_b + \epsilon_{13} \hat{Y}_b$$

Therefore

$$\omega_{Zc} = -\epsilon_{12}$$

$$\omega_{Yc} = +\epsilon_{13}$$

Similarly

$$\hat{Y}_f \times \hat{Y}_b = (\epsilon_{21} \hat{X}_b + \epsilon_{22} \hat{Y}_b + \epsilon_{23} \hat{Z}_b) \times \hat{Y}_b$$

$$= \epsilon_{21} \hat{Z}_b - \epsilon_{23} \hat{X}_b$$

Therefore

$$\omega_{Xc} = -\epsilon_{23}$$

Table 3-4 does not include operations in the cosine computer (Step 1 above).

Table 3-4. Summary of Major Arithmetic Operations if Guidance Provides Three Euler Angles

High Speed Computations	Low Speed Computations (Calculations Prior to a Maneuver)
Multiplications = 45	Multiplications = 16 Sin = 3 Cos = 3

Interface With Guidance Subsystem

The guidance subsystem attitude commands can have any one of the following forms:

(1) Three Euler angles.

(2) Three sine and three cosine functions of the Euler angles.

(3) Three sine functions of the Euler angles and three signs of the corresponding cosine functions.

(4) Nine numbers which define the T_{o2f} transformation.

The ARS initial alignment procedure will require that the guidance subsystem:

(1) Command vehicle hold using optical sensors with the vehicle body axes aligned along the body reference attitude (body axes along o frame).

(2) Instruct the ARS that it is in the alignment mode.

GYRO SPIN AXIS COMMANDS, $\hat{Q}_1$, $\hat{Q}_2$

Concept

For this concept the vehicle attitude error is computed by comparing the current gyro readout with the commanded readout and then steering the vehicle to null the difference. The geometry is depicted in Figure 3-5.

In Figure 3-5 the gyro spin vectors $\hat{S}_1$ and $\hat{S}_2$ are known in the body axes by the virtue of the gyro readout and some data processing. The vectors $\hat{Q}_1$ and $\hat{Q}_2$ are the desired attitudes of $\hat{S}_1$ and $\hat{S}_2$ in body axes.

These attitudes are defined by processing the command signals (e.g. Euler angles) from the guidance subsystem together with the initial ARS alignment data. The vector difference ($\overline{\Delta S}$) between $\hat{Q}$ and $\hat{S}$ is formed for each gyro and is used in computation of a unique vector θ such that if the vehicle is rotated about $\overline{\theta}$ the readout errors represented by $\overline{\Delta S}_1$ and $\overline{\Delta S}_2$ approach null values simultaneously. Another property of the $\overline{\theta}$ vector is that it becomes a null vector (zero magnitude) when both the $\overline{\Delta S}_1$ and $\overline{\Delta S}_2$ are zero. In fact $\overline{\theta}$ is the desired attitude error in body axes to be used as an input to the SCS.

It should be obvious from the above discussion that during a given maneuver the $\hat{Q}_1$ and $\hat{Q}_2$ are constants and they are precomputed before the maneuver. Consequently, these constants can be precomputed by the Guidance Subsystem or by the ARS G. P. Computer. The ARS computer, before a maneuver may be in the "Standby" Mode, therefore could be available for the computation of $\hat{Q}_1$ and $\hat{Q}_2$ constants.

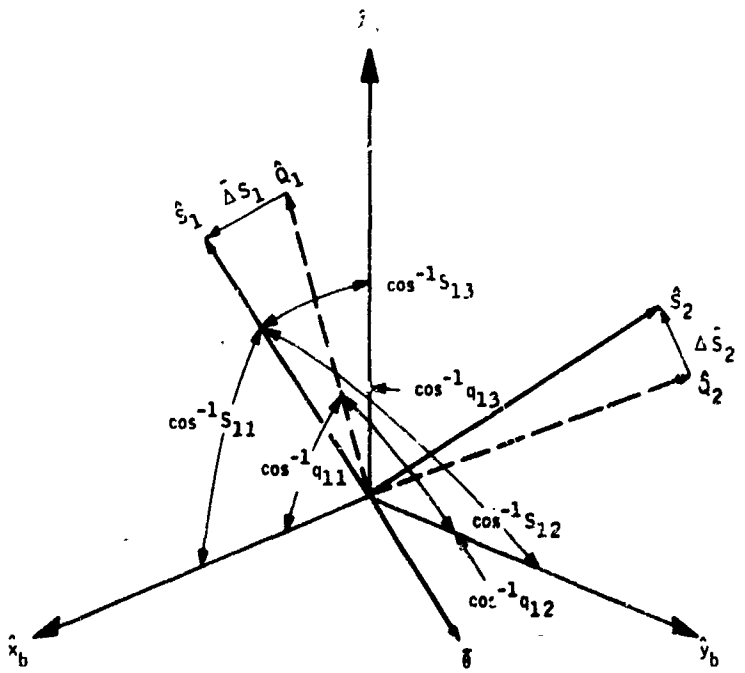

$\hat{x}_b, \hat{y}_b, \hat{z}_b$	UNIT VECTORS ALONG THE BODY AXES
$\hat{S}_1, \hat{S}_2$	UNIT VECTORS ALONG GYRO SPIN AXES
$\hat{Q}_1, \hat{Q}_2$	COMMANDED ATTITUDES OF $\hat{S}_1$ AND $\hat{S}_2$, RESPECTIVELY
S_{11}, S_{12}, S_{13}	$\hat{S}_1$ DIRECTION COSINES
S_{21}, S_{22}, S_{23}	$\hat{S}_2$ DIRECTION COSINES (NOT SHOWN IN THE FIGURE)
q_{11}, q_{12}, q_{13}	$\hat{Q}_1$ DIRECTION COSINES
q_{21}, q_{22}, q_{23}	Q_2 DIRECTION COSINES (NOT SHOWN IN THE FIGURE)
$\bar{\theta}$	ATTITUDE ERROR IN BODY AXES

Figure 3-5. Geometry Used in Control of Vehicle Using $\hat{Q}_1$ and $\hat{Q}_2$ Commands

Computational Requirements

The computational requirements for this ARS concept are summarized below:

(1) Compute six direction cosines.

(2) Compute the command matrix T_{o2f}.

Depending on the form of the guidance command signals, the ARS computer will be required to perform different amounts of computations. However, these computations do not have to be done simultaneously with the computations which enter into real time vehicle control. In other words, the T_{o2f} can be precomputed by the ARS G. P. computer prior to a maneuver when the computer is not used for the vehicle control purposes.

If ψ_c, θ_c, ϕ_c are the commanded Euler angles then

$$T_{o2f} = \begin{bmatrix} (c\psi_c\, c\theta_c) & (s\psi_c\, c\theta_c) & (-s\theta_c) \\ (-s\psi_c\, c\theta_c + c\psi_c\, s\theta_c\, s\phi_c) & (s\psi_c\, s\theta_c\, s\phi_c + c\psi_c\, c\phi_c) & (c\theta_c\, s\phi_c) \\ (s\psi_c\, s\phi_c + c\psi_c\, s\theta_c\, c\phi_c) & (s\psi_c\, s\theta_c\, c\phi_c - c\psi_c\, s\phi_c) & (c\theta_c\, c\phi_c) \end{bmatrix}$$

Use the "Method of Least Work" in Appendix C to verify the above transformation.

Note that in order to evaluate the T_{o2f} matrix the computer must have in its memory the sine subroutine which is the new addition to the functions the computer must perform in its primary mode of operation (vehicle control mode).

In order to eliminate the storage of sine subroutine the guidance system command signals must have one of the following forms:

$\sin\psi_c$, $\cos\psi_c$, $\sin\theta_c$, $\cos\theta_c$, $\sin\phi_c$, $\cos\phi_c$

$\sin\psi_c$, $\sin\theta_c$, $\sin\phi_c$ and

sign of $\cos \psi_c$

sign of $\cos \theta_c$

sign of $\cos \phi_c$

Guidance provides the nine elements of the T_{o2f} transformation.

(3) Compute the command vectors $\hat{Q}_1$ and $\hat{Q}_2$. These computations do not have to be done simultaneously with the computations which enter into the real time vehicle control. In other words, the six direction cosines which describe the $\hat{Q}_1$ and $\hat{Q}_2$ command vectors can be precomputed by the ARS G. P. computer prior to a maneuver when the computer is not used for the vehicle control purposes.

The computation involves multiplication of a 3 by 3 matrix (T_{o2f}) by a 2 by 3 matrix

$$\begin{bmatrix} \hat{Q}_1 & \hat{Q}_2 \end{bmatrix} = \begin{bmatrix} q_{11} & q_{21} \\ q_{12} & q_{22} \\ q_{13} & q_{23} \end{bmatrix} = T_{o2f} \begin{bmatrix} S_{110} & S_{210} \\ S_{120} & S_{220} \\ S_{130} & S_{230} \end{bmatrix}$$

The six direction cosines (S_{ijo}) are available from the ARS computer memory and are the initial ARS alignment data. Before storage of these constants in the computer memory they are computed by the Cosine Computer (Step 1 above) during the ARS alignment mode.

Note that if the $\hat{Q}_1$ and $\hat{Q}_2$ command signals are established by the guidance subsystem then the guidance - ARS interface must accomodate the transmission of six numbers (S_{ijo}) from ARS to the guidance and six numbers (q_{ij}) from guidance to the ARS. Consequently, the ARS design trade-off involves the storage of a subroutine in the ARS computer to solve for $\hat{Q}_1$ and $\hat{Q}_2$ versus the additional requirement on the guidance ARS interface to transmit ARS alignment data to the guidance subsystem and to compute the command vectors $\hat{Q}_1$ and $\hat{Q}_2$ in the guidance computer.

(4) Steer the vehicle according to the law

$$\tilde{\theta} = \hat{Q}_1 \times \hat{S}_1 - \hat{S}_1 \, (\hat{Q}_2 \cdot \hat{S}_1 \times \hat{S}_2)$$

See Attitude Error and Body Rate Computer in Progress Report 20113-PR2.

Table 3-5. Summary of Major Arithmetic Operations if the Guidance Provides Three Euler Angles

High Speed Computations	Low Speed Computations
Multiplications = 18	Multiplications = 34 Sin = 3 Cos = 3

Table 3-5 does not include operations in the cosine computer (Step 1 above).

Interface with Guidance Subsystem

In the discussion of the "Computational Requirements" section, two approaches were pointed out: (1) The command vectors $\hat{Q}_1$ and $\hat{Q}_2$ are computed by the guidance subsystem, and (2) the $\hat{Q}_1$ and $\hat{Q}_2$ vectors are computed by the ARS computer. The interface requirements will differ for the two approaches.

Interface Requirements for Approach 1 --

(1) Six numbers which describe ARS initial alignment are transmitted to the guidance subsystem.

(2) Six numbers which describe $\hat{Q}_1$ and $\hat{Q}_2$ vectors are transmitted from guidance to the ARS computer.

(3) The ARS initial alignment procedure will require that the guidance subsystem:

(3.1) Commands vehicle hold using optical sensors with the vehicle body axes aligned to the o frame.

(3.2) Instructs the ARS that it is in the alignment mode.

Interface Requirements for Approach 2 --

(1) The Guidance system will transmit to the ARS:

(1.1) Three Euler angles, or

(1.2) Three sine and three cosine functions of the Euler angles, or

(1.3) Three sine functions of the Euler angles and three signs of the corresponding cosine functions, or

(1.4) Nine numbers which define the T_{o2f} transformation.

(2) The ARS initial alignment procedure will require that the guidance subsystem:

(2.1) Commands vehicle hold using optical sensors with the vehicle body axes aligned to the o frame.

(2.2) Instructs the ARS that it is in the alignment mode.

VEHICLE STEERING IN GYRO FRAME

In this concept, the inertial gyro frame is used as a primary reference frame for the computation of the vehicle steering commands. Since the computed steering signals are in the inertial gyro frame, they must be resolved along the vehicle body axes.

Concept

The concept is depicted in Figure 3-6 which shows the vehicle X-axis steering. A similar diagram can be drawn for Y-axis (or Z-axis) steering to control the vehicle about the X-axis.

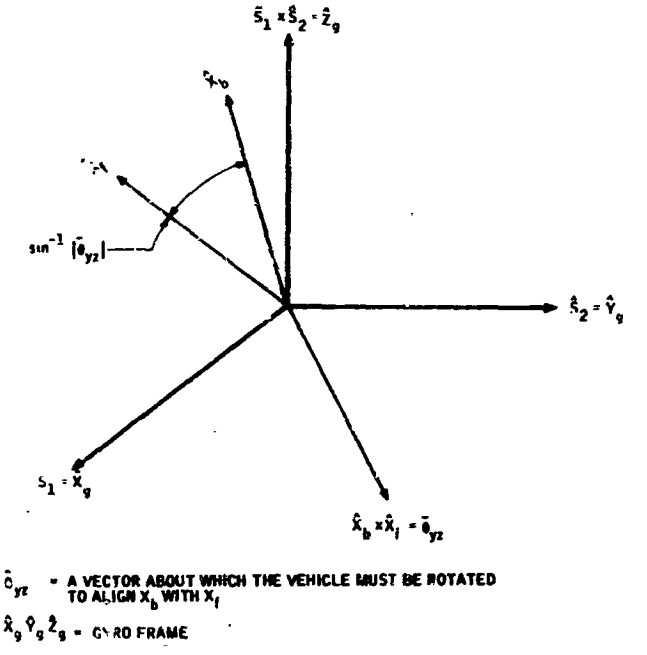

Figure 3-6. The Vehicle X-Axis Steering in Gyro Frame

For the X-axis steering, the actual and desired X-axis attitudes are computed in the gyro frame. The vector cross-product of $\hat{X}_b$ and $\hat{X}_f$ is formed, which, if transformed to the body frame, can be used as input to the Y and Z controllers of the vehicle.

Similarly, the cross-product of $\hat{Y}_b$ and $\hat{Y}_f$, after suitable transformation, can be used as an input to the X-axis controller.

Computational Requirements

The ARS mechanization using the vehicle steering in the gyro frame requires the following computation steps by the digital computer.

(1) Compute six direction cosines (Cosine Computer in Progress Report 20113-PR2).

(2) Perform vector cross-product, hence, define the body-to-gyro transformation (T_{b2g}). This transformation also defines the T_{o2g} ARS alignment matrix when the vehicle is held to the body reference attitude by optical sensors.

(3) Invert matrix T_{b2g} and obtain T_{g2b}. This is a comparatively trivial computation if the gyro spin axes are orthogonal. The orthogonality of the spin axes can be assured if the gyros have caging or torquing capability.

(4) Establish the command matrix T_{o2f}.

Depending on the form of the guidance command signals, the ARS computer will be required to perform different amounts of computations. However, these computations do not have to be done simultaneously with the computations which enter into real time vehicle control. In other words, the T_{o2f} can be precomputed by the ARS G.P. computer prior to a maneuver when the computer is not used for the vehicle control purposes.

If ψ_c, θ_c, ϕ_c are the commanded Euler angles then

$$T_{o2f} = \begin{bmatrix} (c\psi_c\, c\theta_c) & (s\psi_c\, c\theta_c) & (-s\theta_c) \\ (-s\psi_c\, c\theta_c + c\psi_c\, s\theta_c\, s\phi_c) & (s\psi_c\, s\theta_c\, s\phi_c + c\psi_c\, c\phi_c) & (c\theta_c\, s\phi_c) \\ (s\psi_c\, s\phi_c + c\psi_c\, s\theta_c\, c\phi_c) & (s\psi_c\, s\theta_c\, c\phi_c - c\psi_c\, s\phi_c) & (c\theta_c\, c\phi_c) \end{bmatrix}$$

Use the "Method of Least Work" in Appendix C to verify the above transformation.

Note that in order to evaluate the T_{o2f} matrix the computer must have in its memory the sine subroutine which is the new addition to the functions the computer must perform in its primary mode of operations (vehicle control mode).

In order to eliminate the storage of sine subroutine the guidance system command signals must have one of the following forms:

$$\sin\psi_c,\ \cos\psi_c,\ \sin\theta_c,\ \cos\theta_c,\ \sin\phi_c,\ \cos\phi_c$$

$$\sin\psi_c,\ \sin\theta_c,\ \sin\phi_c \text{ and}$$

$$\text{sign of } \cos\psi_c$$

$$\text{sign of } \cos\theta_c$$

$$\text{sign of } \cos\phi_c$$

Guidance provides the nine elements of the T_{o2f} transformation.

(5) Multiply the 3 by 3 T_{o2f} matrix by the 3 by 3 matrix T_{g2o}.

$$T_{g2f} = T_{o2f} \quad T_{g2o}$$

(6) Use information from Step (5) and Step (3) and from two vector cross-products.

$$\hat{X}_b \times \hat{X}_f = \bar{\theta}_{YZ}$$

$$\hat{Y}_b \times \hat{Y}_f = \bar{\theta}_X$$

(7) Calculate the rate commands to be used as inputs to SCS.

$$\begin{bmatrix} \omega_{Yc} \\ \omega_{Zc} \end{bmatrix} = T_{g2b} \begin{bmatrix} \bar{\theta}_{YZ} \cdot \hat{X}_g \\ \bar{\theta}_{YZ} \cdot \hat{Y}_g \\ \bar{\theta}_{YZ} \cdot \hat{Z}_g \end{bmatrix}$$

$$\begin{bmatrix} \omega_{Xc} \end{bmatrix} = T_{g2b} \begin{bmatrix} \bar{\theta}_X \cdot \hat{X}_g \\ \bar{\theta}_X \cdot \hat{Y}_g \\ \bar{\theta}_X \cdot \hat{Z}_g \end{bmatrix}$$

Note that the computations which are described in Steps (4) and (5) can be pre-computed before a re-orientation maneuver either in the ARS or guidance computer. The computations in these steps transform the guidance command signals from the reference frame (o-frame) to the inertially fixed gyro frame (g-frame).

The ARS guidance interface requirements will change depending on whether the ARS or guidance computer transforms the guidance commands to the gyro frame.

Table 3-6 does not include operations in the cosine computer (Step 1 above).

Table 3-6. Summary of Major Arithmetic Operations if Guidance Provides Three Euler Angles

High Speed Computations	Low Speed Computations (Calculations Prior to a Maneuver)
Multipliciations = 27	Multiplications = 43 Sin = 3 Cos = 3

Interface with Guidance Subsystem

In the discussion of the "Computational Requirements" section, two approaches were pointed out: (1) the guidance specifies attitude command in gyro frame, (2) the ARS computer transforms guidance commands from the reference to the gyro frame. The interface requirements will differ for the two approaches.

Interface Requirements for Approach 1 --

(1) Six numbers which describe ARS initial alignment are transmitted to the guidance subsystem.

(2) Six numbers which describe the desired attitude of the vehicle two body axes in the gyro frame (g-frame) are transmitted from guidance to the ARS computer.

(3) The ARS initial alignment procedure will require that the guidance subsystem:

(3.1) Commands vehicle hold using optical sensors with the vehicle body axis aligned to the O-frame.

(3.2) Instructs the ARS computer that it is in the alignment mode.

Interface Requirements for Approach 2 -- The guidance subsystem attitude commands can have any one of the following forms:

(1) Three Euler angles

(2) Three sine and three cosine functions of the Euler angles

(3) Three sine functions of the Euler angles and three signs of the corresponding cosine functions

(4) Nine numbers which define the T_{o2f} transformation

The ARS initial alignment procedure will require that the guidance subsystem:

(1) Commands vehicle hold using optical sensors with the vehicle body axes aligned along the body reference attitude (body axes along o frame)

(2) Instructs the ARS that it is in the alignment mode

CONCLUSIONS

The computer operations which are shown in Tables 3-2 through 3-6 have been selected to show the tradeoffs among the four ARS design approaches. In all tables the assumed attitude command signals from the guidance subsystem were assumed to be Euler angles. The airborne computer operations required to calculate spin vector direction cosines are not included in the tables since these computations are required by all four design approaches of the ARS.

The computations are divided into high and low speed categories.

The high-speed computations are those which are done on-board the vehicle and whose rate is consistent with the control system stability requirements.

The low-speed computations do not enter into the real time control of the vehicle, and can be done either on-board the vehicle prior to a maneuver or in a guidance computer which may be located on the ground.

If the low-speed computations are done on-board the vehicle, in general only airborne computer memory will increase in order to store the necessary program. However, if these computations are performed in a ground based computer, the telemetry link will be required to accommodate six ARS alignment numbers from vehicle to ground and six or nine numbers from ground to the vehicle.

Assume that the low-speed computations are done in the airborne computer. Then by inspection of Tables 3-3 through 3-6 it can be seen that Table 3-5 is the best compromise. Table 3-3 is definitely out because of the relatively complicated high-speed section of the computer. Table 3-5, if compared with Tables 3-4 and 3-6, has not only less high-speed multiplications, but also requires less high-plus-slow multiplications.

Therefore, the ARS design approach represented by Table 3-5 has been selected as the approach for the SDMEG-ARS study.

ARS SYSTEM EQUATIONS

This subsection presents the equations and logic statements that must be mechanized in the computer section of the 12 attitude reference systems. This work is a prerequisite for determining size, weight, power consumption and other parameters for the various systems.

DISCUSSION OF SYSTEM EQUATIONS

For the purposes of this discussion, the data processor has been arbitrarily divided into two categories: the Cosine Computer and the Attitude Error and Body Rate Computer. Flow charts for the two computer sections are shown in Figures 3-7 and 3-8. The flow charts represent a maximum design of the data processing by including all detail necessary for the highest accuracy ADMEG attitude reference system. Therefore, the data processor or computers for all the systems can be discussed as variations of these computers.

Figure 3-7 indicates calculations that would be performed by the cosine computer for one gyro. In a complete system, the computer section performing this function could be duplicated for each gyro or shared by both gyros. The choice is dictated by system accuracy requirements and the delay time the attitude control system can tolerate. In this study it is assumed it is adequate to time share the computer between the gyros.

COSINE COMPUTER

The cosine computer's function is to generate at its output digital signals proportional to the direction cosines of the gyro spin vectors in the vehicle body axes. The cosine computer receives its inputs from the interface logic that couples the gyros and computer. The interface logic provides digital signals proportional to the time interval between the time at which the rotor reference line passes under a pickoff and the time at which the rotor cosine pattern passes under the same pickoff. This information is supplied for two pickoffs on each gyro (referred to here as "partial counts"). Also, the interface logic provides digital inputs proportional to the time of one revolution of each gyro rotor. These inputs will be referred to as "total counts".

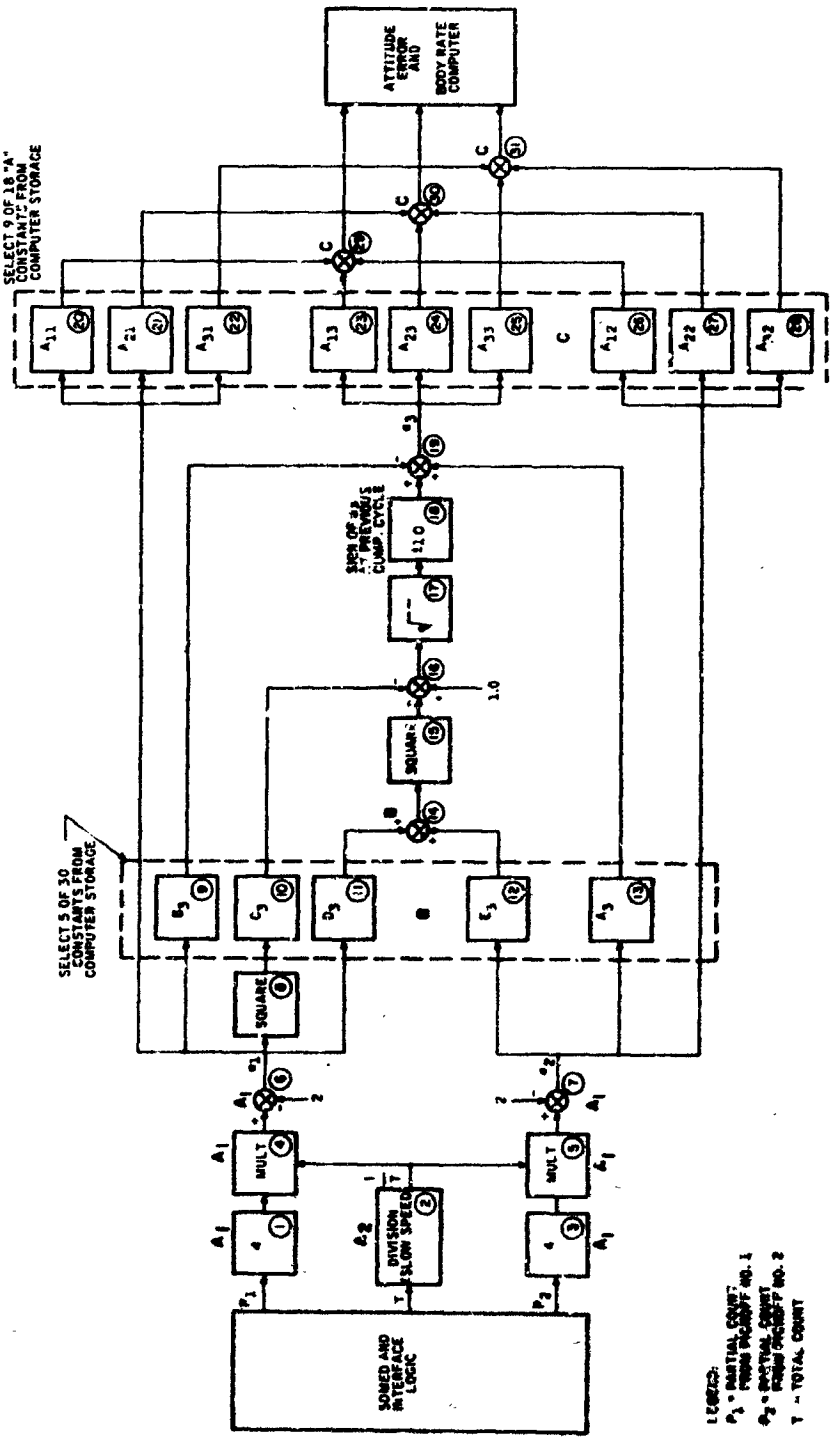

Figure 3-7. Cosine Computer Flow Chart

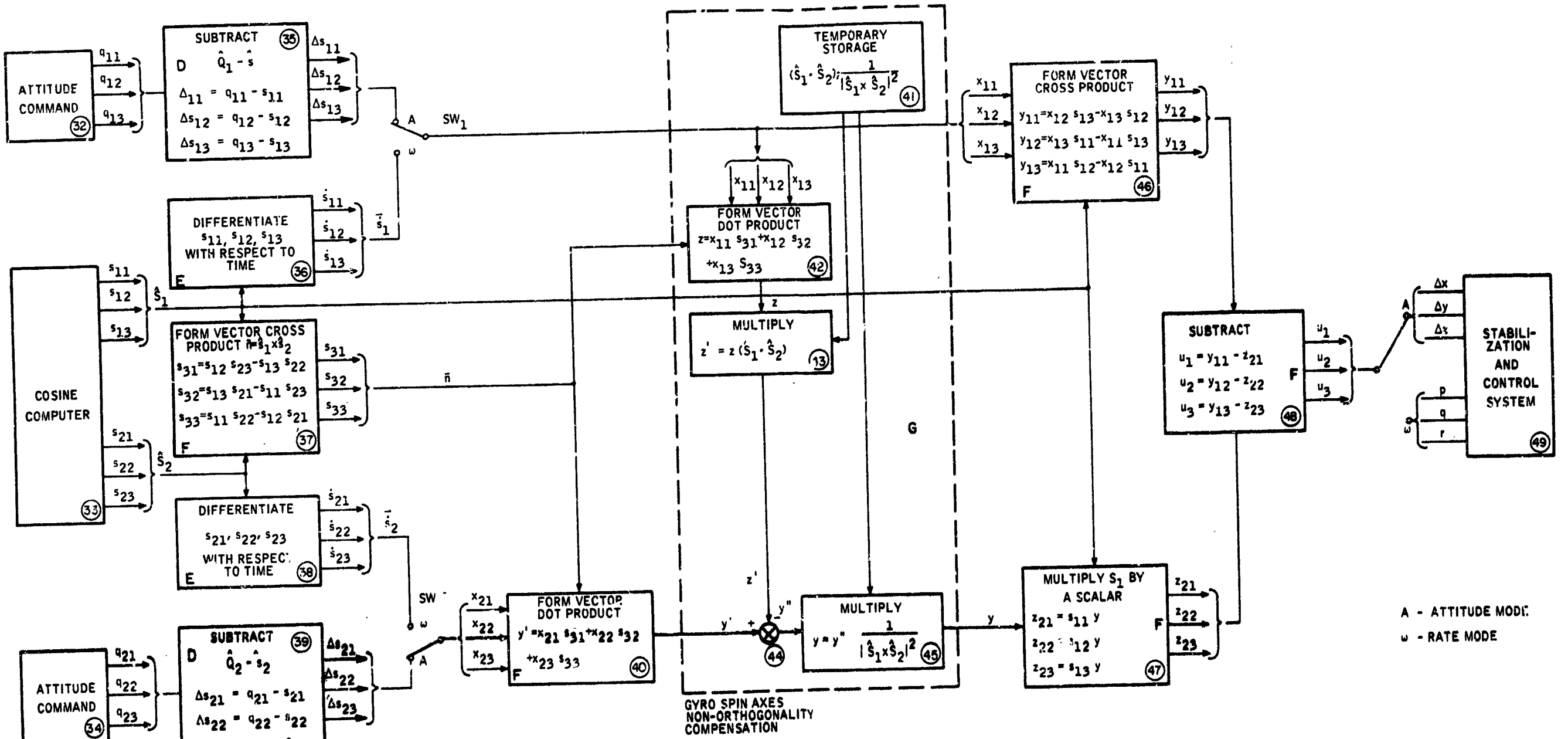

Figure 3-8. Attitude Error and Body Rate Computer Flow Chart

The principal functions of the cosine computer are:

- To compute the spin axis direction cosines relative to the two active pickoffs from which data are obtained.
- To compute the spin axis direction cosine relative to the inactive pickoff axis
- To compute the spin axis direction cosines relative to the vehicle body axes

The computation of the spin axis direction cosines from the outputs of the interface logic is defined by the following equations and indicated in Figure 3-7 in blocks (1) through (7).

$$\alpha_1 = 4 P_1 \left(\frac{1}{T}\right) - 2 \qquad (1)$$

$$\alpha_2 = 4 P_2 \left(\frac{1}{T}\right) - 2 \qquad (2)$$

In Equations (1) and (2), α_1 and α_2 are the direction cosines of the gyro spin vector relative to the axes of the number 1 and 2 pickoffs, respectively. P_1 and P_2 are the partial counts from pickoffs 1 and 2 and T is the total count for the gyro.

The direction cosine of the gyro spin axis relative to the axis of the third pickoff is computed from the following equation:

$$\sqrt{C_2}\,\alpha_3 = -D_2\alpha_1 - B_2\alpha_2 \pm \sqrt{1 - \alpha_2^2 - \left[E_2\alpha_1 \cdot A_2\alpha_2\right]^2} \qquad (3)$$

Equation (3) is derived in Appendix A. In Figure 3-7, blocks (8) through (10) are a graphical representation of the solution of Equation (3) for the third direction cosine, α_3.

If the available partial counts are for two pickoffs other than pickoffs 1 and 2, the equations for calculating direction cosines are of the same form.

The available partial counts may be used in Equations (1) and (2) and corresponding direction cosines will be computed.

If the partial count from pickoff number 1 is not available and if the direction cosine of the spin axis to the number 1 pickoff axis must be computed from direction cosines α_2 and α_3, Equation (3) becomes

$$\sqrt{C_3}\alpha_1 = - D_3\alpha_2 - B_3\alpha_3 \pm \sqrt{1 - \alpha_3^2 - \left[E_3\alpha_2 - A_3\alpha_3^2\right]^2} \qquad (4)$$

and in a similar manner, if α_2 must be computed from α_1 and α_3

$$\sqrt{C_1}\alpha_2 = - D_1\alpha_3 - B_1\alpha_1 \pm \sqrt{1 - \alpha_1^2 - \left[E_1\alpha_3 - A_1\alpha_1\right]^2} \qquad (5)$$

The coefficients for Equations (3), (4) and (5) will be stored and the command that selects the pickoffs to provide the partial counts to Equations (1) and (2) will also select the proper coefficients from storage and the proper program as represented by Equations (3), (4) or (5).

In Figure 3-7, blocks 20 through 31 show the calculations necessary to transform the spin axis direction cosines from the reference frame represented by the axes of the three pickoffs to the vehicle reference frame.

Since the gyros are strapped down in the vehicle, there is a fixed relationship between the pickoff axes and the vehicle reference frame. This relationship can be expressed mathematically by a 3 x 3 matrix whose elements can be determined from measurements made during the installation of the gyros on the vehicle. The transformation of the direction cosines to body coordinates is the product of this alignment matrix and the vector whose components are the direction cosines relative to the pickoff axes.

That is:

$$\begin{bmatrix} s_1 \\ s_2 \\ s_3 \end{bmatrix} = \begin{bmatrix} A_{11} & A_{12} & A_{13} \\ A_{21} & A_{22} & A_{23} \\ A_{31} & A_{32} & A_{33} \end{bmatrix} \cdot \begin{bmatrix} \alpha_1 \\ \alpha_2 \\ \alpha_3 \end{bmatrix}$$

where:

$\hat{S} = (s_1, s_2, s_3)$ = spin vector in body axes

$[A_{ij}]$ = alignment matrix

ATTITUDE ERROR AND BODY RATE COMPUTER

The attitude error and body rate computer's function is to generate digital signals at the computer's output which are suitably related to the vehicle attitude and body rate so that they may drive the vehicle stabilization and control system to produce stable vehicle attitude.

The basis for the attitude error signals generated by the computer is the cross products of the commanded and observed spin vectors in body coordinates. The basis for the body rate signals generated in the computer is the difference between successive observations of the gyro spin vectors.

The computation of the attitude error signal from the outputs of the cosine computer section and the attitude commands supplied to the ARS is defined by the following vector equation:

$$\bar{\theta} = \hat{Q}_1 \times \hat{S}_1 + \frac{1}{/\hat{S}_1 \times \hat{S}_2/^2} \left[\hat{Q}_1 \cdot \hat{S}_1 \times \hat{S}_2 \, (\hat{S}_1 \cdot \hat{S}_2) - \hat{Q}_2 \cdot \hat{S}_1 \times \hat{S}_2\right] \hat{S}_1$$

where:

$\bar{\vartheta}$ = attitude error vector
$\hat{Q}_1$ & $\hat{Q}_2$ = commanded spin vectors
$\hat{S}_1$ & $\hat{S}_2$ = observed spin vectors

The solution of this equation is indicated graphically in Figure 3-8 when switches 1 and 2 are in the position marked A.

The derivation of the attitude error equation is presented later in this section.

The computation of the body rate signal from the observed positions of the gyro spin vectors in body reference axes is defined by the following vector equation:

$$\bar{\omega} = \bar{\dot{S}}_1 \times \hat{S}_1 + \frac{1}{/\hat{S}_1 \times \hat{S}_2/^2} \left[\bar{\dot{S}} \cdot \hat{S}_1 \times \hat{S}_2 \, (\hat{S}_1 \cdot \hat{S}_2) - \bar{\dot{S}} \cdot \hat{S}_1 \times \hat{S}_2 \right] \hat{S}_1$$

where:

$\bar{\omega}$ = body angular velocity vector
$\bar{\dot{S}}_1$ & $\bar{\dot{S}}_2$ = derivatives of $\hat{S}_1$ & $\hat{S}_2$ in body axes

Figure 3-7 is a graphic display of the solution of the above equation when switches 1 and 2 are in position A.

The derivation of the body rate equation is presented later in this section.

It is obvious from the presence of switches 1 and 2 in Figure 3-8 that a large portion of the computation necessary to determine the attitude error signal and the body rate signal is identical. Whether the equipment performing this computation will actually be shared in time between the attitude error and body rate calculations (as implied by the switches) will depend on the system accuracy and performance necessary to the application.

It is anticipated that blocks 36 and 38 in Figure 3-8 will approximate the spin vector derivatives by finite differences between observations of the spin vectors in body axes. The interval between observations will depend on the quality required in the body rate information and may vary between applications.

Blocks 41 through 45 indicate the computations necessary as a result of the gyro spin vectors being non-orthogonal. These computations will be omitted for application that do not require high accuracy, or if the gyros have the facility for making the spin vectors orthogonal.

COMPUTATIONS FOR THE TWELVE SYSTEMS OF THE PARAMETER STUDY

Twelve attitude reference systems were defined for the parameter study of the SDMEG attitude reference system. The systems were defined on the basis of three variations of gyro complexity, two variations of system output and two variations of system accuracy. In order to discuss the computers composed for these independent parameter variations, the following symbols are used:

A. Gyro Complexity
   - A(1) Gyro defined under Contract No. 950607
   - A(2) Gyro with caging capability
   - A(3) Gyro with torquing capability

B. System Outputs

B(1) Three-axes attitude error and body rate

B(2) Three-axes attitude error

C. System Accuracy

C(1) High system accuracy
(Computer error less than 0.01°, a data rate of 100/sec on body rate information, and 10/sec on attitude error information)

C(2) Low system accuracy
(Computer error less than 0.1°, a data rate of 10/sec for body rate and 1/sec on attitude error)

The 12 attitude reference systems may be indicated as follows:

ARS No. 1 =	A(1)	B(1)	C(1)
ARS No. 2 =	A(1)	B(1)	C(2)
ARS No. 3 =	A(1)	B(2)	C(1)
ARS No. 4 =	A(1)	B(2)	C(2)
ARS No. 5 =	A(2)	B(1)	C(1)
ARS No. 6 =	A(2)	B(1)	C(2)
ARS No. 7 =	A(2)	B(2)	C(1)
ARS No. 8 =	A(2)	B(2)	C(2)
ARS No. 9 =	A(3)	B(1)	C(1)
ARS No. 10 =	A(3)	B(1)	C(2)
ARS No. 11 =	A(3)	B(2)	C(1)
ARS No. 12 =	A(3)	B(2)	C(2)

The following discussion defines the functions that must be performed in the cosine computer and attitude error and body rate computer sections of the systems defined above.

These computer definitions serve as the starting point for preliminary design of the ARS computer. The objective of the preliminary computer design is to provide size, weight, power consumption, and relative reliability estimates for the computer portion of the ARS.

ARS No. 1 - A(1) B(1) C(1)

The flow chart of the computer functions for this ARS configuration is shown in Figure 3-7 and 3-8.

Due to accuracy and speed requirements for this configuration the computer design is characterized by the maximum number of functions to be solved. This system is the first to be analyzed in the ARS computer parametric study.

ARS No. 2 - A(1) B(1) C(2)

For this configuration it is assumed that gyro pickoff non-orthogonality, body axes pickoff misalignments and gyro spin axes non-orthogonality do not contribute more than 0.1 degree error at the output.

The computer flow chart is shown in Figures 3-7 and 3-8 with the following modifications:

- The storage of the 30 "C" constants is eliminated and the operations in blocks 9 through 13 become:

  a) Eliminate blocks 9, 11, and 13 since these constants are zero.
  b) The blocks 10 and 12 are unity multipliers.

- The storage of the 18 "A" constants is eliminated and the operations in blocks 20 through 28 become:

  a) Blocks 20, 27, and 25 are unity multipliers.
  b) Blocks 23, 26, 21, 24, 22, 28, have zero constants.

- With the above definition of the "A" constant locations the computer control logic must do the following gating of the direction cosines:

  α_1 is gated to block 20

  α_2 is gated to block 27

  α_3 is gated to block 25

- In figure 3-8 blocks 41, 42 and 43 are eliminated. The information from block 40 to block 47 is transmitted to satisfy the following identity:

  $Y' = Y'' = Y$

ARS No. 3 - A(1) B(2) C(1)

The computer flow chart for this ARS configuration is shown in Figures 3-5 and 3-6 with the following modification:

- In Figure 3-8 only "mode A2" is selected (switch is in the position A)
- The block 36 and 38 are eliminated.

The required computations are essentially the same as for ARS No. 1, however high speed rate computations are not required.

ARS No. 4 - A(1) B(2) C(2)

The computer flow chart for this ARS configuration is shown in Figures 3-7 and 3-8 with the following modifications:

- Incorporate all modifications as in ARS No. 2.
- Incorporate all modifications as in ARS No. 3.

ARS No. 5 - A(2) B(1) C(1)

The computer flow chart for this ARS configuration is shown in Figures 3-7 and 3-8 with the following modifications:

- In Figure 3-8 blocks 41, 42 and 43 are eliminated.
- The information from block 40 to block 47 is transmitted to satisfy the following identity:

$$Y' = Y'' = Y$$

ARS No. 6 - A(2) B(1) C(2)

Due to assumptions introduced for ARS No. 2, ARS No. 6 computer configuration is identical to configuration of the ARS No. 2.

ARS No. 7 - A(2) B(2) C(1)

The computer flow chart is the same as for A(1), B(2), C(1) configuration with the following modification:

- In Figure 3-5 blocks 41, 42, and 43 are eliminated.
- The information for block 40 to block 47 is transmitted to satisfy the following identity:

$$Y' = Y'' = Y$$

ARS No. 8 - A(2) B(2) C(2)

The computer flow chart for this ARS configuration is identical to ARS A(1) B(2) C(2).

ARS No. 9 A(3) B(1) C(1)

It appears at this time that this system configuration will require the same computer capability as ARS No. 5. Additional study of the utility of the precision torquing capability in the gyro may alter this conclusion.

ARS No. 10 A(3) B(1) C(2)

The same comments made under ARS No. 9 also apply to this system and ARS No. 6.

ARS No. 11 A(3) B(2) C(1)

This system configuration will use the same computer capability as ARS No. 7 pending further study of the utility of the precision gyro torquing.

ARS No. 12 A(3) B(2) C(2)

The same comments made under ARS No. 11 also apply to this system and ARS No. 8.

PERFORMANCE ANALYSIS

INTRODUCTION

The SDMEG-ARS performance described in this section contains discussion of the ARS error sources and shows how these errors affect ARS performance in the attitude and rate modes of the ARS operation.

The discussion and evaluation of the error sources is based primarily on the findings arrived at on various SDMEG development programs (e.g., JPL Contract No. 950607, Phases A and B).

SUMMARY

In the ARS parametric study, the ARS configurations were designed on the basis of varying:

- Gyro complexity
  - Gyro defined under Contract No. 950607
  - Gyro with caging capability
  - Gyro with torquing capability
- System outputs
  - Three-axis attitude error and body rate
  - Three-axis attitude error only
- System accuracy
  - High accuracy
  - Low accuracy

For the ARS performance analysis, gyro complexity variation can be disregarded since this variation introduces only second-order error in the performance equations.

From the sole point of view of ARS design, the gyro caging and torquing capability provides the advantage that the gyro spin axes can be maintained in an orthogonal attitude. However, the gyros designed under Contract No. 850607 can be started up so that the non-orthogonality in the spin axes causes only a second-order error in the performance equations. Therefore, the main advantages of the gyro torquing and caging capability is in ARS operational procedures.

The types of system outputs selected are primarily a reflection of computer sampling rate requirements and data filtering requirements for computing body rate. For the ARS performance analysis, this ARS variation means only that the errors must be estimated for both the attitude and rate modes of the ARS. In the estimate of body rate error, the error reduction due to data filters is not included; however, it is pointed out what portion of the total rate error can be subjected to filtering.

The level of system accuracy (high or low) is reflected in ARS design in that the high-accuracy system can compensate for the gyro pickoff axes misalignment and misalignment of the gyro assembly with the vehicle body axes. Therefore, for the ARS performance analysis, the misalignment numbers used for the high-accuracy system are those which reflect state-of-the-art of alignment measurements and stability. The low-accuracy system will reflect the state-of the-art alignment of gyro pickoff axes and alignment to the vehicle body axes.

Consequently, the 12 ARS configurations are grouped for the performance estimate as follows:

- ARS performance in attitude mode

  High accuracy
  Low accuracy

- ARS performance in rate mode

  High accuracy
  Low accuracy

Since the basic function of the ARS is to align or "point" some axis of the spacecraft along a line in space, the attitude performance of the ARS is expressed in terms of the error that could occur in this operation.

In the attitude mode, Table 3-7 gives the vehicle thrust axis alignment uncertainty following a maneuver consisting of initial ARS alignment, vehicle orientation and delta-V thrustings. It is assumed the above maneuver consumes one hour.

Table 3-7. ARS Performance in Attitude Mode

Error Source	Vehicle Pointing Error in Degrees	
	High Accuracy	Low Accuracy
Data Sampling Errors	< 0.004	< 0.004
Readout Errors	0.016	0.016
Alignment Errors	0.006	0.054
Gyro Drift Errors	0.028	0.028
Computer Errors	0.017	0.017
RSS	0.036	0.066

Table 3-8 gives the error in computed body rate in the rate mode. Note that the distinction between high and low accuracy in the ARS rate output is lost in the presence of the high noise level on the gyro readout.

Table 3-8. ARS Performance in Rate Mode

Error Source	Rate Error in Deg/Sec	
	High Accuracy	Low Accuracy
1. Gyro and Readout Noise	2.42	2.42
2. Gyro Drift Rate	0.036	0.036
3. All ARS errors not including 1 and 2 above	0.005	0.017
RSS	2.42	2.42

DISCUSSION OF ERROR SOURCES

Summary

The SDMEG-ARS error sources arise from SDMEG imperfections, ARS misalignments and data processing of the gyro readouts. These error sources can be classified into four groups:

- SDMEG errors
- Physical misalignments or uncertainties in alignment measurements
- Data sampling errors
- Computer errors

The SDMEG errors include the gyro drift mechanizism and the errors in the readout mechanization whose output are the shaped pulses used for gating the counters in the I/O logic of the ARS mechanization. These errors have been extensively analyzed and evaluated by test under various SDMEG development programs (e.g., JPL Contract No. 950607). This discussion will include general description and evaluation of the SDMEG errors per the SDMEG development findings.

The ARS errors due to misalignments deal with the relative alignment among pickoff axes, the two-gyro spin axes non-orthogonality and the alignment of the gyro assembly with the vehicle body axes. Depending on the configuration, the ARS performance will be affected in two ways by the alignment errors. In the low accuracy ARS configuration the ARS performance will be limited by the state of the art of physical alignments without the computer provisions to compensate for the misalignment errors. In the high accuracy ARS configuration ARS performance will be limited by the measurement uncertainties of the misalignments. The computer will compensate for the misalignments to a degree of their measurement uncertainty.

The data sampling errors result from finite sampling rate and time sharing of the equipment used to read the gyros. The magnitude of the data sampling error is the function of SDMEG rotor speed, counting rate of the counters and the vehicle rate. These errors can be minimized by the computer capability and will be equal to zero for the case of no vehicle motion.

The computer errors, by definition in this study, are only the roundoff (word length), and algorithm errors. The system errors which logically could be classifed as computer errors (e.g., pulse shaping, etc.) are treated as SDMEG errors or data sampling errors.

The summary of error sources and the corresponding error magnitudes are shown in Table 3-9. Detailed discussion of the error sources can be found in the remainder of this section.

SDMEG Errors

The SDMEG errors are attributed to gyro drift and the SDMEG readout errors. Both of these types are discussed below.

Gyro Drift -- Drift estimates used in the SDMEG-ARS performance study are based on an analysis published in Honeywell Report 1726-FR1 (15 April 1964).

The assumed SDMEG parameters are:

Size (OD of rotor)	2 inches
Maximum electric field	990v/mil (nigh power) 170 v/mil (low power)
Rotor-to-electrode gap	0.0015 inch
Average rotor wall thickness	0.055 inch
Rotor mass	20 gm
Rotor inertia	90 gm-cm^2
Acceleration capability	30 g (high power) 1 g (low power)
Operational rotor speed	100-200 rev/sec

Table 3-9. ARS Error Sources
(ARS Error Model is Shown in Figure 3-15)

SDMEG-ARS Error Sources	Error in Direction Cosine	Alignment Errors (RAD)	Spin Axis* Attitude Error Vector (RAD)	Spin Axis** Rate Error Vector (RAD/Sec)	Body Rate RAD/Sec
Gyro Drift					
• Axial Mass Unbalance			$\lvert\delta\bar{s}_{MD}\rvert$ 0.000006	$\lvert\delta\bar{s}_{\mu}\rvert$ 0	
• Electric Torque			$\lvert\delta\bar{s}_{ED}\rvert$ 0.000424	$\lvert\delta\bar{s}_{E}\rvert$ 0.00042	
• Magnetic Field Torque			$\lvert\delta\bar{s}_{\mu D}\rvert$ 0.000005	$\lvert\delta\bar{s}_{M}\rvert$ 0.000005	
Readout Errors					
• Spin Axis Uncertainty	$\delta\alpha_s$ 0.0000325			$\lvert\delta\bar{s}_{N}\rvert$ 0.0345	
• Noise Error	$\delta\alpha_N$ 0.000141				
• Trigger Uncertainty	$\delta\alpha_T$ 0.0000108				
• Pattern Uncertainty	$\delta\alpha_p$ 0.0000858				
• Rise Time	$\delta\alpha_{RT}$ 0.0000034				
Alignment Errors					
• Pickoff Alignments		$\delta\theta_a$ 0.0006 0.000064			
• Gyro to Vehicle Alignment		ρ_a 0.0006 0.000064			
• Gyro Spin Axis Non-orthogonality		0.00244			
Data Sampling Errors	$\delta\alpha'$				
• Due to Readout Equation	$< 10^{-5}$				
• Synchronization Error	< 0.00004				
Computer Errors			$\delta\bar{s}_c$ 0.000302		$\delta\bar{\omega}_c$ 0.00008

*Calculated for ARS alignment, vehicle orientation and delta-V thrusting (10,000 ft/sec at 1/2 g) assuming 1 hour for maneuver completion.

**Calculated for 30-g gyro capability in o-g space environment.

For this gyro, 1726-FR1 gives the following one-sigma drift functions:

- Axial mass unbalance ($|\dot{\bar{\delta S}}_\mu|$) drift rate in deg/hr

$$\left|\dot{\bar{\delta S}}_\mu\right| = 0.0042\ a\left(\frac{200}{f}\right)$$

- Electric torque ($|\dot{\bar{\delta S}}_\epsilon|$) drift rate in deg/hr

$$\left|\dot{\bar{\delta S}}_\epsilon\right|^2 = \left\{0.024\left(\frac{a_o}{30}\right)\left[1+\left(\frac{a}{a_o}\right)^2\right]\left(\frac{f}{200}\right)\right\}^2 + \left\{0.262\left(\frac{a}{a_o}\right)a\left(\frac{f}{200}\right)\right\}^2 + \left\{0.056\left(\frac{a}{a_o}\right)a\left(\frac{f}{200}\right)\right\}^2$$

- Magnetic torque ($\dot{\bar{\delta S}}_M$) drift rate in deg/hr

$$\left|\dot{\bar{\delta S}}_M\right| = 0.00028\left(\frac{B}{0.01}\right)^2$$

where

a = vehicle acceleration in g's

a_o = SDMEG acceleration capability in g's

f = rotor speed in rev/sec

B = magnetic field in gauss

$\dot{\bar{\delta S}}$ = rate of change of gyro spin vector in inertial space

To evaluate these drift functions, some assumptions must be made about the vehicle acceleration profile, the mode of SDMEG operation (high- or low-power mode), the rotor speed, and the magnetic field which exists at the SDMEG rotor.

In general, the vehicle and the ARS can be in three different modes of operation:

- Mode 1 -- Cruise:

  Vehicle accelerations at zero; control jet pulsing to maintain a prescribed limit cycle can be neglected

  SDMEG operating in a low power mode, $a_o = 1$ g

  SDMEG rotor speed at 200 rev/sec, f = 200

  Magnetic fields at the rotor are due only to residual fields after SDMEG degaussing, hence B = 0.01

- Mode 2 -- Midcourse delta-V corrections, consisting of the ARS alignment mode, vehicle reorientation and delta-V thrusting mode:

  During the delta-V thrusting the vehicle acceleration may be about 1/4 g to impart a delta-V of 70 ft/sec

  SDMEG operating in the high-power mode, $a_o = 30$ g's

  SDMEG speed at 200 rev/sec, f = 200

  Magnetic field at 0.01 gauss, B = 0.01

- Mode 3 -- Delta-V correction to orbit consisting of the ARS alignment mode, vehicle reorientation and delta-V thrusting:

  During the delta-V correction the vehicle acceleration may be at an average of 0.5 g's to impart a delta-V of 7,000-10,000 ft/sec

  SDMEG operating in the high-power mode, $a_o = 30$ g's

  SDMEG speed at 200 rev/sec, f = 200

  Magnetic field at 0.01 gauss, B = 0.01

It can be assumed that Modes 2 and 3 may take up to two hours for execution, including the two reorientations and thrusting. Therefore, the one-sigma gyro drift equations for the cruise mode are:

$$\left|\delta\dot{\bar{S}}_{\mu}\right| = 0$$

$$\left|\delta\dot{\bar{S}}_{\epsilon}\right| = 0.0008 \text{ deg/hr} = 1.4 \times 10^{-5} \text{ rad/sec}$$

$$\left|\delta\dot{\bar{S}}_{M}\right| = 0.00028 \text{ deg/hr} = 0.49 \times 10^{-5} \text{ rad/sec}$$

and, the RSS gyro drift rate during cruise is

$$\sqrt{\left|\delta\dot{\bar{S}}_{\mu}\right|^2 + \left|\delta\dot{\bar{S}}_{\epsilon}\right|^2 + \left|\delta\dot{\bar{S}}_{M}\right|^2} = 0.00084 \text{ deg/hr} = 1.5 \times 10^{-5} \text{ rad/sec}$$

During ARS alignment and the reorientation maneuver gyro drift rates are

$$\left|\delta\dot{\bar{S}}_{\mu}\right| = 0$$

$$\left|\delta\dot{\bar{S}}_{\epsilon}\right| = 0.024 \text{ deg/hr} = 42 \times 10^{-5} \text{ rad/sec}$$

$$\left|\delta\dot{\bar{S}}_{M}\right| = 0.00028 \text{ deg/hr} = 0.49 \times 10^{-5} \text{ rad/sec}$$

$$\text{RSS} = 0.0242 \text{ deg/hr} = 42.2 \times 10^{-5} \text{ rad/sec}$$

The RSS value of 0.0242 deg/hr for gyro drift occurring during the ARS alignment and the vehicle reorientation maneuver are used as estimated gyro drift in the ARS performance equations.

During the delta-V thrusting at 1/4 g, gyro drift equations are

$$\left|\dot{\bar{\delta S}}_{\mu}\right| = 0.0010 \text{ deg/hr}$$

$$\left|\dot{\bar{\delta S}}_{\epsilon}\right| = \sqrt{(0.024)^2 + (0.00054)^2 + (0.000118)^2} = 0.024 \text{ deg/hr}$$

$$\left|\dot{\bar{\delta S}}_{M}\right| = 0.00028 \text{ deg/hr}$$

$$\text{RSS} = 0.024 \text{ deg/hr} = 42 \times 10^{-5} \text{ rad/sec}$$

During delta-V thrusting at 1/2 g, gyro drift equations are

$$\left|\dot{\bar{\delta S}}_{\mu}\right| = 0.0021 \text{ deg/hr}$$

$$\left|\dot{\bar{\delta S}}_{\epsilon}\right| = \sqrt{(0.0242)^2 + (0.00218)^2 + (0.00047)^2} = 0.0242 \text{ deg/hr}$$

$$\left|\dot{\bar{\delta S}}_{M}\right| = 0.00028 \text{ deg/hr}$$

$$\text{RSS} = 0.0244 \text{ deg/hr} = 42.5 \times 10^{-5} \text{ rad/sec}$$

Assume that the midcourse delta-V correction consumes one hour to align the ARS and to orient for delta-V correction. The time taken for thrusting is

$$\frac{70}{3600 \left(\frac{1}{4}\right) 32.2} = 0.00242 \text{ hr}$$

Therefore, the gyro error at the end of the delta-V thrusting is

$$(0.0242 \times 1) + 0.024 \times 0.00242 = 0.0242 + 0.000058$$
$$= 0.0243 \text{ degree}$$
$$= 4.24 \times 10^{-4} \text{ radians}$$

Assuming one hour for the ARS alignment and orientation for the delta-V correction for an orbit injection, the gyro error at the end of delta-V thrusting is

$$0.0042 \times 1 + 0.0244 \times \frac{10,000}{3600 \left[\frac{1}{2}\right] 32.2}$$

$$= 0.0242 + 0.00424 = 0.0284 \text{ degree}$$

$$= 4.96 \times 10^{-4} \text{ radians}$$

The attitude error due to gyro drift of 0.0284 degree as estimated above will be used in the ARS performance equations.

Readout Errors -- The SDMEG readout errors are:

- Spin axis uncertainty $\delta\alpha_S$
- Signal noise, rotor noise and counter error $\delta\alpha_N$
- Trigger uncertainty $\delta\alpha_T$
- Pattern uncertainty $\delta\alpha_P$
- Rise time $\delta\alpha_{RT}$

Numerical estimates of the readout errors for the SDMEG-ARS are based on the analysis and development of the SDMEG component in Phases IA and IB. In Phase IB, one of the major tasks included breadboarding of the SDMEG readout logic to be used for the checkout of the readout performance.

Spin Axis and Pattern Uncertainty -- Patterning the SDMEG rotor involves determination of the preferred inertia axis about which the rotor will exhibit a stable spin. After the spin axis is determined, the rotor pattern can be applied relative to this axis so as to satisfy a suitable mathematical relationship between the rotor polar coordinate angles. The mathematical relationship between the polar

coordinates of the rotor provides the means of reading out the spin axis orientation relative to the gyro case.

The errors attributed to the patterning process will result from:

- Inability to specify exactly the spin axis location in the rotor (spin axis uncertainty)
- Pattern line deviation from a mathematical configuration (pattern uncertainty)

The corresponding direction cosine errors of the SDMEG readout have been estimated as:

$\delta\alpha_S$ = 0.0000325 (1σ) - spin axis uncertainty

$\delta\alpha_P$ = 0.0000855 (1σ) - pattern uncertainty

The $\delta\alpha_S$ and $\delta\alpha_P$ errors can be classified as systematic errors, meaning that they are either bias or slowly varying errors with the angle between spin axis and a pickoff axis.

Noise Error -- Noise errors arise from three sources:

- Signal noise, described by the signal-to-noise ratio of the readout
- Rotor noise, resulting from microscopic deviations of the pattern line
- Counter uncertainty

The readout scatter caused by these errors will occur at the frequency of the computer sampling rate; therefore, these errors will contribute to the uncertainty in the derived body rate signal.

During the Phase IB, all three noise errors were experimentally determined, and these findings are being used in the SDMEG-ARS performance analysis. The one-sigma values of these errors are:

- Direction cosine error due to signal noise = 0.0000917 (1σ)
- Direction cosine error due to rotor noise = 0.000033 (1σ)

The counter error is attributed only to uncertainty of the last count. Therefore, the contents of the counter will be in error by a maximum of one count. However, if a uniform distribution for this error is assumed, it can be shown that the one-sigma of the uniform distribution will be $\frac{1}{\sqrt{3}}$ of one count unit.

The counter error of $\frac{1}{\sqrt{3}}$ of one count unit can be converted to the corresponding error in the readout direction cosine as follows:

The SDMEG readout mechanization equation is:

$$\alpha = 4\frac{P}{T} - 2 \quad \text{(see system equations)}$$

where

α = readout direction cosine
P = partial count
T = total count

From the above, the error in α due to errors in P and T is:

$$(\delta\alpha)^2 = \left(\frac{4}{T}\right)^2 (\delta P)^2 + \left(\frac{4}{T}\right)^2 \left(\frac{P}{T}\right)^2 (\delta T)^2$$

If a 5-mc counter and 200 rev/sec for the rotor speed is assumed, then

$$T = \frac{5 \times 10^6}{200} = 2.5 \times 10^4 \text{ counts/rev}$$

Due to rotor pattern geometry

$$0.31 \leq P/T \leq 0.69$$

Therefore, let $(P/T) = 0.50$.

If $\delta P = \delta T$, then

$$(\delta\alpha)^2 = (4/T)^2 \ (\delta P)^2 \ 1.25$$

or

$$\delta\alpha = (4/T) \ \delta P \ (1.12)$$

$$= \frac{4}{2.5 \times 10^4} \frac{1}{\sqrt{3}} (1.12) = 1.03 \times 10^{-4}$$

Therefore, the RSS $(\delta\alpha_N)$ of the three noise errors is

$$\delta\alpha_N = \sqrt{(0.917)^2 + (0.33)^2 + (1.03)^2} \times 10^{-4} = 1.41 \times 10^{-4}$$

Since the direction cosine rate is computed in the SDMEG-ARS by forming direction cosine differences between direction cosine values on successive computer cycles,

$$\left(\dot{\delta\alpha}_N\right)_K = \frac{\pm\left|\delta\alpha_N\right|_K - \left[\pm\left|\delta\alpha_N\right|_{K-1}\right]}{\Delta t}$$

If it is assumed that $\left|\delta\alpha_N\right|_K$ and $\left|\delta\alpha_N\right|_{K-1}$ are statistically independent and have normal distributions, then

$$\sigma_{\dot{\delta\alpha}_N}{}^2 = \sigma_{\delta\alpha_{NK}}{}^2 + \sigma^2_{\delta\alpha_{N(K-1)}} = 2 \ \sigma_{\delta\alpha_N}{}^2$$

Therefore,

$$\left|\delta\dot{\alpha}_N\right|_K = \delta\alpha_N \frac{\sqrt{2}}{\Delta t} = \frac{1.41 \times 10^{-4}}{0.01}\sqrt{2} = 0.020 \text{ rad/sec}$$
$$= 1.14 \text{ deg/sec}$$

where Δt = time interval for one computer cycle.

If $\left|\delta\bar{\dot{S}}_N\right|$ is the error in the magnitude of the gyro spin axis rate due to readout noise

then

$$\left|\delta\bar{\dot{S}}_N\right| = \sqrt{3}\ \delta\dot{\alpha}_N = \sqrt{3}\ 0.02 = 0.0345 \text{ rad/sec}$$
$$= 1.975 \text{ deg/sec}$$

Error in Counter Triggering Logic -- The error which will introduce an uncertainty when the counters are started and stopped can be attributed to the following sources:

- Reflectance variation
- Rise time
- Triggering uncertainty
- Illumination variation and field-of-view irregularity

In general, the readout electronics which provide the stop and start pulses to the counters accomplish the functions of pulse discrimination, pulse shaping and gating of the train of pulses into the stop and start pulses for the counters. Consequently, the particular main circuit sections are: the pulse-width discriminator (PWD); height-insensitive trigger (HIT); and start-stop gating.

Consider a general pulse (Figure 3-9) occurring at the preamplifier output of a pickoff.

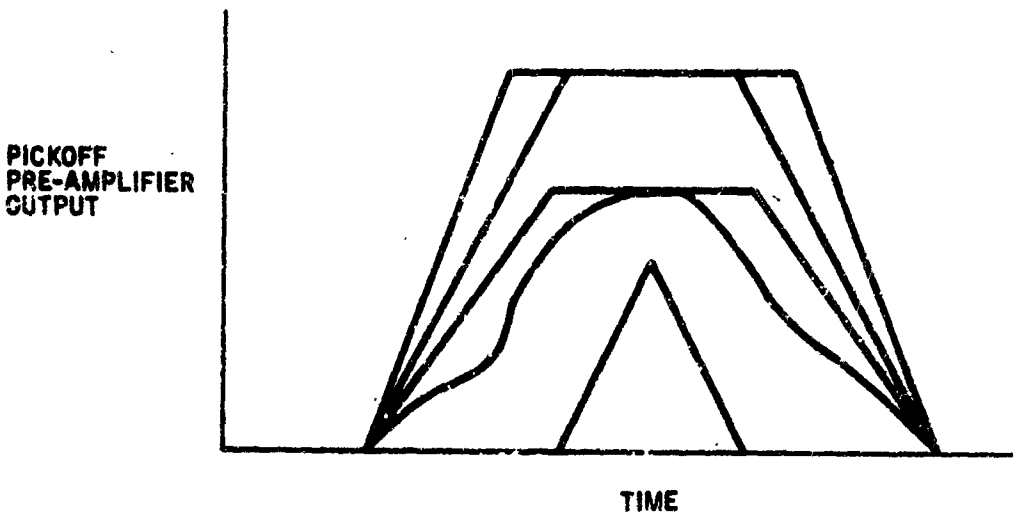

Figure 3-9. Pulse Shape from a Pickoff Preamplifier

In Figure 3-9 five different pulse shapes are shown which differ from one another either in height, slop (rise time), pulse width, or irregular slope of the pulse. These pulse shapes are attributed to reflectance variation and changes in pickoff lamp output, response time (rise time) of the pickoff, illumination variation, and field-of-view irregularity. The fact that the rotor surface has arc marks may produce pulses. These pulses, however, will exhibit much smaller pulse widths than the pulses due to pattern lines.

Since any pulse shape in Figure 3-9 may occur at the gyro readout, the readout electronics must interpret the pulses as to minimize the time errors when commanding the counters to stop and start.

The pulse-width discriminator (PWD) circuit compares the widths of all pulses to a fixed percentage of the gyro rotor period. If the input pulse is narrower than the fixed percentage of rotor period, the PWD has no output. Thus, the noise pulses due to rotor arc marks are eliminated.

Since the electronic trigger circuits are voltage-sensitive, a HIT circuit is used which enables the trigger device to be sensitive to a fixed percentage of pulse height rather than to a fixed voltage. The test results of this circuit indicate a large degree of error compensation due to reflection and trigger level variation. With the electronics as described, the readout errors were evaluated by controlled experiments to evaluate:

- Trigger uncertainty ($\delta\alpha'_T$)
- Reflectance and rise time variation ($\delta\alpha_{RT}$)
- Illumination and field-of-view irregularity ($\delta\alpha''_T$)

The one-sigma error values in the direction cosines were determined to be:

$$\delta\alpha'_T = 0.0000034$$

$$\delta\alpha''_T = 0.0000100$$

$$\delta\alpha_{RT} = 0.0000034$$

Therefore,

$$\delta\alpha_T = 10^{-4} \times \sqrt{(0.034)^2 + (0.1)^2} = 0.0000105$$

and

$$\delta\alpha_{RT} = 0.0000034$$

Alignment Errors

Pickoff Alignments -- The routine physical alignment of the pickoff axes will result in a misalignment of 2 arc minutes per alignment. The misalignments can be measured to an accuracy of 10 seconds of arc.

The aligned pickoff assembly was subjected to an environmental test. Following the exposure to the shock, vibration and temperature environments the pickoff alignments remained constant within 3 arc seconds.

The environmental test was as follows:

Temperature cycling	140 to 170° for 3 hours
Shock	±200 g's with rise time of 1.5 milliseconds
Vibration	
White noise, 28 g-rms, 15-2000 cps, for 18 seconds	
White noise, 10 g-rms, 15-2000 cps plus 4 g-rms sinusoid between 15 and 40 cps	
White noise, 10 g-rms, 15-2000 cps plus 18 g-rms sinusoid between 40-2000 cps. The frequency of the sinusoid is swept from 40 to 2000 and back to 15 cps in a total time of 10 minutes at a rate proportional to frequency.	

Each gyro has three pickoff axes arranged in an orthogonal orientation with respect to each other. However, due to the above mentioned misalignments they will differ from the orthogonal orientation.

If $\delta\theta_a$ is the non-orthogonality between any two axes, then

$$\delta\theta_a = \sqrt{(120)^2 + (8)^2} = 120 \text{ arc-seconds}$$
$$= 6 \times 10^{-4} \text{ radians}$$

The measurement uncertainty in the $\delta\theta_e$ is

$$\sqrt{(10)^2 + (8)^2} = 12.8 \text{ arc-seconds}$$
$$= \text{ 4 x } 10^{-5} \text{ radians}$$

Therefore, in the ARS Computer designs which have provisions for misalignment compensation, 6.4×10^{-5} rad pickoff misalignment will be used in the ARS performance estimate. In the computer which has no misalignment compensation the misalignment is 6×10^{-4} rad.

Gyro Alignment to Vehicle Axes -- Assume that it is desired to align the three orthogonal pickoff axes with the vehicle body axes. The misalignment between the two sets of axes can be defined by three Euler rotations through small misalignment angles which can be expressed in a matrix equation as follows:

$$\begin{bmatrix} 1 & \rho_3 & -\rho_2 \\ -\rho_3 & 1 & \rho_1 \\ \rho_2 & -\rho_1 & 1 \end{bmatrix}$$

The ρ_1, ρ_2, and ρ_3 are the small Euler rotations.

For the error analysis it will be assumed that $\rho_1 = \rho_2 = \rho_3 = \rho_a$. Furthermore, it is assumed that the physical alignment can be accomplished to $\rho_a = 6 \times 10^{-4}$ rad. and this misalignment can be measured to an accuracy of 6.4×10^{-5} rad.

Gyro Spin Axis Non-Orthogonality -- An all-attitude ARS requires that its two attitude sensor-sensitive axes subtend an angle which is approximately equal to 90 degrees. One or two co-linear vectors can define only two degrees of attitude freedom. Reasonable deviations from orthogonality can be accounted for in the ARS mechanization. However, since some ARS designs in the present study do not have the provisions to compensate for the gyro spin axis non-orthogonality, errors will result.

During the SDMEG development program (JPL Contract No. 950607) spin-vector caging repeatability was determined to be within 0.10 degrees. The results of this test can be found in the Honeywell final report (1726-FR1 April 15, 1964) to the JPL.

Therefore, for error analysis purpose, it will be assumed that the gyro spin axis non-orthogonality will be within 0.14 degrees.

Data Sampling Errors

The data sampling errors result from finite sampling rate and time sharing of the equipment used to read the gyros. The gyro readout concept uses the relative motion of the gyro rotor and the case, and from this information deduces the spin vector attitude with respect to gyro case. Using this readout concept the readout will be in error due to vehicle motion.

Therefore, the following discussion is presented to describe the errors due to vehicle motion and equipment time sharing in terms of the chosen SDMEG readout mechanization.

SDMEG Readout Mechanization -- Figure 3-10 illustrates the rotor pattern geometry involved in readout of the spin vector direction cosines. The locus of points occupied by the rotor pattern is given by:

$$\cos\theta = 2\left(1 - \frac{\phi}{\pi}\right) \qquad (6)$$

where θ and ϕ are the angular coordinates of a point on the curved pattern.

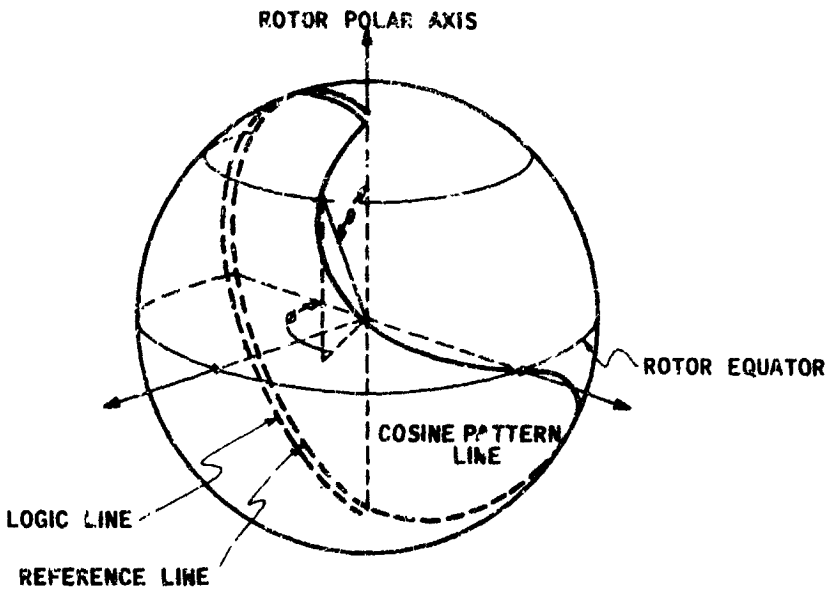

Figure 3-10. Modified Cosine Pattern

Figure 3-11 illustrates what might be a typical traversal over the rotor surface by one of the pickoffs due to vehicle angular motion. In terms of the angles ϕ_1 and ϕ_2, which are measured in the constant latitude plane and are shown in Figure 3-11, the readout equation is:

$$\cos\theta = \frac{4\phi_1}{\phi_1+\phi_2} - 2 = \frac{2(\phi_1 - \phi_2)}{\phi_1 + \phi_2} = \frac{2(2\pi - 2\phi_2)}{2\pi} = 2\left(1 - \frac{\phi_2}{\pi}\right) \qquad (7)$$

The readout logic deduces the angles ϕ_1 and ϕ_2. High speed counters, if gated by the pulses emitted from the pickoffs, will accumulate counts which will be proportional to the angles ϕ_1 and ϕ_2.

Figure 3-12 illustrates a sequence of pulses emitted and what the counters measure. The illustration is for a four-counter I/O interface logic and typical for one pickoff readout.

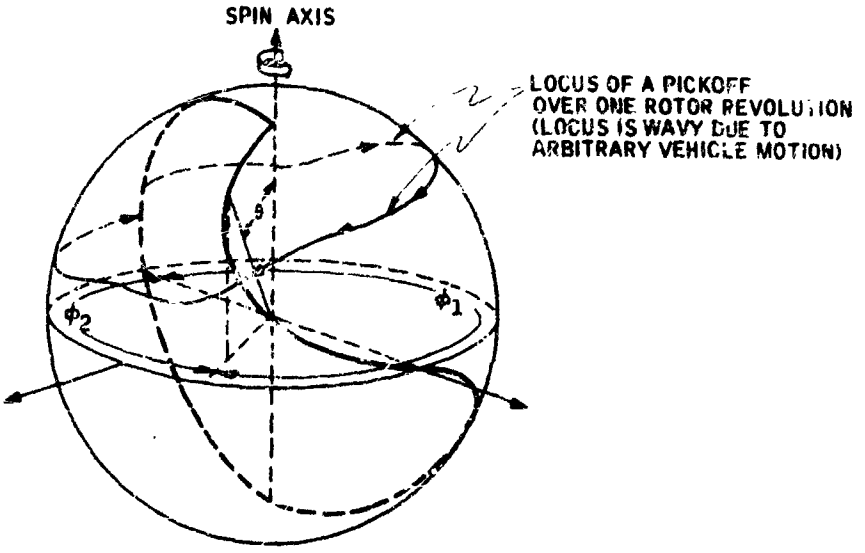

Figure 3-11. Locus of Pickoff Under Arbitrary Vehicle Motion

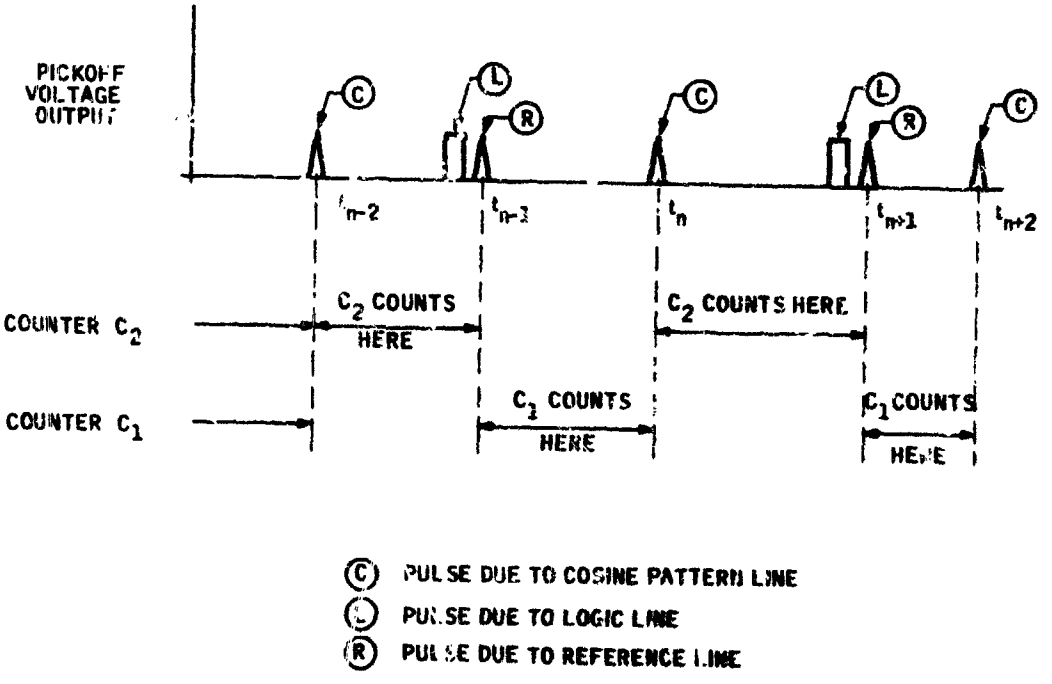

Figure 3-12. Counter Timing

The counter C_1 value is:

$$\begin{aligned} C_1(t_n) &= f(t_n - t_{n-1}) \\ C_1(t_{n+2}) &= f(t_{n+2} - t_{n+1}) \end{aligned} \tag{8}$$

The counter C_2 value is:

$$\begin{aligned} C_2(t_{n-1}) &= f(t_{n-1} - t_{n-2}) \\ C_2(t_{n+1}) &= f(t_{n+1} - t_n) \end{aligned} \tag{9}$$

where f is a fixed count frequency in pulses per second.

Hence, the value of the cos θ at the discrete time t_n of cosine line crossing is:

$$\cos\theta(t_n) = \frac{4C_1(t_n)}{C_1(t_n) + C_2(t_{n+1})} - 2 = \frac{4\phi_1(t_n)}{\phi_1 + \phi_2} - 2$$

$$= \frac{4f(t_n - t_{n-1})}{f(t_n - t_{n-1}) + f(t_{n+1} - t_n)} - 2 \tag{10}$$

$$= \frac{4(t_n - t_{n-1})}{(t_{n+1} - t_{n-1})}$$

Note that if there is no vehicle motion the cos θ value as computed from the counts in Equation 10 is exact. However, if the vehicle has an arbitrary motion the readout will, in general, be in error.

A possible wavy locus of a pickoff due to an arbitrary vehicle motion is illustrated in Figure 3-11. The above discussion of the readout equation may have implied that the locus must close and remain at a constant latitude while the data is accumulating to be used in the readout equation. However, upon further analysis of the problem it can be deduced that the non-closing and non-constant latitude locii do not necessarily decrement the validity of the readout equation.

The wavy locus results from the vehicle angular rates and accelerations about the gyro spin axis and about directions which are perpendicular to the gyro spin axis.

It will first be shown that any angular rate (less than 13 rev/sec) or acceleration about any axis of rotation which is perpendicular to the gyro spin axis does not introduce an error in the readout equation. It will then be shown how the angular accelerations about the spin axis result in the readout error. The constant rate about the spin axis does not introduce any errors in the readout.

Although the vehicle motion about an axis perpendicular to the spin axis does not introduce an error in the readout equation an error may result due to insufficiently accurate computer mechanization. Since three pickoffs "read" the spin vector direction cosines at different times, unless this is properly interpreted, this can result in dynamic errors in the determination of the direction cosine matrix. Because of this, the timing of the direction cosine readout must be synchronized against the computer computational time base. In the present computer design for the SDMEG-ARS the synchronization is neglected; therefore, the ARS will suffer from the synchronization error among the six readouts of the two gyros. However, it can be shown that for a realistic vehicle motion these errors are considerably smaller than the other ARS errors; therefore, lack of computer capability to account for the synchronization errors is justified.

Error From Vehicle Motion Normal to Spin Axis -- In interpreting what happens to the gyro readout when the vehicle motion is perpendicular gyro spin axis refer to Figure 3-13, below.

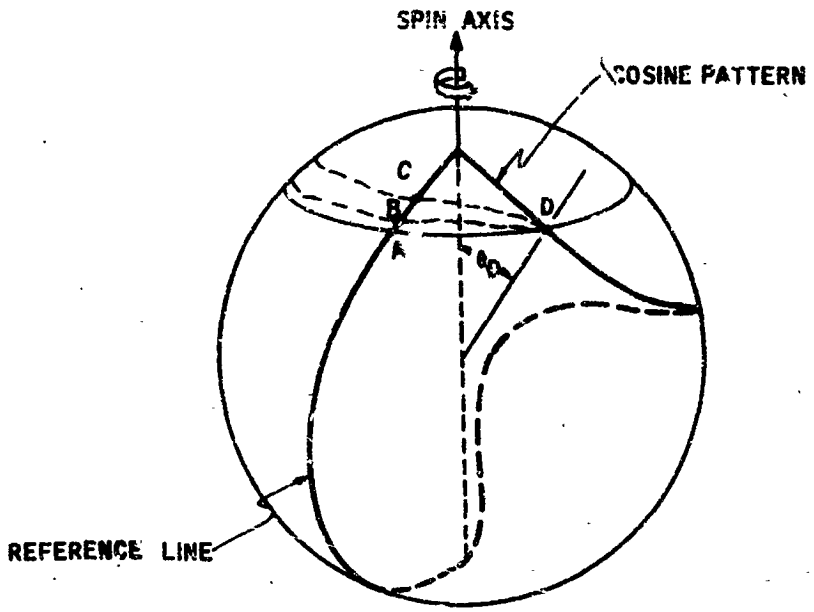

Figure 3-13. Pickoff Locus Under Vehicle Motion

First assume that a counter is counting from a pulse due to reference line to a pulse due to reference line when it passes under the pickoff again. The contents of the counter will be the total count (T). Since the reference line is the Great Circle which contains the gyro spin axis it is obvious that the pickoff motion (vehicle motion) perpendicular to the gyro spin axis will not affect the total count T.

Investigate paths AD, BD, and CD and conclude that it takes the same amount of time for the pickoff to traverse these distances provided, of course, that the case rate does not change about the spin axis.

The cos θ_D for no vehicle motion is:

$$\cos \theta_D = \frac{4C_{AD}}{T} - 2 \qquad C_{AD} = \text{count on path AD}$$

If the vehicle is moving and pickoff goes through point D, then the direction cosine of the spin axis is cos θ_D at the time when pickoff passes through D. If the pickoff paths were BD or CD, then the direction cosine at the point D is:

$$\cos \theta_D = \frac{4C_{AD}}{T} - 2 = \frac{4C_{BD}}{T} - 2 = \frac{4C_{CD}}{T} - 2$$

$$\text{Since} \quad = C_{AD} = C_{BD} = C_{CD}$$

Therefore, using the proposed readout equation and synchronizing the readout with the time when the pickoff crosses the cosine pattern the direction cosine can be determined exactly under the vehicle motion if it is perpendicular to the gyro spin axis.

Error From Vehicle Motion About the Spin Axis -- The gyro readout is based on the relative motion of the gyro case and rotor about the gyro spin axis. If the relative rate is a constant, there will be no error due to the readout equation. Angular accelerations in the relative rate will result in readout error. However, due to relatively small angular accelerations of the vehicle these errors can be neglected. The order of magnitude for the readout error due to acceleration can be obtained as follows:

$$C\,\theta(t_n) = \frac{4\phi_1(t_n)}{2\pi} - 2 \qquad \text{(see Equation 10)}$$

and the differential of cos $\theta(t_n)$ is:

$$\Delta \left[\cos \theta(t_n)\right] = \frac{2\delta \phi_1(t_n)}{\pi}$$

If the average vehicle acceleration during the time interval $t_n - t_{n-1}$ is $\dot{W}(t_n)$ then:

$$\delta\phi_1(t_n) = \frac{\dot{W}(t_n)\left[t_n - t_{n-1}\right]^2}{2}$$

Then the error in readout is:

$$\Delta \left[\cos \theta(t_n)\right] = \frac{\dot{W}(t_n)\left[t_n - t_{n-1}\right]^2}{\pi}$$

assume that

$$\dot{W}(t_n) = 1 \text{ RAD/sec}^2$$

$$(t_n - t_{n-1}) = \frac{1}{200} \text{ sec} \quad \text{(200 RPS rotor speed)}$$

Then the error in the readout equation due to the vehicle acceleration of 1 RAD/sec^2 is:

$$\Delta\left[\cos \theta(t_n)\right] = (1)\left[\frac{1}{200}\right]^2 \frac{1}{\pi} \cong \frac{2}{5} \times 10^{-5}$$

Synchronization Error -- The previous section described the readout mechanism and it was shown that vehicle angular motion does not appreciably affect the readout accuracy. However, the three pickoffs in general "read" the spin vector direction cosines at different times and, unless this is properly interpreted, can result in dynamic error. In the present computer design for the SDMEG-ARS the readout synchronization is neglected for the 1, 2, 3, 4, and 6 counter mechanizations.

The worst synchronization error will result if the I/O logic is using only one counter, and it can be shown that the error for this mechanization is on the order of 0.00075 deg. if the vehicle limit cycle rate is at 0.1 deg/sec. The one counter timing is illustrated in Figure 3-14.

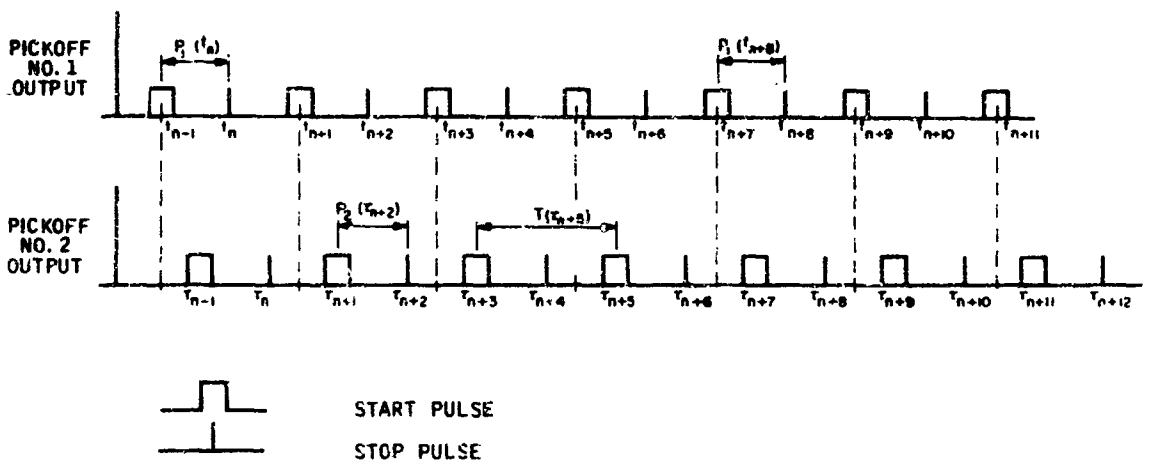

Figure 3-14. One Counter Timing

From Figure 3-14 the readout equations may be written as:

$$\alpha_1(t_n) = \frac{4P_1(t_n)}{T(\tau_{n+5})} \quad -2$$

$$\alpha_2(\tau_{n+2}) = \frac{4P_2(\tau_{n+2})}{T(\tau_{n+5})} \quad -2$$

The errors in partial (P) and total count (T) due to vehicle motion during time intervals $t_n - t_{n-1}$; $\tau_{n+2} - \tau_{n+1}$; and $\tau_{n+5} - \tau_{n+3}$ can be neglected as determined in the previous sections.

Assuming rates of 0.1 deg/sec. and 200 rev/sec. for the vehicle and the rotor, respectively, then $\alpha_1(t_n)$ is out of synchronism with $\alpha_2(\tau_{n+2})$ by

$$(0.1)\ (\tau_{n+2} - t_n) = (0.1)\left[\frac{1.5}{200}\right] = 0.00075 \text{ degrees}$$

Therefore, the error due to lack of synchronization while reading one gyro is 0.00075 degrees.

Similarly, if both gyros read with one counter the first readout on the first gyro may be out of synchronism with last readout on the second gyro by:

$$(0.00075) \times (3) = 0.00225 \text{ degrees}$$

The 0.0025 degrees error includes the readout logic "waiting period" while switching from first to second gyro.

Computer Errors

By definition, the computer errors arise only from the limited word length and the type of algorithm selected in the computer design.

The computers are being designed for 0.01-degree accuracy per one direction cosine computation. Therefore, the error in a gyro spin vector attitude, $|\delta\bar{S}_c|$, due to computer errors is

$$|\delta\bar{S}_c| = \sqrt{3}\ \frac{0.01}{57.3} = 3.02 \times 10^{-4} \text{ radians}$$

The body rate is computed to the resolution of 0.002 deg/sec about each vehicle axis; therefore, the total rate error, $|\delta\bar{\omega}_c|$, due to computer errors is

$$|\delta\bar{\omega}_c| = \sqrt{3}\ 0.002 = 0.0046 \text{ deg/sec}$$
$$= 0.8 \times 10^{-4} \text{ rad/sec}$$

MATHEMATICAL CONSIDERATIONS

Assumptions

Since the SDMEG-ARS outputs are the vehicle attitude and rate, its performance will be specified in terms of the uncertainties of the attitude and rate outputs.

If $\delta\bar{\theta}$ and $\delta\bar{\omega}$ are the attitude and body rate uncertainties then, in general, the SDMEG performance equations are:

$$\delta\bar{\theta} = \bar{f}_\theta(\epsilon_1, \epsilon_2 \ldots \epsilon_n)$$

$$\delta\bar{\omega} = \bar{f}_\omega(\epsilon_1, \epsilon_2 \ldots \epsilon_n)$$

where $\epsilon_1, \epsilon_2 \ldots \epsilon_n$ are the errors as listed

The vector functions $\bar{f}_\theta$ and $\bar{f}_\omega$ are extremely non-linear and demanding in their derivation and use. Therefore, simplifying assumptions must be introduced.

A list of reasonable assumptions that will simplify the mathematical detail and still result in a good estimate of the ARS performance is:

1. The terms which contain ϵ of second or higher order can be neglected.
2. The system errors can be entered into the error equation as shown graphically in Figure 3-15.
3. The influence coefficients (or error gain coefficients) in the error equation for the cosine computer can be evaluated for the condition that the gyro pickoff axes are orthogonal and aligned to the vehicle body axes.
4. The influence coefficients in the error equation for the attitude and body rate computer can be evaluated for the condition that the gyro spin axes are orthogonal.

Item 1 is the commonly used assumption in the error analysis; therefore, it does not require special explanation. Nominally, the gyro pickoff axes are orthogonal and aligned to vehicle axes; they depart from the condition only due to misalignment errors. Therefore, the error equations can be expanded and linearized about this condition.

Similar reasoning holds for the justification of assumption 4.

Assumption 2 deals with defining the SDMEG-ARS error model. This model is illustrated graphically in Figure 3-15. In the model, the blocks numbered 1 through 7 represent the same data processing steps as explained in the system section of this report. The extraneous inputs (e.g. readout errors, alignment errors, etc) represent all of the ARS errors as they were defined in the section

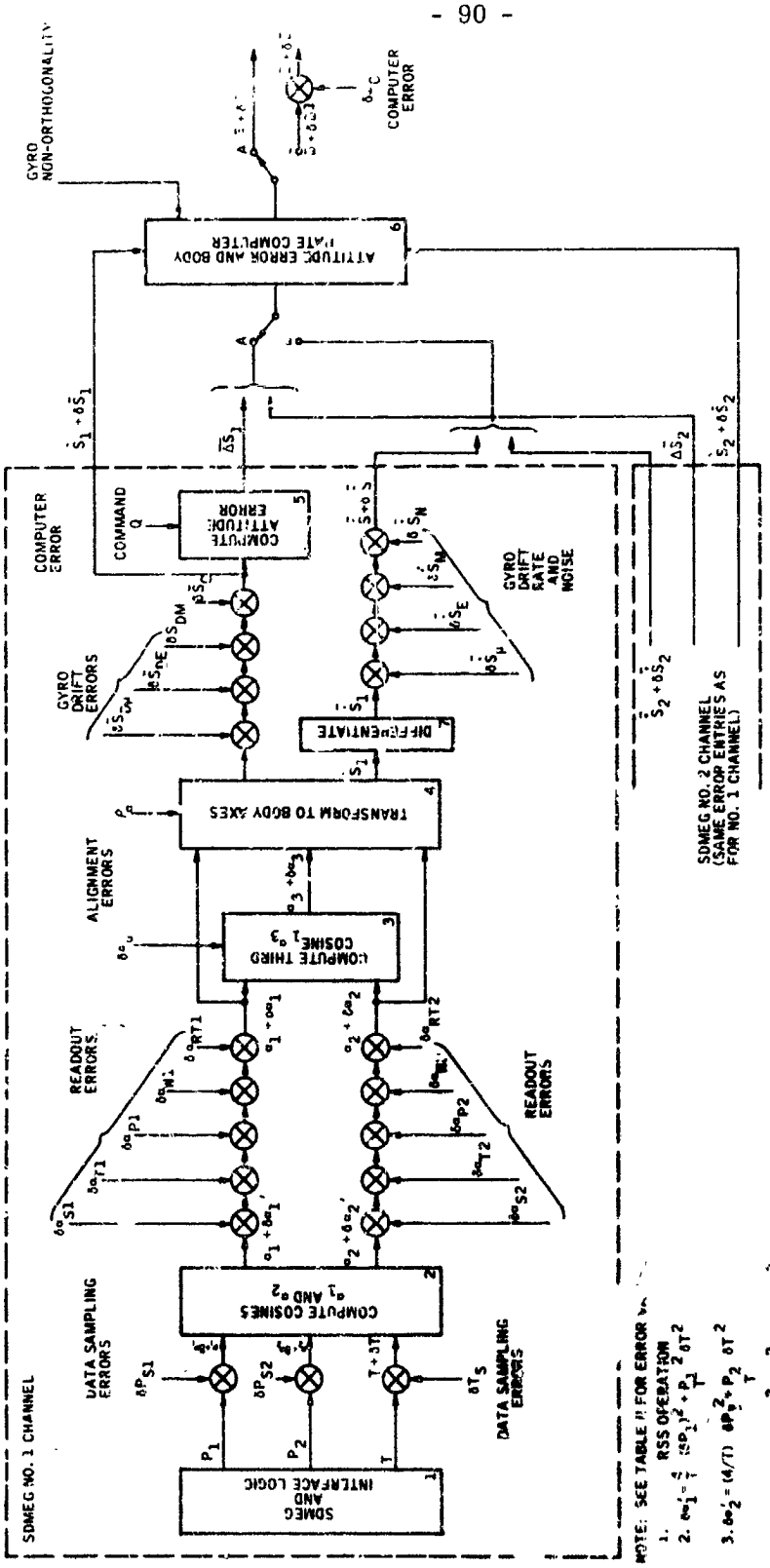

Figure 3-15. SDMEG-ARS Error Model

on the error sources. The summing points (⊗) in the diagram are interpreted as the root-sum-square (RSS) operations.

Specifically, assumption 2 deals with "where" in the system equations a particular error is entered.

Due to linearization of the error equations (assumption 1) the error terms, with proper gain factors, can be entered at any desired point of the system; thus, assumption 2 is justified.

Error Sensitivity

Under assumptions of this section it was pointed out that the error analysis will establish the ARS performance by the estimate of the attitude, $\delta\bar{\theta}$, and body rate, $\delta\bar{\omega}$, uncertainties.

The meaning and derivation of the attitude uncertainty, $\delta\bar{\theta}$, is not obvious without further clarification.

First, the attitude error will have different meanings, depending on whether the ARS is used in the closed vehicle attitude control loop or used in an open loop as an attitude monitor.

Second, if the ARS is used in the closed attitude control loop, not all of the ARS errors should be used in the ARS performance estimate.

If the ARS is used as an attitude monitor, its performance will be specified by determining the magnitude of $\delta\bar{S}$ (see Figure 3-15). In the case of closed loop operation the spin vector error, $\delta\bar{\Sigma}$, is only a partial answer since, in this case, the error in the vehicle attitude is of prime importance and will appear as an error in $\bar{\theta}$ (see Figure 3-15).

To estimate the error in $\bar{\theta}$ one must differentiate between the ARS errors occurring in the forward and feedback portions of the loop, since they have different effects on the loop performance. The appropriate block diagram showing the closed loop and the error entries appears in Figure 3-16.

In Figure 3-16 the two modes of the ARS operation are shown by switch positions A (attitude mode) and W (rate mode). The SDMEG-ARS includes blocks numbered (1), (2), (4), (5), and (6). The block (3) contains the autopilot and the vehicle which complete the attitude control loop.

In the attitude control loop (ARS in attitude mode) the autopilot will drive the errors ($\Delta\bar{S}_1$ and $\Delta\bar{S}_2$) to zero independently of the non-bias type errors in the ARS computer block (2). The block (2) serves the purpose of making a transformation of the attitude signals to torque command signals about the three vehicle control axes. This transformation can be regarded as a gain factor although of extremely non-linear nature. Therefore, since the transformation is essentially a gain factor, the errors in this block can be neglected in the system performance analysis as an attitude reference. However, the analysis of the system's performance as an attitude rate sensor must consider the errors occurring in block (2).

The block 2 is subjected to two types of errors: gyro non-orthogonality; transformation error due to error in $\hat{S}_1$ and $\hat{S}_2$ ($\delta\bar{S}_1$ and $\delta\bar{S}_2$). These errors do not contribute to the error in $\bar{\theta}$; therefore, when deriving the $\delta\bar{\theta}$ error care must be taken to avoid including these errors.

ARS PERFORMANCE IN ATTITUDE MODE

So far, it has been established that vehicle attitude error ($\delta\bar{\theta}$) will be a function of the readout, alignment, gyro drift and data sampling errors, and the errors introduced in block 2 of Figure 3-16 do not contribute to the error in $\bar{\theta}$. Next, it will be shown how to arrive at an expression which relates the above errors to $\delta\bar{\theta}$.

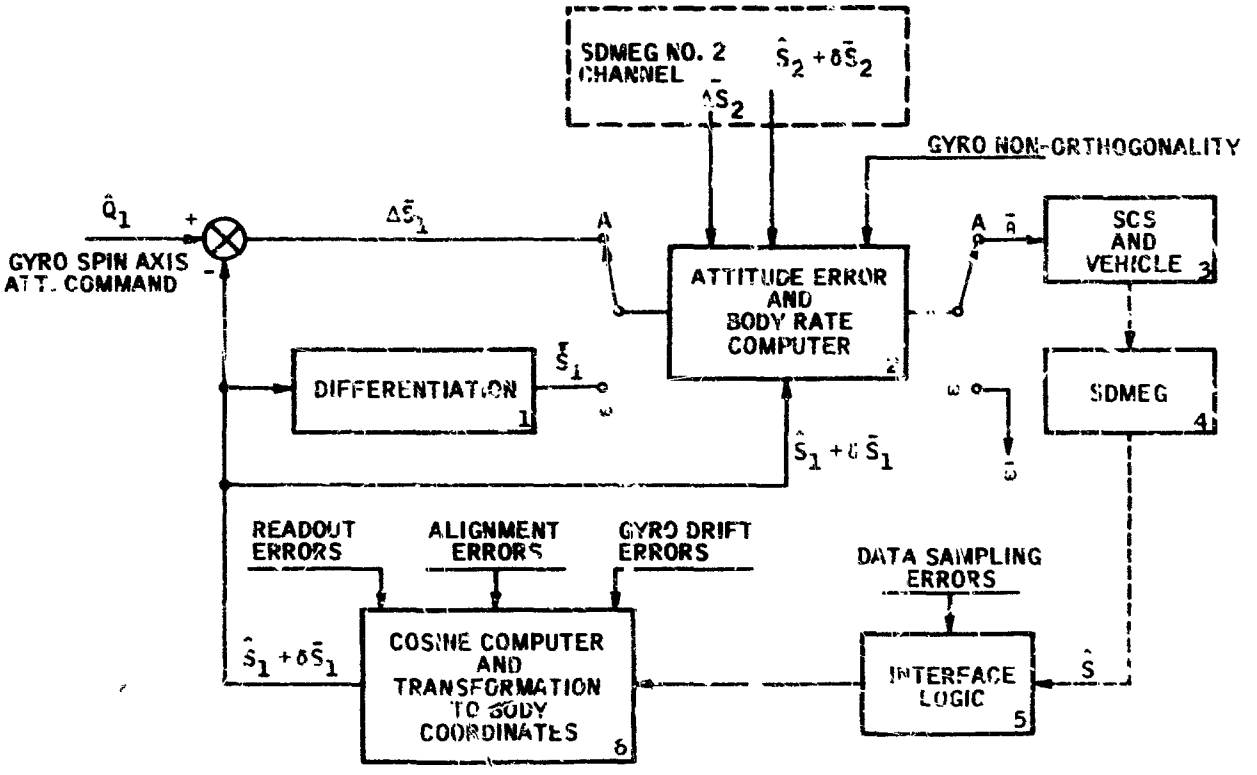

Figure 3-16. Attitude and Rate Modes of ARS Performance

It can be seen in Figure 3-16 that the readout, alignment, gyro drift and data sampling errors make up the error in gyro spin axis attitude (δS). Therefore, the desired error equation must establish the relationship between $\delta\bar{S}_1$, $\delta\bar{S}_2$ and $\delta\bar{\theta}$.

This relationship can be derived as follows:

In the section defining the ARS system equations it was shown that for the orthogonal gyro spin vectors ($\hat{S}_1 \cdot \hat{S}_2 = 0$)

$$\bar{\theta} = \Delta\bar{S}_1 \times \hat{S}_1 - \hat{S}_1 (\Delta\bar{S}_2 \cdot \hat{S}_1 \times \hat{S}_2)$$

Differentiate the equation for $\bar{\theta}$ and obtain

$$\delta\bar{\theta} = \delta(\Delta\bar{S}_1) \times \hat{S}_1 - \hat{S}_1 (\delta(\Delta\bar{S}_2) \cdot \hat{S}_1 + \hat{S}_2)$$

$$+ \quad \Delta\bar{S}_1 \times \delta\bar{S}_1 - \delta\bar{S}_1 (\Delta\bar{S}_2 \cdot \hat{S}_1 \times \hat{S}_2)$$

$$- \hat{S}_1 (\Delta\bar{S}_2 \cdot \delta\bar{S}_1 \times \hat{S}_2 + \Delta\bar{S}_2 \cdot \hat{S}_1 \times \delta\hat{S}_2)$$

The first two terms on the right side of the equation represent the error in $\delta\bar{\theta}$ due to errors in $\Delta\bar{S}_1$ and $\Delta\bar{S}_2$. The remaining terms, enclosed in the sequence bracket, represent the error in $\delta\bar{\theta}$ due to errors in the transformation (error in block 2 in Figure 3-16) and must be neglected for the above reasons.

Therefore, the error in $\delta\bar{\theta}$ is

$$\delta\bar{\theta} = \delta(\Delta\bar{S}_1) \times \hat{S}_1 - \hat{S}_1 (\delta(\Delta\bar{S}_2) \cdot \hat{S}_1 \times \hat{S}_2)$$

Since

$$\delta(\Delta\bar{S}_1) = \delta\bar{S}_1$$

$$\delta(\Delta\bar{S}_2) = \delta\bar{S}_2$$

$$\delta\bar{\theta} = \delta\bar{S}_1 \times \hat{S}_1 - \hat{S}_1 \, (\delta\bar{S}_2 \cdot \hat{S}_1 \times \hat{S}_2)$$

The magnitude of $\delta\bar{\theta}$ is

$$\left|\delta\bar{\theta}^{\,2}\right| = \left|\delta\bar{S}_1\right|^2 \sin(\delta\bar{S}_1, S_1) + \left|\delta\bar{S}_2\right|^2 \cos^2(\delta\bar{S}_2, \hat{S}_1 \times \hat{S}_2)$$

Since by definition the $\hat{S}_1$ and $\hat{S}_2$ are unit vectors, $\delta\bar{S}_1 \cdot S_1 = 0$ and $\delta\bar{S}_2 \cdot S_2 = 0$

Then it follows that the sine and cosine values in the above equations are

$$\sin^2(\delta\bar{S}_1, \hat{S}_1) = 1$$

$$0 \leq \cos^2(\delta\bar{S}_2, \hat{S}_1 \times \hat{S}_2) \leq 1$$

Let the argument of the cosine be equal to τ; then the expected value of the cosine is

$$E(\cos^2\tau) = \frac{1}{2\pi} \int_0^{2\pi} \cos^2 \tau \, d\tau = 1/2$$

Therefore, the magnitude of the vehicle attitude error is

$$\left|\delta\bar{\theta}\right|^2 = \left|\delta\bar{S}_1\right|^2 + 1/2 \left|\delta\bar{S}_2\right|^2$$

$$\text{if } \left|\delta\bar{S}_1\right| = \left|\delta\bar{S}_2\right|$$

Then

$$\left|\delta\bar{\theta}\right| = \sqrt{3/2} \left|\delta\bar{S}_1\right|$$

The equation for the vehicle pointing error is derived using the following mathematical definitions.

Let $\delta\bar{\theta}$ be an error vector about which the vehicle is rotated from the commanded attitude through an angle $|\delta\bar{\theta}|$. The $\delta\bar{\theta}$ vector is a function of the ARS error.

Now, if $\hat{X}$, $\hat{Y}$, $\hat{Z}$ are the unit vectors along the vehicle roll, pitch, and yaw axes, then the angular errors about the roll, pitch, and yaw axes are $\delta\bar{\theta}\cdot\hat{X}$, $\delta\bar{\theta}\cdot\hat{Y}$, and $\delta\bar{\theta}\cdot\hat{Z}$, respectively.

Since the $\hat{X}$, $\hat{Y}$, $\hat{Z}$ is an orthogonal triad

$$(\delta\bar{\theta}\cdot\hat{X})^2 + (\delta\bar{\theta}\cdot\hat{Y})^2 + (\delta\bar{\theta}\cdot\hat{Z})^2 = |\delta\theta|^2$$

And the expected angular error about any one of the three vehicle axes is (see Figure 3-17).

$$\text{attitude error/vehicle axis} = \frac{|\delta\theta|}{\sqrt{3}}$$

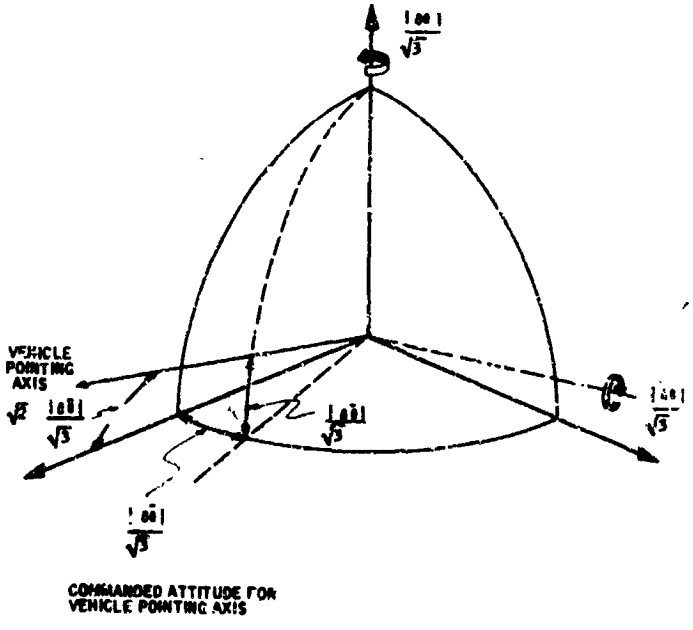

Figure 3-17. Vehicle Pointing Error Geometry

Therefore, the vehicle pointing error is

$$\text{Pointing error} = \sqrt{\left(\frac{|\bar{\delta\theta}|}{\sqrt{3}}\right)^2 + \left(\frac{|\bar{\delta\theta}|}{\sqrt{3}}\right)^2} = \frac{\sqrt{2}}{\sqrt{3}} \; |\bar{\delta\theta}| = |\bar{\delta S}|$$

The equations which relate the $|\delta S|$ error to the system errors are given below. The derivations of these equations will be shown later in this report.

$$\delta P_i^2 = \delta P_{Si}^2 \qquad i = 1 \text{ or } 2 \quad \text{(pickoff number)} \tag{11}$$

$$\delta T^2 = \delta T_S^2 \tag{12}$$

$$(\delta\alpha_i')^2 = \left(\frac{4}{T}\right)^2 \delta P_i^2 + \left(\frac{4}{T}\right)^2 \times \left(\frac{P_i}{T}\right)^2 \times \delta T^2 \tag{13}$$

$$\delta\alpha_i^2 = (\delta\alpha_i')^2 + \delta\alpha_{Si}^2 + \delta\alpha_{Ti}^2 + \delta\alpha_{Pi}^2 + \delta\alpha_{Ni}^2 + \delta\alpha_{RTi}^2 \tag{14}$$

$$\delta\alpha_3^2 = 0.366\,(\delta\alpha_1^2 + \delta\alpha_2^2) + 0.50\,\delta\theta_a^2 \tag{15}$$

$$|\delta\bar{S}'|^2 = \delta\alpha_1^2 + \delta\alpha_2^2 + \delta\alpha_3^2 + 2\rho_a^2 \tag{16}$$

$$|\delta\bar{S}|^2 = |\delta\bar{S}'|^2 + |\delta\bar{S}_{DM}|^2 + |\delta\bar{S}_{De}|^2 + |\delta\bar{S}_{DM}|^2 + |\delta\bar{S}_C|^2 \tag{17}$$

$$|\delta\bar{\dot{S}}|^2 = |\delta\bar{\dot{S}}_\mu|^2 + |\delta\bar{\dot{S}}_\epsilon|^2 + |\delta\bar{\dot{S}}_N|^2 + |\delta\bar{\dot{S}}_M|^2 \tag{18}$$

The simultaneous solution of Equations (11) through (17) yields:

$$|\delta\bar{S}|^2 = \left\{|\delta\bar{S}_{DM}|^2 + |\delta\bar{S}_{De}|^2 + |\delta\bar{S}_{DM}|^2\right\} + 2.732\left\{\delta\alpha_{Si}^2 + \delta\alpha_{Ti}^2 + \delta\alpha_{Pi}^2 + \delta\alpha_{Ni}^2 + \delta\alpha_{RTi}^2\right\} + |\delta\bar{S}_C|^2 + 2\rho_a^2 + 0.5\,\delta\theta_a^2$$

Substitution of the error term values from Table 3-6 yields:

$$|\delta\bar{S}|^2 = \left\{(0.000496)^2\right\} + 2.732\left\{(0.325)^2 + (0.105)^2 + (0.855)^2 + (1.41)^2 + (0.084)^2\right\} \times 10^{-8} + (3.02)^2 \times 10^{-8} + 2\rho_a + 0.5\,\delta\theta_a^2$$

$$|\delta\bar{S}|^2 = 38.72 \times 10^{-8} + 2\rho_a^2 + 0.5\,\delta\theta_a^2$$

For high-accuracy ARS design

$$\rho_a^2 = \theta_a^2 = (0.000064)^2 = 0.41 \times 10^{-8} \text{ radians}^2$$

Therefore, $|\delta\bar{S}|$ for high-accuracy ARS is

$$|\delta\bar{S}| = \sqrt{38.72 + 2.5 \times 0.41} \times 10^{-4}$$
$$= 6.3 \times 10^{-4} \text{ radians}$$
$$= 0.0360 \text{ degree}$$

and

$|\delta\bar{S}|$ = 0.036 degree = vehicle pointing error for high-accuracy ARS

For low-accuracy ARS

$$\rho_a^2 = \theta_a^2 = 3.6 \times 10^{-6} \text{ radians}$$

Therefore, the vehicle pointing error for the low-accuracy ARS is:

$$|\delta\bar{S}| = \sqrt{38.72 + (36)\,2.5} \times 10^{-4}$$

$$= 11.35 \times 10^{-4} \text{ radians}$$

$$= 0.066 \text{ degree}$$

ARS PERFORMANCE IN THE RATE MODE

In the ADMEG-ARS the body rate is computed by two operations (see Figure 3-15):

- Differentiation of six direction cosines (block 7 in Figure 3-15).
- Transformation of direction cosine rates to vehicle body rates resolved along the body axes (block 6 in Figure 3-15).

The quality of the six signals, which represent the six direction cosines, and the errors in the above two operations, affect the quality of the computed body rate.

The direction cosine rate error results from the gyro readout noise, differentiation process and gyro drift.

The transformation error results from the fact that the gyro spin axes attitudes are not absolutely known. Therefore, the computed body rate components may be along some other frame than the true body axes.

The body rate error equation is derived later in this report and is given here in vector form as follows:

$$\delta\bar{\omega}^1 = \delta\dot{\bar{S}}_1 \times \hat{S}_1 + \bar{\omega} \cdot \hat{S}_1 \, \delta\bar{S}_1 + \hat{S}_1 \left\{ \bar{\omega} \cdot \hat{S}_2 \, \delta\bar{S}_2 \cdot \hat{S}_1 + \delta\bar{S}_2 \times \hat{S}_2 \cdot \hat{S}_1 \right\}$$

where

$\delta\bar{\omega}^1$ = body rate error vector (does not include computer error)

$\delta\bar{S}_1$ = error in $\bar{S}_1$ vector

$\hat{S}_1$ = first gyro true spin axis attitude

$\bar{\omega}$ = body rate vector

$\delta\bar{S}_1$ = error in $\hat{S}_1$ vector

$\bar{S}_2$ = second gyro true spin axis attitude

$\delta\bar{S}_2$ = error in $\hat{S}_2$

$\delta\bar{S}_2$ = error in $\bar{S}_2$ vector

By examination of the expression for $\delta\bar{\omega}^{-1}$ it can be deduced that the vectors $\delta\bar{S}_1 \times \hat{S}_1$, $\delta\bar{S}_1$, and $\hat{S}_1$ are an orthogonal set; therefore, the magnitude of the $\delta\bar{\omega}^{-1}$ error vector can be written as follows:

$$\left|\delta\bar{\omega}^{-1}\right|^2 = \left|\delta\bar{S}_1\right|^2 + (\bar{\omega}\cdot\hat{S}_1)^2 \left|\delta\bar{S}_1\right|^2 + [\bar{\omega}\cdot\hat{S}_2\ \delta\bar{S}_2\cdot\hat{S}_1 + \delta\bar{S}_2 \times \hat{S}_2\cdot\hat{S}_1]^2$$

In order to evaluate the above equation certain assumptions must be made about the relative attitude of the vectors appearing on the right side of the equation.

Therefore, let

$$\bar{\omega}\cdot\hat{S}_1 = \bar{\omega}\cdot\hat{S}_2 = \left|\bar{\omega}\right|\frac{1}{\sqrt{2}}$$

The RSS value of the third term on the right side of the equation can be shown to be

$$\frac{1}{2}(\omega\cdot\hat{S}_2)^2 \left|\delta\bar{S}_2\right|^2 + \frac{1}{2}\left|\delta\bar{S}\right|^2$$

Therefore, the magnitude of the $\delta\omega^1$ is

$$\left|\delta\bar{\omega}^1\right|^2 = \left|\delta\bar{S}_1\right|^2 + \frac{\left|\bar{\omega}\right|^2}{2}\left|\delta\bar{S}_1\right|^2 + \frac{\left|\bar{\omega}\right|^2}{2}\frac{\left|\delta\bar{S}_2\right|^2}{2} + \frac{\left|\delta\bar{S}_2\right|^2}{2}$$

Since $\left|\delta\bar{S}_1\right| = \left|\delta\bar{S}_2\right| = \left|\delta\bar{S}\right|$

and $\left|\delta\bar{S}_1\right| \cdot \left|\delta\bar{S}_2\right| = \left|\delta\bar{S}\right|$

$$\left|\delta\bar{\omega}^1\right|^2 = \frac{1}{2}\left|\delta\bar{S}\right|^2 + \omega^2\,\frac{3}{4}\left|\delta\bar{S}\right|^2$$

$$|\delta\bar{\omega}|^2 \quad \frac{3}{2}\,|\delta\bar{S}|^2 + \omega^2\,\frac{3}{4}\,|\delta\bar{S}|^2 + |\delta\bar{\omega}_C|^2 \qquad (19)$$

The vehicle rate error about pitch, yaw or roll axis is:

$$\text{Rate error per axis} = \frac{|\delta\bar{\omega}|}{\sqrt{3}} \qquad (20)$$

The derived body rate error $|\delta\bar{\omega}|$ can be obtained by simultaneous solution of Equations (11) through (19) and substitution of the error term values in Table 3-9.

Simultaneous solution of Equations (11) through (19) yields

$$|\delta\bar{\omega}|^2 = 1.5\left\{|\delta\bar{S}_\mu|^2 + |\delta\bar{S}_\epsilon|^2 + |\delta\bar{S}_M|^2\right\} + 0.75\,\omega^2\,|\delta\bar{S}|^2 + |\delta\bar{\omega}_C|^2 + 1.5\,|\delta\bar{S}_N|^2$$

Substitution of the error term values in Table 3-9 and assumption of a vehicle rate ω of 20 deg/sec yields

$$|\delta\bar{\omega}|^2 = 1.5 \left\langle (4.22)^2 \times 10^{-8} \right\rangle + 0.75 \left|\frac{20}{51.3}\right|^2 |\delta\bar{S}|^2 + (0.6)^2 \times 10^{-8} + 1.5 \times (345)^2 \times 10^{-8}$$

$$\cong 1.5 \times (345)^2 \times 10^{-8}$$

$$|\delta\bar{\omega}| = 0.0422 \text{ rad/sec} = 2.42 \text{ deg/sec}$$

Therefore, the rate error per control axis is

$$\frac{|\delta\bar{\omega}|}{\sqrt{3}} = \frac{2.42}{\sqrt{3}} = 1.4 \text{ deg/sec}$$

In the expression for $|\delta\bar{\omega}|^2$ it can be seen that the contribution of the noise error term $|\delta\bar{S}_N|$ is about 70 times larger than the RSS of all other error terms. Therefore, the ARS performance in the rate mode depeneds entirely on the ability of the data filters to reduce the 1.4-deg/sec computed rate uncertainty.

Note that the distinction between high and low accuracy in the rate output of the ARS is lost in the presence of the high noise level on the gyro readout.

DERIVATIONS OF ERROR EQUATIONS

This section contains the derivations of the error equations which are listed without proof in Figure 3-15. The equations which are derived here are:

$$\delta\alpha_1 = (4/T)\sqrt{\delta P_1^2 + (P_{1/T})^2\ \delta T^2}$$

$$\delta\alpha_2^1 = (4/T)\sqrt{\delta P_2^2 + (P_{2/T})^2\ \delta T^2}$$

$$\delta\alpha_3 = \sqrt{0.366(\delta\alpha_1^2 + \delta\alpha_2^2) + 0.50\ \delta\theta_{\varepsilon}^2}$$

$$\delta S_1 = \sqrt{\delta\alpha_1^2 + \delta\alpha_2^2 + \delta\alpha_3^2 + 2P_a^2}$$

$$\delta\omega = \sqrt{\left|\delta\bar{S}_1\right|^2 + \frac{\left|\delta\bar{S}_2\right|^2}{2} + \frac{\omega^2}{2}\left(\left|\delta\bar{S}_1\right|^2 + \left|\frac{\delta\bar{S}_2}{2}\right|^2\right)}$$

The expression for $\left|\delta\bar{\theta}\right|$ was derived in the section "ARS Performance in Attitude Mode".

Derivation of $\delta\alpha_1^1$ and $\delta\alpha_2^1$

The gyro readout equation which define the direction cosines of the two reading pickoffs with respect to the gyro spin axis are

$$\alpha_1 = \frac{4P_1}{T} - 2$$

$$\alpha_2 = \frac{4P_2}{T} - 2$$

If $\delta\alpha_1^1$ and $\delta\alpha_2^1$ are the errors in α_1 and α_2, respectively, then by differentiation

$$\delta\alpha_i^1 = \left(\frac{4}{T}\right)\delta P_1 - \left(\frac{4P_1}{T^2}\right)\delta T$$

$$\delta\alpha_2{}^1 = \left(\frac{4}{T}\right)\delta P_2 - \left(\frac{4P_2}{T^2}\right)\delta T$$

Forming the RSS of the two terms on the right side of each equation yields:

$$\delta\alpha_1{}^1 = \left(\frac{4}{T}\right)\sqrt{\delta P_1{}^2 + \left(\frac{P_1}{T}\right)^2 \delta T^2}$$

$$\delta\alpha_2{}^1 = \left(\frac{4}{T}\right)\sqrt{\delta P_2{}^2 + \left(\frac{P_2}{T}\right)^2 \delta T^2}$$

Derivation of $\delta\alpha_3$

The α_3 is the third missing direction cosine whose value is determined from the knowledge of α_1, α_2 and the relative alignment among the three pickoff axes.

The expression for α_3 is

$$\sqrt{C_2}\,\alpha_3 = -D_2\,\alpha_1 - B_2\,\alpha_2 \pm \sqrt{1 - \alpha_2{}^2 - \left[E_2\,\alpha_1 - A_2\,\alpha_2\right]^2}$$

The constants A_2, B_2, C_2, D_2, E_2 are determined from the pickoff alignment data. The expressions for these constants are:

$$A_2 = \frac{/\hat{P}_1 \times \hat{P}_2 \,/\, (\hat{P}_1 \cdot \hat{P}_2)}{1 - (P_2 \cdot P_1)^2} = \frac{\sin\theta_{12}\cos\theta_{12}}{1 - \cos^2\theta_{12}} = \frac{\cos\theta_{12}}{\sin\theta_{12}} = \text{ctn}\,\theta_{12}$$

$$B_2 = \frac{/\hat{P}_1 \times \hat{P}_2 \,/(\hat{P}_1 \cdot \hat{P}_2\,\hat{P}_1 \cdot \hat{P}_3 - \hat{P}_3 \cdot \hat{P}_2)}{(P_1\,P_2\,P_3)\left[1 - (\hat{P}_1 \cdot \hat{P}_2)^2\right]} = \frac{1}{X}\left\{\text{ctn}\,\theta_{12}\cos\theta_{13} - \text{CSC}\,\theta_{12}\cos\theta_{23}\right.$$

$$C_2 = \frac{/\hat{P}_1 \times \hat{P}_2 /^2}{(P_1\ P_2\ P_3)} = \frac{1}{X} \sin\theta_{12}$$

$$D_2 = \frac{/\hat{P}_1 \times \hat{P}_2 / (\hat{P}_1 \cdot \hat{P}_2\ \hat{P}_2 \cdot \hat{P}_3 - \hat{P}_1 \cdot \hat{P}_3)}{(P_1\ P_2\ P_3)\ \left[1 - (P_1 \cdot P_2)^2\right]} = \frac{1}{X}\left(\text{ctn}\,\theta_{12} \cos\theta_{23} - \text{CSC}\,\theta_{12} \cos\theta_{1}\right.$$

$$E_2 = \frac{/\hat{P}_1 \times \hat{P}_2 /}{1\ (\hat{P}_1 \cdot \hat{P}_2)^2} = \text{CSC}\ \theta_{12}$$

where

$$(\hat{P}_1,\ \hat{P}_2\ \hat{P}_3) = \hat{P}_1 \cdot \hat{P}_2 \times \hat{P}_3 = X$$

$$\hat{P}_i \cdot \hat{P}_j = \text{Cos}\ \theta_{ij}$$

$$\left|\hat{P}_i \times \hat{P}_j\right| = \text{Sin}\ \theta_{ij}$$

If $\delta\alpha_3$ is the error in α_3 then by differentiation

$$\delta\left(\sqrt{C_2}\right)\alpha_3 + \sqrt{C_2}\ \delta\alpha_3 = -\delta D_2\,\alpha_1 - \delta B_2\alpha_2$$

$$-D_2\,\delta\alpha_1 - B_2\,\delta\alpha_2$$

$$\pm \frac{-2\alpha_2\,\delta\alpha_2 - 2\left(E_2\alpha_1 - A_2\alpha_2\right)\left(\delta E_2\alpha_1 - \delta A_2\,\alpha_2 + E_2\,\delta\alpha_1 - A_2\,\delta\alpha_2\right)}{2\sqrt{1 - \alpha_2^2 - \left[E_2\,\alpha_1 - A_2\,\alpha_2\right]^2}}$$

If, nominally, the pickoff axes are orthogonal then $\theta_{ij} = \pi/2$,

$X = 1$, $\alpha_1^2 + \alpha_2^2 + \alpha_3^2 = 1$ and

$A_2 = 0$, $B_2 = 0$, $\sqrt{C_2} = 1$, $D_2 = 0$, $E_2 = 1$

Therefore, the differential equation for α_3 becomes

$$\delta\left|\sqrt{C_2}\right| \alpha_3 + \delta\alpha_3 = -\delta D_2 \alpha_1 - \delta B_2 \alpha_2 \pm \frac{-2\alpha_2 \delta\alpha_2 - 2\alpha_1 \left|\delta E_2 \alpha_1 - \delta A_2 \alpha_2 + \delta\alpha_1\right|}{2\alpha_3}$$

The differentials for the constants A, B, C, D, E can be evaluated in terms of errors in θ_{ij}. If the error in θ_{ij} in $\delta\theta_{ij}$ then

$$\delta A_2 = \delta\left|\operatorname{ctn}\theta_{12}\right| = -\operatorname{CSC}^2\theta_{12}\ \delta\theta_{12} = -\delta\theta_{12}$$

Similarly,

$$\delta B_2 = \delta\theta_{23}$$

$$\delta\left|\sqrt{C_2}\right| = -\delta X$$

$$\delta D_2 = \delta\theta_{13}$$

$$\delta E_2 = 0$$

The δX is also a function of alignment measurements and it can be neglected since it is of second order.

The proof for this statement goes as follows:

It is given that (21)

$$X = \hat{P}_1 \cdot \hat{P}_2 \times \hat{P}_3$$

Differentiate Equation (21)

$$\delta X = \delta\overline{P}_1 \cdot \hat{P}_2 X \hat{P}_3 + \hat{P}_1 \cdot \delta\overline{P}_2 X \hat{P}_3 + \hat{P}_1 \cdot \hat{P}_2 X \delta\overline{P}_3 \tag{22}$$

The vectors P are unit vectors; therefore their differentials represent small rotations from nominal and can be expressed as follows:

$$\begin{aligned} \delta\overline{P}_1 &= \overline{\phi}_1 X \hat{P}_1 \\ \delta\overline{P}_2 &= \overline{\phi}_2 X \hat{P}_2 \\ \delta\overline{P}_3 &= \overline{\phi}_3 X \hat{P}_3 \end{aligned} \tag{23}$$

where ϕ's are small angular rotations of the P's.

Substitute Equation (23) into Equation (22), expand by vector product identities and obtain:

$$\begin{aligned} \delta X = {} & \overline{\phi}_1 \cdot P_2 \hat{P}_1 \cdot P_3 - \overline{\phi}_1 \cdot \hat{P}_3 \hat{P}_1 \cdot \hat{P}_2 \\ & + \hat{P}_1 \cdot [\overline{\phi}_2 \cdot \hat{P}_3 \hat{P}_2 - \hat{P}_2 \cdot \hat{P}_3 \overline{\phi}_2] \\ & + \hat{P}_1 \cdot [\hat{P}_2 \cdot \hat{P}_3 \overline{\phi}_3 - \hat{P}_2 \cdot \overline{\phi}_3 \hat{P}_3] \end{aligned} \tag{24}$$

Let

$$\hat{P}_2 \cdot \hat{P}_3 = \cos\theta_{23}$$

$$\hat{P}_1 \cdot \hat{P}_2 = \cos\theta_{12}$$

$$\hat{P}_1 \cdot \hat{P}_3 = \cos\theta_{13}$$

and let

$$\theta_{23} = \frac{\pi}{2} + \delta\theta_{23}$$

$$\theta_{12} = \frac{\pi}{2} + \delta\theta_{12}$$

$$\theta_{13} = \frac{\pi}{2} + \delta\theta_{13}$$

Substitute these expressions into Equation (24) and obtain

$$\begin{aligned} \delta X = & -\delta\theta_{12}\left[(\bar{\phi}_2 - \bar{\phi}_1) \cdot \hat{P}_3\right] \\ & -\delta\theta_{13}\left[(\bar{\phi}_1 - \bar{\phi}_3) \cdot \hat{P}_2\right] \\ & -\delta\theta_{23}\left[(\bar{\phi}_3 - \bar{\phi}_2) \cdot \hat{P}_1\right] \end{aligned} \tag{25}$$

Since the ϕ's are of the same order as $\delta\theta$'s, the δX quantity is the second order error; therefore, it can be eliminated from further consideration.

Therefore, the differential equation for α_3 becomes

$$\begin{aligned} \delta\alpha_3 = & -\delta\theta_{13}\alpha_1 - \delta\theta_{23}\alpha_2 \\ & \pm \frac{1}{\alpha_3}\left(\delta\alpha_2\alpha_2 + \alpha_1\delta\alpha_1 + \alpha_1\alpha_2\delta\theta_{12}\right) \end{aligned} \tag{26}$$

The $\delta\theta$'s are angular errors in the relative alignment among the pickoff axes whose expected values are the same for all alignments; therefore, let

$$\delta\theta_{12} = \delta\theta_{13} = \delta\theta_{23} = \delta\theta_a$$

Then the RSS of the Equation (26) is

$$\delta\alpha_3^2 = \delta\theta_a^2\left[\alpha_1^2 + \alpha_2^2 + \frac{\alpha_1^2\alpha_2^2}{\alpha_3^2}\right] + \frac{1}{\alpha_3^2}\left[\alpha_1^2\delta\alpha_1^2 + \alpha_2^2\delta\alpha_2^2\right] \tag{27}$$

It can be deduced that the value for $\delta\alpha_3^2$ will be maximum if α_3 is small and $\alpha_1^2 = \alpha_2^2$.

The α_3, being the missing cosine, will have values ranging between 0.76 to 1.0; therefore, evaluate it at 0.76.

And since

$$\alpha_1^2 + \alpha_2^2 + \alpha_3^2 = 1$$

the value of $\delta\alpha_3^2 = 0.50\,\delta\theta^2 + 0.366\,(\delta\alpha_1^2 + \delta\alpha_2^2)$

Derivation of δS_1 [1]

Write the direction cosine row matrix in pickoff axes $[\alpha]$ and the transformation matrix from pickoff to body axes $[A]$ then the cosine computer output is

$$[S_i] = [\alpha]\,[A]$$

and the error in the cosine computer output is

$$[\delta S_i] = [\delta\alpha]\,[A] + [\alpha]\,[\delta A]$$

The $[\delta\alpha]$ is the row matrix whose elements are the previously derived errors in α_1, α_2, and α_3, namely

$$[\delta\alpha] = [\delta\alpha_1 \;\; \delta\alpha_2 \;\; \delta\alpha_3]$$

Nominally, the pickoff axes are aligned along the vehicle body axes, then the alignment matrix $[A]$ is the unit matrix.

The matrix δA consists of elements which are small misalignment angles between pickoff axes and vehicle body axes. For the error analysis purposes write this matrix as follows (see Alignment Errors):

$$[\delta A] = \begin{bmatrix} 0 & \rho_3 & -\rho_2 \\ -\rho_3 & 0 & \rho_1 \\ \rho_2 & -\rho_1 & 0 \end{bmatrix}$$

Therefore,

$$[\delta S_i] = [\delta\alpha_1 \ \ \delta\alpha_2 \ \ \delta\alpha_3] + [\alpha_1 \ \ \alpha_2 \ \ \alpha_3] \begin{bmatrix} 0 & \rho_3 & -\rho_2 \\ -\rho_3 & 0 & \rho_1 \\ \rho_2 & -\rho_1 & 0 \end{bmatrix}$$

$$[\delta S_i] = [\delta\alpha_1 - \alpha_2\rho_3 + \alpha_3\rho_2 \ \ | \ \ \delta\alpha_2 + \alpha_1\rho_3 - \alpha_3\rho_1 \ \ | \ \ \delta\alpha_3 - \alpha_1\rho_2 + \alpha_2\rho_1]$$

The expression on the right side of the equation is a row matrix whose elements define the error vector $\delta\bar{S}_1{}^1$.

Forming the RSS of each element and solving for the magnitude of $\delta\bar{S}_1{}^1$, and letting $\rho_1 = \rho_2 = \rho_3 = \rho_a$

$$|\delta\bar{S}_i|^2 = \delta\alpha_1^2 + \delta\alpha_2^2 + \delta\alpha_3^2 + \rho_a^2(\alpha_1^2 + \alpha_2^2 + \alpha_3^2)2$$

Since $\alpha_1^2 + \alpha_2^2 + \alpha_3^2 = 1$

$$|\delta\bar{S}| = \sqrt{[\delta\alpha_1^2 + \delta\alpha_2^2 + \delta\alpha_3^2 + 2\rho_a^2]}$$

Derivation of $|\delta\bar{\omega}|^1$

The body rate error equation can be derived as follows:

The time differentials of $\hat{S}_1$ and $\hat{S}_2$ are

$$\dot{\bar{S}}_{1D} = \dot{\bar{S}}_1 + \bar{\omega} \times \hat{S}_1 \tag{28}$$

$$\dot{\bar{S}}_{2D} = \dot{\bar{S}}_2 + \bar{\omega} \times \hat{S}_2 \tag{29}$$

where

$\dot{\bar{S}}_{1D}$, $\dot{\bar{S}}_{2D}$ = gyro drift rates

$\dot{\bar{S}}_1$, $\dot{\bar{S}}_2$ = gyro spin axes rates with respect to the rotating body axes

$\bar{\omega}$ = body rate

$\hat{S}_1$, $\hat{S}_2$ = unit vectors along the two gyro spin axes.

Perturb Equations (28) and (29) about their nominal values and subtract the nominal solutions

$$\dot{\bar{S}}_{1D} - \delta\dot{\bar{S}}_1 = \bar{\omega} \times \delta\bar{S}_1 + \delta\bar{\omega} \times \hat{S}_1 = -\delta\dot{\bar{S}}_1 \tag{30}$$

$$\dot{\bar{S}}_{2D} - \delta\dot{\bar{S}}_2 = \bar{\omega} \times \delta\bar{S}_2 + \delta\bar{\omega} \times \hat{S}_2 = -\delta\dot{\bar{S}}_2 \tag{31}$$

The drift rates $\dot{\bar{S}}_{1D}$ and $\dot{\bar{S}}_{2D}$ appear in Equations (30) and (31) because in the nominal solution their values have been assumed to be zero.

Note that the rate errors $\delta\dot{\bar{S}}_1$ and $\delta\dot{\bar{S}}_2$ are the sum total of gyro drift and gyro readout noise.

Crossing Equation (30) and $\hat{S}_1$, and Equation (31) and $\hat{S}_2$

$$-\delta\dot{\bar{S}}_1 \times \hat{S}_1 = (\bar{\omega} \cdot \hat{S}_1)\,\delta\bar{S}_1 - \delta\bar{S}_1 \cdot \hat{S}_1\,\bar{\omega} + \delta\bar{\omega} \cdot \hat{S}_1\,\hat{S}_1 - \delta\bar{\omega} \tag{32}$$

$$-\delta\dot{\bar{S}}_2 \times \hat{S}_2 = \bar{\omega} \cdot \hat{S}_2\,\delta\bar{S}_2 - \delta\bar{S}_2 \cdot \hat{S}_2\,\bar{\omega} + \delta\bar{\omega} \cdot \hat{S}_2\,\hat{S}_2 - \delta\bar{\omega} \tag{33}$$

If it is assumed that $\hat{S}_1$ and $\hat{S}_2$ remain unit vectors then

$$\delta\bar{S}_1 \cdot \hat{S}_1 = 0 \text{ and } \delta\bar{S}_2 \cdot \hat{S}_2 = 0$$

Dotting Equation (32) by $\hat{S}_2$ and Equation (33) by $\hat{S}_1$

$$-\delta\dot{\bar{S}}_1 \times \hat{S}_1 \cdot \hat{S}_2 = \bar{\omega} \cdot \hat{S}_1\,\delta\bar{S}_1 \cdot \hat{S}_2 + \delta\bar{\omega} \cdot \hat{S}_1\,\hat{S}_1 \cdot \hat{S}_2 - \delta\bar{\omega} \cdot \hat{S}_2 \tag{34}$$

$$-\delta\dot{\bar{S}}_2 \times \hat{S}_2 \cdot \hat{S}_1 = \bar{\omega} \cdot \hat{S}_2\,\delta\bar{S}_2 \cdot \hat{S}_1 + \delta\bar{\omega} \cdot \hat{S}_2\,\hat{S}_1 \cdot \hat{S}_2 - \delta\bar{\omega} \cdot \hat{S}_1 \tag{35}$$

Solve the scalar Equations (34) and (35) simultaneously and eliminate $\delta\bar{\omega} \cdot \hat{S}_2$

$$-\delta\bar{S}_2 \times \hat{S}_2 \cdot \hat{S}_1 = \bar{\omega} \cdot \hat{S}_2 \, \delta\bar{S}_2 \cdot \hat{S}_1 - \delta\bar{\omega} \cdot \hat{S}_1 + \hat{S}_1 \cdot \hat{S}_2 \left\{ \bar{\omega} \cdot \hat{S}_1 \, \delta\bar{S}_1 \cdot \hat{S}_2 + \delta\bar{\omega} \cdot \hat{S}_1 \, \hat{S}_1 \cdot \hat{S}_2 + \delta\dot{\bar{S}}_1 \times \hat{S}_1 \cdot \hat{S}_2 \right\} \tag{36}$$

Solve Equation (36) for $\delta\bar{\omega} \cdot \hat{S}_1$ and substitute this expression into Equation (32).

$$\delta\bar{\omega} = \delta\dot{\bar{S}}_1 \times \hat{S}_1 + \bar{\omega} \cdot \hat{S}_1 \, \delta\bar{S}_1 + \frac{\hat{S}_1}{1 - (\hat{S}_1 \cdot \hat{S}_2)^2} \left\{ \bar{\omega} \cdot \hat{S}_2 \, \delta\bar{S}_2 \cdot \hat{S}_1 + \delta\dot{\bar{S}}_2 \times \hat{S}_2 \cdot \hat{S}_1 + \hat{S}_1 \cdot \hat{S}_2 \, \delta\bar{S}_1 \cdot \hat{S}_2 - \hat{S}_1 \cdot \hat{S}_2 \, \delta\dot{\bar{S}}_1 \times \hat{S}_1 \cdot \hat{S}_2 \right\} \tag{37}$$

Since $S_1 \cdot S_2$ is of the same order (see Error Sources) as the errors in S and in the rate of S the Equation (37) can be simplified by elimination of the products of $S_1 \cdot S_2$ with either δS or $\delta \dot{S}$

$$\delta\bar{\omega} = \delta\dot{\bar{S}}_1 \times \hat{S}_1 + \bar{\omega} \cdot \hat{S}_1 \, \delta\bar{S}_1 + \hat{S}_1 \, \bar{\omega} \cdot \hat{S}_2 \, \delta\bar{S}_2 \cdot \hat{S}_1 + \delta\dot{\bar{S}}^2 \times \hat{S}_2 \cdot \hat{S}_1 \tag{38}$$

And

$$|\delta\bar{\omega}| = \sqrt{|\delta\dot{\bar{S}}_1|^2 + \frac{|\delta\dot{\bar{S}}_2|^2}{2} + \frac{\omega^2}{2}\left(|\delta\bar{S}_1|^2 + \frac{|\delta\bar{S}_2|^2}{2}\right)} \tag{39}$$

The derivation steps leading from Equation (38) to Equation (39) are shown under "ARS Performance in the Rate Mode".

ARS COMPUTER AND I/O LOGIC

INTRODUCTION

The objective of this study is to establish the characteristics of the digital computers necessary to satisfy the computational requirements of 12 different attitude reference systems, each utilizing two SDMEG's. The attitude reference systems are intended to provide three-axis information for control of a spacecraft similar to Voyager. The 12 systems result from variations of the following parameters:

A SDMEG (gyro) configuration

(1) The SDMEG developed under contract No. 950607

(2) SDMEG with caging capability

(3) SDMEG with torquing capablity

B The attitude reference system (ARS) outputs

(1) Three-axis attitude error and attitude rate

(2) Three-axis attitude error only

C Accuracy

(1) High accuracy

(a) Computer output error less than 0.01 degree

(b) Updating of attitude rate information 100 times per second and attitude information 10 times per second

(2) Low accuracy

(a) Computer output error less than 0.1 degree

(b) Updating of attitude rate information 10 times per second and attitude information once per second

Varying the seven parameters results in the following 12 system configurations for which the ARS computer requirements are to be determined.

ARS No. 1 = A(1) B(1) C(1)

ARS No. 2 = A(1) B(1) C(2)

ARS No. 3 = A(1) B(2) C(1)

ARS No. 4 = A(1) B(2) C(2)

ARS No. 5 = A(2) B(1) C(1)

ARS No. 6 = A(2) B(1) C(2)

ARS No. 7 = A(2) B(2) C(1)

ARS No. 8 = A(2) B(2) C(2)

ARS No. 9 = A(3) B(1) C(1)

ARS No. 10 = A(3) B(1) C(2)

ARS No. 11 = A(3) B(2) C(1)

ARS No. 12 = A(3) B(2) C(2)

From the point of view of computer design, the two gyro configurations with the capability of caging or torquing are the same. On the basis of computer design then. ARS configurations 5 through 8 have the same requirements as ARS configurations 9 through 12. This simplification leaves 8 ARS configurations.

- ARS No. 1 - A(1) B(1) C(1) - The flow charts of the functions to be performed for this ARS are shown in Figures 3-18 and 3-19. This system is the most complex, having the maximum number of functions to be solved in the least amount of time with the greatest accuracy. It is the system on which the choice of a computer design was based.

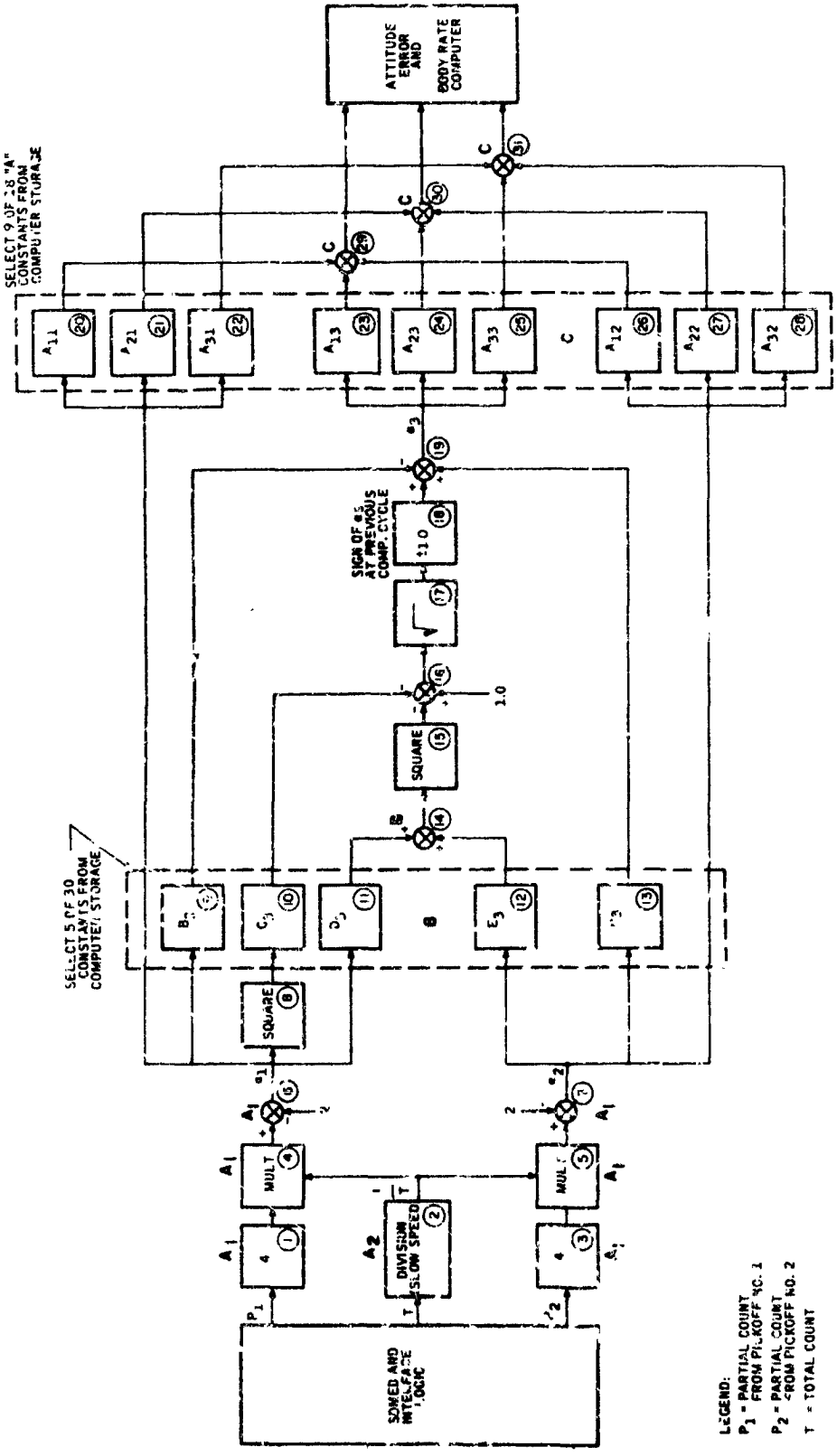

Figure 3-18. Cosine Computer Flow Chart

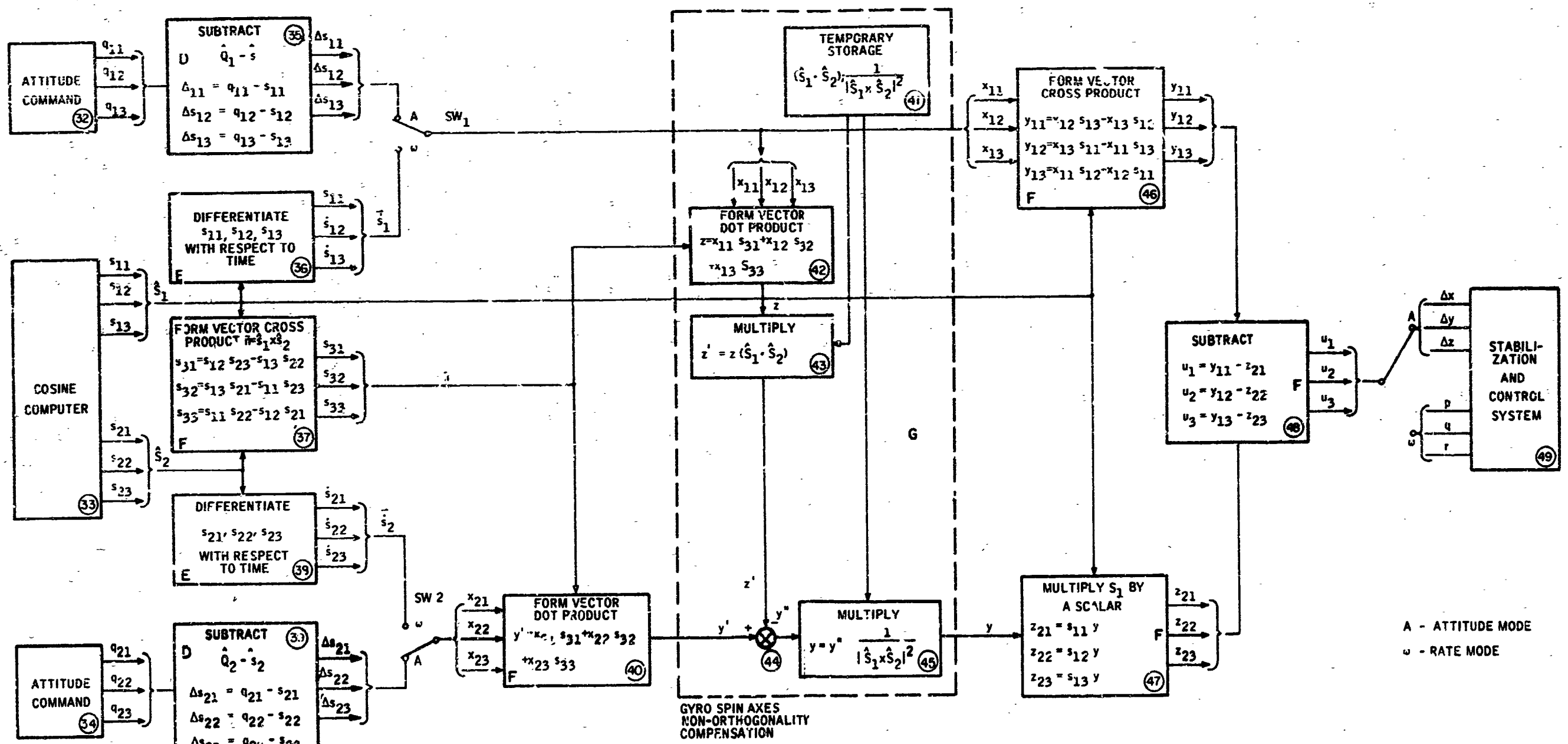

Figure 3-19. Attitude Error and Body Rate Computer Flow Chart

20113-FR1

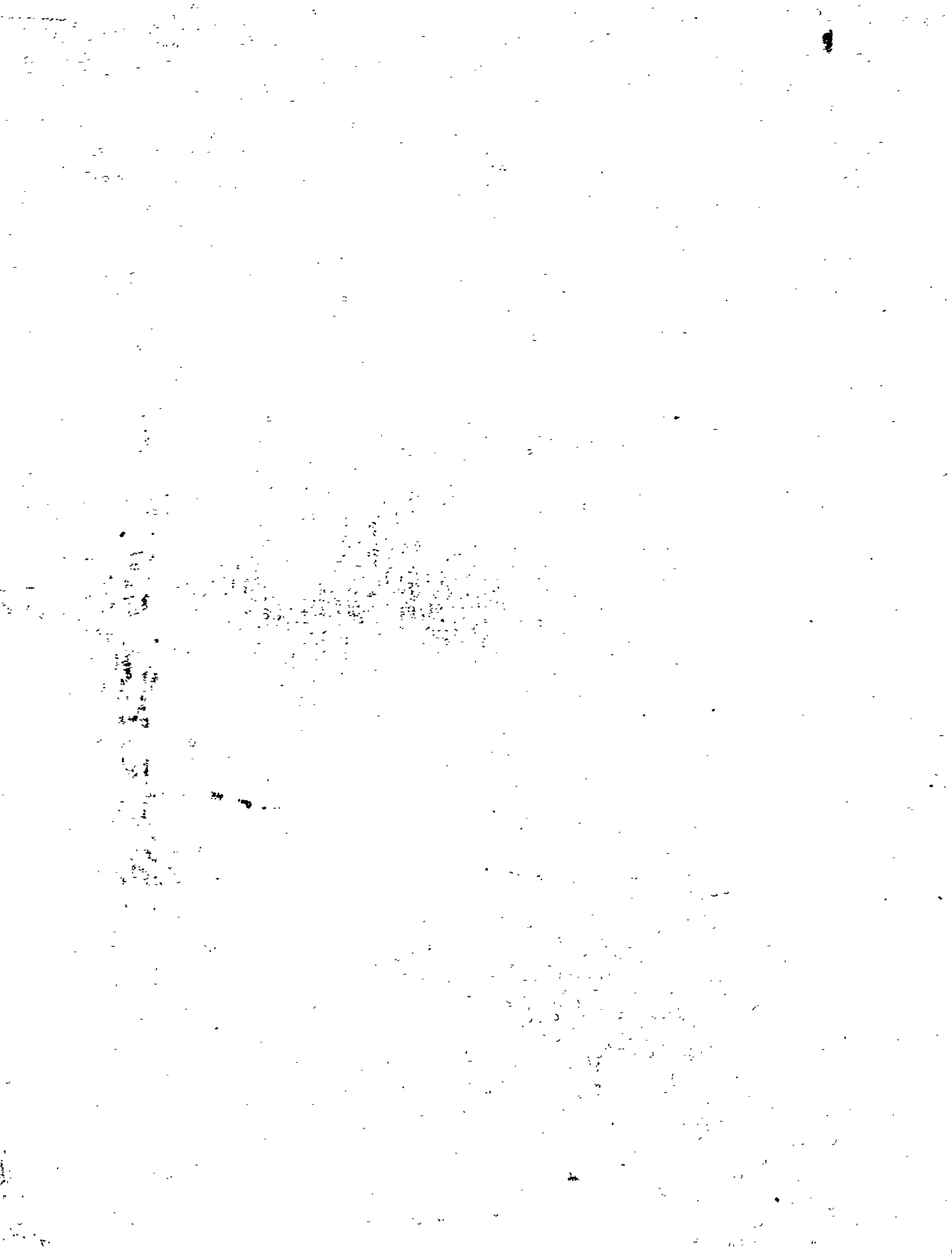

- ARS No. 2 - A(1) B(1) C(2) - Here it is assumed that the gyro pickoff non-orthogonality, pickoff axes misalignments from body axes and gyro spin axes non-orthogonality will have magnitudes such that the total effect will contribute less than 0.19-degree error at the output. The following modifications can be made to the flow charts of Figures 3-18 and 3-19:

  Eliminate the constants in Blocks 9-13

  Eliminate blocks 9, 11 and 13 (constants = 0)

  Blocks 10 and 12 are unity multipliers

  Eliminate 18 constants (Blocks 20-28, Figure 3-18)

  Eliminate blocks 21, 22, 23, 24, 26, 28

  Blocks 20, 25 and 27 have unity multipliers

  Eliminate blocks 41, 42, 43, 45

- ARS No. 3 - A(1) B(2) C(1) - Eliminate blocks 36 and 38

- ARS No. 4 - A(1) B(2) C(2) - Incorporate all modifications made in ARS 2 and 3

- ARS No. 5 - A(2) B(1) C(1) - Eliminate blocks 41, 42, 43, 45

- ARS No. 6 - A(2) B(1) C(2) - Using the assumption introduced for ARS No. 2, this configuration is the same as that for ARS No. 2 - A(1) B(1) C(2)

- ARS No. 7 - A(2) B(2) C(1) - This configuration is the same as ARS No. 3; in addition eliminate blocks 41, 42, 43, 45

- ARS No. 8 - A(2) B(2) C(2) - The capability of torquing or caging is immaterial for a system of low accuracy. The computer flow chart for this configuration is the same as ARS No. 4 - A(1) B(2) C(2).

On the basis of computer requirements, there are six different systems:

- ARS No. 1
- ARS No. 2, 6, 10
- ARS No. 3
- ARS No. 4, 8, 12
- ARS No. 5, 9
- ARS No. 7, 11

Using these six systems, the study was broken down into four areas of investigation:

- Gyro interface logic
- Gyro startup procedure
- ARS computer design
- Telemetry-computer interface

The design of the ARS-SDMEG systems presented here is based on the following information for these four areas of investigation.

Gyro Interface Logic

The basic information derived from the ESG is of an analog nature. It is in the form of two time intervals which are related to the gyro attitude. The interface logic transforms these analog data into binary numbers suitable for use in a digital computer. The acquisition of the two time intervals is complicated by the fact that there are three intervals available from the ESG and only two have valid data. The decision as to which pickoffs have valid data must be made in the interface logic or in the computer.

The design of the gyro interface logic is also influenced by the rate at which data is required in the computer. Data must be available from the SDMEG at least as fast as output data is required from the computer. Where data is required at much lower rates, an I/O configuration can be chosen to minimize hardware.

Gyro Startup Procedure

Since the gyro probably will not be able to survive a launch while suspended, it is necessary to start the gyro in space. Assuming a cosine rotor pattern, this gyro is most accurate if the startup ensures the correct rotation direction of the rotor. The startup procedure involves the transmission of a number of discrete commands (spin, damp, reverse, etc.,) to the gyro which are conditional to past and present states of the gyro. This procedure can be accomplished by either a "black box" which generates the commands at preset intervals or by a stored routine in the computer.

The ARS Computer

Given the data from the ESG in the form of a binary count, the following quantities are computed:

- Three-direction cosines for each of the two SDMEG's
- Vehicle attitude error
- Vehicle attitude rate

The computer takes the two valid digital words from the input-output logic interface and calculates two direction cosines. From these two cosines, a third direction cosine is generated. Inthis manner three direction cosines are obtained for each of the two SDMEG's. The two sets of direction cosines,

along with a set of six direction cosines received from the guidance and navigation system, are used to determine the vehicle attitude error. Also, in some of the six system configurations, attitude rate is also computed from the two sets of three direction cosines and the past history of the vehicle attitude rate

Telemetry-Computer Interface

The scope of this study does not allow for the examination of all the possible schemes for obtaining computer data for telemetry. However, three possible schemes have been selected for discussion here. These selections were made by assuming that only words in the computer memory would be required for telemetry. The main value in discussing the problem here is to indicate the flexibility of the computer in dealing with the problem of telemetry.

GYRO INTERFACE LOGIC

Input-Output

The portion of the gyro interface logic concerned with the ARS computer is called the input-output logic (I/O). The I/O deals with the time interval between pulses from the gyro and converts this time interval into a binary word by counting the pulses from a fixed-frequency source during the time between pulses. It is necessary, then, to determine the frequency of the source and the magnitude of the maximum count necessary to attain the accuracy required by the system specifications.

The following calculations are made to determine the length required in the (I/O) counters and the frequency required in the (I/O) clock. Two binary numbers are generated by the input-output logic -- a partial count (P) and a total count (T). The computer uses these binary numbers in the equation

$$\text{Cos } \theta = 4 \left(\frac{P}{T}\right) - 2$$

to determine the spin axis direction cosine (cos θ).

Neglecting second order errors, the error in the direction cosine as a function of error in (P) and (T) may be expressed as

$$\Delta \cos \theta = 4\left(\frac{\Delta P}{T}\right) - 4\left(\frac{P}{T^2}\right) \Delta T \tag{40}$$

where

$\Delta \cos \theta$ = error in $\cos \theta$

ΔP = error in P

ΔT = error in T

The errors ΔP and ΔT result from reading the counter immediately preceding the recording of a count.

Therefore,

$$\Delta P = \Delta T = 1 \text{ count}$$

and

$$\Delta \cos \theta = \frac{4}{T}\left(1 - \frac{P}{T}\right) \tag{41}$$

Since

$$0.31 \leq \frac{P}{T} \leq 0.69$$

the maximum error in the direction cosine will be

$$\Delta \cos \theta = \frac{4}{T}(1 - 0.31)$$

or (42)

$$\Delta \cos \theta = \frac{2.76}{T}$$

Since it is desired to have an accuracy in the computations equivalent to ±0.01 degree at the system output for the high accuracy systems, and 0.1 degree for the low accuracy systems, the tolerable error in the direction cosine may be expressed as follows:

In terms of the error in θ the error in the direction cosine is

$$\Delta \cos \theta = \sin \theta \cdot \Delta \theta$$

where

$\Delta\theta$ = the error in θ

Therefore, the maximum error in the direction cosine may be expressed as

$$\Delta \cos \theta = \Delta\theta$$

and for the two accuracy levels of 0.01 degree and 0.1 degree

$$\Delta \cos \theta = \frac{0.01 \times 2\pi}{360} \cong 0.000174 \text{ radian}$$

and

$$\Delta \cos \theta = \frac{0.1 \times 2\pi}{360} = 0.00174 \text{ radian}$$

Therefore, substituting these values for $\Delta \cos \theta$ in Equation (42), the following values result for the total count during a rotor period, (T):

$$0.000174 = \frac{2.76}{T}$$

or

$$T = \frac{2.76}{0.000174} = 15,900 \text{ counts}$$

For the low accuracy system

$$0.00174 = \frac{2.76}{T}$$

or

$$T = \frac{2.76}{0.00174} = 1,590 \text{ counts}$$

Therefore, to hold 15,900 counts the high accuracy system will require counters with at least 14 bits; the low accuracy systems will require counters with at least 11 bits to hold 1,590 counts.

Since the minimum period of the gyro rotor is 5 milliseconds, the frequency of the clock for the high accuracy system must be at least

$$\frac{15,900}{5 \times 10^{-3}} = 3.18 \times 10^{6} \text{ cycles per second}$$

For the low accuracy system the clock frequency must be at least

$$\frac{1,590}{5 \times 10^{-3}} = 318,000 \text{ cycles/second}$$

Gyro rundown is another factor affecting counter length. Since it is desired to maintain system integrity until the gyro rotor speed has decreased by 50 percent, the rotor period will increase from 5 milliseconds to 10 milliseconds and the counts during a period of the rotor will double.

Therefore, to accommodate this condition another bit must be added to the length of the counters, thus totaling 15 bits for the high-accuracy counters, and 12 bits for the low accuracy counters.

Gyro Readout Electronics

In normal gyro operation, a readout is obtained from only two pickoffs while the third pickoff is in the "dead zone". For this reason, only two channels of readout electronics were to be provided. This required that the electronics be switched from pickoff to pickoff as they went in and out of the dead zone. In this way, both sets of electronics were always connected to pickoffs not in the dead zone. The sensing of the dead zone and switching of electronics between pickoffs had to be done by the I/O logic. These logic decisions require additional hardware in the I/O logic. Since a general purpose computer was chosen for the ARS, it is best to use the computer as the decision maker wherever possible. For this reason, a third set of readout electronics is to be provided on the gyro, and decisions regarding the pickoff in the dead zone will be made in the computer.

Gyro Output Rate

The maximum-accuracy system requires an output rate of 10 attitude calculations per second and 100 attitude rate calculations per second. To accomplish this requires 100 direction cosine calculations per second. This in turn requires the acquisition of 100 new sets (three counts) of partial counts from each ball. (Total counts are acquired at a much lower rate, perhaps one a second, and are stored in the computer for later use in the computations.)

The maximum time for a partial count occurs for cos 40 degrees.

$$\cos 40^\circ = 4 \frac{P \max}{0.005} - 2 \quad \text{so that } P \max = 0.0035 \text{ second}$$

In the worst case, where the read heads make equal angles with the spin axis, all three heads will pass the start line in two-thirds of a ball rotation

So, to the maximum count time of 3.5 ms, is added two-thirds × 5 ms equals 3 1/3 ms to get a total of about 6.85 ms to complete the outputs of the three pickoffs from one gyro. If a separate counter is provided for each pickoff, then the set of counts can be completed in a maximum of about 6.85 milliseconds This would allow for the acquisition of over 146 sets of counts per second. This allows for a drop in ball speed to 7.3 milliseconds per revolution (137 rpm) to maintain the rate of acquisition of 100 per second. This meets the requirement of 100 sets of partial counts but requires that both gyros have a set of three counters. So, for the maximum information rate (100 direction cosines per second), a six-counter system is required, but the ball speed may not drop below 137 rpm.

Having devised an I/O scheme for the system of maximum output rate (100 per second), it remains to devise one for those systems of lower output rates (10 per second or less). If a single counter is used to acquire counts from all six channels, one at a time, then the maximum total time required for the six acquisitions is 6 × 5 ms = 30 milliseconds. For the 10 acquisitions per second needed in the systems of lower computation rate, there are 100 milliseconds per acquisition. This makes the one-counter system feasible.

The requirement, then, is for only two I/O systems -- a six-counter system for the highest computation rates (100 per second) and a one-counter system for all other computation rates (10 per second or less).

I/O System Operation

The Six-Counter System -- Figure 3-20 is the logic diagram of the channel counter and logic for one channel of the six-counter I/O system. One such logic configuration is used in the single-counter system and six are used in the six-counter system.

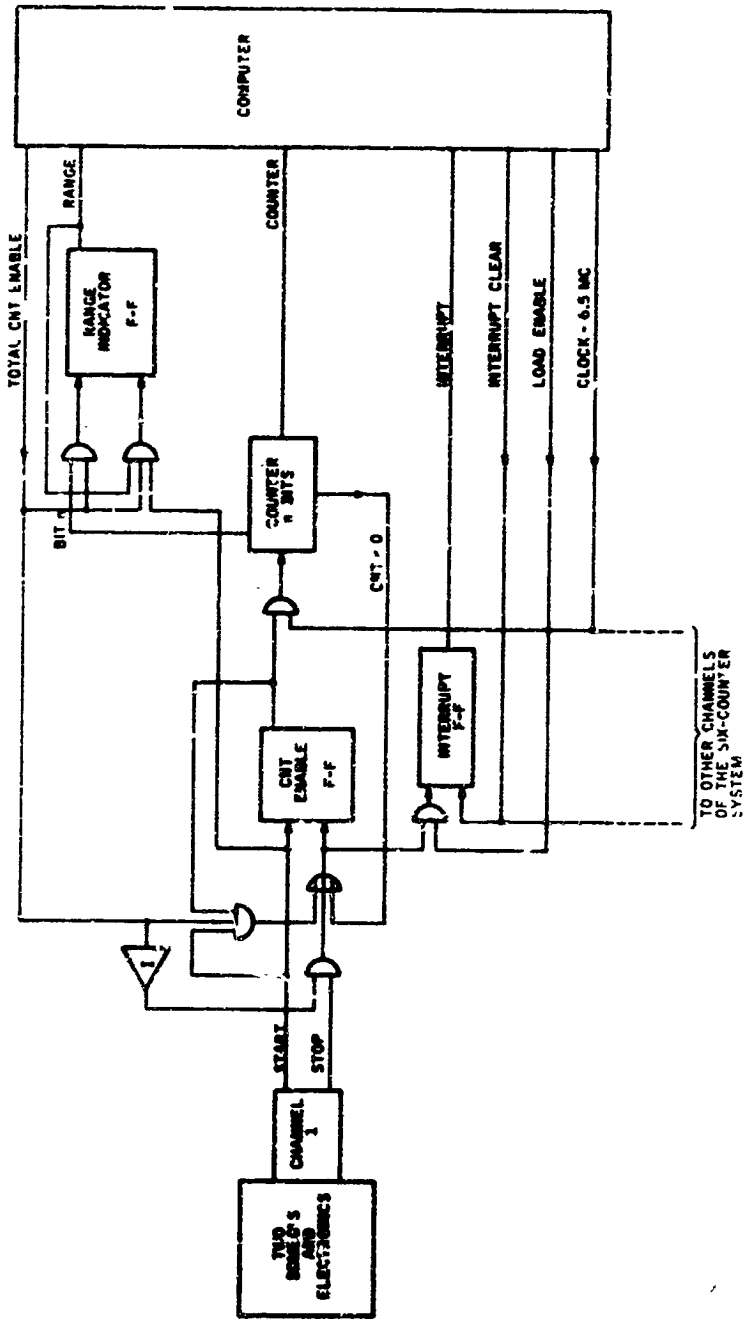

Figure 3-20. Single Channel of Six-Counter System of Gyro-Computer Interface Logic

The following sequence occurs for the acquisition of counts. The decoding of the appropriate I/O instruction sets a flip-flop in the computer, causing the "load enable" line to go to a "one" state and the computer program resumes operation. The "load enable" line, being at a "one", opens the gates to the counter and the interrupt. The I/O is now ready to send data to the computer.

For acquisition of partial counts, the "total count enable" line is a zero. A start pulse from the gyro sets the "count enable" flip-flop which gates the clock into the counter. The counter continues counting until a stop pulse clears the "count enable" flip-flop. If the pickoff is near the dead zone so that no stop pulse occurs, the counter counts through to zero, stops, and generates a pulse to clear the "count enable" flip-flop. (If the pickoff is not in the dead zone the count will be finite, if the pickoff is in or on the edge of the dead zone, the count will be zero.) The clear pulse to the "count enable" flip-flop also sets the "interrupt" flip-flop. On receiving an interrupt, the computer completes its current instruction. The interrupt causes the computer to enter a short subroutine which loads the counter contents into the computer memory. The computer then clears the interrupt flip-flop and resumes operation in the main program. The next start pulse from the gyro starts the cycle over again.

For acquisition of total counts, operation of I/O logic is the same as that for partial counts except for the following: The "total count enable" line is a "one" as a result of the computer. The "count enable" flip-flop will be set by a start pulse and will be cleared by the next start pulse so that the counter counts for a full revolution of the bail.

It was shown previously that an extra bit was necessary in the counter to accommodate the large counts resulting from gyro rundown but not necessary to retain the extra bit in the computer calculations. The "range indication" flip-flop is included to determine whether the most significant bits or the

least significant bits of the count are loaded into the computer. When total counts are required and the "total count enable" line is a "one" the "range indication" flip-flop will be set when the most significant bit of the counter is a one. When the range signal to the computer is a "one", the most significant bits of the total count and all subsequent partial counts will be loaded into the computer. When the range signal is a "zero", the least significant bits will be loaded. The "range indicator" flip-flop will be cleared when a new total count is taken and the first start count occurs.

The One-Counter System -- Where as the six-counter system is made up of six of the configurations just described, the one-counter system (Figure 3-21) uses only one of these configurations, the main difference being that each of the six sets of readout channels must be connected in turn to the "channel counter and logic" previously described. This is done by having the interrupt signal increment a modulo six counter. The new value of the count connects a new channel to the "channel counter and logic" through the "channel select logic". The new channel is counted up and an interrupt is generated to increment the modulo six counter and continue the process. The six channels will continue generating counts, in turn, as long as the "count enable" line is a "one". As before, the state of the "total count enable" line determines whether the outputs of the I/O are total or partial counts.

GYRO STARTUP

Given a general purpose computer, the gyro startup procedure can be accomplished with a stored program. This works particularly well for startup because the computer will not be doing anything else. A programmed startup procedure requires the low-speed real-time clock included in the computer, to time intervals up to one hour. Figure 3-22 is a program flow diagram for the gyro startup routine. It is estimated to require about 75 instructions to mechanize.

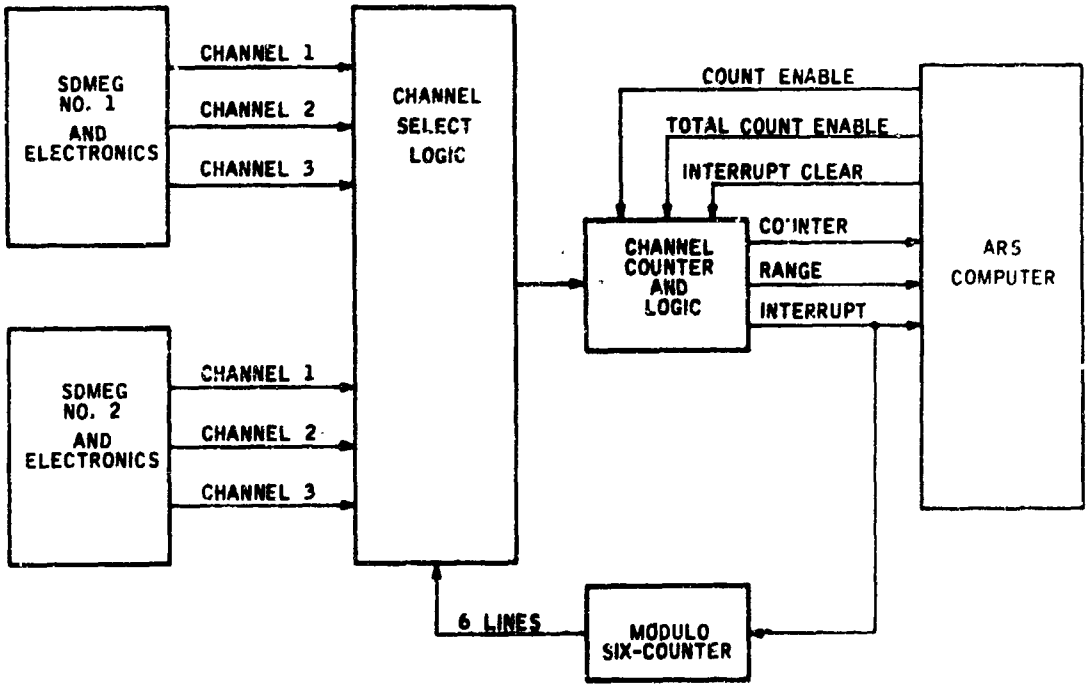

Figure 3-21. One-Counter System of Gyro-Computer Interface Logic

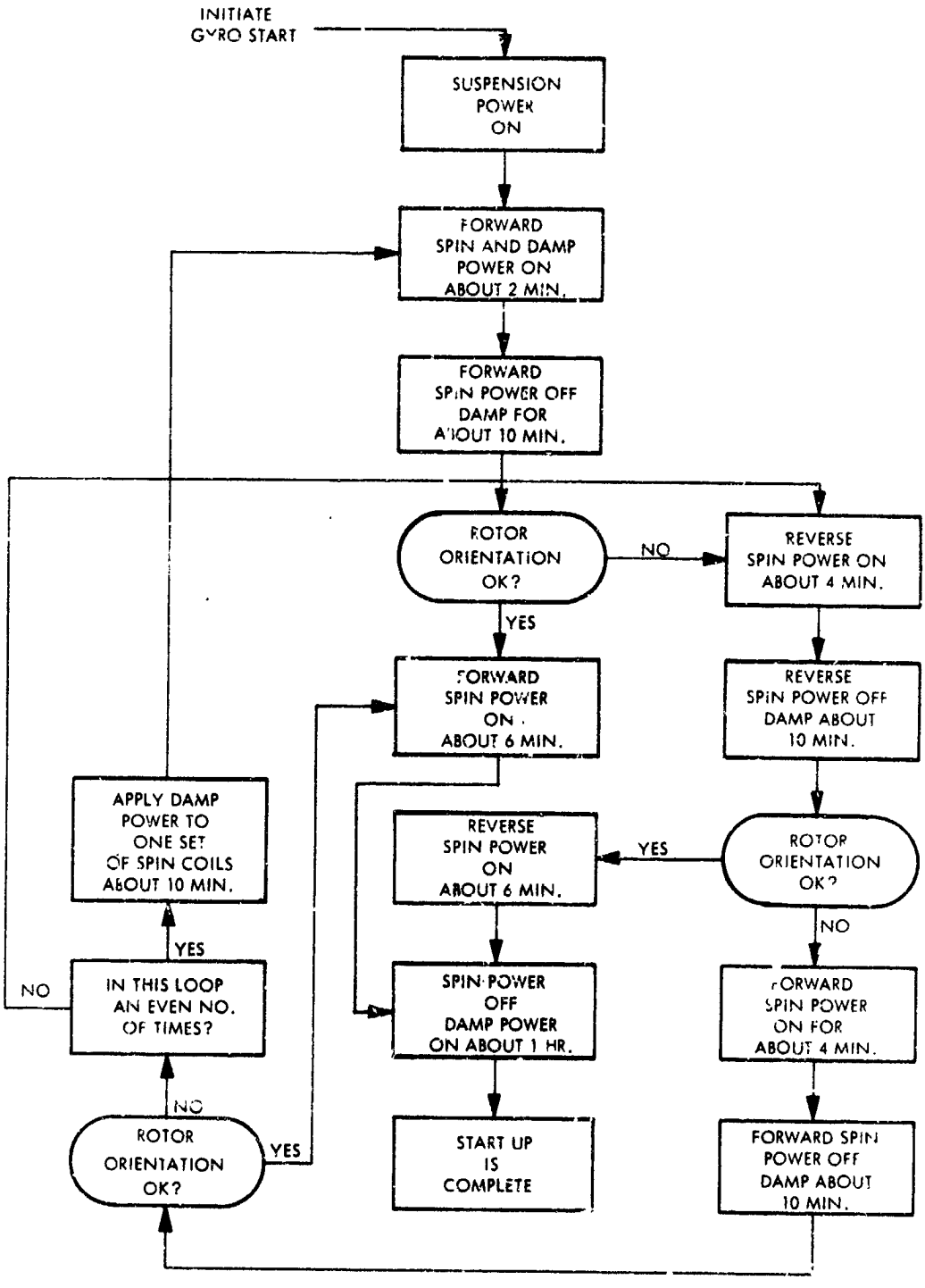

Figure 3-22. Flow Diagram For Gyro Startup Program

THE ARS COMPUTER

In the time available for this investigation, it was not possible to study each of the six different systems and determine an optimum computer configuration for each. Instead, a computer was designed for the maximum complexity system, and portions of this computer were modified or removed as necessary to satisfy the requirements of each of the other systems. In the following discussion, most of the material pertains to the maximum-complexity system.

Selection of Computer Type

The computer for the maximum-complexity ARS could take any one of several forms. The three computer types that might be considered for this application are (1) special-purpose incremental, (2) special-purpose total-value, and (3) general-purpose, stored-program total-value. An approximate comparison of the complexity of each of these three mechanizations under the constraints imposed by this problem is made in the following paragraphs.

Each of the classes of computers mentioned usually is applied to a specific class of problems. General-purpose, total-value computers are used when the computing rates are not excessively high and when a wide variety of problems must be solved. Special-purpose computers are usually employed in situations where a specific type of problem must be solved repeatedly, particularly when it must be solved at a moderately high rate. Incremental computers can be used when the inputs are smoothly varying functions and are particularly useful when extremely high output rates are required. Special-purpose computers as a class increase in complexity with the size of the job and require considerable amounts of hardware for sequencing and controlling the arithmetic operations when a large number of computations must be performed. Also, when a new computational task is required of a special-purpose computer, it usually results in a significant increase in the amount of hardware. On the other hand, in a general-purpose computer, if there is sufficient time remaining in the computational cycle and enough extra memory capacity, additional tasks can often be added without increasing the hardware requirements.

A total of approximately 120 computations is required in the maximum complexity ARS. Of these, approximately 63 are long operations, such as multiplications and divisions, and approximately 57 are short operations, such as additions and subtractions. Some of these computations are performed only once, others are repeated 10 times, and the remaining computations must be repeated 11 times during each computer iteration period. This results in a total of about 1250 computations that must be made during each computer iteration. Since the computer iteration rate is 10 per second, a total of approximately 12,500 computations must be made each second. Of these, approximately 7000 are long computations, and the remaining 5500 are short computations. If we multiply the number of long computations times 16 (16 bits per word) and add to this the number of short computations, we obtain a figure of 117,500. This is roughly the equivalent number of short computations that must be performed by the computer each second. Thus, we have approximately 8.5 microseconds to do each equivalent short computation if they are done sequentially by a total-value computer. This should be more than adequate for either a general-purpose or special-purpose mechanization.

Incremental computation techniques might also be used, since the inputs are continuous functions of time. For a maximum input rate of approximately seven radians per second and with 14-bit direction cosines, the required iteration rate of an incremental computer employed in the solution of these equations can be computed as follows:

$$\text{Minimum Increment Rate} = \frac{1 \text{ increment}}{2^{-14}} \times \frac{7}{\text{second}}$$

$$\approx 115{,}000 \text{ increments/second}$$

Thus, the maximum input and output rate of each computation would be approximately 115,000 increments per second, which corresponds to the minimum iteration rate. Assuming serial/parallel bit processing and a 1.5-megacycle clock rate, each computation would require a minimum of

four microseconds. The computer operates in a 4-bite serial, 4-bit parallel fashion, requiring 2-2/3 microseconds for processing 16 bits, and 1 microsecond for memory access of the operand, totaling about 4 microseconds for the operation. Therefore, at most, two computations could be performed sequentially during each iteration by each arithmetic unit, and a total of about 6000 arithmetic units would be required. Thus, the number of components required by an incremental computer would be many times the number required of a general-purpose computer that performs the same job. Even if special techniques such as variable or multiple increment operation were used, many arithmetic units would be required, and each of them would be more complex than those of a single-increment computer.

Incremental computation is therefore not practical, leaving a choice between the two types of total-value computation -- general-purpose and special-purpose. A special-purpose computer to perform these computations would require a very large and complicated control section to sequence the operations properly. In addition, other tasks, such as the startup routine, would require either additional hardware or additional control section complexity. It would therefore require less hardware if a general-purpose computer were employed, since the startup instructions could be stored in a portion of the memory, and a small control section could be included for interpreting them.

A general-purpose total-value mechanization has been selected for the following reasons:

- It requires less hardware than an incremental mechanization in this particular case.
- It requires somewhat less hardware than a total-value special-purpose mechanization and is much more flexible, allowing for the addition of new tasks at a later date.

- A simple serial/parallel total-value mechanization is permissible with the computation rates required of this problem, yet a large portion of the computation cycle remains available for additional tasks.

- The arithmetic unit can be time-shared to perform appropriate functions in different modes. For example, during startup the ARS computations need not be made, and the entire computation cycle is available for the startup program.

Description of Computer

The block diagram of the proposed general purpose computer for the maximum complexity ARS is shown in Figure 3-23. It consists of three main sections -- memory, arithmetic, and control -- along with input and output registers and a source of computer clock. The memory and control sections are of relatively conventional design. The arithmetic unit, which operates in a serial/parallel mode, consists of two serial/parallel registers, a serial/parallel adder-subtractor, and the necessary logic for performing the time-dependent interconnections of these units. The input registers contain 16 data bits along with address bits and an interrupt bit. They are loaded asynchronously from outside the computer and transferred to the computer memory by halting the normal operation of the computer as soon as possible after the interrupt bit becomes a "1". The output registers are loaded from the accumulator by instructions stored in the memory. The number of input and output registers depend on the requirements of each of the 12 different systems.

Memory -- Three classes of memories were considered for the ARS computer:

- The fixed memory, such as prewired plugboard, core ropes, or the class of reactive element coupling devices in which the information is stored in the absence or presence of a material deposited on a substrate.

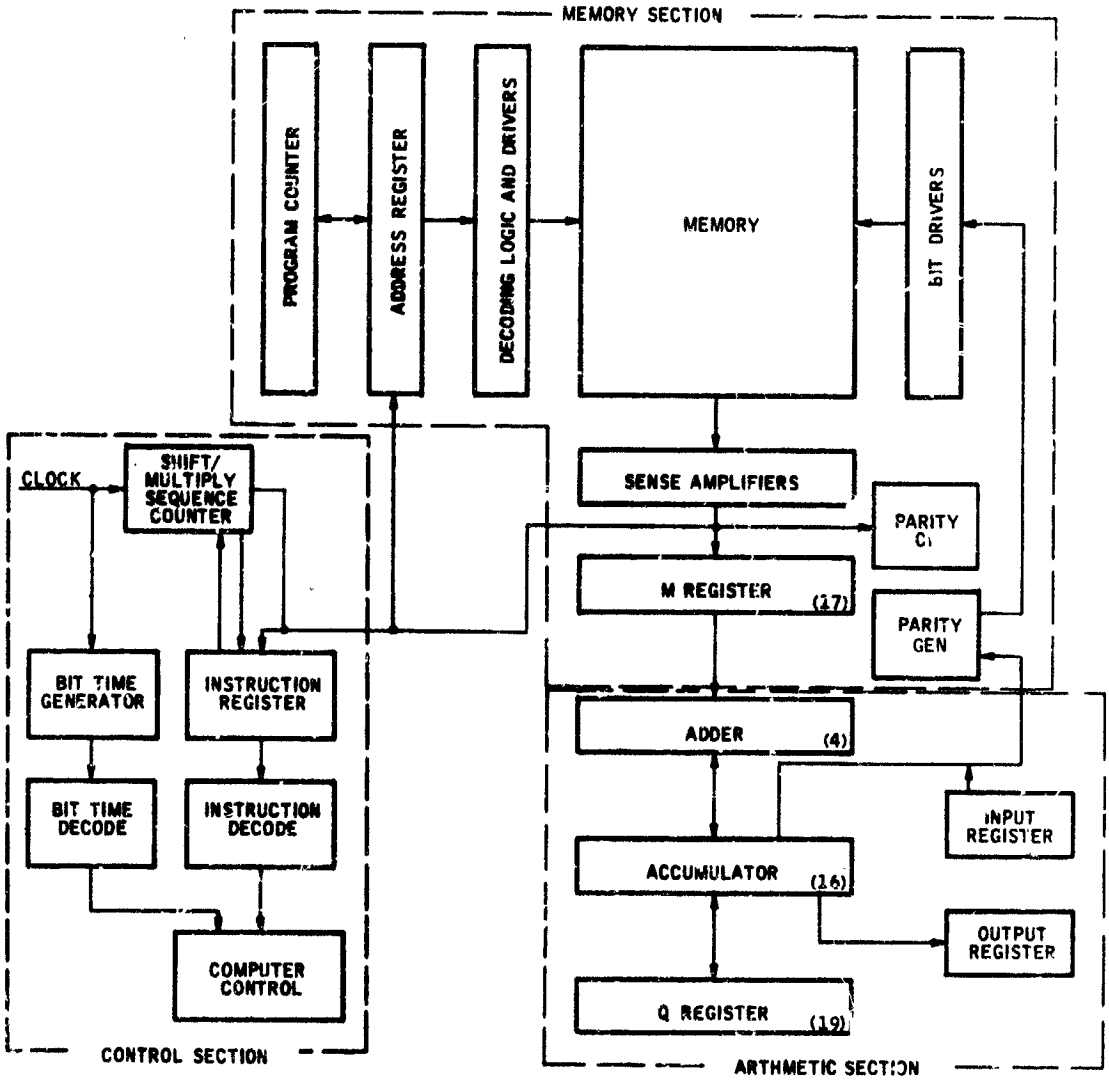

Figure 3-2. Computer Block Diagram

- Nondestructive readout (NDRO) memories in which information contained in memory is unaltered when read. The NDRO memory is generally composed of two-hole storage devices in which information is written in the device through one hold and read from the other hole.

- Destructive readout (DRO) memories in which the reading of a word destroys the memory content so that it must be rewritten after each readout. This type of memory is generally composed of tiny toroids (one for each bit). It is the memory most commonly used in large ground-based computers.

The fixed memory was elimirated from consideration because it is necessary to have the capability of altering the contents of some memory locations in the ARS computer programs. The fixed memory does not have this capability. It would be possible to have fixed memory for the fixed portions of the program and a variable memory for the variable portions of the program. This alternative was eliminated because of the additional hardware required to operate two independent memories. The choice, then, is between the NDRO and the DRO memories.

The DRO memory dissipates about twice as much power as the NDRO memory. The difference is due to the fact that read and write currents of equal magnitude are necessary to read or write in the DRO memory. In the NDRO memory, only a read or write current is necessary. Therefore on the basis of power considerations the NDRO memory was selected for the ARS computer and the hardware requirements of the ARS computer memory will be based on the NDRO configuration.

The memory will contain up to 1024 words. The number will vary with the computational needs of the 12 attitude reference systems. Each word will be 17 bits long. Sixteen bits are for an instruction or data and one bit is for parity. It is generally considered advisable to do error checking at

the computer memory because it is the least reliable portion of the computer. Although it is probably desirable to do some form of error detection in other portions of the computer, the scope of this study does not allow for a full investigation of these needs.

Memory speed requirements are not very severe in this application. Therefore a conservative state-of-the-art NDRO memory with a write time of 4 microseconds and a read time of 1 microsecond will be postulated. It will be seen later that these memory speeds are adequate for the maximum complexity ARS.

A block diagram of the memory section is shown in Figure 3-23. The address register contains the address of the memory word currently in use. This address is decoded and used to enable the proper driver-switch pair which in turn causes either a read or a write to occur upon receipt of the appropriate pulse from the control section. The memory register (M) serves several functions: During a read operation it holds the output word after it is read out of the memory. If the output word is an instruction, the instruction code field is sent to the instruction register and the address field is sent to the address register, both of these transfers being effected in parallel. If the output word is an operand, it is used in serial/parallel form by the arithmetic section.

Arithmetic Section -- The arithmetic section for the maximum complexity ARS contains two registers -- A and Q. The A register is the accumulator which always holds the result of the last operations. For simple operations such as adds, subtracts and shifts, it is the only one of these registers used. During add (subtract) operations, the contents of M is added to (subtracted from) the contents of A directly without any intermediate transfer of the contents of M. For the multiply operation, the multiplicand is held in A, the multiplier is held in M and the double length product forms in A and Q. For the simpler systems in which a programmed multiply is used, the Q register is omitted since it is not necessary.

The adder-subtractor is a logic network that performs serial/parallel addition, subtraction and counting on the input words. The arithmetic timing and control logic implements the subcommands inherent in each operation by making a suitable interconnection of the registers and the adder-subtractor. The required timing is obtained by controlling the shift pulses.

Control Section -- The instruction register of the control section receives the instruction code bits from the M register. They are then decoded, and the appropriate signals are formed and sent to the arithmetic section to perform the required operation. For multistep operations, such as multiply, the iteration counter is used to count and identify each step in the operation. The P counter holds the address of the current instruction, and, at the end of each operation, it is stepped by one count to obtain the address of the next instruction. The control section also controls the reading and writing operations in the memory by means of pulses transmitted at the appropriate times. Interrupt signals are received by the control unit which, in turn, causes the required actions to occur.

Computer Parameters

Some important computer parameters have been omitted in the discussion to this point. These consist of clock rate, memory size, data word length, instruction list and instruction word format. The factors that affected the choice of these parameters and the resulting selections are discussed in the following subsections.

Data Word Length -- The number of binary digits or the length of the computer data word is determined by the accuracy required in the computer output. The desired accuracy in the output of the maximum accuracy computer is 0.01 degree or approximately 0.00017 radian. To establish the relationship between the computer output accuracy and the tolerable error in the round off of the data words, the computer output is assumed to be the product of 12 data words.

Therefore, the error in the product may be related to the roundoff error in the data words as

$$\Delta(X_1 X_2) \ldots X_{12}) = \Delta X_1 (X_2 X_3 \ldots X_{12}) + \Delta X_2 (X_1 X_3 \ldots X_{12}) + \ldots + \Delta X_{12} (X_1 X_2 \ldots X_{11})$$

Since, in the product, the factors will be direction cosines, the factors will have a maximum value of unity, and

$$\Delta(X_1 X_2 \ldots X_{12}) \leqq \Delta X_1 + \Delta X_2 + \ldots \Delta X_{12}$$

From statistics, the variance of a sum of random variables is the sum of the variances for the individual variables. Therefore

$$\sigma_p^2 \leqq \sigma_1^2 + \sigma_2^2 + \ldots + \sigma_{12}^2$$

where

σ_p^2 = variance of the error in the product

σ_i^2 = variance of the error in the individual data words of the product

Since the error in the data words is due to roundoff and the words are direction cosines rounded to the same number of digits, it is reasonable to assume the errors will have equal statistics. Therefore

$$\sigma_p^2 = 12\,\sigma^2$$

where

$$\sigma^2 = \sigma_i^2 \qquad i = 1, 2 \ldots 12$$

Assuming the roundoff error of the data words in the product is uniformily distributed on (-0.5ξ, $+0.5\xi$) and, from the definition of variance, we obtain

$$\sigma^2 = \int_{-0.5\xi}^{+0.5\xi} (\Delta X)^2 \frac{1}{\xi} d(\Delta X)$$

where

ξ = scaling of least significant bit in the data word

or

$$\sigma^2 = \frac{(\Delta X)^3}{3\xi} \Bigg|_{-0.5\xi}^{+0.5\xi}$$

$$\sigma^2 = \frac{\xi^2}{12}$$

Therefore

$$\sigma_p^2 = \xi^2$$

$$\sigma_p = \xi$$

Since the error in the product is made up of 12 errors with uniform distribustions, the probability distribution of the error in the product will be approximately Gaussian. Therefore, the error in the product will be less than ξ 68 percent of time, less than 2ξ 95 percent of the time, and less than 3ξ 99 percent of the time. It is desired to have the error in the computer output, or product, less than 0.00017 radian. If it is satisfactory to have this occur 68 percent of the time, then the scaling of the least significant bit in the data word may be 0.00017. Since the direction cosines in the

product have a maximum value of unity, the data word length must have a range of 1/0.00017 or 5880. This will require a word length of 13 bits, but, to avoid noninteger scaling within the computer, the word length is selected to have 15 bits plus sign or 16 bits.

Clock Rate and Memory Size -- To obtain the data essential to establishing clock rate, memory size, and instruction requirements, it was necessary to formulate an approximate computer program for the ARS computations based on a preliminary list of instructions. The instructions in the program were then divided into two groups, the first consisting of those containing long operations (multiplications) and the second consisting of those containing short operations (additions and subtractions). The instructions in the second group that contained operations requiring a "write" operation in memory were also tabulated in a third group.

The divide and square root operations appear only once, and, since the direction cosines are continuous functions of time, it is possible to replace these operations by iterative subroutines such as the following:

$$\text{Divide: } \mu_{n+1} = \mu_n(2 - \mu_n b)$$

where

$$\mu_n \to \frac{1}{b} \text{ as } n \to \infty$$

$$\text{Square root: } x_{n+1} = \frac{1}{2}\left(x_n + \frac{a}{x_n}\right)$$

where

$$x_n \to \sqrt{a} \text{ as } n \to \infty$$

The magnitude of n need not be very great in continuous, real-time situations such as this, since we can use the previously computed value of μ or x as the initial value for each new iteration. In fact, worst-case calculations have shown that from 3 to 5 iterations of these formulas are sufficient to achieve the required accuracy, depending on the computer iteration rate of the particular system configuration. Thus, the proper number of multiples of the operations required to implement the iterative formulas above are included in the instruction count rather than the two operations.

For the maximum-complexity ARS, a total count of 2958 short operations, 890 "write" operations, and 773 long operations was obtained. Since with a 16-bit word length, a long operation takes approximately 16 times as long to execute as does a short operation, we obtain

$$890\left(\frac{3}{2}\right) + 2958 + 773\,(16) = 16,661 \text{ equivalent short operations}$$

For a 16-bit word length and a 1.5-megacycle clock rate, a serial/parallel word time (which corresponds to the execution of a short operation) is 4 microseconds. Thus, the operations themselves required 16,661 (4) = 66,644 microseconds. Since 100,000 microseconds are available during each computer cycle for the maximum complexity ARS, approximately one-third of the computer time is available for processing I/O interrupts and any other computations that may be necessary.

The actual number of instructions that must be stored in the memory is about 300. In addition, approximately 145 instructions are required for the startup program, subroutines, bookkeeping and input-output. Approximately 100 memory locations are required for variable or scratchpad storage and 50 for storage of constants. Thus, a total of at least 595 storage locations are required for the maximum-complexity ARS computer. A memory size of 1024 words will be assumed, since this represents the next largest power of two. A 10-bit address field is required to specify a memory of this size.

Instruction Word Format -- The ARS computer word, based on the accuracy requirements of the more accurate systems, contains 15 binary digits (bits), numbered 0 through 15 starting at the left:

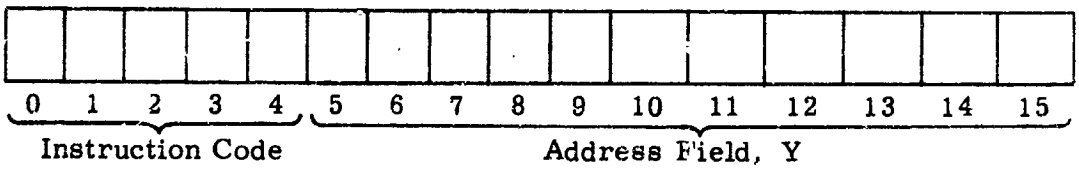

Bits 5 through 15 are used to determine the memory address referred to by the instruction code. The 11-bit field can address up to 2048 words in memory.

The five bits, 0 through 4, are used to represent 32 different instructions (add, subtract, jump, etc.). Since the required tasks can be accomplished in the ARS computer with fewer than 32 instructions, not all combinations of the five bits are used.

In the simpler systems, a 12-bit word is used and is broken down into a nine-bit address field, capable of addressing 512 words, and a three-bit instruction code representing eight different instructions.

Instruction Repertoire

Following is a list of the instructions that are available for programming the ARS computer. Along with each is a brief description of the instruction. Except for the instruction which deals with some of the special requirements of input-output equipment, the list is composed of instructions commonly used in digital computers. Some of these instructions will not be used in the simpler systems.

(1) ADD (A) + (M) → A (Add) -- Contents of the addressed cell in memory are added to the contents of the accumulator; the sum being placed in the accumulator. Execution time is 4 microseconds.

(2) SUB (A) - (M) → A (Subtract)-- Contents of the addressed cell in memory are subtracted from the contents of the accumulator, the difference being placed in the accumulator. Execution time is 4 microseconds.

(3) CAD (M) → A (Clear and Add) -- Contents of the addressed cell in memory are transferred to the accumulator. Execution time is 4 microseconds.

(4) CSB -(M) → A (Clear and Subtract) -- The (2's) complement of the addressed cell in memory is transferred to the accumulator. Execution time is 4 microseconds.

(5) NEG -(A) → A (Negate) -- The (2's) complement of the accumulator is formed and placed in the accumulator. Execution time is 4 microseconds.

(6) WRT (A) → M (Write) -- Contents of the accumulator are transferred to the addressed cell in the scratch pad memory. Execution time is 6 microseconds.

(7) MPY (A) × (M) → A, Q (Multiply) -- Contents of the addressed cell in memory are multiplied by the contents of the accumulator. The most significant half of the product is formed in the accumulator, and the least significant half is formed in the Q register. Execution time is 65 microseconds.

(8) SMY $\left|\frac{1}{2}A\right|$ × $\left|\frac{1}{2}M\right|$ → A (Short Multiply) -- Contents of the most significant half of the addressed cell in memory are multiplied by the contents of the most significant half of the accumulator; the product being formed in the accumulator. Execution time is 17 microseconds.

(9) LQP (A) $\wedge$ (M) → A (Logical Product) -- The logical bit-by-bit product of the contents of the addressed cell in memory and the contents of the accumulator are formed in the accumulator. Execution time is 4 microseconds.

(10) LQS (A) $\vee$ (M) → A (Logical Sum) -- The logical bit-by-bit sum of the contents of the addressed cell in memory and the contents of the accumulator are formed in the accumulator. Execution time is 4 microseconds.

(11) SHR (A) × 2^{-N} → A (Right Shift) -- Contents of the accumulator are shifted to the right N bits specified by the operand address portion of the instruction ward. The sign is extended in the high order end of the accumulator. Execution time is 2 + 2/3N microseconds.

(12) SHL (A) × 2^{N} → A (Left Shift) -- Contents of the accumulator are shifted to the left N bits specified by the operand address portion of the instruction ward. Zeros are inserted into the low order end of the accumulator. Execution time is 2 + 2/3N microseconds.

(13) ATQ (A)←→(Q) (A-Q exchange) -- Contents of the accumulator and the Q register are exchanged. Execution time is 2 microseconds.

(14) BPA (Addr.) → iff (A) ≥ 0 (Branch if Positive) -- If the contents of the accumulator are positive, the contents of the address register are written into the program counter. Execution time is 2 microseconds.

(15) BZA (Addr.) → P iff (A) = 0 (Branch if Zero) -- If the contents of the accumulator are zero, the contents of the address register are written into the program counter. Execution time is 2 microseconds.

(16) BMA (Addr.) → P iff (A) < 0 (Branch if Minus) -- If the contents of the accumulator are negative, the contents of the address register are written into the program counter. Execution time is 2 microseconds.

(17) JMP (Addr.) → P (Branch Unconditionally) -- Contents of the address register are written into the program counter. Execution time is 2 microseconds.

(18) OUT (Output) -- This instruction is used when it is necessary to transfer data from the computer to the output register. This instruction differs from the other instructions in that the operand address field is a "function code. The "function code" is decoded in the output register to determine the piece of output equipment being dealt with. In this manner a single instruction can deal with the output needs of all the equipment which receives information from the computer in this system.

Interrupt Operation -- Interrupt operation allows the computer program to operate normally except for the short time it takes to load the input register into the computer memory.

As the main computer program is running, a piece of auxiliary equipment becomes ready to transmit a word to the computer. Operation is as follows: The auxiliary equipment sends an interrupt signal to the computer (a single line going to a "one"). On receiving the interrupt, the computer stops executing the main program upon completion of the current instruction. A particular memory address, determined by the interrupt, is read out. (Each interrupt line has associated with it one particular memory location.) The word read out of this address is a jump instruction to a short subroutine which will load the input data word in a manner prescribed by the subroutine. Upon completion of the subroutine a jump is made back to the main program.

Computer Descriptions for 12 ARS

Earlier in the study, 12 ARS systems were synthesized on the basis of the variation of certain system parameters. It was also shown that, on the basis of the computer requirements, there are only six different systems. In this subsection it is shown that three different systems of computer hardware are adequate to satisfy the computer requirements of the six systems. In other words, some of the six systems require identical hardware even though they do computing jobs of different complexity.

Instruction Count -- As previously stated, an approximate program was written for the ARS computations. Not all of these computations are required of all six systems. The number of computations for each of the systems is grouped by computing function in Table 3-10. The letters A_1, A_2 through F at the extreme left of Table 3-10 serve as a key between the instruction count of Table 3-10 and the calculations indicated in Figure 3-18 and 3-19.

Table 3-10. Instruction Count

Key (see Figures 5 and 6)	L	S	Wr	ARS 1			ARS 2, 6, 10			ARS 3			ARS 4, 8, 12			ARS 5, 9			ARS 7, 11		
				L	S	Wr	L	S	Wr	L	S	Wr	L	S	Wr	L	S	Wr	L	S	Wr
A_1	6(8)	42	10	60	420	100	60	420	100	0	42	10	--	--	--	60	420	100	6	42	10
	16	64	8																		
A_2	36	164	18	180	840	80	360	1640	180	36	164	18	64	280	32	160	840	80	33	164	184
	64	280	32																		
B	12	18	10	120	180	100	--	--	--	12	18	10	--	--	--	120	180	100	12	18	10
C	18	54	22	180	540	220	--	--	--	18	54	22	--	--	--	180	540	220	18	54	22
D	0	18	6	0	18	6	0	18	6	0	18	6	0	18	6	0	18	6	0	18	6
E	0	30	12	0	300	120	0	300	120	--	--	--	--	--	--	0	300	120	--	--	--
F	18	50	20	180	550	220	180	550	220	18	50	20	18	50	20	180	550	220	18	50	20
G	5	10	4	55	110	44	--	--	--	5	10	4	--	--	--	--	--	--	--	--	--
Instructions/Cycle				773	2968	890	618	2928	826	96	356	90	82	348	58	718	2840	846	90	346	86
Instructions in Program				59	222	84	24	140	48	59	192	72	18	68	26	54	212	80	54	182	68
Constants					50			0			50			0			50			48	

NOTE: L = Long Instruction
S = Short Instruction
Wr = Write Instruction

Some of the systems provide attitude and rate outputs while others provide only attitude. For each of those that provide only attitude, the figures on the left in Table 3-10 are multiplied by one. For those that provide both attitude and rate, some of the figures are multiplied by 11, some by 10 and others by one. This is necessary because rate must be computed ten times as fast as attitude. Note that computational block A_2 has three sets of figures. The divide and square root operations make up this group. Since they are implemented by programmed subroutines, the number of iterations for a given accuracy depend on the computing rate; the lower speed systems require more iterations than the higher speed systems since the subroutine begins with a less accurate initial value.

Again, three categories have been provided for the instructions -- one for long instructions, one for short instructions, and one for instructions requiring a write operation (these are all short instructions). All of the instructions have been totaled at the bottom of the table. Also included are the total number of constants that are required by the computations for each system. The results of this tabulation have been used to determine memory size and instruction complement, thereby establishing the word length.

Memory Size -- The number of instructions in the program for the ARS computations required by each of the six systems is given in Table 3-11 along with the number of constants that must be stored. The startup program would require about 75 instructions and subroutines, bookkeeping, and input-output would require about 70. The requirements for short-term or scratchpad storage vary between systems from about 40 words to about 100. These figures are tabulated and totaled in Table 3-11. The actual memory size for each system (next highest power of two) and the number of bits required in the address field are also included in this table. Only two different memory sizes result, and fortunately the systems which can utilize the smaller memory are the less accurate system in which we can afford the smaller word length.

Table 3-11. Storage Requirements

	ARS 1	ARS 2, 6, 10	ARS 3	ARS 4, 8, 12	ARS 5, 9	ARS 7, 11
Instructions						
ARS Computers	300	175	275	100	275	250
Startup	75	75	75	75	75	75
Subroutines	20	20	20	20	20	20
Bookkeeping	50	50	50	50	50	50
Data						
Variable	100	60	85	40	100	80
Constants	50	0	50	0	50	50
Total	595	380	555	285	570	525
Actual Number in Memory	1024	512	1024	512	1024	1024
Address Word Length (bits)	10	9	10	9	10	10

Computer Speed and Instruction List -- It was previously shown that the ARS computations could be performed at the maximum required ra provided certain assumptions were made concerning clock rate, memc cycle times, and the list of built-in instructions. It will now be shown that, for some of the system requirements, multiplication and some of the other instructions can be programmed, resulting in a simpler control section in these cases.

The following assumptions were made to calculate the time required tc perform the ARS computation for each of the six systems:

- A 1.5-megacycle clock rate was assumed, resulting in a serial parallel word time (for a 16-bit word) of 4 microseconds.

- It was assumed that a nondestructive readout (NDRO) memory would be employed with a read-only time of about 1 microsecond and a write time of 4 microseconds. These are the times for a complete cycle.

- Square root and divide computations would be programmed rather than built in, and multiply would also be programmed if there were sufficient time available.

The number of computations and memory operations required for each of the six systems are listed in Table 3-12. Each of these are then multiplied by a number corresponding to the execution time of the operation and the total cycle time is obtained. The total time available is also given.

Programmed multiplication is permissable in four of the six systems. Since there is still additional time available, some of the other instructions can also be programmed. It appears to be possible to reduce the number of instructions to eight in these cases, thereby reducing the number of bits in the instruction code to three. The list of instructions for the simpler systems would probably include the following instructions from the list previously given: 1, 2, 3, 6, 11, 12, 16, and 18.

For programmed multiplication, the wired-in multiplication instruction is omitted from the computer, which amounts to removing the Q-register and a small amount of control logic.

Computer Systems -- Combining the results from Tables 3-10, 3-11, and 3-12, the six sets of different computer requirements can be satisfied by three computer configurations. The characteristics of each of these configurations and a list of the original ARS system numbers whose requirements are met by each computer configuration is given in Table 3-13. The appropriate gyro interface system is also specified in each case.

Table 3-12. Computer Speed and Instruction Requirements

Operations	ARS 1 (N = 18)	ARS 2, 6, 10 (N = 12)	ARS 3 (N = 16)	ARS 4, 8, 12 (N = 12)	ARS 5, 9 (N = 16)	APS ..11 (N = 16)
Long (L)	773	618	95	82	718	90
L × N	12,368	7,416	1,520	984	11,488	1,440
Short (S)	2,958	2,928	356	348	2,848	348
Write (W)	890	626	90	58	846	86
$S + (L \times N) + W\left\lfloor\frac{3}{2}\right\rfloor = A$	16,661	11,283	2,011	1,419	15,605	1,915
4A (microseconds)	66,644	45,832	8,044	6,476	62,420	7,660
Prog multiply time L × N × 6 × 4	296,832	177,984	36,480	23,616	275,712	34,560
Total with prog multiply (microseconds)	363,476	223,116	44,524	30,092	338,132	42,220
Time available (microseconds)	100,000	1,000,000	100,000	1,000,000	100,000	100,000
Multiply	Built in	Program	Program	Program	Built in	Program

Table 3-13. Final Computer Configurations

Computer Configuration	System Numbers	Word Size (Bits)	Memory Size (Words)	Multiply	Gyro Interface
A	1, 5, 9	18	1024	Built in	6 counters
B	2, 6, 10	12	512	Program	1 counter
C	3, 7, 11	16	1024	Program	1 counter

TELEMETRY-COMPUTER INTERFACE

The following schemes for obtaining useful ARS operating data via telemetry link are only intended to show the flexibility of adopting the ARS computer to the problem. Such unknown factors as available bandwidth, mission length, number of data points to be taken, etc., would determine the choice of a telemetry system. In each case data is obtained by reading certain selected memory locations.

Telemetry Data Points by Program

This is the simplest scheme but requires that all memory locations to be read out must be selected before launch. In this method the main program within the computer runs in a normal manner. A jump instruction is placed at points within the main program at fairly regular intervals (about every 10 seconds, for example). The jump will be to a short subroutine which controls the loading of the contents of one of a set of predetermined memory locations into telemetry equipment. A jump from the subroutine to the main program is made to resume normal operation after loading is complete. This method of obtaining data for telemetry requires additional program space but no added hardware.

Telemetry Data Points by Local Exerciser

In addition to the need for selecting memory locations before launching this scheme also requires some additional hardware over the previous method.

The block diagram of this data acquisition system along with the associated computer hardware is shown in Figure 3-24. The additional required hardware consists of the pulse generator and counter. (The telemetry register is considered part of the computer because it is necessary for any of the telemetry data acquisition techniques.) Operation is as follows: The pulse generator generates a pulse at the desired acquisition rate (perhaps one pulse every 10 seconds). This pulse increments the counter and also goes to the computer, where it is interpreted as an interrupt. The interrupt causes the computer

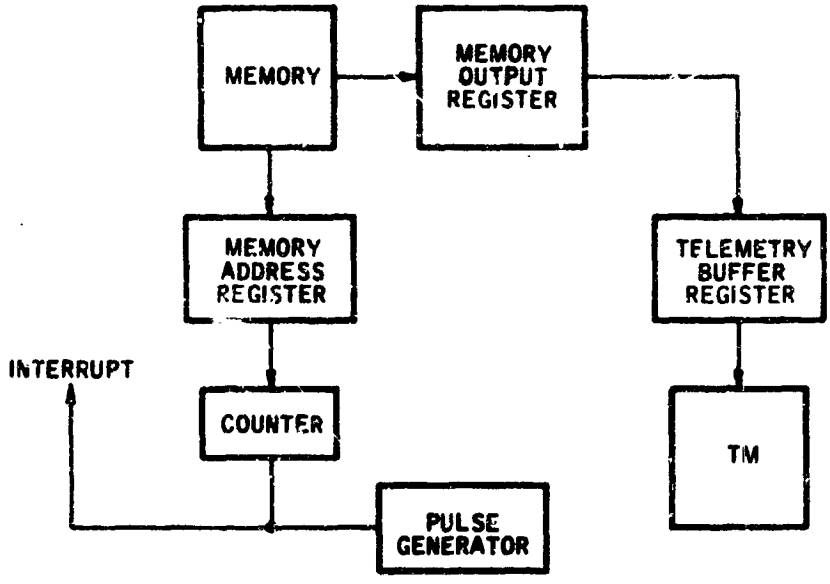

Figure 3-24. Telemetry Data by Local Exerciser

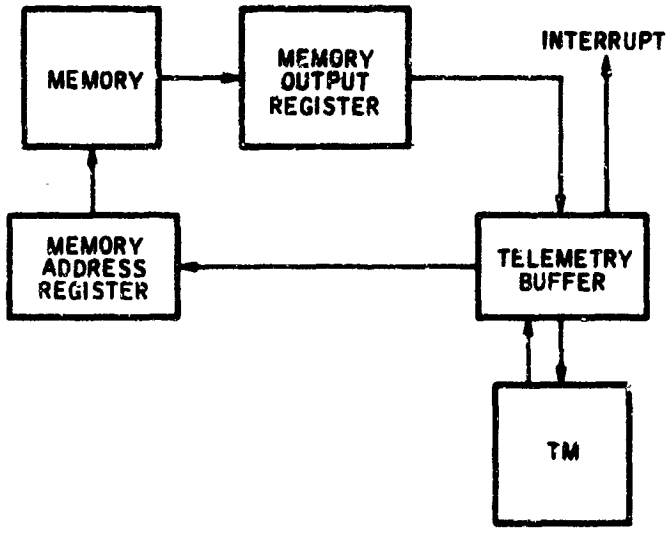

Figure 3-25. Telemetry Data by Remote Interrogation

to enter a short subroutine which loads the counter into the memory address register, reads the contents of that address and transfers them into the telemetry buffer for transmission to the ground. The counter, then, is used as the address of words to be read out at a rate determined by the pulse generator frequency. The counter length determines whether all or just a portion of the memory will be transmitted.

Telemetry Data Points by Remote Interrogation

In this scheme it is intended that the address of the data to be transmitted is sent to the computer by telemetry link. Figure 3-25 is the block diagram for this method.

The memory address of the desired data is transmitted to the vehicle. The address is then loaded into the telemetry buffer. This action causes an interrupt to be sent to the computer. The computer enters a short subroutine which transfers the address from the telemetry buffer register to the memory address register. The data word at that address is read into the memory output register and is then transferred to the telemetry buffer. Finally, the data word is fed into the telemetry equipment for transmission. As in the other telemetry schemes, these functions are under control of a short subroutine. When the subroutine is complete the main program resumes operation.

VEHICLE BODY RATE FROM THE END AXIS ROTOR PATTERN

INTRODUCTION

The purpose of this investigation is to determine if it is feasible to derive a signal proportional to vehicle body rate from the output signal of the end axis rotor pattern. Previous study indicates that the noise present on the readout from the cosine pattern results in a derived rate of approximately 1.4 degrees per second. Since it is desired to measure the vehicle body rate while the attitude control system is holding attitude in a limit cycle, it is necessary to measure rates of the order of 0.001 to 0.0001 degrees per second. In the event the end axis readout is suitable for measuring vehicle body rates of this magnitude, it may be possible to use an end axis readout during attitude hold operation and use the cosine pattern readout during attitude maneuvers involving the high body rates.

EFFECT OF ATTITUDE ON DERIVE RATE SIGNAL

Section IV describes the operation of the readout system using the end axis rotor pattern and indicates that the effective protion of the readout signal from the polar pickoff is

$$\left\langle A_1 \right\rangle = \frac{1}{2} \cos \frac{4a}{\pi r} \sin \left[\frac{4b}{\pi r} \sin (\omega t + \phi) \right] \qquad (43)$$

The quantities a and b are defined in Figure 3-26, r is the radius of the pickoff field of view, ω is the rotor angular velocity, t is time and ϕ is the phase angle determined by the direction of the pickoff displacement from the null position. For the purpose of this investigation both a and ϕ will be assumed zero, which results in considerable mathematical simplification and does not affect the general nature of the conclusions.

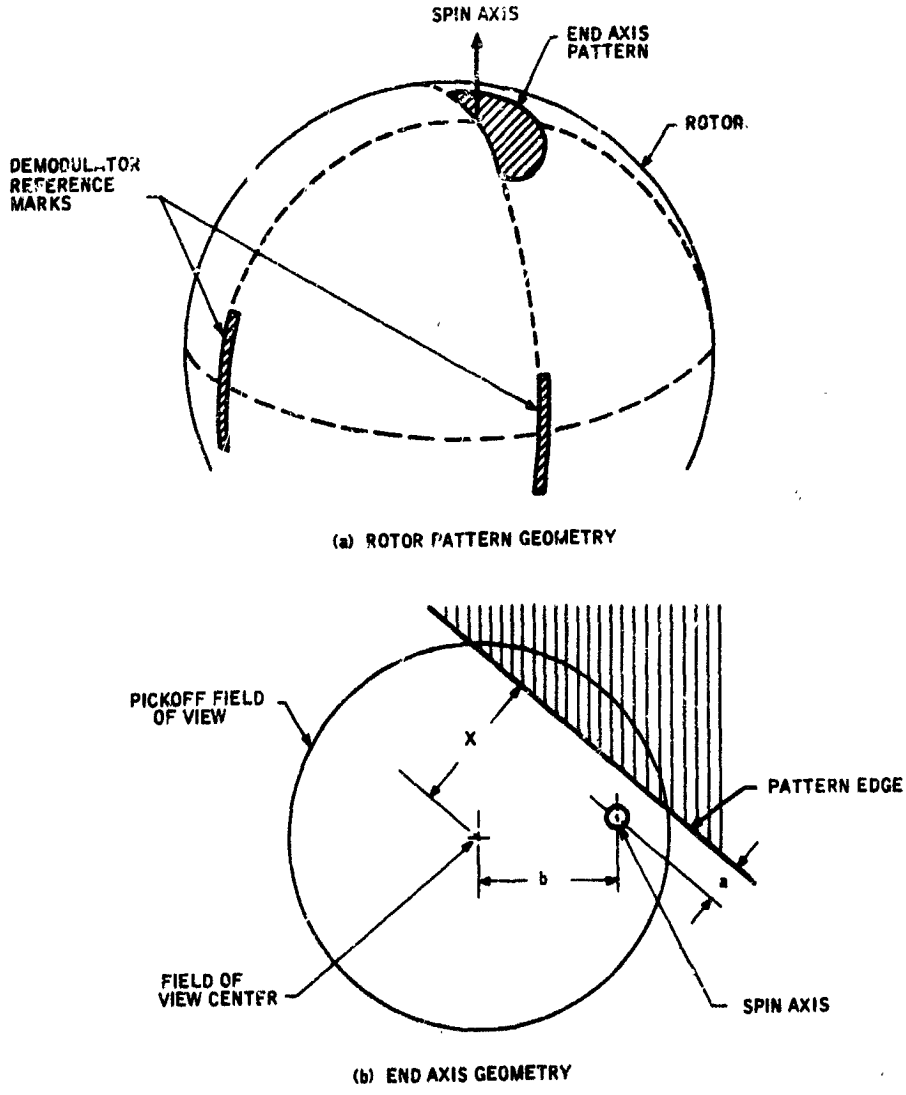

Figure 3-26. Conventional End-Axis Pattern and Pickoff Geometry

Under these assumptions Equation (43) becomes

$$\left\langle A_1 \right\rangle = \frac{1}{2} \sin \left[\frac{4b}{\pi r} \sin \omega t \right] \qquad (44$$

In Equation (44) the term b is proportional to the tangent of the angle of body rotation and is therefore proportional to the angle with an error of less than 1 percent for angles of 10 degrees or less. The output of the synchronous demodulator is essentially the time average of Equation (44) over one-half cycle of the square wave used to switch the demodulator.

That is,

$$\frac{\omega}{\pi} \int_0^{\pi/\omega} \frac{1}{2} \sin \left[\frac{4b}{\pi r} \sin \omega t \right] dt = \bar{A}_1 \qquad (45$$

The integrand in Equation (45) may be expanded in an infinite series of Bessel functions as

$$1/2 \sin (m \sin \omega t) = \sum_{n=1}^{\infty} J_{2n-1}(m) \sin (2n-1) \omega t \qquad (46$$

where

$$m = \frac{4b}{\pi r}$$

Substituting Equation (46) in Equation (45) and integrating

$$\bar{A}_1 = \frac{2}{\pi} \sum_{n=1}^{\infty} \frac{J_{2n-1}(m)}{(2n-1)} \qquad (47$$

Expanding the Bessel functions in powers of m the first terms of the series in Equation (47) becomes

$$\bar{A}_1 = \frac{1}{\pi}\left[m - \frac{m^3}{12} + \frac{m^5}{1200} - \cdots\right] \tag{48}$$

Differentiating Equation (48) with respect to time

$$\frac{d\bar{A}_1}{dt} = \frac{1}{\pi}\frac{dm}{dt}\left[1 - \frac{m^2}{4} + \frac{m^4}{240} - \cdots\right] \tag{49}$$

From Equation (49) it is apparent that the time rate of change of $\bar{A}_1$ is a function of the attitude (m) as well as the rate of change of attitude $\left(\frac{dm}{dt}\right)$. If $\frac{dA_1}{dt}$ is to represent the attitude rate with an error of 1 percent or less,

$$\frac{m^2}{4} \leq 0.01$$

or

$$m \leq 0.2$$

since $m = \frac{4b}{\pi r}$

then

$$\left(\frac{b}{r}\right) \leq 0.15$$

That is to say the attitude angle must not exceed 0.15 of the angle subtended by the radius of the pickoff field of view if an error of less than 1 percent is to be maintained in the attitude rate signal. In the event the attitude angle is equal to the angle subtended by the radius of the pickoff field of view the error in the rate signal would be approximately 40 percent. In the event

the attitude angle exceeds the angle subtended by the radius of the pickoff field of view, but does not exceed the limits of the rotor pattern, the attitude signal, $(\bar{A}_1)$, saturates, and any rate signal derived from it would indicate zero body rate. If the attitude angle exceeds the limits of the rotor pattern the readout system would give no information of either attitude or body rate.

PICKOFF FIELD OF VIEW

From the above discussion it is apparent that the usefulness of both the attitude and attitude rate signals obtained from the end axis rotor pattern is limited by the pickoff field of view. In turn the pickoff field of view is limited by the sensitive area on the pickoff sensor. Sensors currently available for this application have a useable area with a diameter of about 0.050 inches. The pickoffs as currently designed have a magnification of 5 and therefore the diameter of the field at the rotor is about 0.010 inch. This subtends an angle of about 0.6 of a degree. Therefore, the radius of the field of view subtends about 0.3 degree. Since the end axis pattern will be used for attitude hold type operation rather than for maneuvers, and the limit cycle amplitudes is typically ±0.1 degree, this field of view would be sufficiently large to ensure presence of the rate signal. At the extreme of the limit cycle the ratio of the attitude angle to the angle subtended by the radius of the field of view, $\left(\frac{b}{r}\right)$, is 1/3 and

$$\frac{m^2}{4} = \frac{1}{4} \cdot \left(\frac{4}{\pi}\right)^2 \left(\frac{b}{r}\right)^2$$

$$\frac{m^2}{4} = 0.0441$$

On the basis of Equation (49) this represents an error of about 4.4 percent in the attitude rate signal. Since the limit cycle rates are typically 10^{-4} deg/sec the absolute error is approximately $4.4(10^{-6})$ deg/sec.

In the event it is necessary to have the rate signal over a range of attitude greater than ±0.3 deg, or if greater accuracy is required in the rate signal, it may be possible to redesign the pickoffs to have an optical system with a magnification of one. This would result in a field of view at the rotor equal to the sensitive area of the optical sensor -- 0.050 inch in diameter -- which would permit an attitude change from the null position of ±1.4 degrees before saturation of the attitude signal. Therefore, the rate signal could be derived in this range. At the extremes of a limit cycle with an amplitude of ±0.1 degree, the error in the rate signal due to attitude would be about 0.2 percent. The absolute error for a limit cycle rate of 10^{-4} deg/sec would be $2(10^{-7})$ deg/sec.

EFFECT OF NOISE ON DERIVE RATE SIGNAL

The relationship in Equation (50) will be used to estimate the effect of readout noise on the attitude rate signal derived from the end axis pattern readout.

$$\Phi_R(\omega) = |G(\omega)|^2 \Phi_n(\omega) \tag{50}$$

where

$\Phi_n(\omega)$ = power spectral density of readout noise

$\Phi_R(\omega)$ = power spectral density of the noise on the derived rate

$G(\omega)$ = Fourier transform of the system used to derive rate

Test information on polar pickoffs used in the ESG Monitor program indicate a noise level of the order of 5.0 arc seconds (rms). Assuming this noise is "white" its power spectral density will be a constant equal to the mean square of the noise.

That is

$$\Phi_n = \overline{n^2} \tag{51}$$

$$\Phi_n = (5.0)^2 \text{ arc sec/rad/sec} \tag{52}$$

$\overline{n^2}$ = mean squared readout noise

Assuming the rate signal is obtained by differentiation

$$G(\omega) = j\omega$$

and

$$|G(\omega)|^2 = \omega^2 \tag{53}$$

From statistics, the average square of the noise on the rate signal will be given by:

$$\overline{R_n^2} = \frac{1}{2\pi} \int_{-\infty}^{\infty} \Phi_R(\omega)\, d\omega \tag{54}$$

where

$\overline{R_n^2}$ = mean squared rate noise

Substituting from Equations (50), (51) and (53) into Equation (54)

$$\overline{R_n^2} = \frac{\overline{n^2}}{2\pi} \int_{-\infty}^{+\infty} \omega^2\, d\omega \tag{55}$$

Obviously, the above integral is infinite if the entire frequency spectrum is considered. However, for attitude control of a space vehicle only noise in the bandwidth of the control system is of interest. If the bandwidth of the control system is $\omega_c/2$ radians per second, evaluation of the integral in Equation (55) between the limits $+\omega_c$ and $+\omega_c$ will provide a reasonable estimate of the mean square noise on the rate signal. That is,

$$\overline{R_n^2} = \frac{n^2}{2\pi} \int_{-\omega_c}^{+\omega_c} \omega^2 \, d\omega \tag{56}$$

and

$$\overline{R_n^2} = \frac{\overline{n^2}}{2\pi} \frac{\omega^3}{3} \Bigg|_{-\omega_c}^{+\omega_c} \tag{57}$$

or

$$\overline{R_n^2} = \frac{\overline{n^2}}{\pi} \frac{\omega_c^3}{3} \tag{58}$$

Assuming the bandwidth of the control system is 5 cps,

$$\omega_c \cong 60 \text{ rad/sec}$$

and from Equations (51) and (52)

$$\overline{n^2} = (5.0)^2$$

substituting in Equation (58)

$$\overline{R_n^2} = 57.4 \times 10^4 (\text{arc sec/sec})^2$$

$$\overline{R_n^2} = 4.5 \times 10^{-2} (\text{deg/sec})^2$$

$$\overline{R_n^2} \cong 0.2 \text{ deg/sec}$$

Obviously, the above noise level of 0.2 deg/sec will make it impossible to detect rates of the desired level of 0.001 to 0.0001 deg/sec. In order to detect a rate of 0.001 degrees per second or greater

$$R_n < 0.001 \text{ deg/sec}$$

or

$$R_n < 3.6 \text{ arc sec/sec}$$

and

$$\overline{R_n^2} < (3.6)^2$$

From Equation (58)

$$\overline{n^2} = \frac{3\pi \overline{R_n^2}}{\omega_c^3}$$

substituting for $\overline{R_n^2}$ and ω_c

$$\overline{n^2} = \frac{3\pi (3.6)^2}{(60)^3}$$

$$\overline{n^2} = 5.75 \ (10^{-4})$$

$$n = 0.024 \text{ arc sec (rms)}$$

This indicates that the noise on the readout must be less than 0.024 arc seconds if vehicle body rates as low as 0.001 degree per second are to be detected by differentiation of the signal from the end axis readout.

CONCLUSIONS

The principal conclusion of this investigation is that the level of noise on the readout limits usefulness of the rate signal derived from the end axis readout system. Also, the investigation reveals that the noise level must be reduced by a factor of approximately 200 if vehicle rates of 0.001 degree per second are to be detected.

Further, the investigation indicated that the optical pickoff has an adequate field of view for deriving the vehicle rate signal during the attitude hold limit cycle.

GYRO CAGING AND TORQUING CAPABILITY

CAGING

One objective of the SDMEG-ARS parameter study was to establish the utility of SDMEG caging capability. ("Caging" means precisely aligning the gyro spin axis with a line in the gyro case.) When the attitude reference system study program was conceived it was felt that a caging capability in the SDMEG would permit simplification of the data processing required to obtain information useful to the autopilot or attitude control system. This is true to some extent; however, there is little to be gained from a caging precision greater than that available from the use of the damping coils on the current gyro design.

Theoretically, the caging capability will align the gyro spin vectors orthogonal with each other. Since the proposed calculation for the attitude error signal to the autopilot is

$$\bar{\theta} = \hat{Q}_1 \times \hat{S}_1 + \frac{1}{|\hat{S}_1 \times \hat{S}_2|^2} \left\{ \hat{Q}_1 \cdot \hat{S}_1 \times \hat{S}_2 (\hat{S}_1 \cdot \hat{S}_2) - \hat{Q}_2 \cdot \hat{S}_1 \times \hat{S}_2 \right\} \hat{S}_1 \quad (59)$$

where

$\bar{\theta}$ = attitude error

$\hat{Q}_1$ and $\hat{Q}_2$ = commanded positions of spin vectors in body coordinates

$\hat{S}_1$ and $\hat{S}_2$ = observed positions of spin vectors in body coordinates

The calculation is simplified to

$$\bar{\vartheta} = \hat{Q}_1 \times \hat{S}_1 - \left\{ \hat{Q}_2 \quad \hat{S}_1 \times \hat{S}_2 \right\} \hat{S}_1 \tag{60}$$

when the spin vectors are orthogonal and

$$\hat{S}_1 \cdot \hat{S}_2 = 0 \text{ and } |\hat{S}_1 \times \hat{S}_2| = 1$$

In the event the spin vectors are assumed orthogonal and the signal for the autopilot is calculated from Equation (60) (when in fact the spin axes are not orthogonal) the error in the calculated signal is the difference between Equations (59) and (60). That is

$$\overline{\delta\theta} = \left\{ \frac{1}{|\hat{S}_1 \times \hat{S}_2|^2} \left[\hat{Q}_1 \cdot \hat{S}_1 \times \hat{S}_2 \, (\hat{S}_1 \cdot \hat{S}_2) \right] - \right. \tag{61}$$

$$\left. - \frac{1}{|\hat{S}_1 \times \hat{S}_2|^2} \left[\hat{Q}_2 \cdot \hat{S}_1 \times \hat{S}_2 \right] + \left[\hat{Q}_2 \cdot \hat{S}_1 \times \hat{S}_2 \right] \right\} \hat{S}_1$$

If the angle between $\hat{S}_1$ and $\hat{S}_2$ is α, then

$$|\overline{\delta\theta}| = \frac{\cos \alpha}{\sin^2 \alpha} \left[\hat{Q}_1 \cdot \hat{S}_1 \times \hat{S}_2 \right] - \frac{1}{\sin^2 \alpha} \left[\hat{Q}_2 \cdot \hat{S}_1 \times \hat{S}_2 \right] + \left[\hat{Q}_2 \cdot \hat{S}_1 \times \hat{S}_2 \right] \tag{62}$$

Since

$$|\hat{S}_1| = |\hat{S}_2| = |\hat{Q}_1| = |\hat{Q}_2| = 1$$

The quantities in the parenthesis approach $\cos\alpha$ as the system approaches a null. Therefore,

$$|\overline{\delta\theta}| \cong \frac{\cos^2\alpha}{\sin^2\alpha} - \frac{\cos^2\gamma}{\sin^2\alpha} + \cos\alpha \qquad (63)$$

Report 1726-FR1 on JPL Contract No. 950607 indicates in Figure 12-3 that gyro spin axis can be aligned to a line in the case within 0.1 degree, using the damping coils of the current gyro design. Therefore, error in the orthogonality of the spin axes of the two gyros (due to caging error in the present gyro design) would be of the order of ±0.2 degree.

Using $\alpha = (90° \pm 0.2°)$ in Equation (63) then

$$|\overline{\delta\theta}| \cong 12 \times 10^{-6} \text{ radians}$$

This would obviously have negligible effect on the accuracy of pointing the vehicle.

Since the above is the error associated with the caging capability of the current gyro design, it does not appear further development of caging will be required. Also, since the caging is accomplished by the gyro damping coils, no further system additions will be required. When initially spun up the gyros are damped as a normal part of the start-up procedure. They will therefore be initially caged to the axis of their damping coils. If it can be assumed the spacecraft is held to the sun-Canopus reference frame by optical sensors during cruise, with the gyros used for attitude maneuvers from the sun-Canopus reference, the damping coils should be energized prior to such attitude maneuver to cage the gyros and remove any gyro drift that may have occurred.

TORQUING

It was originally thought that having capability to precisely position the gyro spin vectors in any selected direction (torquing) would simplify system calculations, and thus reduce system size. Results of the study did not bear this out. If gyro torquing were to simplify system calculations it would occur as a result of initial alignment of the gyro spin vectors coincident with two of the vectors defining the master or navigation reference frame. To do this it is necessary to have on board the orientation of the master reference system because the gyro torquing mechanism is fixed to the gyro case and thus the vehicle. This information is not generally available. In general the orientation between the master and vehicle references is known only when the sun sensor is locked on the sun and the star tracker is locked on Canopus, with vehicle attitude being held by the outputs of these sensors. Under these conditions, gyro torquing is not necessary for initial alignment. Proper mounting of the gyros enables alignment of the spin vectors with the master reference with the damping coils of the gyro as presently designed. The result of such an alignment of the gyro spin vectors is to reduce two direction cosines for each spin vector to zero. This saves four storage locations plus the time required for 12 multiplications and 12 additions, which is not a large or significant saving. In the ARS configuration selected for the parameter study, these savings would occur in the ground-based equipment.

Another tentative application of gyro torquing was directed at the solution of a noise problem encountered during the parameter study.

In the course of the parameter study it was determined that the noise on the gyro readout from the cosine patterned rotor produced a threshold of about 1.4 degrees per second on the derived vehicle body rate signal. Since it is desired to measure body rates of the order of 0.001 degree per second, this is excessive. However, it was thought that a cleaner rate signal might be derived from the end axis pattern readout. If this were the case, a gyro torquing capability would provide the means fo

positioning the end axis pattern under the pickoff at such times as necessary to measure the lower rates. Unfortunately an analysis of the process of deriving vehicle body rate from the end axis pattern readout did not reveal the desired improvement.

This analysis is presented under a separate heading in Section III of this report. Although the readout noise from the end axis pattern is somewhat reduced, the rate signal threshold is still too great to measure the desired low body rates encountered during the limit cycle of attitude hold operations. The calculated threshold due to noise was 0.2 deg/sec.

CONCLUSIONS

In view of the results discussed above, it was concluded that additional caging and torquing capability beyond that provided by the damping coils of the current gyro design does not produce a simplification of the ARS considered in this study.

SIZE, WEIGHT, POWER AND RELIABILITY

The SDMEG attitude reference systems considered in the parameter study were divided into three major subsystems to determine system size, weight, power, and reliability. The subsystems are:

- Gyros
- Computer
- Power supply

The gyro subsystem includes the gyro mechanical assembly, the vacuum electronics, the suspension electronics, and the readout electronics that produce the start and stop pulses.

The computer subsystem has a digital computer for processing the gyro outputs to obtain vehicle attitude error and vehicle body rate signals suitable for the autopilot. The computer also controls the gyros during startup. The computer subsystem also has the interface electronics which condition the gyro outputs to be compatible with the digital computer input.

The power supply subsystem includes the equipment necessary to convert the primary power (2400 cycle, square wave) to the voltages and frequencies needed for operating the gyros and computer.

SIZE, WEIGHT, POWER AND RELIABILITY OF GYROS

Estimates of the size, weight, power and reliability of the gyro subsystem are based on the results of the study program contracted under JPL Contract No. 950607 and published in the reports 1726-FR1, 1726-FR2 and 1726-SR1.

The estimates of the gyro electronics assume potted welded module construction techniques. Microminiaturization of the electronics would probably result in smaller weight and size. In order to accommodate the microminiature circuits, the present circuit designs would have to be modified or redesigned. However, under the ground rules of the system parameter study the SDMEG is to be used as currently defined.

Since it was concluded that torquing and caging capability beyond that available with the damping coils will not simplify the system, no provision has been made made for torquing capability in the size, weight, and power estimates of the system. However, Table 3-15 does present the estimates of size, weight, and power of the torquing hardware for information. The gyro size, weight and reliability estimates are summarized in Table 3-14. Table 3-16 summarizes gyro power requirements.

Table 3-14. Summary of Gyro Size, Weight and Reliability

	Size (in^3)	Weight (lbs)	Reliability (% Failures/1000 hrs)
Mechanical Assembly	65	5.0	1.4704
Suspension and Readout Electronics	60	5.5	1.5399
Vacuum Electronics	8	0.7	0.0678
Total for one Gyro	133	11.2	3.0781
Total for two Gyros	266	22.4	6.1562

Table 3-15. Sizing Estimates for Gyro Torquing Hardware

	Size	Weight	Power
3 Coarse Drivers	7.4 in^3	0.74 lbs.	3 watts
3 Fine Drivers	18.7 in^3	1.9 lbs.	8 watts
3 Torquing Amps	50 in^3	10 lbs.	30 watts
TOTALS	76 in^3	13 lbs.	41 watts (6 VDC)

.6

Table 3-16. Power Inputs Required for SD MEG per Gyro

Function	Power Form	One Gyro Watts	Two Gyros Watts
Suspension High g Mode	±22.5 vdc; 500 ma; 1% reg; 0.1% ripple	22	44
Suspension Low g Mode	±6 vdc; 300 ma; 1% reg; 0.1 ripple	3.6	7.2
Spin	50 v; 1 a; 2400 cps; variable level; 2 phase	20	40
Damp	6 vdc; 1 a; 10% ripple; variable level	6	12
PO Lamps	4 vdc; 420 ma; variable level current; 0.05% reg	2	4
Preamps	±22.5 vdc, 20 ma; 1% reg, 0.1% ripple	0.5	1
Vacuum Pump Filaments	3 vdc; 1.5 a; controlled by grid current	4.5	9
Vacuum Pump Grid	+180 vdc; 10 ma; 1% ripple; 10% reg; controls filament current	1.8	3.6
Rotor Caging	Same as damping	6	12
Maximum Load		38.4	76.8

COMPUTER SIZE, WEIGHT, POWER AND RELIABILITY

In the discussion of the ARS computer, three computers A, B and C were defined. It was indicated that these three computer designs would satisfy the data processing requirements of the 12 attitude reference systems being considered in the SDMEG-ARS parameter study.

Component Counts

Approximate component counts have been made for each of the three computer subsystems. It was assumed that integrated circuit elements would be used wherever possible. At the present time, all computer circuits are available in integrated circuit form, except for memory drive circuits. Thus, integrated circuits were assumed for the logic elements, flip-flop, and sense amplifiers, and conventional, discrete element circuits for the memory drivers.

Although identical circuits were assumed for each system, this need not be the case. System B could be operated at a lower clock rate than the others, since there is considerable extra time remaining in the computer cycle. The lower speed circuits that could be employed as a result of lowering the clock rate would cut the power requirements considerably and possibly increase the permissable packing density.

The component counts are given in Table 3-17. Each section of the computer has been divided into sub units, each consisting of several stages of similar logical design such that the number of components in each sub unit can be more readily estimated. Flip-flops and special elements (such as sense amplifiers) have been separated from the logic elements because their power consumption generally differs. It is also possible that shift registers may become available with several stages on a single chip. This would reduce the size and increase the reliability of the computer.

Table 3-17. Component Count for the Three Systems

Computer Section	System A			System B			System C		
	Integrated Circuit Logic Element	Integrated Circuit Flip-Flops and Special Element	Transistor Circuits	Integrated Circuit Logic Element	Integrated Circuit Flip-Flops and Special Element	Tranaistor Circuits	Integrated Circuit Logic Element	Integrated Circuit Flip-Flops and Special Element	Transistor Circuits
Memory									
Sense Amplifiers		17			13			17	
Bit Drivers			68			52			68
Decode Logic	26			20			26		
Drivers			48			48			48
Switches			68			32			68
Address Register	11	11		5	9		11	11	
Memory Register	32	17		13	13		32	17	
Arithmetic									
A Register	8	16		6	12		8	16	
Q Register		16							
Add/Sub	20	16		5	1		5	1	
Timing and Control	15	8		8	2		8	2	
Control									
P Counter	8	10		6	9		8	10	
Instruction Register	3	5			3			3	
Iteration Counter	3	5							
Control Logic	15	8		10	3		10	3	
Clocks									
Computer Clock	5	10		5	10		5	10	
Real Time Clock	5	5		5	5		5	5	
I/O Clock	4			4			4		
Register Drivers	7			5			5		
Input-Output Registers		16			13			16	
Gyro Interface Logic	234	120		46	23		46	23	
Totals	396	280	184	138	116	132	173	134	184

The total component counts show that systems B and C do not differ greatly in complexity, while system A is approximately twice as complex as the others. These results are about what might be expected. Elimination of the builtin multiply (and other instructions) results in considerable hardware savings in the arithmetic and control sections. Systems B and C differ only in word length and in the size of the memory. Only one input-output register was included in these totals. It was assumed that the remaining registers would be associated with the equipment with which they communicate. This approach was taken because the number of registers and their structure would depend on the design of the associated equipment.

In order to compare these systems with similar systems constructed from conventional discrete component circuits, the Table 3-17 figures were translated into equivalent transistors, diodes, and resistors. The resulting figures are given in Table 3-18. Although a few additional capacitors and other components may be required, those listed in the table constitute most of the system components. The relative complexities of the three system remain about the same as in Table 3-17.

Table 3-18. Component Count for Mechanization with Discrete Components

	Transistors	Diodes	Resistors
System A	3,346	14,120	8,898
System B	1,378	5,644	3,726
System C	1,644	6,568	4,416

Size, Weight, and Power Comparisons

Size, weight, and power estimates were made based on current state-of-the-art packaging schemes for integrated circuits, drivers, and memory. These figures, given in Tables 3-19 and 3-20 do not include power supplies.

Table 3-19. Power Requirements for Computer Configurations

Computer	4 vdc (amp)	12 vdc (amp)	50 vdc 10% Duty Cycle (amp)	
			Peak	Avg
Computer A	3.0	3.6	1.0	0.1
Computer B	1.0	2.7	1.0	0.1
Computer C	1.5	2.7	1.0	0.1

Table 3-20. Size, Weight, and Power Comparisons

System Components	System A			System B			System C		
	Size (cu. in.)	Weight (lbs)	Power (watts)	Size (cu. in.)	Weight (lbs)	Power (watts)	Size (cu. in.)	Weight (lbs)	Power (watts)
Integrated Circuit Elements	66	1.33	12	26	0.52	4	30	0.6	6
Transistor Drive Circuits	117	2	48	88	1.5	37	117	2	38
Memory	30	1		20	0.78		30	1	
Case, Connectors, etc.	175	8		125	6.3		150	7	
Totals	388	12.33	60	259	9.1	41	327	10.6	54

The ratios between the figures for the three systems are much closer in terms of size, weight, and power than they are in terms of complexity. Reason for this difference is that the figures for the driver circuits, memory, and case (where appropriate) are much greater than those for the integrated circuit elements and their supporting cards. As a result, the integrated circuit elements, while varying in number between systems more than any other part of the system, contribute only about 10 percent to the size and weight figures and about 25 to 50 percent to the power figures.

Reliability

System reliability is expected to increase considerably with greater use of integrated circuits. Each integrated circuit element may replace 20 to 50 discrete components and their interconnecting leads and will be much more reliable than the circuit it replaces. In the future an integrated circuit may have several shift register stages on a single chip and the system reliability should increase still further. All of these expectations depend on an ultra-reliable method of interconnecting the circuit elements. Althouth methods have been proposed to achieve these goals, none have been tested under actual "in service" conditions.

In calculating the reliability for these three systems, failure rates given in the current literature as estimates of those expected from integrated circuits were used. Each driver transistor was assumed to have a failure rate about three times greater than a logic transistor or an integrated circuit because driver transistors operate at higher voltage and current levels. The driver circuits have additional elements that result in a further increase in the overall failure rate. For the majority of the interconnections, a special technique, such as the Honeywell MICPAK, was assumed. The composite failure rate for each of the three computer configurations is summarized in Table 3-21.

Table 3-21. Reliability Comparisons

	Failure Rate ($/K. Hrs.)	System A		System B		System C	
		No. of Units	Total Failure Rate ($/K. Hrs.)	No. of Units	Total Failure Rate ($/K. Hrs.)	No. of Units	Failure Rate ($/K. Hrs.)
Integrated Circuit Elements	0.002	676	1.352	254	0.508	307	0.614
Driver Transistor Circuits	0.008	184	1.472	132	1.056	184	1.472
Connections	0.00005	8800	0.440	3800	0.190	4600	0.230
Computer Failure Rate ($/K. Hrs.)			3.264		1.754		2.316

POWER SUPPLY SIZE, WEIGHT, POWER AND RELIABILITY ESTIMATE

The estimate of size and weight for the SDMEG power supply is based on the use of a separate supply for each voltage required. They will be packaged in a single housing, including the a-c spin supply.

All the supplies operate continuously; only loading requirements vary. Therefore, the switching logic could be placed on the outputs of the supplies. Regulation would have to be such as to maintain constant voltage throughout the load range of each supply.

The 6 vdc to the damping circuit requires a voltage build-up and tail-off. This can easily be accomplished with an R-C network on the supply's output.

The +4 vdc to the pick-off lamps must be variable through some range, necessitating a variable output from the regulator.

The spin supply will use the 2400 cps input power, which will be fed into a wave shaper to produce a sine wave from the input square wave. It will then be fed through an amplifier into a phase splitter. The outputs

are fed into power amplifiers and thus to the spin coils. The buildup and decay of spin power can be accomplished with an R-C circuit in the biasing of the input amplifier.

The input to the supplies will be through a transformer. Each voltage required will have its own secondary windings. The transformer will suffice for both isolation and voltage conditioning.

The three voltages needed for the computer will be non regulated. Input voltage is regulated and tolerance on these supplies is 10 percent. Therefore, no regulators should be necessary.

It is estimated the power supply will weigh 12 pounds and have a volume of 240 cubic inches. Although the three computer configurations use slightly different amounts of power, the difference is not sufficient to make a significant change in the power supply size. Also, it is estimated the power supply will have a failure rate of 1 percent per 1000 hours.

The estimate includes the following: ±22.5-vdc supply for gyro high G suspension and pickoff preamps; a ±6-vdc supply for gyro low G suspension and damping; a precision 4-vdc supply for pickoff lamp filaments; a 180-vdc supply for the vacuum pump grids; a 3-vdc supply for the vacuum pump filament, a 50-volt, 2400-cycle, two-phase supply for gyro spinup; and 4-, 12-, and 50-vdc supplies for the computer.

SUMMARY

Although the parameter study began with 12 different configurations for the attitude reference system, it was concluded that gyros designed with precision torquing and caging capability did not permit system simplification. Therefore, it was assumed all attitude reference systems would use the same gyros, rather than three different gyros. Thus, the original 12 system configurations were reduced to four. It was then concluded

that three computer configurations would satisfy the requirements of the remaining systems. Therefore, three different attitude reference systems resulted, all using the same gyros and gyro power supplies, but differing in the computer and computer power supply.

The size, weight, power and reliability estimates for the gyro, computer, and power supply subsystems were presented in Tables 3-14, 3-16, 3-19, and 3-20. The information from these tables has been combined in Tables 3-22, 3-23, and 3-24.

Table 3-22. Summary of Sizing Estimates

	Size (in. ^{3})	Weight (pounds)	Input Power (watts)		Reliability (%/1000 hours)
			Standby	Maximum	
Gyros	266	22.4	7.2	77	6.1562
Computer A	388	12.3	55	60	3.2640
Computer B	259	9.1	36	41	1.7540
Computer C	327	10.6	49	54	2.3160
Power Supply	240	12.0			1.0000

Combining the above information the estimates for the resulting three attitude reference systems are:

Table 3-23. Sizing Estimate for Total Systems

	Size (in. ^{3})	Weight (pounds)	Input Power (watts)		Reliability (%/1000 hours)
			Standby	Maximum	
System A	898	46.7	62	137	10.4202
System B	765	43.5	43	118	8.9102
System C	833	45.0	56	121	9.4720

Table 3-24. Summary of Size, Weight, Power and Reliability for ARS

System	Size ($in.^3$)	Weight (pounds)	Input Power (watts)		Reliability (%/1000 hours)
			Standby	Maximum	
ARS No. 1	898	46.7	69	151	10.4202
ARS No. 2	765	43.5	48	130	8.9102
ARS No. 3	833	45.0	62	144	9.4720
ARS No. 4	765	43.5	48	130	8.9102
ARS No. 5	898	46.7	69	151	10.4202
ARS No. 6	765	43.5	48	130	8.9102
ARS No. 7	833	45.0	62	144	9.472
ARS No. 8	765	43.5	48	130	8.9102
ARS No. 9	898	46.7	69	151	10.4202
ARS No. 10	765	43.5	48	130	8.9102
ARS No. 11	833	45.0	62	144	9.4720
ARS No. 12	765	43.5	48	130	8.9102

Table 3-22 summarizes the sizing estimates for the gyros, computer and power supplies. Table 3-23 presents the sizing estimates for the three distinct ARS configurations resulting from the study. Table 3-24 indicates system sizing estimates relative to the original selection of system configurations. This table shows that as a result of the conclusions, original configurations 1, 5, and 9 are the same size; 2, 4, 6, 8, 10 and 12 are the same size and 3, 7, and 11 are the same size.

FILTERS FOR BODY RATE OUTPUT

INTRODUCTION

Use of the SDMEG for spacecraft attitude reference and stabilization requires deriving the body rates by differentiating the available body attitude signals or using a pseudo-rate type control law. In any practical application, both types of control would probably be most effective. Any spacecraft maneuver requiring constant rates, typical of acquisition search patterns, necessitates deriving or approximating the spacecraft body rates. Since most spacecraft have severe fuel limitations, these rates must be controlled at all times.

The nature of the SDMEG readout and the proposed following computational electronics indicate that, for large body rates, satisfactory rate information results using the straightforward difference equation:

$$\frac{[\dot{\bar{X}}]}{[\bar{X}]} = \frac{1 - z^{-1}}{T} \qquad (64)$$

where

$[\bar{X}]$ = a body attitude column vector

$z = e^{st}$

T = sampling period

As the body rates decrease to the point where only a few of the least significant bits of the input buffer counters differ, the rate computation (Equation 7) becomes highly sensitive to the input counter noise caused by ball pattern errors, etc., and some other filter is required to provide, or approximate, the actual body rates. For instance, if the actual body rate is zero

and the input counter (representing a binary number $\sum_{n=0}^{N} a_n 2^n$ differed in the LSB during successive sampling periods, the indicated rate would be

$$\dot{X}_i = \pm \frac{2A}{T}$$

where

A is the scale factor of the LSB

If A is 36 arc-seconds and T is 0.01 second

$$\dot{X}_i = 7200 \text{ arc-seconds/second} = 2 \text{ deg/sec}$$

Obviously this introduction of noise is intolerable in any spacecraft application where the body rates are on the order of < 0.01 - 1.0 deg/sec.

The following preliminary analysis is intended to provide relative tradeoff data on the abilities and requirements necessary to provide an adequate rate signal from a SDMEG. Comparative data ultimately to be established includes rate limitations and computational requirements for:

- Digital pseudo rate
- Derived rate using

  Optimum differentiating filter
  Averaged rate computations
  Differenced - lagged attitude signal

DIGITAL PSEUDO RATE

Stable low rate limit cycle operation is possible using a pseudo-rate approach in much the same fashion as in continuous systems.* The flow diagram shown

*Nicklas, J. C.; Vivian, H. C.; Derived-Rate Increment Stabilization. JPL TR 32-69, 31 July 1961.

Cronquist, R. G.; Welp, D. W.; An Analysis of Compensation Techniques and Sensor Nonlinearities in a Mass Explusion Single Axis Satellite Attitude Control System, Thesis GGC/EE/64-6, USAF-IT; June 1964.

in Figure 3-27 provides both stabilization in the large and convergence to limit cycles with rates on the order of 0.001 deg/sec. Again this computation, which compares successive values of a filtered input attitude signal, will be influenced by counter noise and would probably function better with a lower sampling rate. The low rate limit cycle is achieved by comparing successive differences to a prestored number and, in the event it is exceeded, enabling the reaction system and updating the prestored number as shown. If the reaction system is not enabled during a sample period, the prestored number is replaced by its original value. Figure 3-28 is a typical phase plane portrait of a limit cycle acquisition using this control law. Although this computation will not provide rate information explicitly, it permits satisfactory control signals for both hold and maneuver modes.

DERIVATION OF BODY RATES

Typical Input Buffer Noise

The SDMEG output buffer counter will accumulate pulses to represent a number $\sum_{n=0}^{M} a_n 2^n$. In the event that the output attitude is drifting at a low constant rate, the absolute value of the counter contents will increase or decrease at the spacecraft body rate. If the body rate is near zero the buffer counter LSB varies randomly due to system defficiences with equal probability of recording $a_o = +1, 0, -1$. The input attitude signal appears as shown in Figure 3-29. This noise signal n(t) is represented by an auto-correlation function.

$$\phi_{nn}(\tau) = \overline{n(t)\, n(t+\tau)}$$

$$= \frac{2A^2}{3T}\,(T - |\tau|) \qquad \tau \leq T \qquad (66)$$

$$= 0 \qquad \tau > T$$

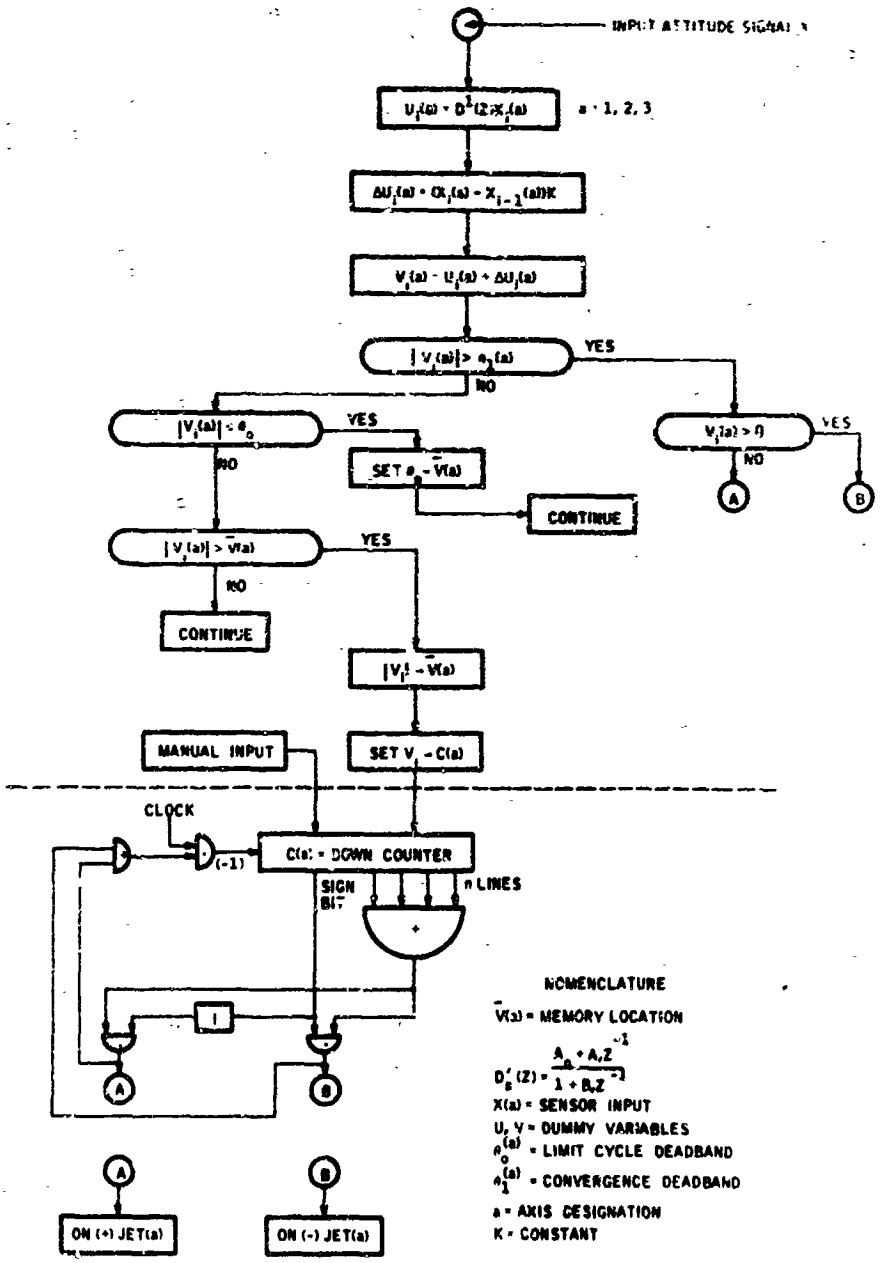

Figure 3-27. Pseudo-Rate Computational Flow Diagram

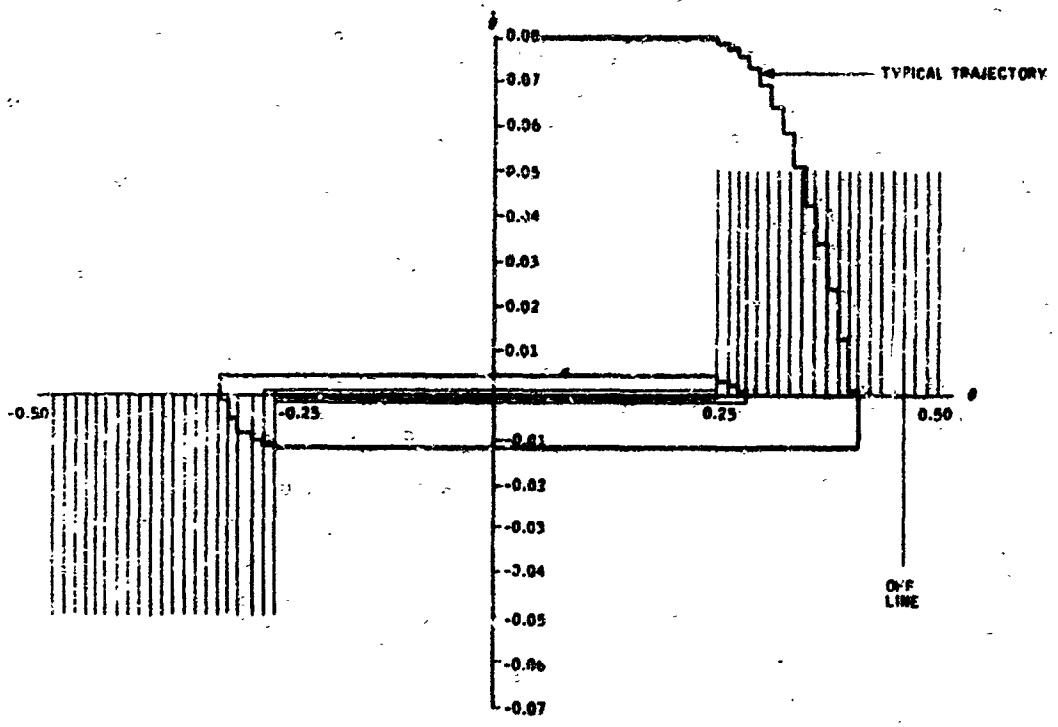

Figure 3-28. Typical Phase-Plane Portrait of Digital Pseudo-Rate Response for a Pure Inertia Plant

Figure 3-30 is a plot of this noise correlation function.

Although it is recognized that possible signal and noise correlation will be evident at specific attitudes $[\bar{X}]$ due to the SDMEG pattern uncertain, for the purposes of this study effort, the signal as shown in Figure 3-29 adequately represents the actual readout noise.

The spectral density of this noise is

$$\begin{aligned} \Phi_{nn}(j\omega) &= \text{Fourier transform of } \phi_{nn}(\tau) \\ &= \int_{-\infty}^{\infty} \phi_{nn}(\tau)\ e^{-j\omega\tau}\, d\tau \\ &= \frac{4A^2}{3T\omega^2}\ [1 - \cos \omega T] \end{aligned} \tag{67}$$

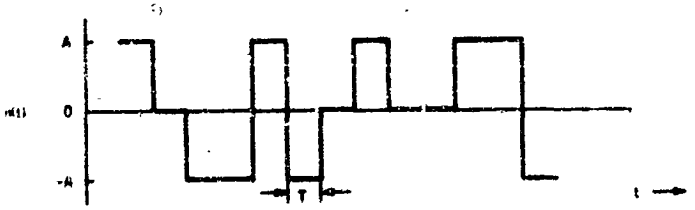

Figure 3-29.
Counter Binary Noise n(t)

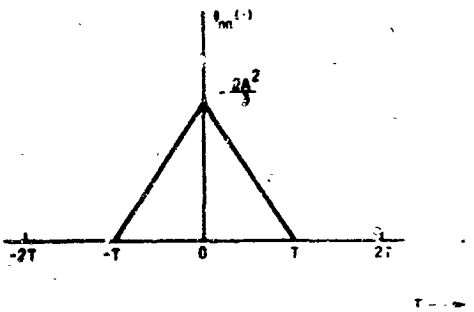

Figure 3-30.
Autocorrelation Function of n(t)

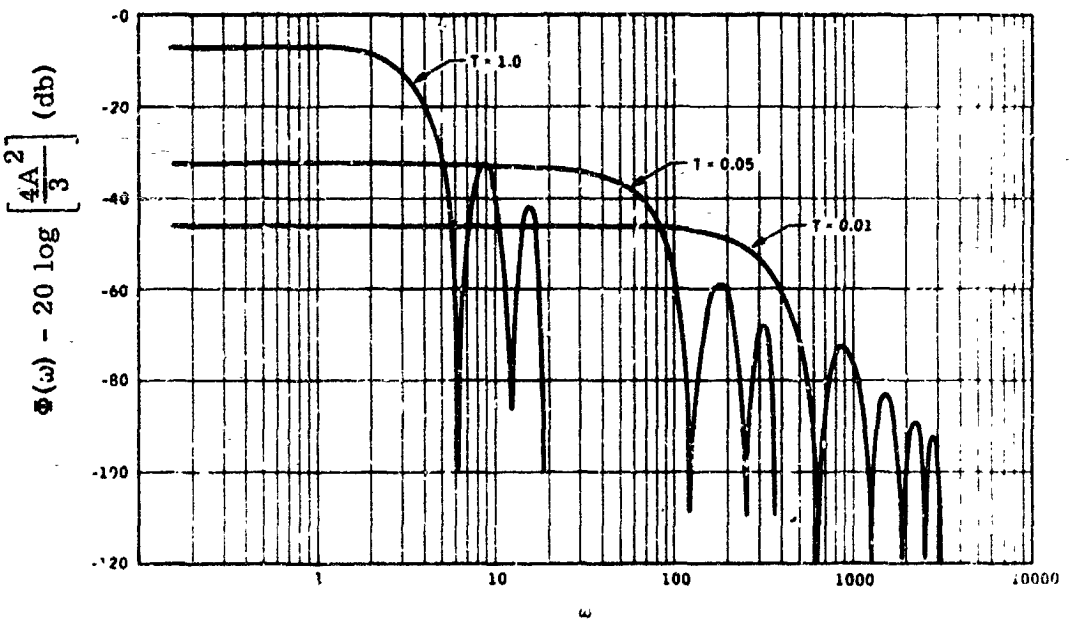

Figure 3-31. Normalized Spectral Density of n(t)
(ω in radians per second)

A normalized plot of the spectral density of $n(t)$ is shown in Figure 3-31 for various sampling periods. An interesting point is that the rms of the noise is independent of the sampling period T and as such, the area under each curve shown on Figure 3-31 will be identical.

A little foresight would suggest rearranging Equation (67) to

$$\Phi_{nn}(s) = \frac{4A^2T}{3}\left|\frac{1}{ST}\right|(-1)\left[1 - \cos(-iST)\right]$$

$$= \frac{4A^2T}{3}\left[\frac{\text{Cosh}(-ST)-1}{(TS)^2}\right]$$

$$= \frac{2A^2T}{3}\left[\frac{e^{ST} + e^{-ST} - 2}{(TS)^2}\right]$$

or

$$\Phi_{nn}(Z) = \frac{2A^2T}{3}\left[\frac{Z^2 - 2Z + 1}{Z}\right]\left[\frac{1}{T^2}\right]\mathcal{Z}\left[\frac{1}{S^2}\right]$$

$$= \frac{2A^2T}{3}\left[\frac{(Z-1)^2}{Z}\right]\left[\frac{1}{T^2}\right]\left[\frac{TZ}{(Z-1)^2}\right]$$

so

$$\Phi_{nn}(Z) = \frac{2A^2}{3}$$

The above expression for the noise power spectral density in the Z domain results in simplification of the following analysis.

Typical Input Information Signals

In order that a filter be derived that best approximates the spacecraft body rates, it is necessary to accurately represent realistic input signals that will be applied to the system. In almost all cases, the inputs will be of the form shown in Figure 3-32. This input is represented by

$$x_n^i = a_n^i \, t, \quad t_{n-1} \leq t \leq t_n \tag{68}$$

where

$\bar{t}_n$ is the average constant rate period

$\sqrt{\bar{a}_n^2}$ is the rms of the constant rates a_n^i

As shown in Figure 3-32, if the input rates $\dot{x}^i(t)$ obey a poisson distribution in amplitude and period with a zero mean rate:

as shown by Solodovnikov*, the spectral density of this input rate signal is,

$$\Phi_{\dot{x}\dot{x}}(s) = \frac{2\beta \, \bar{a}_n^2}{-S^2 + \beta^2} \tag{69}$$

where

$$\beta = \frac{1}{\bar{t}_n}$$

*Solodovnikov, V. V.; Introduction to the Statistical Dynamics of Automatic Control Systems, Dover Book, p. 166.

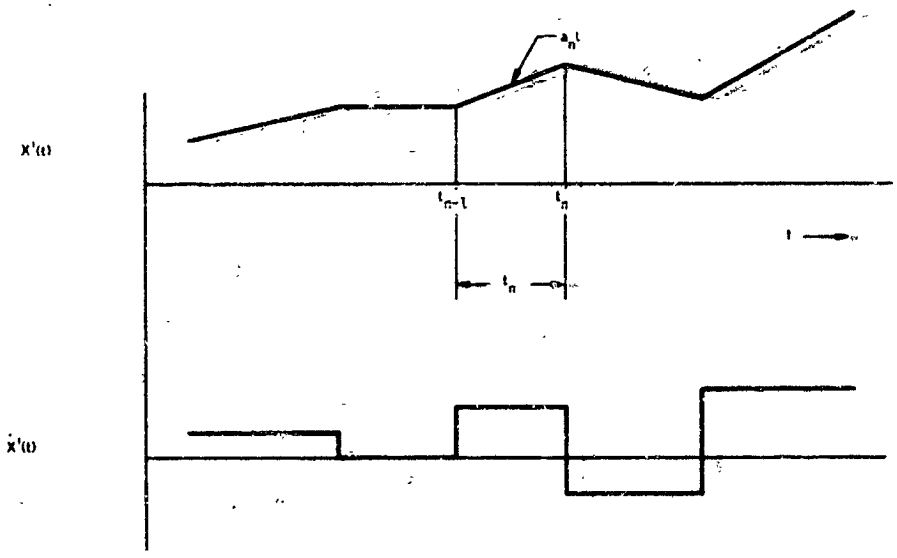

Figure 3-32. Representative Input Signals

Even though it has been assumed that $\dot{x}^i(t)$ is a stationary signal, it is obvious that $x^i(t)$ is not stationary since

$$\Phi_{xx}(s) = \left(\frac{1}{-S^2}\right)\left(\frac{2\beta\,\bar{a}_r^{\,2}}{-S^2+\omega_n^{\,2}}\right) \qquad (70$$

has a double pole at the origin and hence the rms of the attitude signal $x^i(t)$ will grow as the half power of time. As such $x^i(t)$ is nonstationary. Since we are only interested in $x^i(t)$ over the periods t_n, it is possible to represent the spectrum of $x^i(t)$ by the following expression:

$$\Phi_{xx}(s) = \lim_{\substack{h \to t_n \\ \epsilon \to 0}} \left[\left(\frac{1-e^{-hs}}{S+\epsilon}\right)\left(\frac{1-e^{hs}}{-S+\epsilon}\right)\left(\frac{2\beta\,\bar{a}_n^{\,2}}{-S^2+\beta^2}\right)\right] \qquad (71$$

This method of approximating the integration by

$$\frac{1 - e^{-hs}}{S + \epsilon} \tag{72}$$

to eliminate the singularity was based on a work by Newton* and was found to be identical to that used by Monroe†.

Derivation of the Rate Approximating Filter

Upon establishing satisfactory representations for the input signal and counter noise what remains is to determine what filter will permit the best approximation, according to some criteria, and exactly what degree of improvement can be realistically achieved with this filter. Recognizing that any criteria established will not provide the best performance for all requirements (frequency response - time response, etc.), the following subsections will attempt to develop sufficient different approaches to enable an intelligent comparative study.

Optimum Differentiating Filter -- Assuming the criteria established is to minimize the variance of the difference between the actual output signal and the desired output signal, it is relatively straightforward to apply the statistical analysis advanced by Wiener for continuous systems to the sampled system under consideration. This technique, which is covered in most texts on sampled data analysis (for instance, Kuo‡) is based on minimizing a mean square quantity (error signal).

---

*Newton, G. C. Jr.; Inertial-Guidance Limitations Imposed by Fluctuation Phenomina in Gyroscopes, Proc of IRE, April 1960.

†Monroe, A. J.; Digital Processes for Sampled Data Systems, John Wiley Book, 1962.

‡Kuo, B. C.; Analysis and Synthesis of Sampled Data Systems, Prentice-Hall Inc., 1963.

Since we are only interested in the information generated at the sampling instants (and the relatively short computational time required afterwards), it is expedient to use Z transform methods in the analysis. Thus the sampled input signal and noise spectral densities are as shown below:

$$\Phi_{x\,x}(Z) = \left[\sum_{k=0}^{\infty} \phi_{xx}(-kT)Z^{k} + \sum_{k=0}^{\infty} \phi_{xx}(kT)Z^{-k} - \phi_{xx}(0)\right]$$

$$= \left[A(Z^{-1}) + A(Z) - \phi_{xx}(0)\right] \qquad (73)$$

$$A(Z^{\pm 1}) = z\left[\Phi_{xx}(s)\right]^{\pm}$$

where

$[\Phi]^{\pm}$ represents the terms of partial fraction expansion of Φ in the left half plane and right half plane respectively.

Hence

$$\Phi_{x\,x}(Z) = \left[\frac{K_3 Z + K_3 Z^{-1} - C(Z - e^{-\epsilon T})(Z^{-1} - e^{-\epsilon T})(Z - e^{-\beta T})(Z^{-1} - e^{-\beta T})}{(Z - e^{-\epsilon T})(Z^{-1} - e^{-\epsilon T})(Z - e^{-\beta T})(Z^{-1} - e^{-\beta T})}\right] \qquad (74)$$

where

K_3 = residue at $z = -\beta$

$$= \left|\frac{1 - e^{mT\beta}}{-\beta + \epsilon}\right| \left|\frac{1 - e^{-mT\beta}}{\beta \quad \epsilon}\right| (\alpha) \left|\frac{\alpha}{2\beta}\right|$$

m = integer, $t = mT \rightarrow \frac{1}{\beta} = \bar{t}_n$

$$C = \phi_{x\,x}(0)$$

$$\alpha = \sqrt{2\beta\, a_n^{2}}$$

and as previously shown the noise spectrum is:

$$\Phi_{nn}(Z) = \frac{2A^2}{3}$$

Thus, using these signals and the diagram shown in Figure 3-33, the expressions can be derived that will yield the transfer function M(Z) that will enable the best approximation of the body rates $\dot{x}^i(t)$.

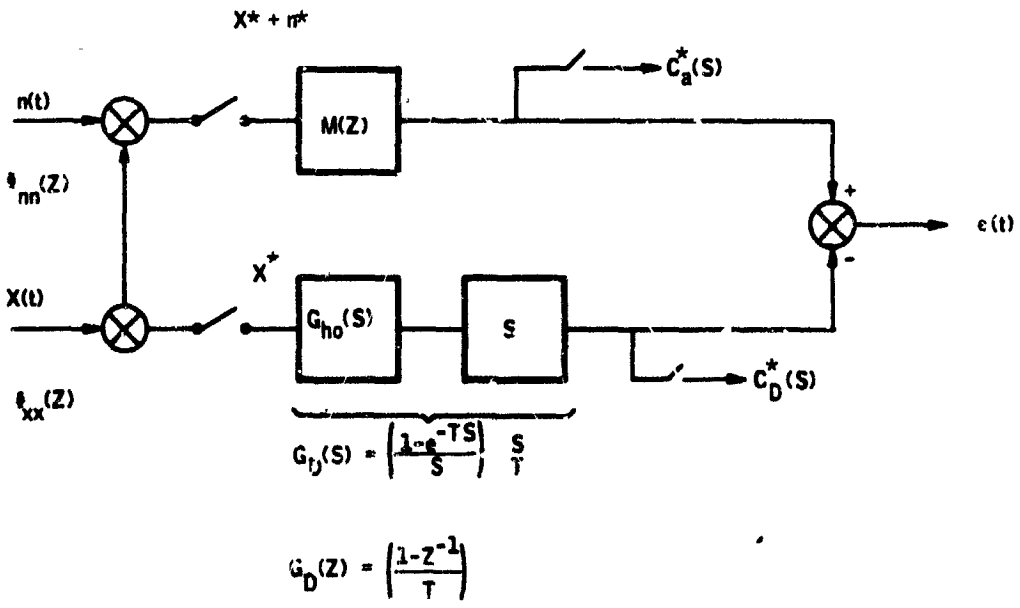

Figure 3-33. Block Diagram Established to Derive the Desired Filter M(Z)

Thus

$$\epsilon^2(nT) = \frac{1}{2\pi j}\oint_\Gamma \left\langle \Phi_{\epsilon\,\epsilon}(Z) \right\rangle Z^{-1}\,dZ$$

$$= \frac{1}{2\pi j}\oint_\Gamma \left[\Phi_{C_d C_d}(Z) + \Phi_{C_x C_x}(Z) + \Phi_{C_n C_n}(Z) - \Phi_{C_d C_x}(Z) - \Phi_{C_x C_d}(Z) \right] Z^{-1}\,dZ \qquad (75)$$

where

Γ is the integration path $|Z| = 1$

$$\Phi_{C_d C_d}(Z) = M_d(Z)\, M_d(Z^{-1})\, \Phi_{xx}(Z)$$

$$\Phi_{C_x C_x}(Z) = M(Z)\, M(Z^{-1})\, \Phi_{xx}(Z)$$

$$\Phi_{C_n C_n}(Z) = M(Z)\, M(Z^{-1})\, \Phi_{nn}(Z)$$

$$\Phi_{C_d C_x}(Z) = M(Z)\, M_d(Z^{-1})\, \Phi_{xx}(Z)$$

$$\Phi_{C_x C_d}(Z) = M(Z^{-1})\, M_d(Z)\, \Phi_{xx}(Z)$$

From the above expressions, the desired rate approximating transfer function is found to be

$$M(Z) = \left\{ \frac{M_d(Z)\, \Phi_{x\,x}(Z)}{\Phi^-_{x+n\,,\,x+n}(Z)} \right\}_+ \frac{1}{\Phi^+_{x+n\,,\,x+n}(Z)} \qquad (76)$$

where

$\Phi^{\pm}_{x+n\,,\,x+n}(Z)$ are the poles and the zeros in the LHP and RHP of

$\Phi_{x+n\,,\,x+n}(Z)$ respectively.

The resulting expression for this spectral density of the signal plus noise is

$$\Phi_{ii}(Z) = \Phi_{xx}(Z) + \Phi_{nn}(Z) = \Phi_{x+n,\ x+n}(Z)$$

$$= \left[\frac{(N - C)(Z - F)(Z^{-1} - F)(Z - D)(Z^{-1} - D) + K_3 Z + K_3 Z^{-1}}{(Z - F)(Z^{-1} - F)(Z - D)(Z^{-1} - D)}\right]$$

where

$$D = e^{-\beta T}$$

$$F = e^{-\epsilon T} \qquad \epsilon \to 0$$

thus

$$\Phi_{ii}(Z) = \frac{A^2 \left\{\frac{2}{3} - \frac{a_1 a_2 K^2}{T^2}\right\} C_3}{DF} \left[\frac{Z^4 + G_3 Z^3 + G_2 Z^2 + G_1 Z + G_0}{(Z - F)(Z - F^{-1})(Z - D)(Z - D^{-1})}\right] \tag{77}$$

where

$$G_3 = \frac{\frac{a_1 a_2 K^2}{T^2} - \left(\frac{2}{3} - \frac{a_1 a_2 K^2}{T^2}\right) C_2}{\left(\frac{2}{3} - \frac{a_1 a_2 K^2}{T^2}\right) C_3}$$

$$G_2 = \frac{C_1}{C_3}$$

$$G_1 = C_{73}$$

$$G_0 = 1$$

where

$$a_1 = \left(\frac{1 - e^{mT\beta}}{-\beta}\right)$$

$$a_2 = \left(\frac{1 - e^{-mT\beta}}{\beta}\right)$$

$$K = \frac{\sqrt{a_n^{\,2}}\,T}{A}$$

$$C_1 = 1 + D^2 + F^2 + 2DF + F^2D^2$$

$$C_2 = D + F + FD^2 + F^2D$$

$$C_3 = FD$$

A = input attitude data LSB

Thus factoring Equation (77) and substituting the result into Equation (76) defines the optimum rate-producing filter, with respect to minimum integral error squared. This filter must be studied with respect to realistic values of β_1 for typical spacecraft maneuver histories, to establish the optimum observation period MT.

Averaging Computed Rate Signals -- Another method that could be used is to average the successively computed rate signals using K samples at a time. Given that the probability density function of the noise shown in Figure 3-29 is

$$p(nt) = 1/3[\delta(-A) + \delta(o) + \delta(A)] \tag{78}$$

where

$\delta(x)$ is the Dirac delta function of arg x

Then the variance of n(nt)

$$\begin{aligned} \overline{n^2} &= \int_{-\infty}^{\infty} n^2 p(n)\, dn \\ &= \frac{1}{3}\int_{-\infty}^{\infty} n^2 [\delta(-A) + \delta(o) + \delta(A)]\, dn \\ &= \frac{2A^2}{3} \end{aligned} \tag{79}$$

which agrees with the previously defined value of $\phi_{nn}(0) = \overline{n^2}$ shown in Equation (66).

If this noise signal is differentiated in the manner shown in Equation (64), it is clear that

$$p(\dot{n}) = \frac{1}{9}\left[\delta\left|\frac{-2A}{T}\right| + 2\delta\left|\frac{-A}{T}\right| + 3\delta(o) + 2\delta\left|\frac{A}{T}\right| + \delta\left|\frac{2A}{T}\right|\right] \tag{80}$$

and

$$\begin{aligned} \overline{(\dot{n})^2} &= \int_{-\infty}^{\infty} (\dot{n})^2\, p(\dot{n})\, d\dot{n} \\ &= \frac{1}{9T^2}\,[4A^2 + 2A^2 + 2A^2 + 4A^2] \end{aligned} \tag{81}$$

and

$$\overline{(\dot{n})^2} = \frac{4}{3}\left|\frac{A}{T}\right|^2 \tag{82}$$

By averaging the computed rate signal n with a finite memory filter, as shown in Figure 3-34, the central limit theorm indicates that the original impulse modulated trapazoidal probability density function would tend toward an impulse modulated normal for $\dot{n}_1$ (nt)

Thus

$$\overline{[\dot{n}_1(nt)]^2} = \frac{1}{K^2}\sum_{k=1}^{K}\left\{\frac{4}{3}\left|\frac{A}{T}\right|^2\right\}_k = \frac{4}{3K}\left|\frac{A}{T}\right|^2 \tag{83}$$

Since the averaging bounds $\dot{n}_1$ (nt) within $\frac{-2A}{T} \leq \dot{n}(nt) \leq \frac{2A}{T}$, the effect of the averaging is illustrated in Figure 3-35. As shown by Equation (83), the variance of $\dot{n}(t)$ is reduced inversely proportional to the number of samples averaged K. Thus to decrease the rms rate noise one order of magnitude requires averaging 100 samples. The associated lag and memory requirements may preclude using this filter approach.

IMPLEMENTING SAMPLED DATA FILTERS

Progress Report 20113-PR5 included a discussion on possible ways to reduce dispersion of the computed rate signals using the sampled attitude data. The form of the resulting filters was:

$$G(z) = \frac{A_0 + A_1 z^{-1} + \ldots + A_m z^{-m}}{1 + B_1 z^{-1} + \ldots + B_n z^{-n}}$$

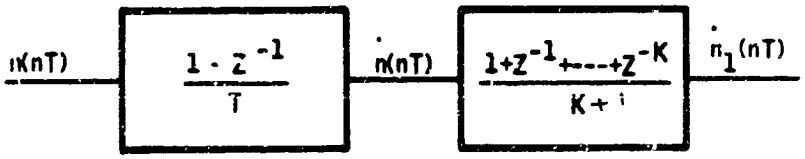

Figure 3-34. Rate Averaging Filter Block Diagram

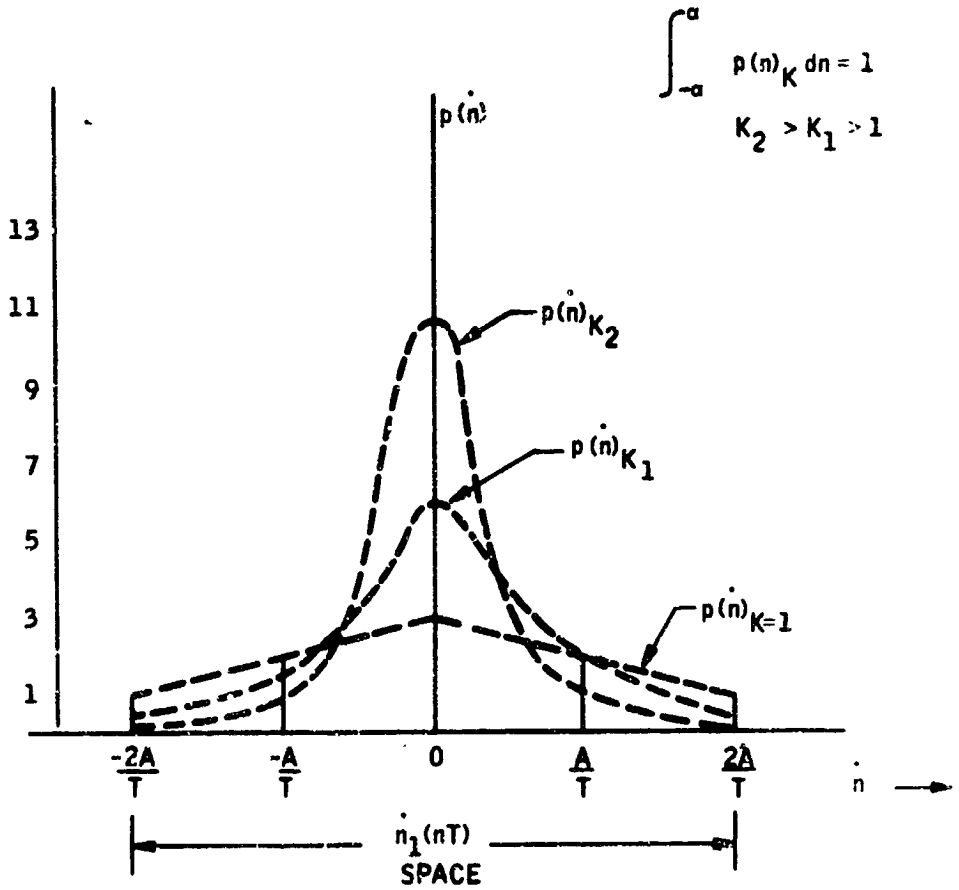

Figure 3-35. Effect of Finite Memory Averaging Rate Filter on Quantized Noise Filter

where

A_1 and B_i are specific constants

$z = e^{ST}$

T = Sample period

S = Laplace transform variable

$= \sigma + j\omega$

The operational requirements of the above filter are clear when the nature of the delay operator z^{-1} is considered. From Laplace transform calculus recall that

$$\mathcal{L}[f(t - T)] = e^{-ST} F(S) = z^{-1} F(S)$$

Thus, multiplying the function F(S) by z^{-n} implies that the time function f(t) has been delayed by nT. For a simple case where

$$G(z) = \frac{A_0 + A_1 z^{-1}}{1 + B_1 z^{-1}} = \frac{e_0}{e_i}$$

Thus

$$e_0 = A_0 e_i + A_1 e_i z^{-1} - B_1 e_0 z^{-1}$$

or

$$e_0(nT) = A_0 e_i(nT) + A_1 e_i[(n-1)T] - B_1 e_0[(n-1)T]$$

From this above expression it is clear that implementing this first-order transfer function requires:

- Storing three permanent constants (A_0, A_1, B_1)
- Storing two temporary data points $\left\{e_i[(n-1)T],\ e_0[(n-1)T]\right\}$
- Three multiplications $\left\{(A_0 \cdot e_i),\ [A_1 \cdot e_i(n-1)],\ [B_1 \cdot e_0(n-1)]\right\}$
- Two additions to form the desired result $e_0(nT)$
- Miscellaneous program instructions to accomplish the above operation

A sample computer program for a first-order transfer function that uses an instruction repertoire inherent to most spaceborne computers is shown below:

Instruction		Comment
LDA	e_i	$e_i \Rightarrow A$
MULT	A_1	$A_1 \cdot (A) = A_1 e_i \Rightarrow A$
STA	M_a	$(A) = A e_i \Rightarrow M_a$
ADD	M_3	$(A) + A_2 \cdot e_i z^{-1} \Rightarrow A$
SUB	M_2	$(A) - B_2 e_0 z^{-1} = e_0 \Rightarrow A$
LOR	R_i	$(A) = e_0 \Rightarrow R_i$ (This is the transfer function, filter, output.)

Instruction		Comment
MULT	B_2	$B_2 \cdot e_0 \Rightarrow A$
STA	M_2	$(A) = B_2\ e_0 \Rightarrow M_2$
LDA	M_a	$(M_a) = A_1\ e_i \Rightarrow A$
MULT	A_2/A_1	$A_2/A_1 \cdot (A) = A_2\ e_i$
STA	M_3	$(A) = A_2\ e_i \Rightarrow M_3$
.		
.		
.		
Continue		

It can be seen that rather than storing both A_1 and A_2 in the permanent memory, A_1 and A_2/A_1 are stored and multiplied times $A_1\ e_i$ at the appropriate time. This approach enables use of fewer program insturctions to accomplish the desired result. In addition, for higher order transfer functions, it will reduce the temporary memory locations required by about a factor of two.

This simple example illustrates the techniques required to implement a sampled data difference equation. The advantage of this approach over a standard numerical method is that the impulse-modulated difference equations (z transforms) permit exact representation of the continuous function at the sample periods. More important, all the analysis and synthesis tools available for frequency domain studies also apply to the sampled system studies.

Continuous system analysis techniques are made applicable for the sampled system by elementary conformal mapping techniques. By letting the new complex variable

$$z = e^{ST} \quad , \quad S = \sigma + j\omega$$

The entire complex S plane is mapped into a new complex z plane, as shown in Figure 4. The entire left half of the S plane is included within the unit circle of the z plane. All S plane root locus techniques apply in the z domain analogous to the S plane.

If the z plane is mapped to another complex plane by the bilinear transformation

$$z = \frac{1 + w}{1 - w}$$

The z plane transfers to the w plane, as shown in Figure 5.

The w domain is generally used for frequency response (bode plots) analysis. The advantage of using the w-z domain for synthesis and analysis is that the transformation is linear between them. Thus, individual compensation blocks can be manipulated without influencing the entire transfer function, as in the S → z plane case.

This elementary discussion of sampled data analysis and application is intended to serve as a brief introduction. For a more thorough discussion, the interested reader is referred to the works of Ragazzini and Franklin, Tou, Kuo, Truxal, Monroe, etc.

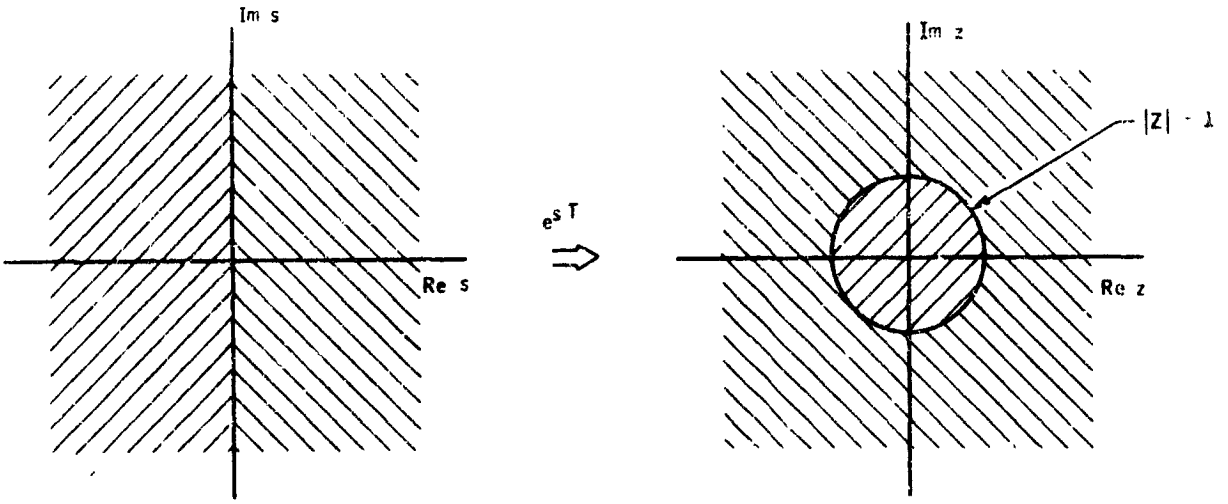

Figure 3-36. S → z Plane Map

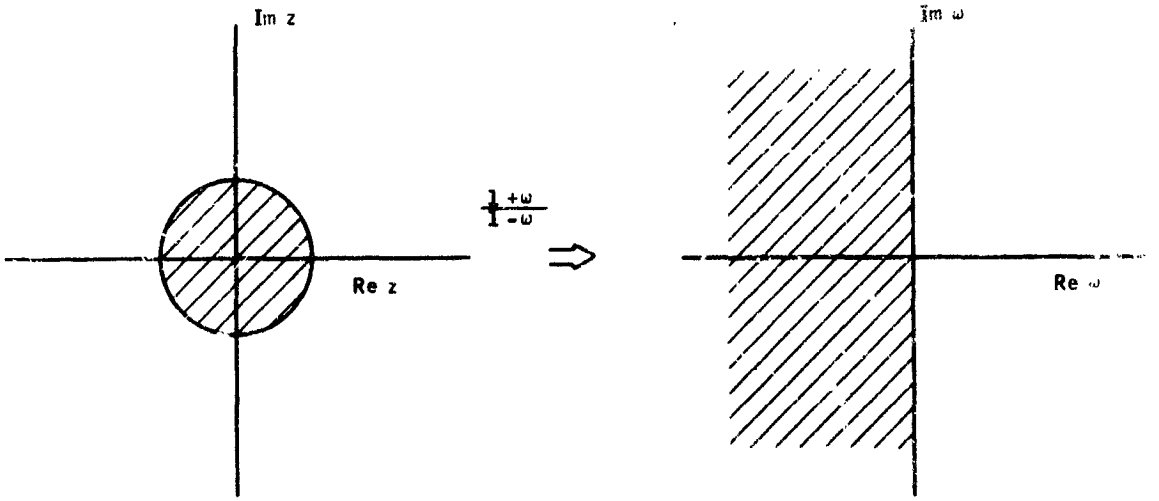

Figure 3-37. Z → w Plane Map

CHECKOUT OF SDMEG-ARS

INTRODUCTION

Telemetry for the monitoring of the gyro operation was discussed in Report No. 1726-FR2, on JPL Contract No. 958607. The following discussion is concerned with telemetry for the monitoring of the attitude reference system computer and the gyro-computer interface logic.

The SDMEG-ARS parameter study is principally concerned with unmanned spacecraft applications; therefore, any verification of the system operation must be through telemetered data. However, since the telemetry capacity available for this function is quite limited, it is essential that the minimum amount of data necessary to establish the status of the system operation be transmitted.

Ideally, the telemetry between the spacecraft and the earth-based facility would provide the capability for:

- Detection of failure
- Isolation and analysis of failure
- Elimination of failure

Although it would be desirable to provide all the above capabilities for the SDMEG-ARS computer, the elimination of a failure requires redundancy in the system. Since the current study assumes a non-redundant system, the data selected for telemetry from the ARS computer will be selected to provide the first two capabilities.

CHECKOUT AND MONITORING OF ARS COMPUTER

It is proposed that two methods be used for detection of a failure in the ARS computer. Since the ARS will not be used continuously, but will be put in service at such times as it is necessary to change the spacecraft attitude from the attitude provided by the Sun and Canopus sensors, the computer should be put through a checkout routine before each use of the ARS. Also, during operation of the ARS in control of the spacecraft, data should be telemetered to verify that the computer and control system are functioning properly.

The computer checkout routine would be the same problem the computer solves in normal operation. Data would be stored in the computer memory to simulate the output of the interface logic. On command from the central controller and sequencer, the program for computation of the gyro spin vector direction cosines would process the simulated data, and the results would be telemetered to the ground facility. On the ground, the correct results for the test problem would be compared with the telemetered data to establish whether or not the computer was properly performing the direction cosine calculation.

A similar procedure could be used for checking the attitude error and body rate computation. However, little or no additional information would be obtained about computer operation. The same computer subsystems are used for the direction cosine computations, the attitude error computation, and the body rate computation. It is extermely unlikely that the computer can fail on any one of these programs without failing on all three; therefore, it should only be necessary to process information through one of the programs to ensure that the computer is functioning properly.

To monitor the actual operation of the ARS, it is suggested that the outputs of the direction cosine computations, the attitude error computations, and the body rate computation be telemetered to the ground facility. The frequency with which this information is transmitted is not critical; however, it should be several times the limit cycle frequency of the attitude control system, and synchronization with the limit cycle should be avoided.

The output of the direction cosine computation will be six binary numbers representing the direction cosines of the two gyro spin vectors in body coordinates. This information could be checked on the ground in two ways: The sum of the squares of the direction cosines for each spin vector should be equal to unity, and, in the steady state, the measured spin vectors should equal the commanded spin vectors. These checks should be made with some tolerance. The magnitude of the tolerance will require further investigation but will be a function of the accuracy of the ARS and telemetry.

The output of the attitude error calculation will be three binary numbers. These numbers represent commands to the autopilot or attitude control system and ideally in the steady state are zero. Since it is anticipated that the spacecraft steady-state condition will be a limit cycle, the attitude error signal will oscillate, and a check of the telemetered output of the attitude error calculation should show this oscillation.

The output of the body rate calculation will be three binary numbers representing the components on the body axes of the angular body rate in inertial space. Since the spacecraft attitude control system will establish a limit cycle about the commanded attitude, the body rate output of the ARS should reflect the limit cycle rate and frequency after the system has had sufficient time to respond to any commands. These characteristics may be used to check the validity of the body rate calculation on the ground.

CHECKOUT OF GYRO-COMPUTER INTERFACE LOGIC

The gyro-computer interface can be checked by providing simulated start-stop pulses at the input and observing the resulting output from the counters in the interface logic. If the computer is checked out prior to the interface logic, it may generate the start-stop pulses and provide the interface with the telemetry system for transmitting the counter outputs to the ground facility. Since the time between the simulated pulses is known, the correct counter outputs are known and can be compared with the data received on the telemetry at the ground facility.

SUMMARY

The preceding paragraphs suggest that the checkout of the ARS computer and gyro-computer interface logic be accomplished by telemetering the result of a checkout routine to the ground facility. Also, it is suggested that the computer operation in the control system be monitored by telemetering the outputs of the direction cosine computation, the attitude error computation and the body rate computation.

The suggested checkout and monitoring schemes are feasible and can readily be programmed on the ARS computer described in this report. The actual details of the checkout program, such as initiation, termination, etc., will require further definition of the interfaces of the computer with the telemetry system and the command system.

SECTION IV
SDMEG ARS FOR A CAPSULE LANDER

INTRODUCTION AND SUMMARY

Task II of the SDMEG ARS study contract requires the synthesis of an attitude reference system for a specific mission. This mission is that of a landing capsule which is separated from a parent space vehicle. After separation, the capsule is two-axis stabilized (pitch and yaw) to the constant ESG spin axis position with roll rate stabilization only. Rate signals for autopilot stabilization are also required in the pitch and yaw channels. The major requirements for this system, as specified by JPL, are presented in Table 4-1.

This section of the report discusses the synthesis and preliminary design of a system to meet the given specifications. The form this system assumes is shown in Figure 4-1. The gyro is the same as the one presently being developed for JPL, with two minor modifications. Two pickoffs would be required instead of three and a more easily applied rotor pattern would be used. The gyro electronics (suspension and vacuum) are also the same as the SDMEG electronics presently being developed. Only the readout electronics have been extensively revised to meet the ARS requirements specified by JPL. The selected readout electronics are comprehensively described as part of the system description.

The projected physical characteristics and major performance parameters of the selected system are presented in Table 4-2. The system was synthesized primarily to meet the attitude output requirements of Table 4-1, and comparison of the two tables shows that this goal was accomplished. (In the absence of direction, the performance specifications of Table 4-1 were assumed the equivalent of three sigma values, and the values listed for comparison in Table 4-2 were also calculated as three sigma. If the performance values of

Table 4-1. Specified Requirements for a Capsule Lander ARS

Time periods of the mission

Delivery to earth launch - 6 months to 1 year
Earth launch to gyro spin up - 200 days
Gyro spin up to capsule separation - 3 hours maximum
Capsule separation to retrofire ignition - 10 to 30 minutes
Retro firing time - 10 minutes maximum
End of retrofire to end of control requirements - 5 to 20 days

Expected environments

Acceleration - separation - 0.1g
retrofire - 0.5g
Rates - separation - 2 deg/sec
retrofire - 2 deg/sec

ARS attitude output requirements (pitch, yaw)

Form - analog
Accuracy ± 0.1 deg to end of retrofire
± 5 deg after retrofire
Threshold 0.05 deg
Linear Range ± 3 deg
Usable Range (Saturated signal, but sign sense retained) ± 10 deg
Bandwidth 15 cycles/second
Quality (i.e. allowable peak to peak noise over frequency range)
0.05 deg up to 20 cps
0.1 deg 20 cps and over

ARS rate output requirements (pitch, yaw)

Separate signal desired
Form - analog
Accuracy ± 0.05 deg/sec
Threshold 0.02 deg/sec
Linear Range ± 1.5 deg/sec
Bandwidth 5 cycles/second
Quality 0.02 deg/sec up to 20 cps
0.05 deg/sec 20 cps and over

ARS rate output requirements (roll)

Form - analog
Accuracy
Linear Range
Threshold
Usable Range
Bandwidth
Quality if analog

} Provide signal with sign information (no magnitude required) whenever roll rate exceeds 1.0 ± 0.3 rad/sec

General ARS requirements

Power Source

2400 ± 0.01% cycles/second square wave
Rise and fall times 5 ± 4 microseconds
Amplitude controlled to produce 50 volts RMS ± 3% absolute
Spikes 5 volts maximum amplitude
5 microseconds maximum duration

Packaging

Any assumed technique must be of standard practice by January 1966. The assumed technique must be capable of surviving the sterilization and launch environment requirements given in JPL Spec Nos. GMO-50198-ETS-A, XSO-30275-TST-A, and 30250B, respectively.

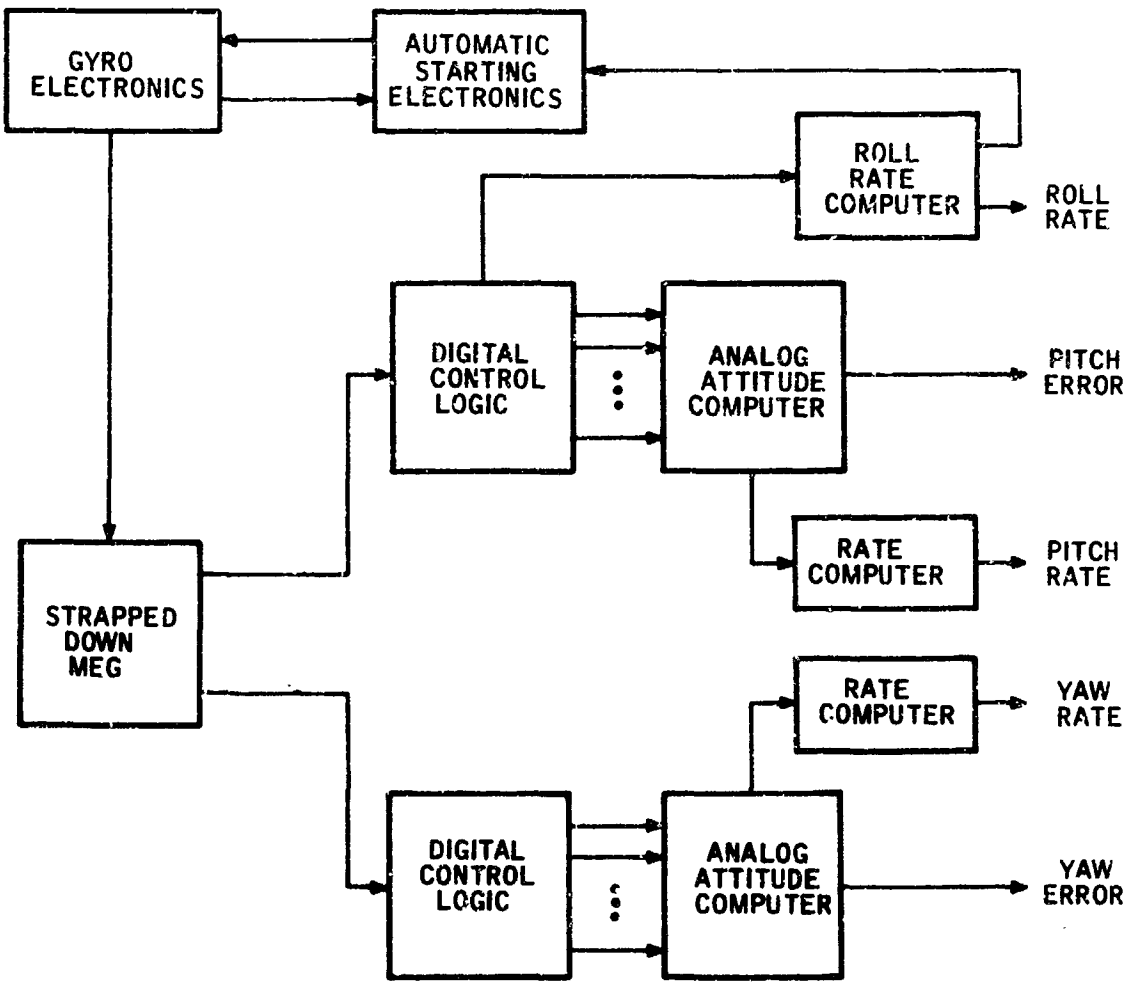

Figure 4-1. Two-Axis ESG-ARS Block Diagram

Table 4-1 were intended as one sigma the same comparison can be made by dividing the projected performance shown in Table 4-2 by three.) However, the accuracy and quality of the rate outputs are not as good as desired. As shown in the performance analysis, this is a consistent result; for the type of noise in the SDMEG ARS the attitude and rate performance requirements of Table 4-1 are not compatible.

The following discussion is divided into these four major topics:

- The analysis and reasoning leading to the selection of a particular system configuration is presented
- The system's general requirements are translated into specific hardware requirements; both the required gyro modifications and readout electronics are described
- A performance analysis is used to estimate the performance of the selected system
- The selected systems's reliability, size, weight, and power requirements are estimated, and along with the basis for these estimates are presented and discussed.

Table 4-2. Summary Characteristics for Selected ARS

Physical Characteristics		
Size	Gyro Assembly	104 in.^{3}
	Electronics Assembly	160 in.^{3}
Weight	Gyro Assembly	6.0 lbs.
	Electronics Assembly	8.5 lbs.
Power Requirements	Steady State	11.9 watts
	Peak Power	53.7 watts
Reliability	0.9814	(5 day descent)
	0.9523	(20 day descent)
Performance Parameters (3σ)		
Pitch and Yaw Attitude Outputs		
Accuracy	End of retro	±0.074 deg.
	5 days	±1.44 deg.
	20 days	±5.76 deg.
Quality	less than 20 cps	0.027 deg.
	over 20 cps	0.002 deg.
Pitch and Yaw Rate Outputs		
Accuracy		±0.19 deg/sec
Quality	less than 20 cps	0.37 deg/sec
	over 20 cps	0.048 deg/sec
Roll Rate Output		
The required ±0.3 rad/sec roll rate accuracy can be supplied for only the first 24 hours after separation.		

SYSTEM CONFIGURATION

Two basic types of systems can be considered for this application, with the system type dictated by the basic gyro configuration. The first type, employing a conventional SDMEG, is basically a digital system since the conventional gyro requires extensive digital data processing to provide intelligence. Digital

data processing could then be used to calculate error signals, and a digital-to-analog converter would be necessary to obtain the required analog outputs. A functional block diagram of such an ARS system is shown in Figure 4-2a. The second type of ARS assumes a modified SDMEG readout system with either a direct analog readout (e.g., end axis pattern) or a pulsed readout system which could be used to directly control an analog error angle calculation. A functional block diagram of an ARS which assumes the latter type of modified MEG readout system is shown in Figure 4-2b. The functional blocks of Figure 4-2 which change significantly between the two systems are so indicated.

Even a cursory examination and comparison of the two types of systems indicates that the synthesis of a system with the desired simplicity depends in turn on using a simplified ESG readout system. The following paragraphs present the analysis used to select a particular ESG readout scheme. The discussion is divided into two parts - end axis patterns, and equatorial patterns.

END-AXIS PATTERNS

One ESG readout mechanization which has been considered for application in the subject attitude reference system is the end-axis pattern. The following paragraphs discuss both conventional and nonconventional end-axis readout techniques.

The geometry of a conventional end-axis readout pattern and pickoff are shown in Figure 4-3. Let A be defined as the ratio of the high reflectivity rotor surface in the pickoff field of view to the total field of view area.

$$A = \frac{1}{2} + \frac{X}{\pi r}\sqrt{1 - \frac{X^2}{r^2}} + \frac{1}{\pi}\sin^{-1}\frac{X}{r}; \quad -r \leq X \leq r \tag{84}$$

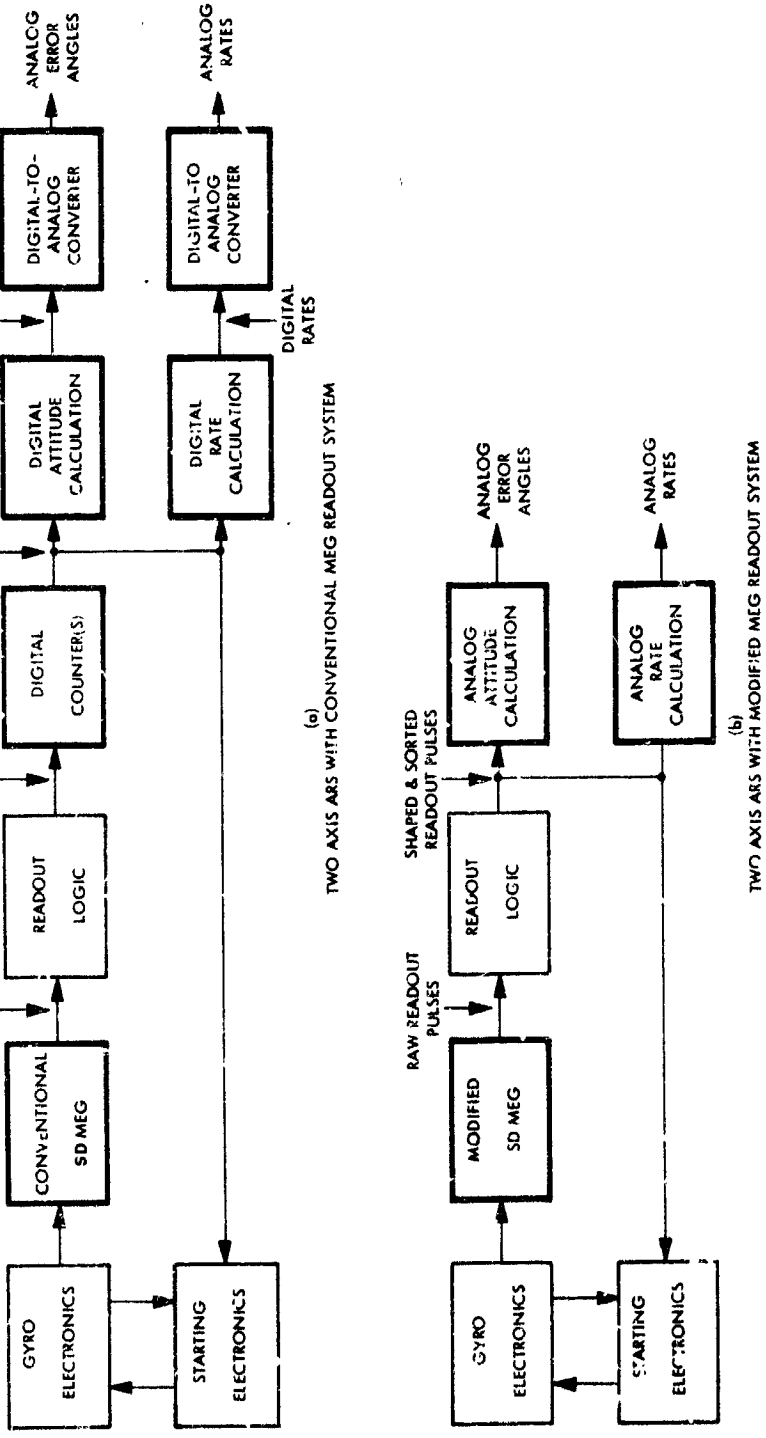

Figure 4-2. Functional ESG-ARS Block Diagram

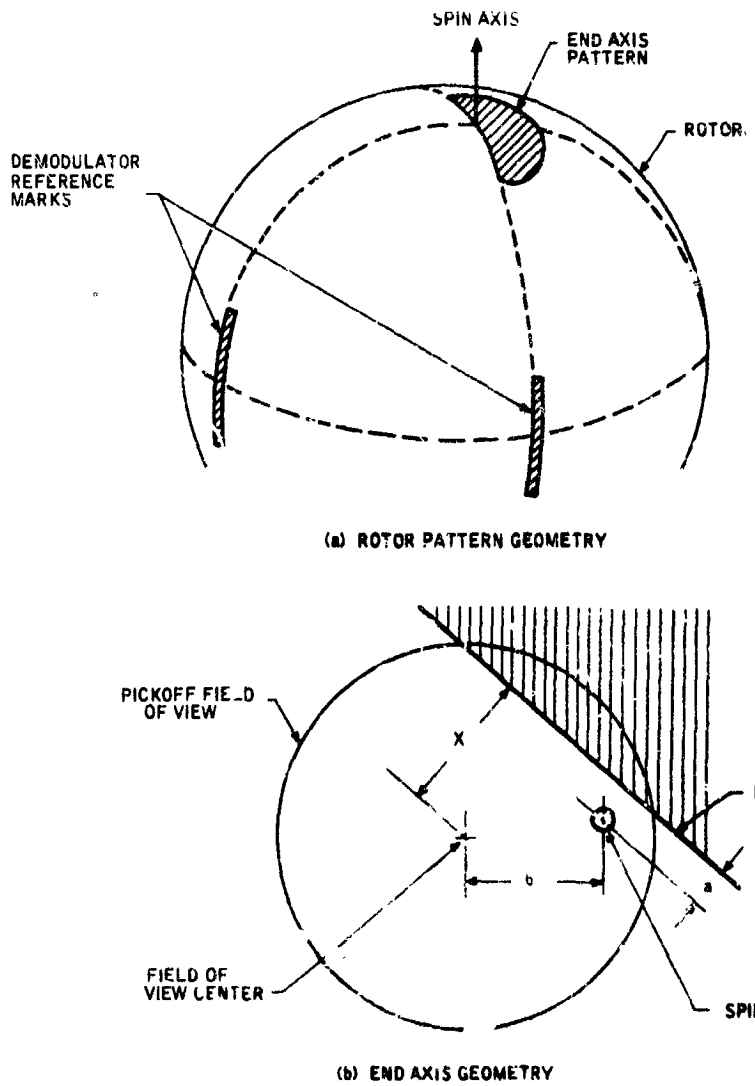

Figure 4-3. Conventional End-Axis Pattern and Pickoff Geometry

where

r = pickoff field-of-view radius

For a uniformly responsive pickoff, the pickoff output is proportional to A. Considerable analytical simplification results if this function is approximated by the center slope matched sinusoid.

$$A_1 = \frac{1}{2}\left[1 + \sin \frac{4X}{\pi r}\right] \quad ; \quad -r < X < r \tag{85}$$

The difference between Equations (84) and (85) is shown in Figure 4-4. Since the rounding of the sinusoidal function representing A_1 (relative to A) near $|X| = r$ approximates the expected effects of diffraction and residual aberration at the edge of the pickoff field of view, the response represented by A_1 is likely to be closer to reality than the exact expression.

The variation of X with time will be

$$X = a + b \sin (\omega t + \phi) \tag{36}$$

where

a, b = (shown in Figure 4-3)
ω = rotor speed
ϕ = arbitrary phase angle determined by direction of pickoff displacement

Substituting Equation (86) into Equation (85) then yields:

$$A_1 = \frac{1}{2}\left\{1 + \sin \frac{4a}{\pi r} \cos \left[\frac{4b}{\pi r} \sin (\omega t + \phi)\right] + \cos \frac{4a}{\pi r} \sin \left[\frac{4b}{\pi r} \sin (\omega t + \phi)\right]\right\} \tag{87}$$

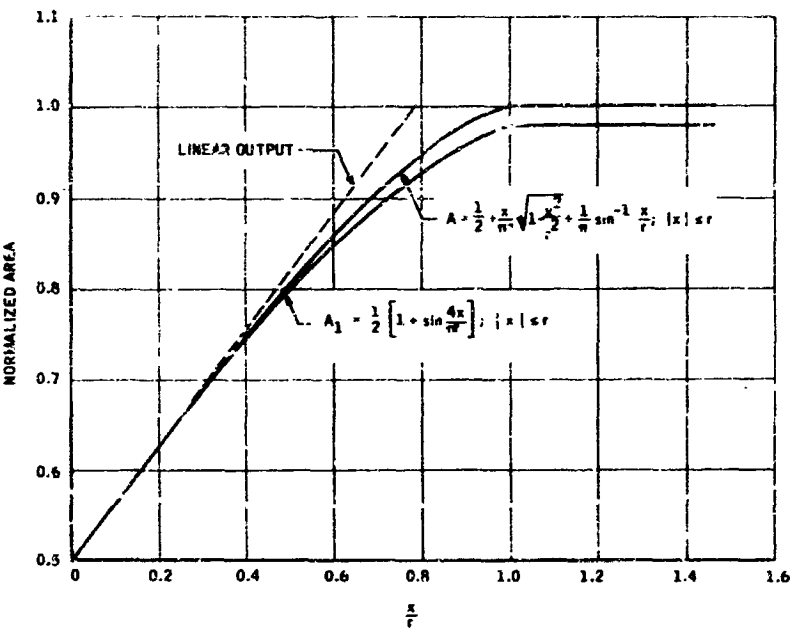

Figure 4-4. Pickoff Output for Conventional End-Axis Readout

A simple and effective method to get the desired information from this signal is the use of a square wave switched synchronous demodulator. A block diagram of such a system is shown in Figure 4-5. The reference square waves must, of course, be generated from the output of a second optical pickoff's viewing reference marks on the rotor (see Figure 4-3) so that this square wave is of the same frequency as the polar pickoff signal. Since this synchronous demodulator rejects all d-c and even harmonics, and a term of the form $\cos\left[K \sin(\omega t + \phi)\right]$ consists of only even harmonics, the effective portion of the signal represented in Equation (87) may be written as:

$$\left\langle \begin{matrix} A \\ 1 \end{matrix} \right\rangle = \frac{1}{2} \cos \frac{4a}{\pi r} \sin \left[\frac{4b}{\pi r} \sin(\omega t + \phi) \right] \tag{88}$$

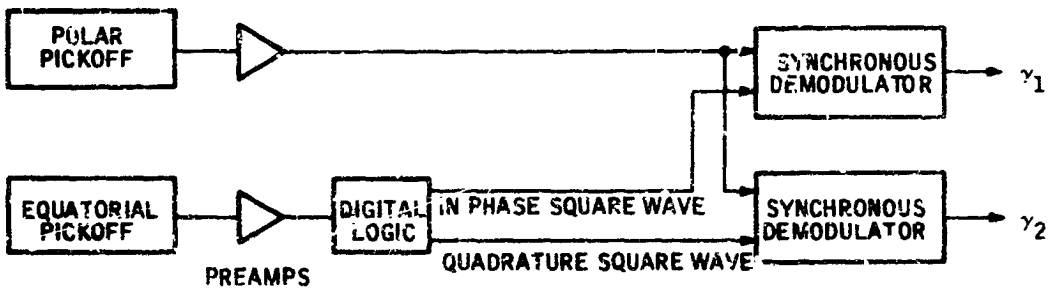

Figure 4-5. End-Axis Pickoff Readout Electronics

The zero-degree phase and 90-degree phase components of this signal (outputs of the synchronous demodulators) would then be directly proportional to the pitch and yaw error angles desired for the attitude reference system. It should be noted that the dimension a, which is caused by improper pattern application, does not affect null position or signal phasing, but merely results in a slight change in sensitivity.

An indication of the linear range of the polar pickoff readout scheme can be obtained by examining Figure 4-4. More accurately, the ideal linear output may be defined by the slope of Figure 4-4 at X = 0 as

$$A_2 = \frac{1}{2} + \frac{2X}{\pi r} \tag{89}$$

and the linear range, as a function of percent linearity P, is then found by solving

$$P(10^{-2}) = \frac{A_2 - A_1}{A_1} = \frac{\frac{2X}{\pi r} - \frac{1}{2}\sin\frac{4X}{\pi r}}{\frac{2X}{\pi r}} \tag{90}$$

For 10 percent linearity the solution yields X/r equal to 0.62. Since present pickoff technology limits the optical pickoff field of view to about 10 mil-inches, this result indicates a 10 percent linear range of about ±0.175 degree for a 1-inch radius rotor and a total range in which the signal output is at all proportional to displacement of ±0.286 degree (equal to pickoff field of view).

These extreme limitations on linear range make the conventional end-axis readout scheme unsuitable for the attitude reference system being studied and have led to a consideration of other end-axis readout schemes - particularly mechanizations in which the linear range of the readout system is not limited by the pickoff field of view. However, no completely applicable readout scheme based on end-axis patterns has been envisaged. As an example of the difficulties encountered, the readout mechanization associated with the modified end-axis pattern shown in Figure 4-6 is briefly discussed below.

The end-axis pattern of Figure 4-6 is applied so that the relationship between the rotational angle ϕ and the error angle γ (total pickoff displacement) is given by

$$\phi = A + K\gamma \tag{91}$$

This simple readout equation would allow a corresponding simple readout mechanization using a combination of analog and digital circuitry. The actual mechanization of such a readout system would be similar to that presented in the discussion of Equatorial Patterns (following subsection). The shortcoming of such a readout system is obvious from an examination of Figure 4-6b, which is drawn approximately to scale for $A = \pi/2$, $K = 18$. The finite line width of the pattern [line widths of about $8(10^{-3})$ inches are presently used] causes a proportional readout null uncertainty. For a 1-inch radius rotor, the corresponding null uncertainty of nearly ±0.5 degree is excessive for the attitude reference system under consideration.

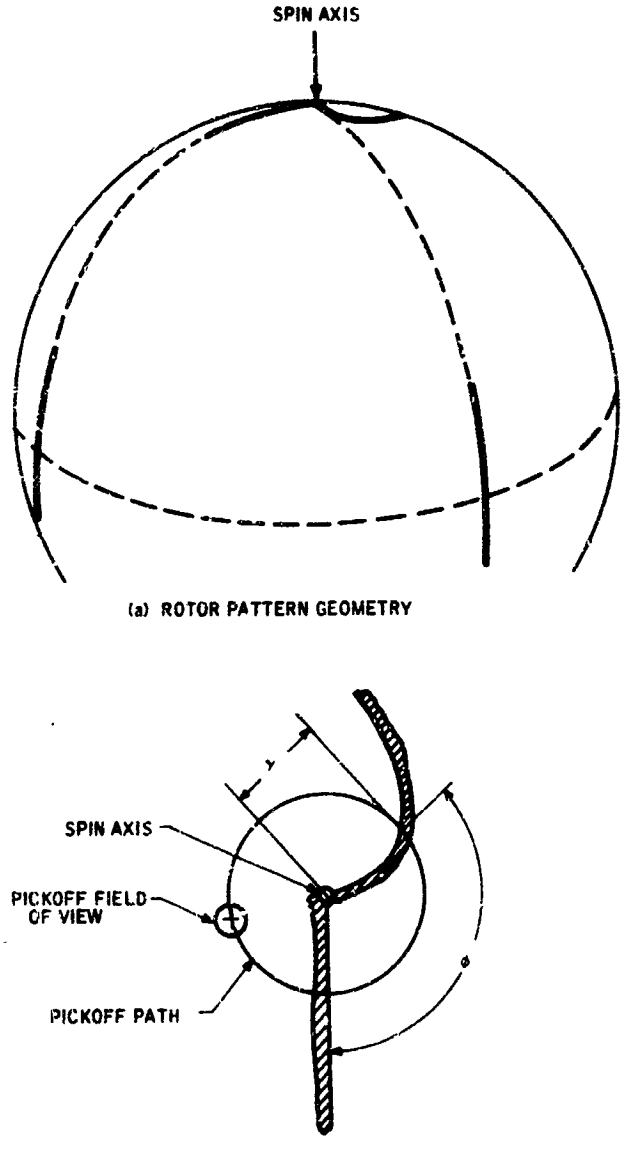

Figure 4-6. Modified End-Axis Pattern Geometry

The possibility still remains that a dual range end-axis readout system -- using the conventional end-axis pattern to provide the required null accuracy and the modified end-axis pattern to provide the required linear range -- could be mechanized. However, the apparent complexity of such a system, the difficulty of matching scale factors in the two ranges, etc., dictates investigating alternate approaches first.

EQUATORIAL PATTERNS

Pattern and pickoff geometry for a very attractive ESG readout mechanization employing an equatorial pattern is shown in Figure 4-7. This pattern appears desirable for the ARS under consideration because of the relatively simple readout equation. The assumed patterning equation is:

$$\phi = \pi \left(1 - \frac{\gamma}{B}\right) \quad ; \quad -B \leq \gamma \leq B \tag{92}$$

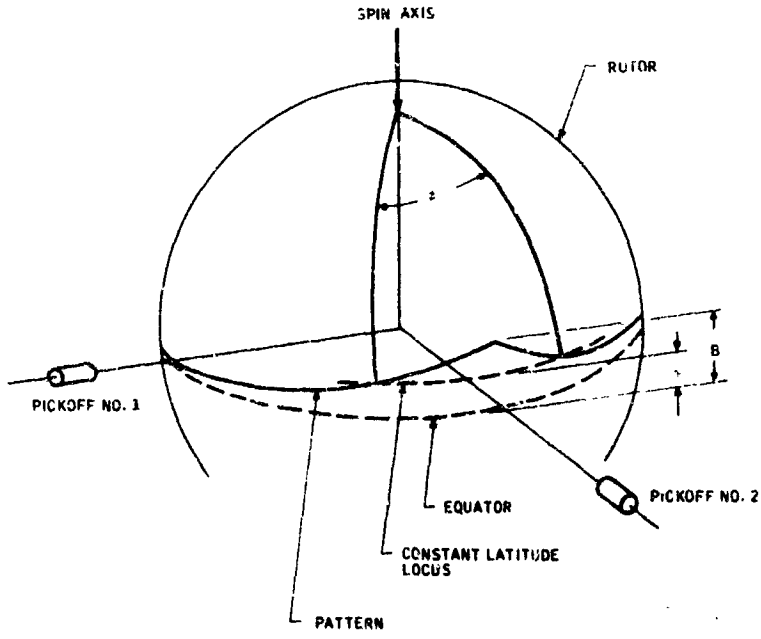

Figure 4-7. "Constant Slope" Equatorial Pattern Geometry

Variation of the parameter B in Equation (92 trades off sensitivity (scale factor) for linear range. Since the derivative of the included rotational angle ϕ with respect to the pickoff displacement angle γ is a constant, this type of pattern may be named a "constant slope" pattern. The two pickoffs shown in Figure 4-7 would be mounted parallel to vehicle pitch and yaw axes; hence, angle γ sensed by each pickoff would be a direct measure of the required attitude reference system error angles.

For the rotor pattern of Equation (92), linear range and usable range are the same and are equal to approximately B (ignoring linewidth effects). Selection of the constant B requires consideration of not only the desired readout range, but also the manner in which the readout errors are affected by this constant. Since the derivative of γ with respect to ϕ is directly proportional to B, and ϕ is the angle which is actually sensed in the readout scheme, any increase in B will cause a proportional increase in the readout angle errors caused by inaccuracies in determining ϕ. It is therefore desirable from the standpoint of accuracy and sensitivity to keep B as small as possible consistent with the system linear range requirements.

The readout equation to be mechanized in the readout system is readily obtained by solving Equation (92) for γ.

$$\gamma = B\left(1 - \frac{\phi}{\pi}\right) \tag{93}$$

Figure 4-8 demonstrates a conceptual (single-axis) readout electronics mechanization which could be used to solve this readout equation. Since, in terms of the pickoff output of Figure 4-8,

$$\phi = 2\pi \frac{T_1}{\tau} \tag{94}$$

where τ = rotor period

Equation (93) may be rewritten as

$$\gamma = B\left(\frac{\tau - 2T_1}{\tau}\right) \tag{95}$$

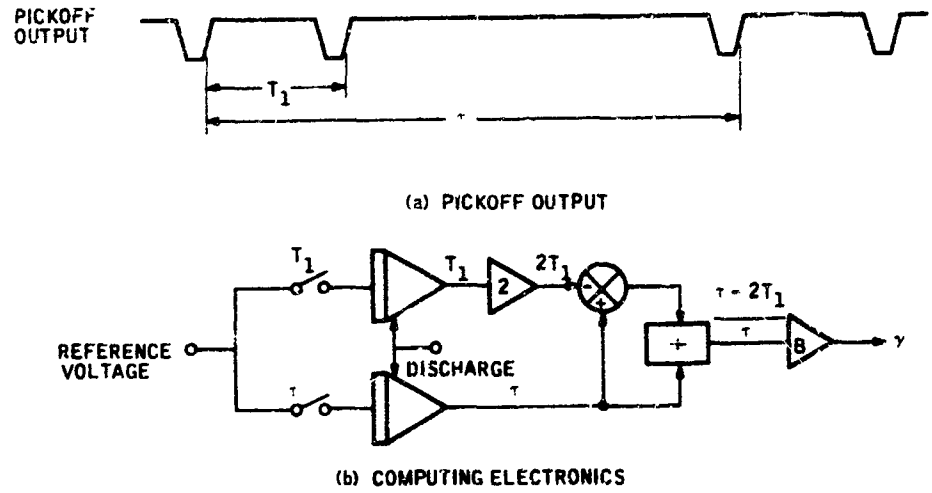

Figure 4-8. Conceptual Readout Mechanization

Equation (95) can be solved by a computing mechanism such as shown in Figure 4-8. The switches(digital controls) are closed for times T_1 and τ, respectively. The outputs of the integrators, when operated upon as shown, then yield the required error angle γ. Two such computing channels, operating on alternate rotor revolutions and discharged between each operating cycle, would provide a continuous analog attitude signal for one channel of the ARS under investigation.

The extreme simplicity of the ESG readout equation and the resulting simplicity of the readout mechanization has been obtained, at least in part, at the expense of a relatively complex rotor pattern. The simplest ESG rotor pattern to apply is a great circle pattern since it requires rotating the ESG rotor (or patterning tool) about a single axis. Any pattern which is not a great circle requires (at least theoretically) simultaneous rotations about two axes. The difficulties associated with the precision control of two simultaneous rotations greatly increases the complexity of the rotor patterning process. Fortunately, the

"constant slope" rotor pattern of Figure 4-7 can be very accurately approximated, at least in the critical region near $\gamma = 0$, by a great circle pattern of low inclination. The appropriate readout equation for a great circle pattern is:

$$\gamma_1 = \tan^{-1}\left[\tan i \cos\frac{\phi}{2}\right] \tag{96}$$

where i = great circle inclination angle

For the type of attitude reference system under consideration here, where the primary concern is accuracy near the null ($\gamma = 0$ or $\phi = \pi$), the "best" approximation is obtained by matching slopes at the critical point. From Equations (93) and (96)

$$\frac{d\gamma}{d\phi} = -\frac{B}{\pi} = \left.\frac{d\gamma_1}{d\phi}\right|_{\phi=\pi} = -\frac{1}{2}\tan i$$

or

$$i = \tan^{-1}\frac{2B}{\pi} \tag{97}$$

The accuracy with which the great circle pattern of Equations (96) and (97) approximates the "constant slope" pattern of Equation (93) may readily be calculated as:

$$\Delta\gamma = \gamma_1 - \gamma = \tan^{-1}\left\{\frac{2B}{\pi}\cos\frac{\phi}{2}\right\} - B\left(1 - \frac{\phi}{\pi}\right) \tag{98}$$

This error is plotted in Figure 4-9 as a function of γ_1 (the actual readout angle) for several different values of B. The 10 percent error line included in Figure 4-9 as an aid in interpretation demonstrates the extreme nonlinearity of the readout error contributed from this source. As expected, increased linear range (by increasing B or i) can be obtained at the expense of scale

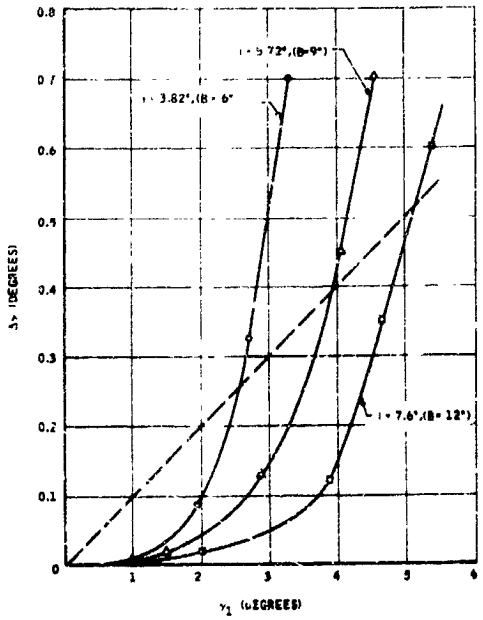

Figure 4-9. Error Contribution - Great Circle Approximation of "Constant Slope"

factor sensitivity. The errors involved are such, however, that for the attitude reference system under consideration reasonable pattern linearity can be provided for the total required usable system range (±10 degrees). This would be accomplished by selecting a great circle of suitable inclination (approximately 7.5 degrees) and patterning the rotor in the critical area near $\gamma = 0$ with this great circle. When the systematic error of the great circle pattern approaches that which could be easily obtained (requiring no expensive pattern development or patterning equipment or procedures) with the more complex "constant slope" pattern - about 0.1 degree - the rotor pattern would then be extended to approximate the "constant slope" equatorial pattern. Even a piecewise linear (continuous) approximation to the "constant slope" rotor pattern would be adequate.

These considerations lead to the type of pattern shown in Figure 4-10. In addition to the combined great circle - constant slope rotor pattern, a reference line (pattern line along a rotor meridian) has been added to this pattern.

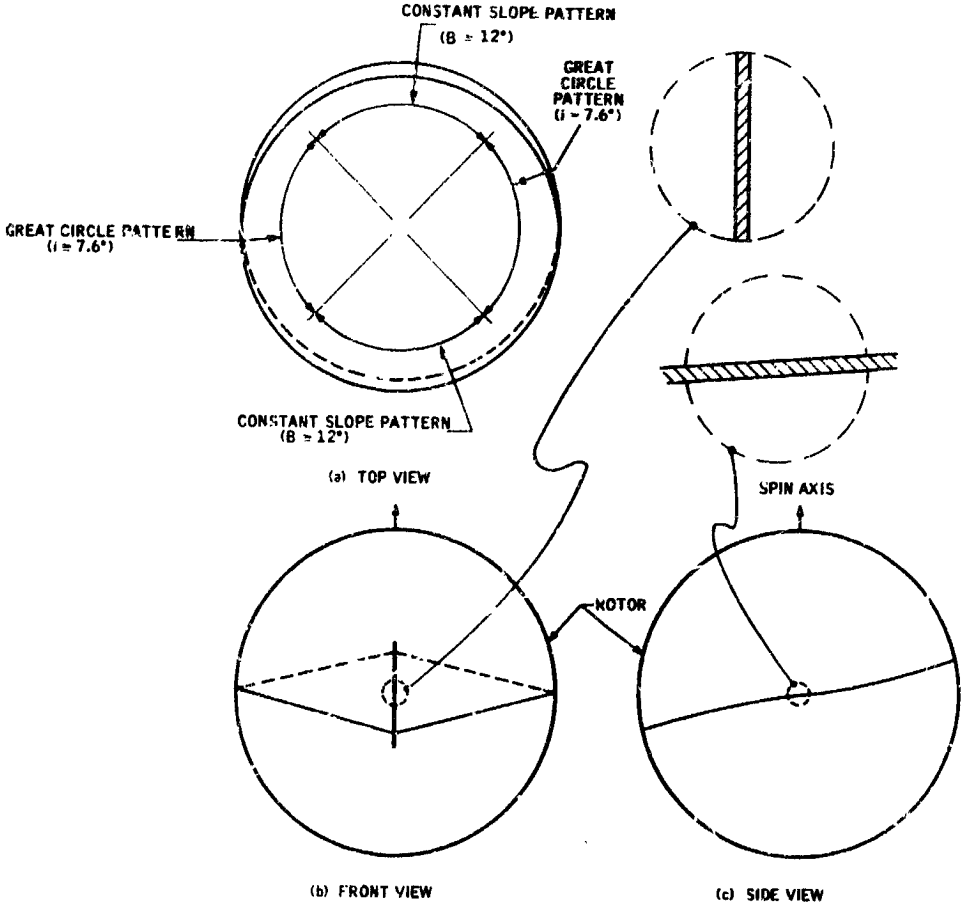

Figure 4-10. Combined Great Circle - Constant Slope Pattern

This reference line is useful in decoding the information in the readout pulses (e.g., without the reference line, how can the pulse at which the two-time measurements of Figure 4-8 are initiated be identified?).

Careful study of the pattern represented in Figure 4-10 reveals one major deficiency - it does not exhibit the required type of symmetry. Since the gyro will have to be started remotely, by an automatic starting system, it is desirable that the pattern be equivalent (fulfill the same readout equation) when the rotor is spun in either of the two possible orientations. Further explanation of this consideration is contained in MH Report 1726-PR10. If the pattern line from which the times of Figure 4-8 are measured is defined as that pattern line immediately following the reference line (the reference line can be detected, for example, by pulse width discrimination), the pattern represented in Figure 4-10 then fulfills Equation (93) in the orientation shown. However, in the other orientation the readout equation would be

$$\gamma_i = - B \left| 1 - \frac{\phi}{\pi} \right| \qquad (99)$$

This is effectively a 180-degree phase change in the indicated output (error) angles.

There are two immediately obvious methods which can be used to remedy this deficiency. First, enough intelligence could be included in the rotor pattern to sense rotor orientation (e.g., two reference lines - one wider than the other) and the readout angles can then be switched to reflect the rotor orientation. Second, the rotor pattern could be modified so that it exhibits the desired symmetry. A pattern which, with no additional patterning difficulty, exhibits this symmetry is shown in Figure 4-11. The two pattern halves are again combination great circle - constant slope patterns, with one pattern half rotated by an angle 2i about a line through its center.

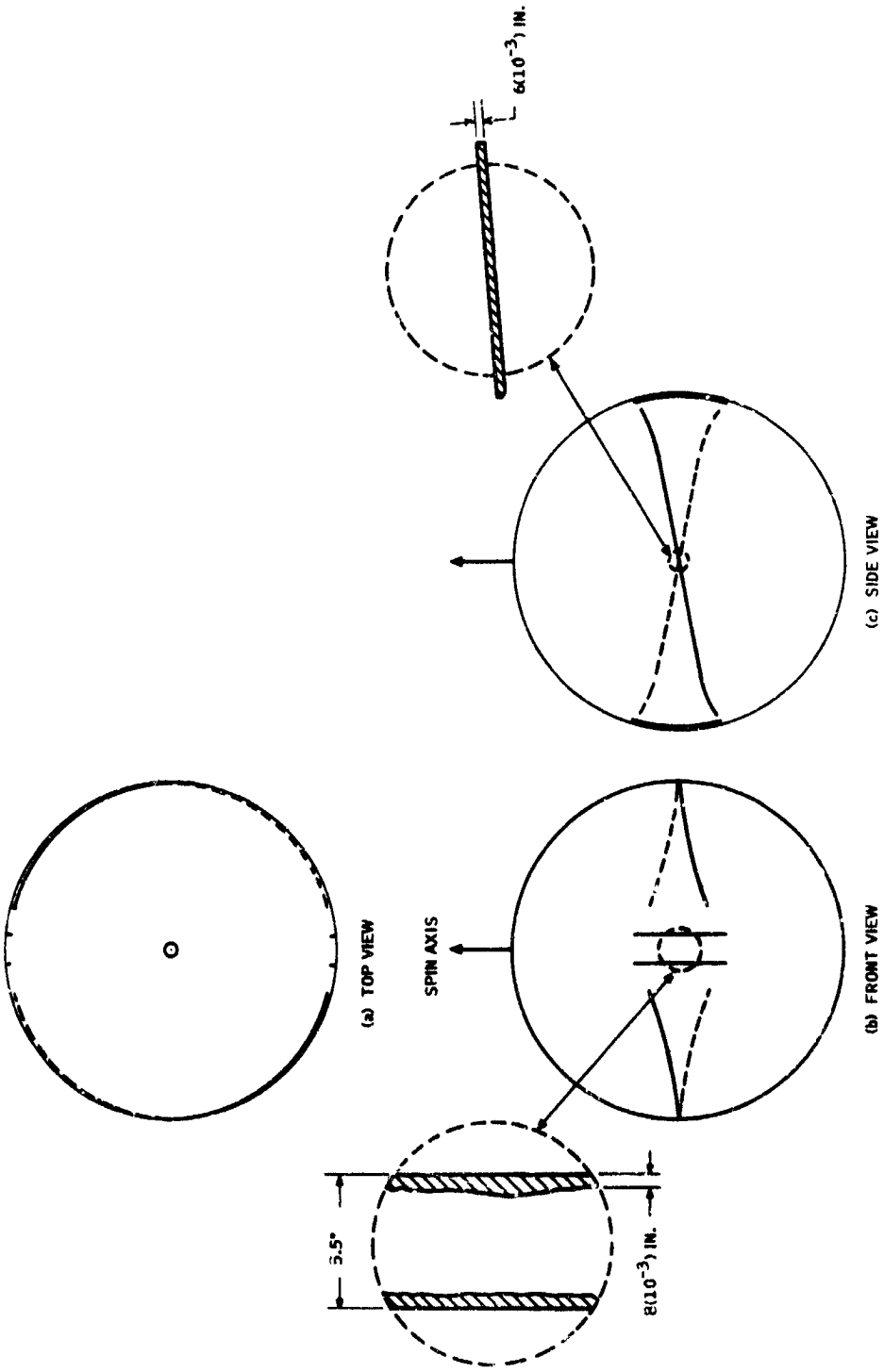

Figure 4-11. Symmetric Great Circle - Constant Slope Pattern

if the parameters associated with the pickoff output when using the pattern of Figure 4-11 are defined as in Figure 4-14, the readout equation to be solved may be shown to be

$$\gamma = B\left[\frac{\tau_b - 2T_1}{\tau_b}\right] \tag{100}$$

This is exactly of the same form as the previously developed readout equation [Equation (95)]. Hence, an identical (conceptual) computing mechanism can be used to effect the required solution.

Some of the practical patterning details associated with the limited range equatorial patterns are also presented in Figure 4-11. First, the line width of the "constant slope" pattern is represented as $6(10^{-3})$ inches. This width has been specified somewhat narrower than the usual pattern line width of about $8(10^{-3})$ inches in order to minimize the "effective" width of the pattern -- the rotor rotational angle included between the constant latitude points on opposite sides of the pattern line. For a 1-inch radius rotor the $6(10^{-3})$ inch pattern width still has an "effective width" of about 5.15 degrees. Therefore, in order that the rotor pattern satisfy Equation (100) in either of the two possible orientations, it is necessary that the trailing edges of the two reference meridians (trailing edge triggering in the electronics is assumed) be separated by 5.15 degrees. The $6(10^{-3})$ inch line width of the constant slope pattern is considered near the minimum of what can be tolerated without encountering severe sensitivity to noise (particularly rotor blemishes) in the readout system. Even this line width supplies only about 70 percent of the maximum possible output of an optical pickoff with a $10(10^{-3})$ inch field of view, thereby making use of pulse width discrimination in the readout system desirable (this type of discrimination minimizes the sensitivity to noise spikes).

A preliminary investigation of the complexity of the computing electronics necessary to decode the pickoff signals from the rotor patterns of Figures 4-10 and 4-11 showed very little tradeoff on this basis. The necessary electronics for the

two-rotor patterns is very nearly the same. The pattern of Figure 4-11, however, has two very definite advantages. First, a data rate of twice per revolution (instead of once per revolution for the pattern of Figure 4-10) can be provided. Second, the maximum time delay in the basic readout system is limited to the ESG rotor period (instead of twice the rotor period for the pattern of Figure 4-10).These two advantages have subsequent desirable effects on the system's frequency response, the ease of differentiating the attitude data to obtain rate information, and the ease of designing an adequate attitude control system for the carrying vehicle. Because of these advantages, and because the pattern of Figure 4-11 appears to provide more than adequate accuracy for the application being considered (this point will be further investigated in a performance analysis), it is the one which has been selected for further development.

SYSTEM DESCRIPTION

GYRO MODIFICATIONS

The functional characteristics of the SDMEG for the subject ARS will necessarily differ from the standard SDMEG being developed for JPL (see Honeywell Reports 1726-FR1 and 1726-FR2) in only two ways:

- Rotor Pattern
- Optical Pickoff Configuration

The selected rotor pattern was described in a previous paragraph of this report. The simplicity and low accuracy requirements of the selected rotor pattern should result in a correspondingly small patterning development effort. As a matter of fact, substitution of this pattern for the present cosine pattern represents a significant gyro simplification.

Furthermore, it is obvious that this pattern requires only two optical pickoffs (instead of the standard three) to accomplish the readout process. Hence, the additional gyro simplification of omitting one of the optical pickoffs would be used for this ARS.

In addition to the above indicated modifications, it might also be desirable to include provisions for mechanically adjusting and stabilizing the ESG damping coil alignment in the gyro design. Tests have shown that the ESG spin axis repeatably cages to an orientation accuracy of about one arc minute during damping. Since this one-arc minute accuracy is accurate enough for this ARS, precision caging would probably be used for initial spin axis alignment. The above caging orientation adjustment would then be used to align the initial spin axis orientation parallel with the vehicle roll axis (normal to the plane of the two optical pickoffs).

ELECTRONICS DESCRIPTION

The operating principles of both the standard electronics associated with every ESG - suspension electronics, vacuum electronics, optical pickoffs - and some of the special purpose electronics necessary for this ARS - remote starting electronics - are available in other documents and will not be repeated here. The physical characteristics of all these electronics are included as part of the size, weight, and power summary.

The following paragraphs present the operating principles of only the electronics which are unique to this ARS configuration, the gyro readout electronics. The presentation is divided into two major headings, attitude calculations and rate calculations.

Attitude Calculations

The gyro readout equation to obtain attitude information from the ESG was given in Equation (100), and a conceptual mechanization of the computation electronics which could be used to solve this equation was presented in Figure 4-8. The most difficult part of these electronics to mechanize -- at least with an analog mechanization -- is the indicated division. A considerable electronics simplification can be effected by recognizing that, for the period of time which the subject ARS must operate (5 to 20 days), the rotor period in the denominator of Equation (100) can be well approximated by a constant. If τ_{b1} is the assumed constant value, the readout equation may then be written as

$$\gamma \sim \frac{B}{\tau_{b1}} \left| \tau_b - 2T_1 \right| \qquad (101)$$

Since the factor B/τ_{b1} is constant, the solution to this equation no longer requires division. Typically, an ESG with the configuration of the JPL SDMEG would be expected to have a rundown rate of one-half rpm per day or less, causing a difference of less than five percent between the actual and (assumed)

constant rotor period for a nominal 200 rps operating speed. Furthermore, the approximation used to obtain Equation (101) is seen to cause no null offset or error; it merely results in a five percent sensitivity (gain) variation.

The operational characteristics of the assumed electronics components used to synthesize a functional block diagram of the readout electronics are presented in Figure 4-12. Both analog and digital circuits are shown. This figure is not meant to represent functioning of the circuits which would be used in an actual design; the represented building blocks are merely idealized logic elements which aid the synthesis of a functional block diagram.

An analog computing module which could advantageously be used to solve Equation (101) is presented in Figure 4-13. The operation of this circuit may be readily understood by first considering only the upper one-half of the network and the corresponding digital control waveforms of Figure 4-14. Assume the integrators have zero initial conditions. Then, at a slight increment of time after the reference pulse ($\omega t = 0 + \epsilon$ in Figure 4-14) control signals (14) and (16) switch appropriate reference values to the inputs of the two integrators. Subsequently, with the same time lag at $t = T_1 + \epsilon/\omega$ signal (16) removes the input to one of the integrators and at $t = \tau_b + \epsilon/\omega$ signal (14) removes the input to the remaining integrator. Also, at $t = \tau_b/\omega$, signal (9) turns on the summing amplifier so the difference of the two integrator outputs is transmitted to the system output through an appropriate gain constant. This output is maintained for one-half a rotor revolution. Then, at $t = 360°/\omega$, signal (9) removes the integrator outputs from the system output, signal (10) is used to discharge the integrators and restore zero initial conditions, and the cycle is repeated. The remaining half of the computing module of Figure 4-13 performs exactly the same function for the alternate half cycles of rotor revolution. The lag ϵ which is built into the system provides a means of discharging the integrators without introducing any significant transients into the system output, and allows the entire computing job (for one readout channel) to be done with just two identical computing circuits.

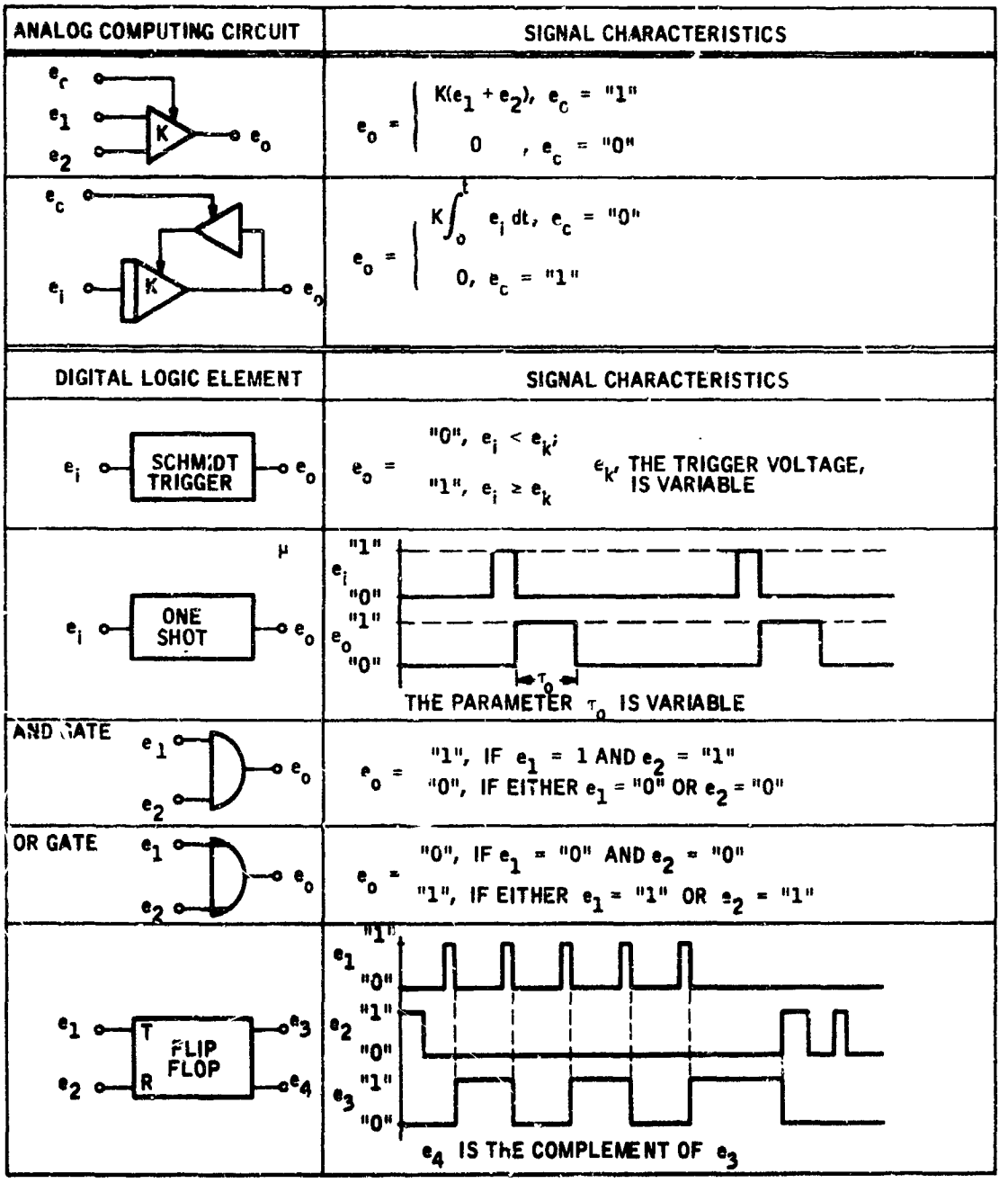

Figure 4-12. Platform Components for Readout Electronics

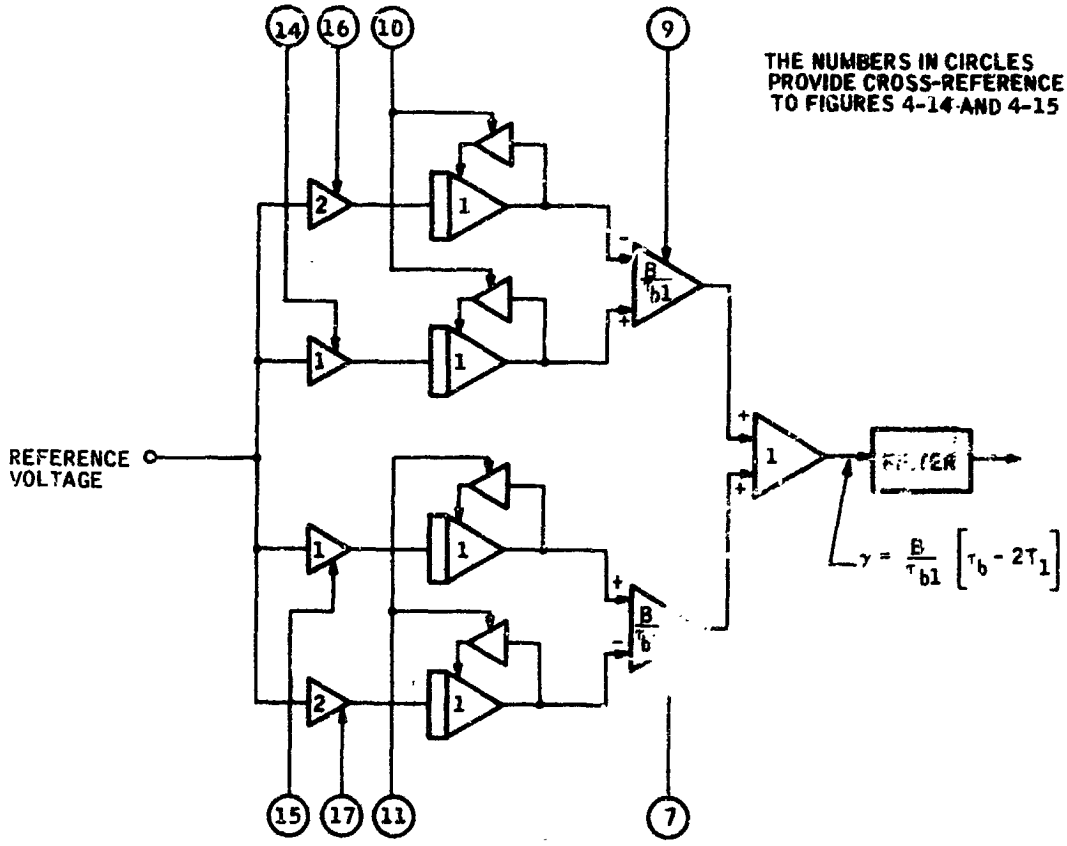

Figure 4-13. Analog Attitude Computing Module Functional Block Diagram

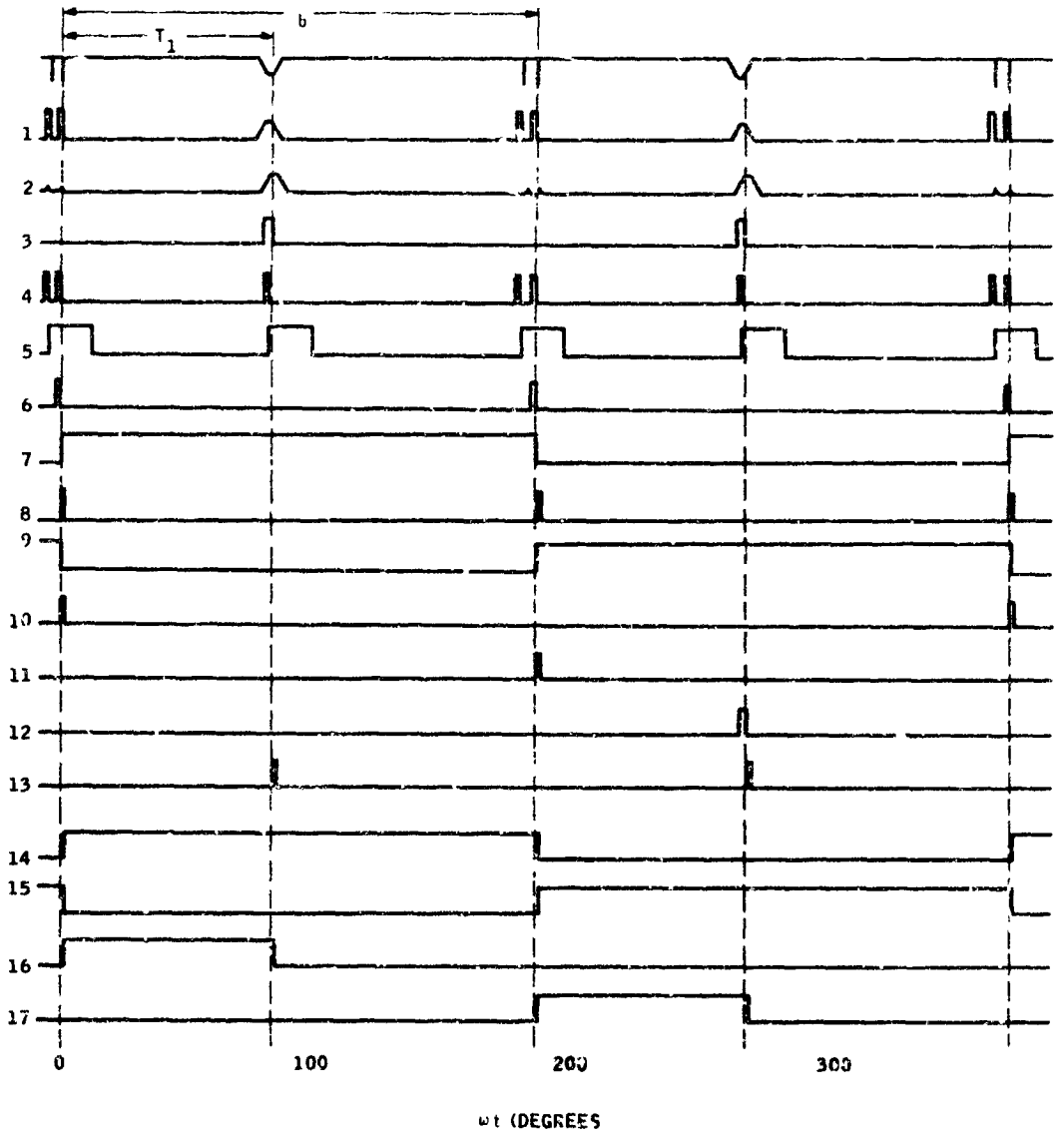

Figure 4-14. Digital Control Signal Waveforms

Alternately, an analog attitude computing module which employs only one-half of the computing circuitry of Figure 4-13, in conjunction with a "sample and hold" type of circuit to provide a continuous analog output, could be mechanized. A brief investigation of this concept indicated that calculations would then be accomplished only on alternate cycles of the ESG readout signals, and that no appreciable equipment savings would be effected. Hence, the system of Figure 4-13 was adopted.

The digital control logic used to generate the necessary control signals for the analog attitude computing module is shown in Figure 4-15. The operation of this circuitry, when examined in conjunction with the waveforms of Figure 4-14 and the individual element characteristics of Figure 4-12, is relatively straightforward. However, several special features built into this control logic deserve further attention. First, a pair of one shots (output signals (8) and (13)) are used to provide the lag ϵ discussed in the previous paragraphs. Second, the reset signals to the three flip-flops on the extreme right side of Figure 4-15 have no effect on the circuit during steady-state operation. These reset signals do, however, provide synchronization when the circuit is first started so that the initial acquisition process is entirely automatic. Third, separate triggers for the reference and constant slope pattern pulses are provided so that different voltage triggering levels may be used. The Height Insensitive Trigger (see MH Report 1726-FR1) for the constant slope pattern pulses is used in conjunction with a pulse width discriminator to provide rejection of all but the desired pulse. The triggering level for this pulse may then be set at quite a low value without introducing noise susceptability, thereby allowing use of a narrow pattern line. For the (assumed) nearly constant rotor speed operation of ESG and the pattern geometry of Figure 4-11, the pulse width discriminator of Figure 4-15 need be nothing more than a simple lag. The Schmidt trigger used for the reference pattern line would be set at a higher level; the circuits attached to the output of this Schmidt trigger provide very good noise rejection and will operate properly regardless of whether or not the incoming pulses from the constant slope pattern trigger the circuit.

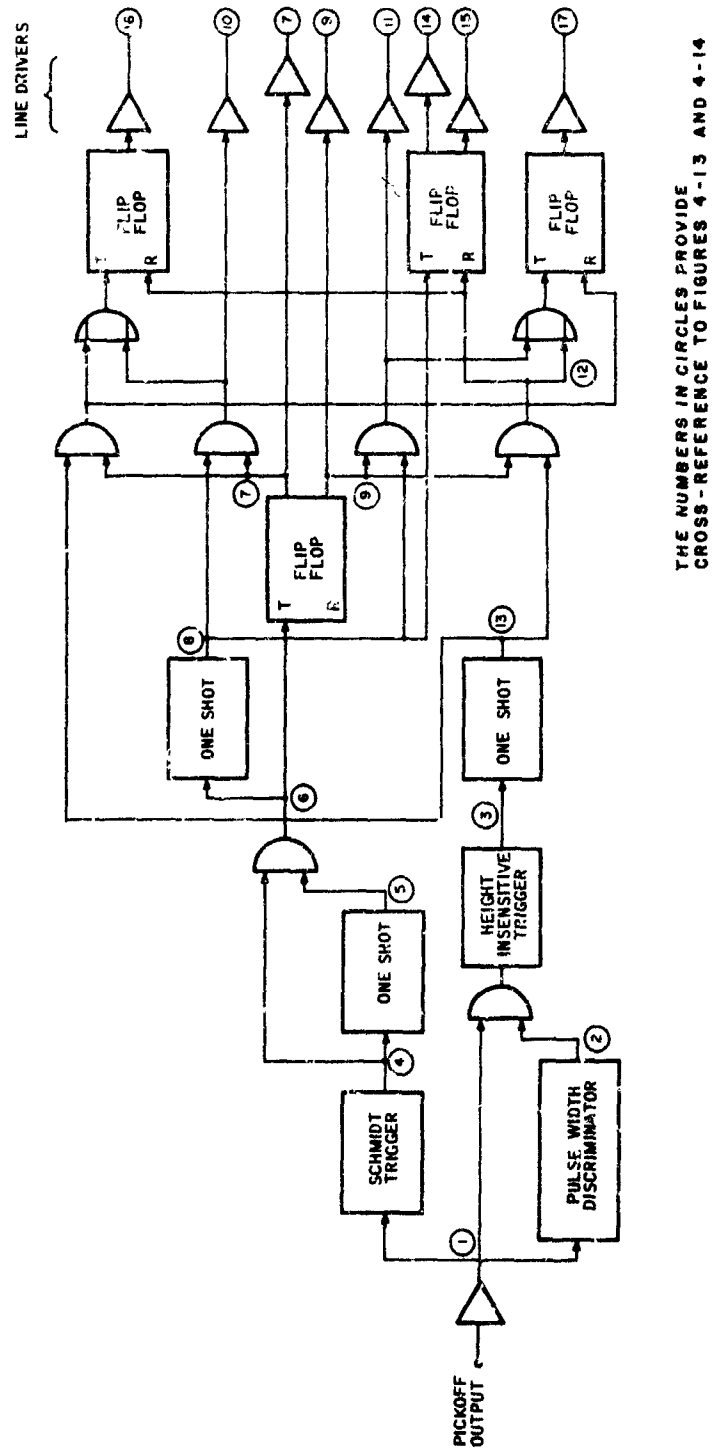

Figure 4-15. Digital Control Logic Functional Block Diagram

Rate Calculations

The required pitch and yaw rate signals are obtained quite simply by "differentiating" the output of the (corresponding) attitude computing module (Figure 4-13). The circuit chosen to approximate the required differentiation is shown in Figure 4-16. The transfer function of this lead-lag circuit is simply

$$\frac{E_o}{E_i} = \frac{K}{\tau(1+K)} \left[\frac{\tau S + 1}{\frac{\tau}{HK} S + 1} \right] \simeq \left(\frac{1}{\tau} \right) \frac{\tau S + 1}{\frac{\tau}{K} S + 1}$$

This circuit is used because it can be adjusted to closely approximate an ideal differentiator over the frequency range of interest.

Selection of the break points for this differentiating circuit is partially a matter of judgment. The rate signal has a required bandwidth of 5 cps. The magnitude of the lead-lag circuit approximates the magnitude of the ideal differentiator at the 5 cps point to about one percent if the frequency of the lag is chosen as 30 cps. A practical value for the (low frequency) lead is about 0.01 cps ($\tau \simeq 16$ seconds) indicating a required gain in the forward loop of about $3(10^3)$. The gain stability of this amplifier should be about one percent to achieve accuracy compatible with the differentiator approximation. The adequacy and performance of this approximation to the desired differentiator is further discussed in the system performance analysis.

For the third vehicle axis a signal with sign information (no magnitude) is required whenever the roll rate exceeds 1.0 ± 0.3 radians per second. This rate signal is much more difficult to derive than the other two. Two possible methods for obtaining this signal have been investigated, and neither method is wholly satisfactory. The first method assumes that the speed of the ESG rotor is known; the vehicle roll rate is then obtained by comparing the

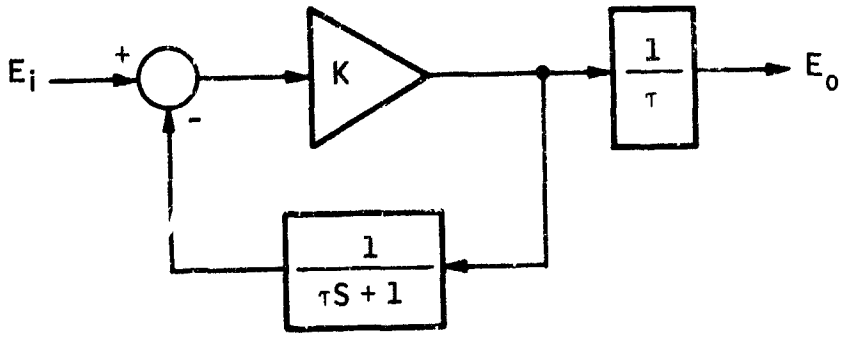

(a)

Rate Computer Block Diagram

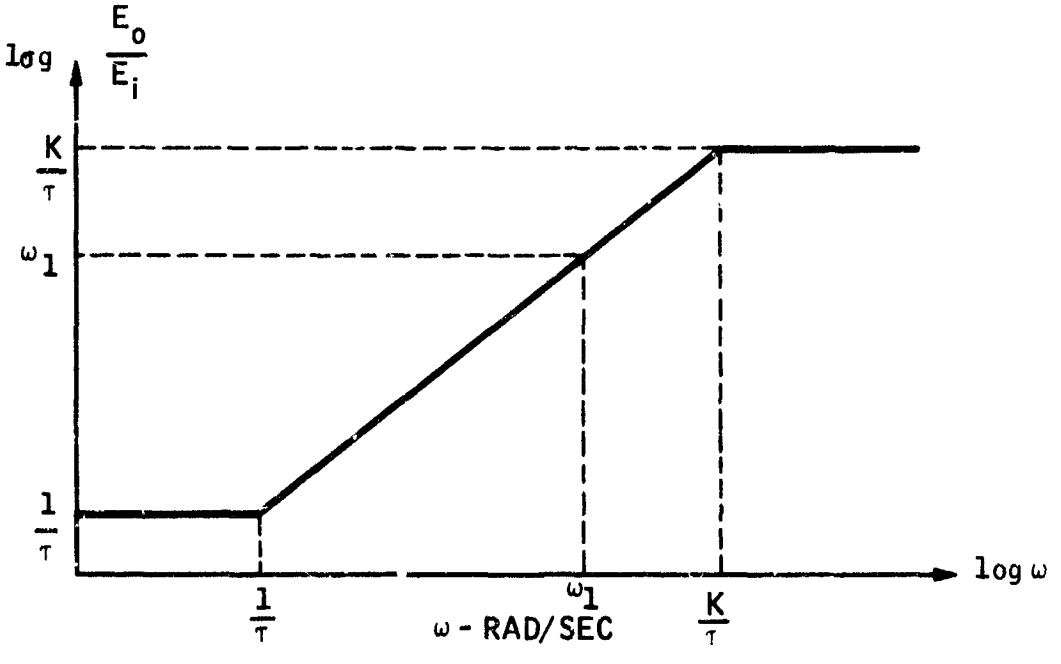

(b)

Rate Computer Transfer Function

Figure 4-16. Pitch and Yaw Rate Computer

measured speed and the known speed. The second method assumes that the ESG is mounted as far as possible (more than one foot) from the roll axis of the capsule lander. Roll rate is then sensed by measuring the associated centripetal acceleration.

The first method has an immediately evident limitation. It requires a knowledge of the ESG rotor speed to the same accuracy as the rate calculation. The JPL SDMEG configuration is expected to have a rundown rate of about 0.5 rps per day. When the effects of unknown magnetic fields, temperature variations, and possible pressure changes inside the ESG envelope are all considered it seems unlikely that the gyro rundown rate can be predicted better than about ten percent, or 0.05 rps per day. Hence, the precise rotor speed knowledge necessary to make the required roll rate measurement (0.3 rad/sec = 0.05 rps) would not be available for more than about one day of ARS operation.

Given that this one day of operation is adequate, the rate calculation still permits a formidable mechanization task. The required measurement accuracy of ±0.3 radians per second requires measuring a nominal rotor speed of about 100 rps to a precision ± 0.05 percent. This requirement means that analog techniques similar to those previously employed cannot be used here. Also, the use of familiar demodulation techniques to detect the difference between a (for example) 100-cps reference signal and 100.15-cps rotor speed signal cannot be used since they do not supply sign information.

The block diagram of a mechanization which could be used for the roll rate calculation is shown in Figure 4-17. The variable frequency pulse generator and clock drive are pre-set to generate a pulse train proportional to nominal ESG rotor speed. The pulse frequency would be given by:

$$PPS = K \left[\omega_{ro} - \dot{\omega}_r \ (t - t_o)\right]$$

where:

ω_{ro} = initial rotor speed

$\dot{\omega}_r$ = nominal rotor rundown rate.

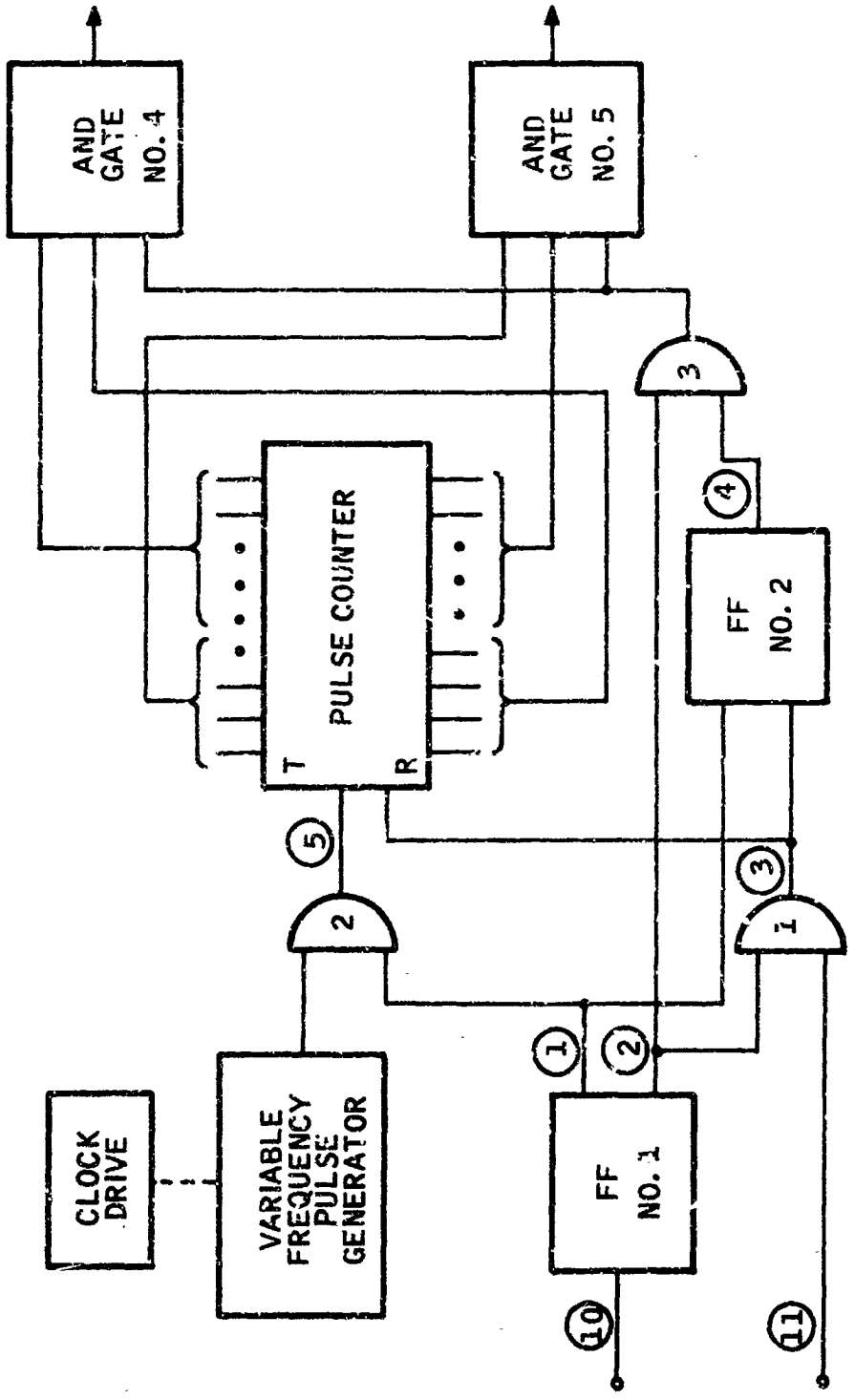

Figure 4-17. Roll Rate Calculation

Signals 10 and 11 are obtained from the circuit of Figure 4-15.

20113-FR1

This pulse generator would typically consist of a voltage controlled or capacitance controlled oscillator followed by appropriate shaping circuits.

AND gates numbers 1, 2, and 3 and the two flip-flops, are used as control elements. The signals which provide the control function are illustrated in Figure 4-18. Signals (10) and (11) are both one pulse per rotor revolution signals, but are 180 degrees out of phase. Signal (1) is used to control the pulse counter so it counts only on alternate rotor revolutions. During the first half of the rotor revolutions when the pulse counter is not counting, signal (2) enables AND gates 4 and 5 so that the remainder of their inputs may be examined. Then, signal (11) resets the pulse counter and FF No. 2 so the cycle may be repeated. The pulse counter circuits and AND gates 4 and 5 are interconnected so that AND gate 4 is fulfilled if the pulse count is less than N_1, and AND gate 5 is fulfilled if the pulse count is greater than N_2. For either of these conditions, corresponding to roll rates outside the accepted limits, a square wave output will be supplied from the appropriate AND gate. For a pulse count between N_1 and N_2 the vehicle roll rate will be less than the specified amount, and zero outputs are provided.

In order to further clarify the roll rate calculation, a numerical example is presented in this paragraph. Assume an ESG with its rotor speed set at exactly 100 rps at the beginning of the mission and a nominal (pre-measured) rundown rate of 0.5 rps per day. The variable frequency pulse generator, with a nominal frequency of one mc., will then be adjusted to provide a pulse rate output varying from 10^6 pps at the beginning of the mission to $0.99(10^6)$ pps at the end of the first day. This frequency is chosen high enough so the normal counter uncertainty of ±1 pulse causes an insignificant system error. In the $\frac{1}{100}$ of a second rotor period 10^4 pulses will occur, hence a 13-stage counter with a total counting capacity of 16,383 pulses is indicated. The ±1 radians per second roll rate limits correspond to an apparent rotor speed change of ±0.159 rps, or a corresponding count deviation of ±15.9 pulses per rotor revolution. Hence, the N_1 and N_2 valves would be set at 9984 and 10,016 respectively.

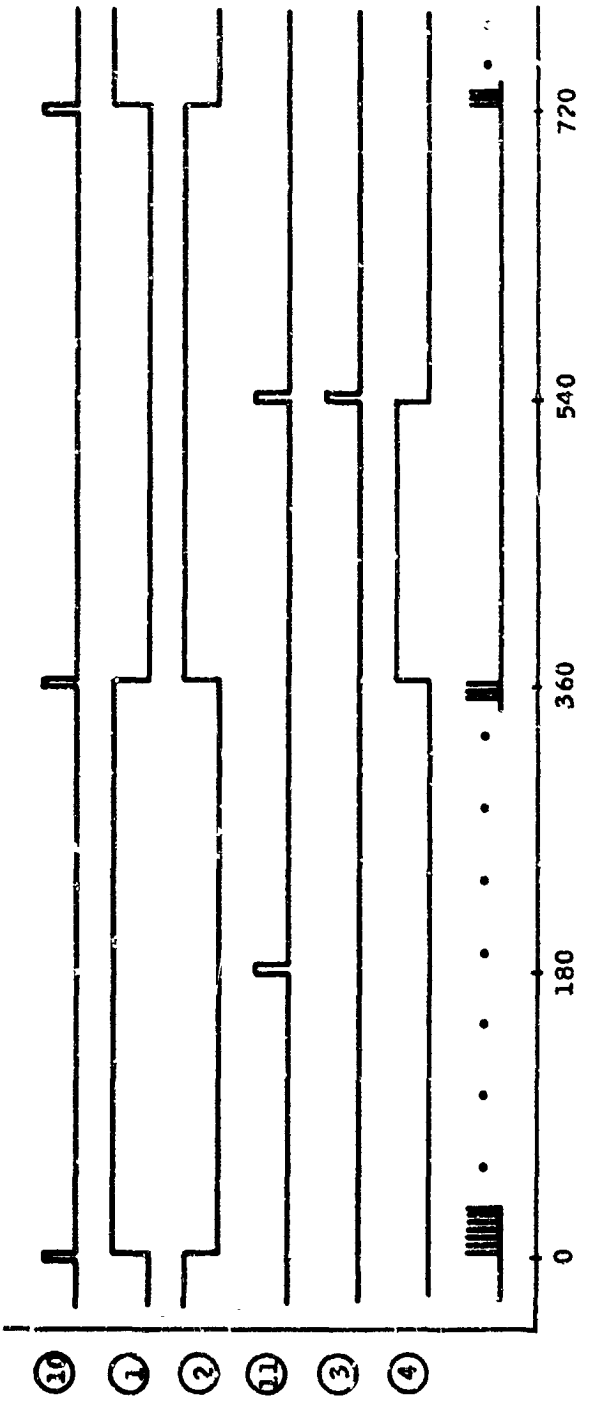

Figure 4-18. Control Signals for Roll Rate Calculation

If the requirement of sign information in the roll rate signal can be omitted, a much simpler alternate mechanization can be used. Assume that the SDMEG is mounted so the gyro is separated from the roll axis of the vehicle, and oriented so the centripetal acceleration associated with a steady roll rate will be impressed on a single ESG suspension channel. The error signal (directly proportional to rotor sag) which generates the suspension voltages necessary to balance this centripetal acceleration can then be directly used as an indication of vehicle roll rate. The direction of the roll rate, however, is obviously missing from this information.

The sensitivity of the JPL SDMEG suspension electronics is such that an error signal of about 0.1 volts per g is available. Selecting a reasonable precision of 1 mv measuring accuracy then indicates that the ESG should be mounted at least one foot from the vehicle roll axis. The 1 ± 0.3 radians per second roll rate signal requirement then corresponds to sensing at 3 ± 1 mv suspension electronics error signal.

The above considerations show that calculating vehicle rate about an axis parallel with the roll axis of a single strapped-down ESG is at best cumbersome and inaccurate. It is therefore recommended that this calculation <u>not</u> be included as a part of the subject ARS. The state of the art of rate gyros is such that a relatively inexpensive version of such a gyro could readily be used to provide the desired roll rate information with minimal size, weight, power, and reliability penalties to the SDMEG ARS.

PERFORMANCE ANALYSIS

INTRODUCTION AND SUMMARY

The performance analysis presented below assumes an SDMEG-ARS as defined in the previous paragraphs. Specifically, a rotor with pattern as shown in Figure 4-11 is to be used. The pattern is assumed to have a 3 degree linear range and 12 degree total range. A nominal gyro operating speed of 100 rps is assumed.

The individual error sources as considered in this performance analysis are presented in Figure 4-19. The effects of these errors on both the attitude and rate outputs are discussed individually below.

A summary of the attitude output errors is presented in Table 4-3. The low frequency, or bias, errors are presented in two different classes. First, errors at the end of the retrofire period (a maximum of 40 minutes after separation) are presented in terms of null errors and maximum errors. The null errors occur at the center of the linear range. The maximum errors occur at the three degree limits of the ARS linear range where pattern and calculation approximations begin to contribute significant additional errors. These errors are nearly invariant with time. The second type of error (e.g., gyro drift) is an error which is time dependent and increases with mission length.

Additionally, high frequency or noise errors are also presented in Table 4-3. The error functions and magnitudes presented in Table 4-3 are explained in the following discussion of error representations. These high frequency errors are used to calculate both the noise on the attitude output and the accuracy of the rate outputs.

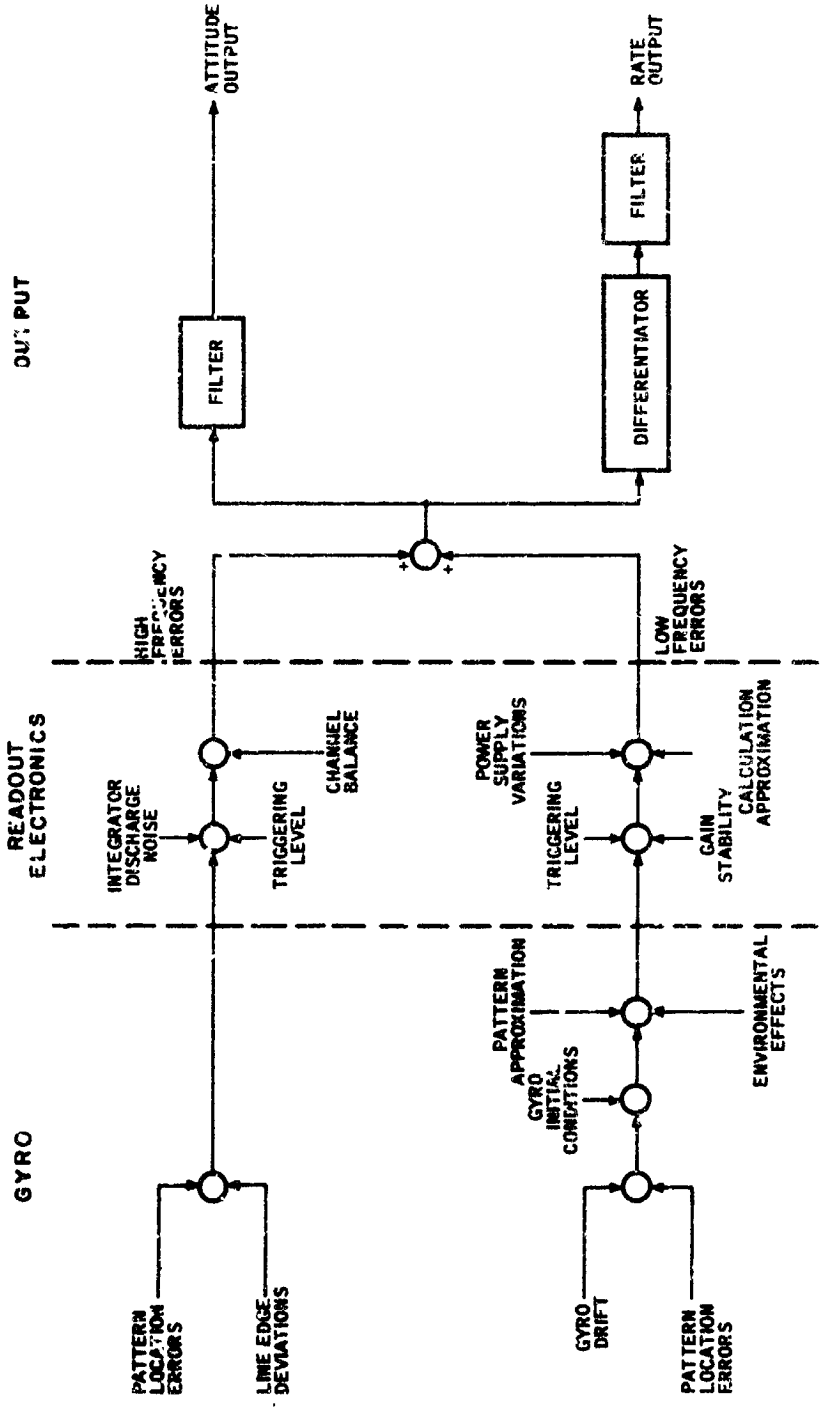

Figure 4-19. SDMEG-ARS Error Diagram

Table 4 3. Attitude Output Errors

Error Source	Magnitude	High Frequency Errors		Low Frequency Errors		
				End of Retrofire		
		Function	Magnitude (3σ deg.)	Null (3σ deg.)	Maximum (3σ deg.)	Time Dependent (3σ deg/day)
Pattern Errors						
Location	5×10^{-4} in	B	0.029	0.020	0.020	
Edge Definition	2×10^{-4} in	A	0.011	0.007	0.005	
Approximations					0.030	
Triggering Level	0.5%	A	0.015	0.017	0.017	-
Integrator Discharge						
Noise	0.1%	A	0.017	0.010	0.010	
Bias				0.010	0.030	
Calculation Approximations		C	0.0075	0.004	0.030	0.015
Gain Balance and Stability		B	0.024	0.017	0.017	
Gyro Drift				0.009	0.009	0.288
Power Supply Variations						
Gyro Initial Conditions	Not Incl.					
Totals (RSS)		A B	0.0252 0.0376	0.035	0.074	0.29

A summary of the most important system performance parameters is presented in Table 4-4. The attitude accuracies and linear range are taken directly from Table 4-3 or from previous discussions. The calculations necessary to obtain the quality of the attitude outputs and the quality and accuracy of the rate outputs are presented in the following discussion of error representations.

Comparison of the required and projected performance parameters presented in Table 4-4 shows that all the specifications on the attitude signals can be met. However, both the accuracy and quality of the pitch and yaw rate signals are less than desired. This comparison has been made assuming that the stated requirements are the equivalent of 3σ values. If the more lenient interpretation that the stated requirements represent one sigma values were used, the appropriate numerical values for the projected performance column of Table 4-4 could be obtained by dividing the given values by three. This interpretation would enable meeting all the required performance parameters except the low frequency noise on the rate signal.

The inability to meet this noise requirement is not surprising. In fact, it might be expected, since the attitude and rate requirements of Table 4-4 are not entirely compatible. Assume that ideal low pass filters (infinitely sharp cutoff) with bandwidth equal to the required system bandwidth are used for the system of Figure 4-19 (this is as good as can be done for noise rejection purposes). A further reasonable assumption is that the spectrum of the noise inside the system bandwidth resembles white noise (power spectral density a constant value). This second assumption is verified by the following error analysis. The relationship between the noise in the rate signal may then be found as:

$$n_{\dot{\gamma}} = \frac{2\pi}{3}\left[\frac{f_2}{f_1}^3\right]^{1/2} n_{\gamma}$$

where:

f_2 = bandwidth of rate filter.

f_1 = bandwidth of attitude filter.

n = rms noise in system output.

Table 4 4 SDMEG ARS Performance Characteristics

Parameter	JPL Requirement	Projected SDMEG System Performance
Attitude Outputs (Pitch Yaw)		
Form	Analog	Analog
Accuracy	±0 1 deg. (end of retro) ±5 deg (end of flight)	±0. 074 deg (end of retro) ±1. 44 deg (5 days) ±5. 76 deg. (20 days)
Linear Range	±3 deg.	±3 deg
Usable Range	±10 deg.	±12 deg.
Bandwidth	15 cps	15 cps nominal (variable)
Threshold	0. 05 deg.	~0. 007 deg.
Quality (peak-to-peak noise)	0. 05 deg. up to 20 cps 0. 10 deg. over 20 cps	~0. 029 deg. ~0. 002 deg.
Rate Outputs (Pitch. Yaw)		
Form	Analog	Analog
Accuracy	±0. 05 deg. /sec.	±0. 19 deg. /sec.
Threshold	0. 02 deg. /sec.	0. 064 deg. /sec.
Linear Range	±1. 5 deg. /sec.	±1. 5 deg. /sec.
Bandwidth	5 cps	5 cps
Quality	0. 02 deg. /sec. up to 20 cps 0. 05 deg. /sec. over 20 cps	0. 37 deg. /sec. 0. 048 deg. /sec.
Roll Rate Output	Signal with sign information (no magnitude required) whenever roll rate exceeds 1. 0 ±0. 3 rad. /sec.	Required roll rate accuracy can be supplied only for first 24 hours of mission Alternately roll rate information without sign can be supplied for an unlimited time.

For the requirements of Table 4-4 (5 and 15 cps bandwidths), the multiplying factor in the above equation is about 6. Hence, if the noise on the attitude signal is 0.05 degrees the minimum noise on the rate signal would be approximately 0.3 degrees per second.

The preliminary design of the attitude reference system described here has been achieved primarily to meet the specifications on attitude performance. It is doubtful, however, that the noise requirement on the rate signal could be met with less than a complete change in the mechanization concept.

ERROR REPRESENTATIONS

The error representations and approximations described below will be useful in mathematically describing the performance of the subject ARS.

Useful Relationships

The analysis includes use of autocorrelation functions and power spectral densities. The autocorrelation function of a process X(t) is, in general, defined as an ensemble average.

$$R_X(\tau) = \overline{X(t_1)\ X(t_1 + \tau)}$$

When the quantity with which we are concerned is stationary this ensemble average becomes independent of the time t_1

$$R_X(\tau) = \overline{X(t)\ X(t + \tau)}$$

The further assumption of ergodicity allows the computation of the autocorrelation function by a time average.

$$R_X(\tau) = \lim_{T \to \infty} \frac{1}{2T} \int_{-T}^{T} X(t)\ X(t + \tau)\, dt$$

The power spectral density of the process X(t) is simply defined as the Fourier transform of the autocorrelation function.

$$S_x(f) \triangleq \int_{-\infty}^{\infty} R_x(\tau)\, e^{-i2\pi f\tau}\, d\tau$$

The mean square value of the process X(t) is simply the autocorrelation function at zero τ.

$$R_x(0) = \lim_{T\to\infty} \frac{1}{2T} \int_{-T}^{T} X^2(t)\, dt = \bar{X}^2 + \sigma_x^2$$

σ_x - variance of X(t)

$\bar{X}$ - mean of X(t)

Alternately, the same quantity may be found from the power spectral density as:

$$R_x(0) = \int_{-\infty}^{\infty} S_x(f)\, df$$

"Random" Square Wave

Assume event points equally spaced at a period T. The value of the process is constant between event points, succeeding values are uncorrelated and all the process values form a gaussian random process with variance σ_A^2. The autocorrelation function may then be found as.

$$R_A(\tau) \quad \begin{matrix} \sigma_A^2 \left(1 - \frac{|\tau|}{T}\right) + \overline{A(t)}^2 & : & |\tau| < T \\ \bar{A}^2 & : & |\tau| > T \end{matrix}$$

and the corresponding power spectral density is:

$$S_A(f) = \bar{A}^2\, \delta(f) + \sigma_A^2\, T \left(\frac{\sin \pi f T}{\pi f T}\right)^2$$

The form of this process is shown in Figure 4-20a. For the previously assumed parameters, of course, T is 1/200 of a second. This error function is designated as a type "A" function in the following error analysis.

"Deterministic" Square Wave

Consider the error process formed by switching alternately (and instantaneously) between two independent, slowly varying, zero mean random processes. The switching is assumed to be done at a rate very much higher than the highest frequency in the processes. A small portion of such a process is shown in Figure 4-20b. The expected average of this process over a time T_1 still much smaller than the period of the highest frequency in the random functions is:

$$\frac{1}{T_1}\int_0^{T_1} B(t)\,dt = \frac{\sqrt{\sigma_{B1}^2 + \sigma_{B2}^2}}{2} \longrightarrow \frac{\sigma_B}{\sqrt{2}}$$

where the σ_{Bi}'s represent the variances of the two processes. As shown in Figure 4-20b, this average may be considered the low frequency (or dc) component of the error process. The expected (statistical) amplitude of the residual after this low frequency component is removed is simply:

$$E[B] = \frac{\sigma_{B1} + \sigma_{B2}}{2} \longrightarrow \sigma_B$$

This residual square wave may then be represented as a Fourier series, as shown in Figure 4-20b.

$$B(t) - \overline{B(t)} = \sum_{m=0}^{\infty} \frac{4\sigma_B}{(2m+1)\pi} \cos\frac{(2m+1)\pi t}{T}$$

and the Fourier transform is:

$$B(f) = \frac{\sigma_B}{\sqrt{2}}\,\delta(f) + \sum_{m=0}^{\infty} \frac{2\sigma_B}{(2m+1)\pi}\left[\delta\left(f - \frac{2m+1}{2T}\right) + \delta\left(f + \frac{2m+1}{2T}\right)\right.$$

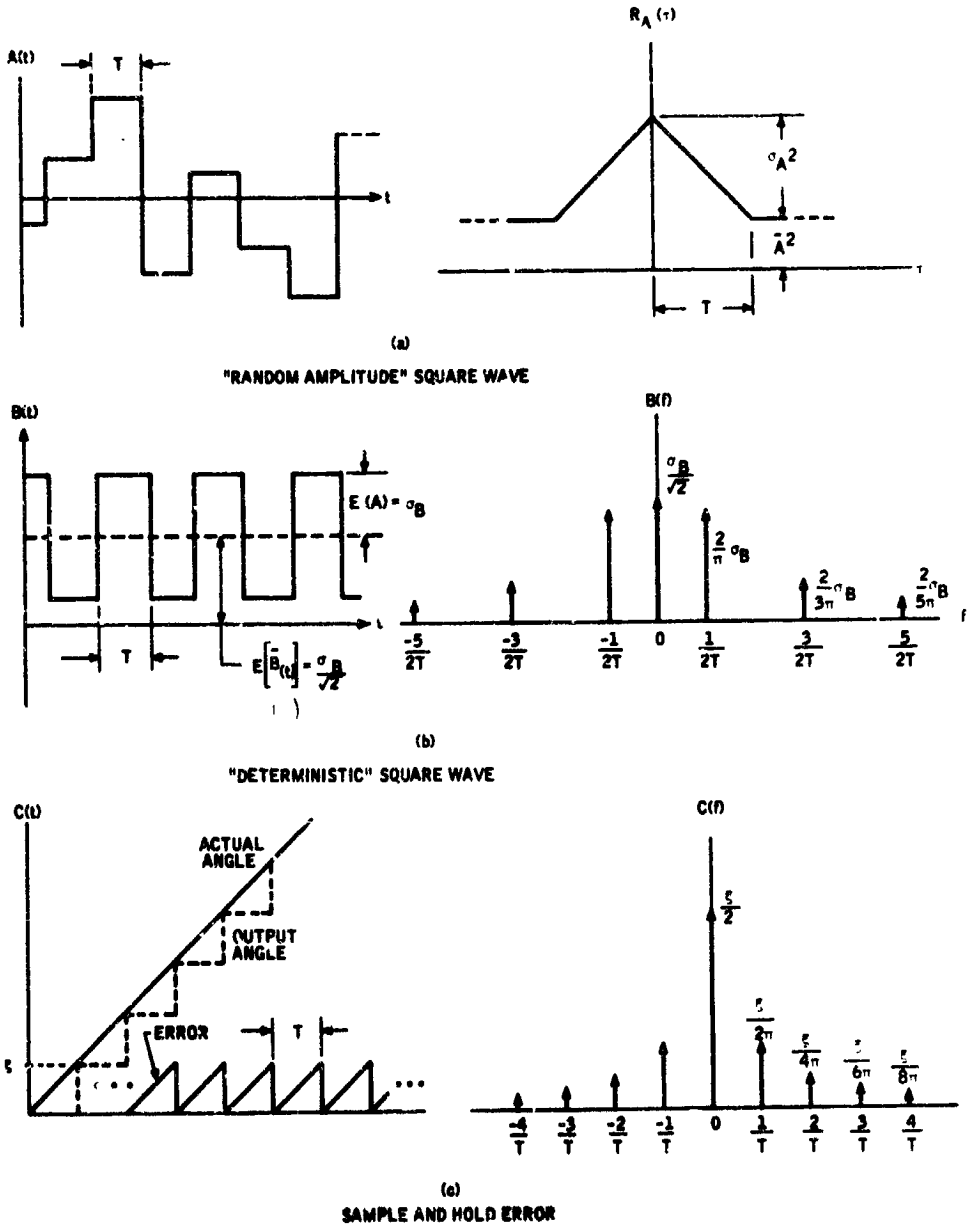

Figure 4-20. SDMEG-ARS Error Functions

For a 200 per second sampling rate the process consists of a low frequency component plus discrete sinusoids at 100, 300, 500, etc. cps.

This error function is referred to as a type "B" process in the following error analysis.

Sample-and-Hold Effect

The final error representation to be discussed here is an approximation to the sample and hold effect introduced by the attitude computing module. This error process may be approximated by assuming a constant vehicle body rate as shown in Figure 4-20c. The difference between the actual body angle and system output results in an effective saw tooth error (as shown) which may be represented as a Fourier series.

$$C(t) = \frac{\xi}{2} + \sum_{n=1}^{\infty} \frac{\xi}{n\pi} \sin \frac{2\pi nt}{T}$$

The frequency spectrum of this process is also shown in Figure 4-20c. For a 200 per second sampling rate the process consists of a low frequency component (average value) plus components at 200, 400, 600, etc. cps.

This error function is designated a type "C" process.

Error Calculations

Consider the system shown in the sketch below (the functions of frequency refer to Fourier transforms). The power spectral

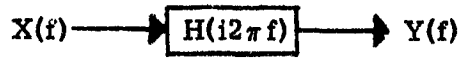

density of the output may be found as

$$S_Y(f) = \left|H(i2\pi f)\right|^2 S_x(f)$$

And the mean square value (power) of the output may again be found as the integral of the output power spectral density. These relationships are first useful in calculating the quality of the attitude signals.

For the attitude errors being considered in this analysis the $H(i2\pi f)$ is simply a filter, and is assumed to have the form

$$H_1(i2\pi f) = \frac{1}{\left(\frac{i\omega}{\omega_{1n}}\right)^2 + \frac{2\rho}{\omega_{1n}}(j\omega) + 1}$$

Three types of noise are put into this filter. The first type, the power spectral density represented by the type "A" function, is well approximated by the value of the function at zero frequency $\left(\text{since } f_{1n} = \frac{\omega_{1n}}{2\pi} << \frac{1}{T}\right)$. This is readily evident by examining the form of the power spectral density function shown in Figure 4-21.

$$S_x(f) \cong S_x(o) = \sum_i \sigma_{Ai}^2 \, T$$

Hence, the total mean square noise power in the output attitude signal due to the type "A" error is found as:

$$\overline{Y^2}_A = \int_{-\infty}^{\infty} \left| \frac{1}{\left(\frac{i\omega}{\omega_{1n}}\right)^2 + \frac{2\rho}{\omega_{1n}}(i\omega) + 1} \right|^2 S_x(o)\, df = \frac{\omega_{1n}}{2\rho} S_x(o)$$

Assuming:

$$\omega_{in} = 2\pi f_{1n} = 2\pi\,(15) \text{ rad./sec.}$$

$$\rho = 0.7$$

And using the rss of the (1σ) type "A" errors from Table 4-3 yields:

$$\overline{Y^2}_A = \frac{2\pi\,(15)}{2\,(0.7)} \frac{(0.0084)^2}{200}$$

$$\left[\overline{Y^2}_A\right]^{1/2} = 0.0049 \text{ degrees}$$

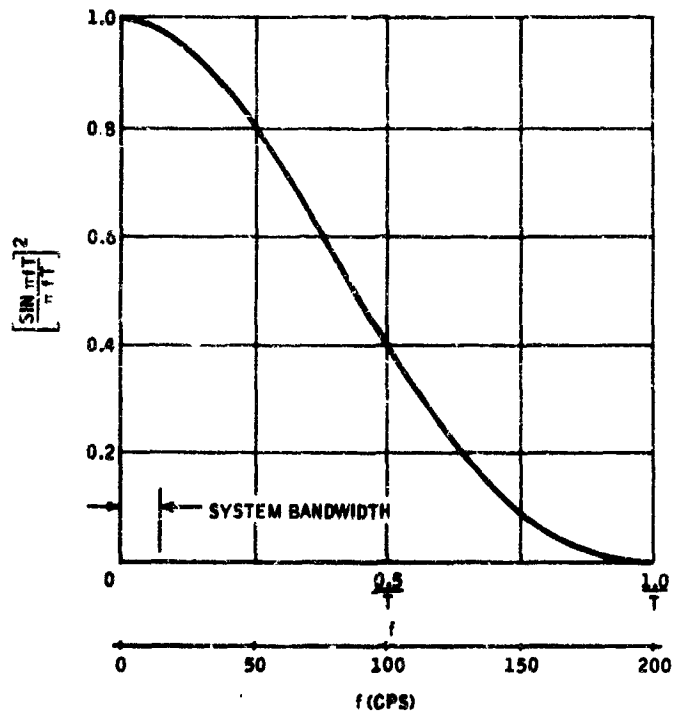

Figure 4-21. Power Spectral Density Function

This type of error is almost entirely contained in the less than 20-cps frequency region and is the only noise error in this frequency region (the type "B" and "C" errors have a minimum frequency of 100 cps). If this attitude error is assumed normally distributed, the above rms value corresponds to a one sigma value. The required peak-to-peak noise specification is taken as 6σ (3σ represents zero-to-peak) and this value is entered in Table 4-4.

The second and third types of noise are the previously described Fourier series which represent the type "B" and "C" error functions. These sinusoids are simply attenuated by the magnitude of the second order filter. Substituting the appropriate numerical values yields:

$$y_B(t) = \frac{4}{\pi}\sigma_B \left[\frac{\cos\left(\frac{\pi t}{T}\right)}{44.5} + \frac{\cos\left(\frac{3\pi t}{T}\right)}{3(400)} + \ldots \right]$$

$$y_C(t) = \frac{\xi}{\pi} \left[\frac{\sin\left(\frac{2\pi t}{T}\right)}{177} + \frac{\sin\left(\frac{4\pi t}{T}\right)}{2(710)} + \ldots \right]$$

The numbers 44.5, 177, 400, 710, . . . are the attenuation of the filter at the 100, 200, 300, . . . cps frequencies. The indicated peak-to-peak noise may therefore be approximated as:

$$y_{P\text{-}P} \sim 2 \left[\frac{4}{\pi} \frac{3\sigma_B}{44.5} + \frac{\xi}{177\pi} \right] = 0.0022 \text{ degrees}$$

where:

$3\sigma_B = 0.0376$ degrees

$\xi = 0.0075$ degrees

from Table 4-3

The threshold of the attitude signal specified in Table 4-4 has been quite arbitrarily assigned at the unity signal-to-noise level.

The circuit used to differentiate the pitch and yaw attitude outputs was presented in the discussion of readout electronics. The projected accuracy of these rates is summarized in Table 4-5. The assumed one percent gain stability in the differentiator circuits translates directly into a possible one percent magnitude error in the rate signals. One percent of the required linear range, ±1.5 degrees per second, yields the ±0.015 degree per second error indicated in Table 4-5.

A second rate calculation error occurs because of the lead-lag circuit used to approximate the desired differentiator. The lag frequency was selected as 30 cps to give adequate performance at the 5 cps bandwidth point. The difference in the magnitude of the transfer function of the ideal differentiator and the

selected approximation at a 5 cps frequency is only 1.4 percent. Similarly, the lead-lad approximates the differentiator to within one percent at the low end of the spectrum for frequencies over 0.07 cps. Hence, a maximum bias error of one percent, or 0.015 degrees per second, has been assumed from this source.

The remaining rate errors are caused by the various types of noise in the pitch and yaw attitude signals. Analytically, the type "B" and "C" errors are easiest to handle. For the frequencies involved in these noise signals the gain of the differentiator is constant at $\frac{K}{\tau} = 200$. A second order filter analagous to that used for the attitude signals, but with the undamped natural frequency at the required five cps bandwidth, is assumed. The noise in the rate output from these two noise errors is then well approximated by the first two terms of the appropriate series.

Table 4-5. Pitch and Yaw Rate Errors

Error Source	Bias Magnitude (3σ - deg./second)	Noise Magnitude (peak-to-peak)
Gain Stability	0.015	-----
Differentiator Approximation	0.015	-----
Type "A" Attitude Noise	0.19	0.37 [2]
Type "B" Attitude Noise	-----	0.0479 [1]
Type "C" Attitude Noise	-----	0.0006 [1]
TOTAL	0.19	-----

1. These errors are primarily high frequency errors.
2. The majority of this error occurs in the 0 to 20 cps frequency range.

$$\dot{y}_B(t) = 200 \frac{4}{\pi} \sigma_B \left\{ \frac{\cos\left(\frac{\pi t}{T}\right)}{400} + \frac{\cos\left(\frac{3\pi t}{T}\right)}{3(2700)} + \ldots \right\}$$

$$y_C(t) = 200 \frac{\zeta}{\pi} \left\{ \frac{\sin \frac{2\pi t}{T}}{1600} + \frac{\sin \frac{4\pi t}{T}}{2(6400)} \right.$$

Where 400, 1600, 2700, 6400, . . . are the attenuation of the 5 cps second order filter at the 100, 200, 300, 400, . . . cps frequencies. The indicated high frequency peak-to-peak noise in the pitch and yaw rates is then seen to be well approximated by:

$$Y_{p-p} \sim 2 \left\{ \frac{200}{400} \frac{4}{\pi} \left| 3\sigma_B \right| + \frac{200}{1600} \frac{\zeta}{\pi} \right\} = 0.0485 \text{ degrees}$$

In calculating the effect of the type "A" noise on the ARS rate outputs the previously assumed approximation for the power spectral density function is still a valid one.

$$S_x(f) \cong S_X(0)$$

The total rms noise in the rate outputs due to the type "A" noise in the attitude signals is then found as:

$$\overline{\dot{y}_A^2} = \int_{-\infty}^{\infty} S_x(0) \left| \frac{i\omega}{\left(\frac{i\omega}{\omega_{2n}}\right)^2 + \frac{2\rho}{\omega_{2n}} (i\omega) + 1} \right|^2 df = S_x(0) \frac{\omega_{2n}^3}{4\rho}$$

$$\left[\overline{\dot{y}_A^2} \right]^{1/2} = 0.0624 \text{ degrees/sec.}$$

This is again a low frequency error, and the above value corresponds to a one sigma value. Hence, using the same interpretations as previously, the possible (3σ) rate error is three times the above value, or 0.19 degrees per second, and the possible peak-to-peak noise error is six times the above value or 0.37 degrees per second. These values have been entered into Table 4-4.

The rate threshold specified in Table 4-4 has again arbitrarily been set at the unity signal-to-noise point.

ERROR SOURCES

The source, form, and magnitude of the individual errors as shown in Figure 4-19 are discussed in the following paragraphs.

Pattern Accuracy

Readout errors caused by pattern accuracy may be considered in three separate categories -- patern location errors, pattern line edge deviations, and patterning approximations.

Pattern Location Errors -- Patterr location errors result from the gross (average) positioning of the "constant slope" patterns with respect to the referenc (meridian) pattern line. Present state-of-the-art rotor patterning techniques limit the pattern location accuracy to about 10^{-4} inches. This accuracy, however, is not required for this application. A $5(10^{-4})$ inch pattern location accuracy can be obtained much easier (and at a more reasonable cost). For the pattern assumed here the sensitivity of readout angle to pattern location is seen to be:

$$\frac{d\gamma}{dy} \simeq 1 \frac{\text{rad}}{\text{in.}}$$

This type of error yields a type "B" function with a 3σ value of about 0.029 degrees.

Pattern Line Edge Deviations - Pattern line edge deviations refer to localized deviations of the actual line edge location from the average location. This type of error is somewhat a function of the technique used to scribe the pattern line (scribing, sand blasting, etc.) but can generally be held to slightly less than the pattern location errors. A 3σ magnitude of about $2(10^{-4})$ inches is assumed for this error analysis. The time representation of these errors would approximate a type "A" function.

The type "A" error function contributes not only noise but also a probable rms (bias) component to the low frequency attitude output. The magnitude of this bias component, at the output of the assumed second order filter, is about 60 percent of the noise magnitude. This quantity is therefore entered as a low frequency error in Table 4-3.

Pattern Approximation Errors -- Patterning approximation errors refer to the fact that a great circle pattern is being used to approximate the "constant slope" pattern near the null. This approximation contributes no error at the null (γ = 0 degrees). Within the linear range the approximation error is maximum at the linear range limit (γ = 3 degrees) and amounts to about 0.05 degrees (see Figure 4-9). This maximum error is used as a 3σ value for this error analysis. The error is consistent between pattern halves and therefore contributes only a d-c component.

Triggering Level

The sensitivity of the EsG readout system to deviations in the electronics triggering level may be obtained by referring to Equation (85). A change in the electronics triggering level means that the time pulses are generated at other than the pre-set percent of non-reflective area in the pickoff field of view. The change in readout angle for an area change may be found as:

$$\delta\gamma_1 = B\frac{r_p}{r}\delta A \quad ; \text{ (reference meridian)}$$

$$\delta\gamma_2 \simeq \frac{\pi}{2}\frac{r_p}{r}\delta A \quad ; \text{ (constant slope pattern)}$$

where:

r_p = pickoff field of view radius

r = rotor radius

A = normalized pickoff field of view area

Assumed nominal trigger level at A = 50 per cent.

Two general levels of triggering accuracy are available. If standard voltage sensing triggering circuits are used, the triggering level variations might be as much as 10 percent (3σ). This triggering accuracy results in an excessive error from the second equation above. Alternately, height-insensitive triggering techniques (e.g., see 1726-FR1, pp 65-77) can be employed to limit the triggering level variations to less than one percent. The difference in the two error equations allows the use of a Schmidt trigger for the reference meridian pulses (See Figure 4-15) with a corresponding error of 0.012 degrees. The triggering on the constant slope pattern (discriminated with pulsewidth discrimination) requires the more complex height insensitive triggering circuitry. The error is then $0.9(10^{-2})$ degrees. The total (3σ) error is the rss of these two, or $1.5(10^{-2})$ degrees. The time function associated with this error would be expected to resemble the type "A" function

In addition to these high frequency errors, long-term variations in triggering circuit gains, rotor illumination and photosensor sensitivity are expected to contribute an additional error of about the same magnitude. The low frequency attitude error (rss of bias and filtered high frequency error) attributable to triggering level is therefore about $1.65(10^{-2})$ degrees.

Integrator Discharge Noise

Discharging the integrators in the analog attitude computing module affects the attitude reference system readout accuracy in two ways. First, any residual voltages on the integrators after the reset procedure are the equivalent of non-zero initial conditions and cause proportional readout errors. Second, the time used to reset the integrators is taken from the computing cycle (see Figure 4-14) thereby causing a systematic readout error.

The sensitivity of the attitude reference system to the first type of readout error is readily found by examining the readout equation.

$$\gamma = \frac{B}{\tau_b} \left[\tau_b - 2T_1\right]$$

An integrator reset error may be interpreted as a time error (i.e., percent of integrator full-scale output), and the corresponding readout error is:

$$\delta\gamma_3 = \frac{B}{\tau_b} \left[\pm \delta\tau_b \pm \delta\tau_b\right] \longrightarrow \sqrt{2} \quad B \quad \frac{\delta\tau_b}{\tau_b}$$

The required integrator reset accuracy is therefore about 0.1 percent of full scale, with a corresponding readout error of 0.017 degrees. This requirement is obtainable, but will demand particular attention to the design of the reset circuits and an allowance of adequate reset time in the computing cycle.

If this reset time is any significant portion of a computing period (one-half rotor period) a further computational error appears. Let the reset time be T_r. The computational error caused by keeping the integrators off (for reset) during the first T_r seconds of the computing cycle is:

$$\delta\gamma_4 = \frac{T_r}{\tau_b} \quad (B + \gamma)$$

This is, however, a predictable and repeatable effect and can therefore be compensated. The compensation, which might consist of either gain adjustments or biasing, would be the equivalent of adding the quantity $\frac{T_r}{\tau_b} B$ to the calculated output angle, and would therefore by wholly effective only at the null ($\gamma = 0$ degrees). A residual null error (after compensation) of 0.01 degrees and maximum error of 0.03 degrees (corresponding to $\frac{T_r}{T_b} = 10^{-2}$) have been assumed for this error analysis.

Calculation Approximations

The most significant calculation approximation in the proposed readout scheme results from the assumption of constant rotor speed (Equation 101) which was employed to avoid the indicated division. If $\delta\tau_b$ is the difference between assumed and actual rotor period the resulting readout error may be found as:

$$\delta\gamma_5 = \frac{\delta\tau_b}{\tau_b}\gamma$$

This error disappears at the null of the readout system, irrespective of the error in the assumed rotor speed.

A reasonable numerical value for this error can be obtained by assuming an initial speed within about one percent of the selected nominal and an SD MEG rundown rate of about one-half rps per day. These values yield the maximum low frequency error listed in Table 4-3.

An additional calculation approximation error appears from the sample and hold effect on the attitude computing modules. This approximation results in a Type "C" error with maximum value equal to the vehicle rate multiplied by the sampling time. Assuming a rate of 1.5 degrees per second (the required linear range of the rate outputs) yields a Type "C" error with

$$A = \dot{\gamma}_{max} \frac{\tau_b}{2} = \frac{1.5}{200} = 0.0075 \text{ °/sec.}$$

The average or bias value of this error, as shown in Table 4-3, is A/2.

Gain Balance and Stability

The accuracy of the ARS output is obviously a function of the gain balance and stability of the analog computing elements. Consider only one of the two parallel computing channels. The sensitivity of output angle to gain stability is well approximated by:

$$\delta\gamma_6 \approx \sqrt{2}\ B\ \frac{\delta K}{K}$$

where:

$\frac{\delta K}{K}$ = fractional gain stability

Assuming an equal (probabalistic) error in each of the two channels would then yield an output noise error (type B) with 3σ value of 2B times the fractional gain instability. This result demonstrates that overall gain stability of about 0.1 percent will be required; this gain stability can be achieved with high feedback around active elements, since the overall gain requirements are low.

Gyro Drift Errors

The gyro drift performance assumed here is the same as has been previously used for SD MEG performance analyses (see Honeywell Report 20113-PR5, pp 16-20).

The first portion of the flight, separation to end of retrofire, will last a maximum of 40 minutes. This 40 minutes includes an assumed 10 minutes of retro firing time with actual acceleration of 0.5 g's and the SD ESG suspension electronics at a 30 g level. The calculated (1σ) gyro drift rate during power flight is 0.0127 degrees per hour. In the free fall condition of the remaining 30 minutes the suspension electronics pr load is assumed at one g and the corresponding SD MEG (1σ) drift rate is 0.004 degrees per hour. The total (3σ) drift angle for this 40 minute portion of the flight is then readily calculated as 0.009 degrees.

The second portion of the flight, during which control must be maintained, has a specified duration of 5 to 20 days. Using the same (free fall) gyro drift rate yields a total error angle of 1.45 degrees after five days or 5.8 degrees after 20 days (0.288 degrees per day 3σ).

Power Supply Variations

The power supplies for the SD MEG ARS will provide adequate regulation and isolation from the vehicle power so that the power variations will cause only second order attitude errors. The ARS preliminary design includes features (e.g., height insensitive triggering, common reference source for attitude computing module integrators, low gain and high gain stability in parallel computing paths) intended to minimize power supply variation effects. A preliminary estimate indicates that one to two percent power regulation will provide adequate performance.

Gyro Initial Conditions

Gyro initial conditions are a function of both the ESG mechanization, the ESG alignment in the carrying vehicle, and the pointing accuracy of this vehicle during the gyro starting procedure. Because of the obvious unknowns in the gyro alignment and startup process, this error has not been included in the performance analysis. The ARS has been designed, however, so that approximately 50 percent of the total allowable system error can be alloted for the initial erection process. The difference between the allowable error of 0.1 degrees and the predicted errors at the end of retrofire (on an rss basis) is 0.067 degrees for the maximum error and 0.093 degrees for the null error. These error allowances are considered more than adequate for the initial gyro alignment and erection procedures.

SYSTEM PHYSICAL CHARACTERISTICS

Size, weight, power, and reliability estimates for the projected capsule lander ARS are presented in the paragraphs below.

SIZE AND WEIGHT

The ARS would logically be divided into at least two separate packages. The single SDMEG with its associated optical pickoffs, vacuum pump, spin and damping coils, and magnetic shielding, would comprise one of the two packages. The mounting provisions for this gyro assembly would have to include precision alignment capabilities. The gyro-associated electronics would be placed in one or more separate packages.

The size and weight of the electronics and mechanical assemblies necessary to perform the various functions are listed in Table 4-6. The physical parameters listed in Table 4-6, with exception of the suspension electronics weight and the readout electronics size and weight, have all been published in other documents (see 1726-FR2). The parameters for the suspension electronics assume welded module packaging of presently existing circuits. The remainder of the electronics parameters were obtained assuming maximum use of prepackaged integrated circuits (gates, flip-flops, operational amplifiers, each in a single TO-5 can or flat pack) with plug-in circuit card type construction. This type of construction would yield a unit suitable for airborne applications (reasonable size, weight, and power) with minimum development time and cost. Use of more advanced packaging techniques -- multilayer circuit boards or three-dimensional integrated circuit matrices -- would permit a 50 percent or more improvement in all Table 4-6 electronics parameters at the expense of considerably more development effort.

The estimates presented in Table 4-6 do not include allowances for power supplies. If the required form of electrical power (specified in the next paragraph) is not available from a separate source, additional electronics

Table 4-6. SDMEG ARS Size and Weight Characteristics

Item	Size (in^3)	Weight (pounds)
Gyro Assembly	104	6.0
Suspension Electronics	60	5.0
Remote Starting Electronics	40	1.3
Readout Electronics *	60	2.2
Totals		
Gyro Assembly	104	6.0
Electronics Assembly	160	8.5

*Add 20 in^3 and 0.7 pound for roll rate calculation

allowance would have to be included in the size and weight parameters. Also, as indicated in the table, the electronics necessary for the roll rate calculations have not been included in the primary figures. Meeting this requirement (for only the first 24 hours of the flight) would require an additional 20 cubic inches and 0.7 pounds.

POWER REQUIREMENTS

The most recent estimates (or measured values) of the power which will be necessary to start and operate the SDMEG and associated electronics of this ARS are presented in Table 4-7. The values in this table indicate that a total of about 61.6 watt-hours of energy will be required during the 1.6 hour starting procedure, with a peak power requirement of 53.7 watts. After the system is started, the steady-state power requirement will be 11.9 watts, except that 30.3 watts peak power is required during retrofire when the suspension electronics are switched to the high g mode.

Table 4-7. SDMEG ARS Power Summary

Function	Power Form	Regulation	Power (watts)	Time (hours)	Energy (watt-hours)
Spin	800 ~ 2ϕ	--	20	0.13	2.6
Damp	22.5 vdc	--	6	1.63	9.8
Vacuum System	180 vdc	5%	0.2	continuous	--
	±22.5 vdc	--		continuous	--
	2.5 vac	--	0.8	continuous	--
Suspension Electronics	2.4 KC ± 0.1%	--	--	continuous	--
1 g	±6 vdc	1%	3.6	continuous	--
30 g	±22.5 vdc	1%	22	1.8	39.6
Starting Logic and Control	±22.5 vdc	--	4.7	1.6	7.5
Readout Electronics *	6 vdc	1%	1.2	continuous	--
	±22.5 vdc	1%	6.1	continuous	--
Totals	11.9 watts continuous 61.6 watt-hours for starting 30.3 watts peak power during retro				

*Add 1.5 watts for roll rate calculation

Except for the readout electronics, most of the values shown in Table 4-7 are taken directly from 1726-FR2. The suspension electronics and spin and damp power levels have been modified to reflect the latest laboratory values, and most of the regulation requirements on the precision power have been relaxed slightly. The conditions on the readout electronics power, the maximum use of integrated circuits, are the same as specified previously. As indicated, an additional 1.5 watts must be added to the readout electronics level of Table 4-7 if the roll rate requirement is to be fulfilled for the first 24 hours.

RELIABILITY

A summary of the reliability predictions for the various subassemblies included in an SDMEG ARS is presented in Table 4-3. These predictions are based on component failure rates presently being used by Honeywell for the Apollo stabilization and control system, and assume proper part application and derating.

The mission reliability may be calculated using the mission parameters, operational sequence, and subassembly failure rates. During the first 200 days of the flight, earth launch to gyro spin up, only the vacuum system will be operated. Hence, with a failure rate of 0.180 (assuming open loop vacuum pump operation with a simple power supply) the reliability (probability of success) for this portion of the mission is

$$R_i = \epsilon^{-\lambda_1 t_1} = \epsilon^{-0.18\,(10^{-5})\,(200)\,(24)} = 0.9914$$

The failure rate during the system start-up phase is 5.367 percent per 1000 hours; but this phase only lasts for about 1.6 hours. The resulting $8.61\,(10^{-5})$ probability of failure during this portion of the flight is insignificant. The system failure rate during the descent portion of the mission is 8.402 percent per 1000 hours or 0.2016 percent per day which indicates a reliability of 0.9900 for a five-day descent or 0.9604 for a twenty-day descent. The total probability of success (product of individual reliabilities) may be found as

$$R \approx 0.9914\ \epsilon^{-0.1875\,(10^{2})\,T}$$

where T is descent time in days.

The total mission reliability ranges from 0.9814 for a 5-day descent to 0.9523 for a 20-day descent.

Table 4-8. Reliability Predictions for SDMEG ARS Subassemblies

Item	n	λ (%/1000 hrs)	$n\lambda$
Mechanical Assembly (without vacuum)	1	0.050	0.050
Vacuum Pump and Electronics	1	0.180	0.180
Suspension Electronics	1	2.988	2.988
Pickoff Assembly	2	0.594	1.188
Automatic Starting Electronic	1	2.025	2.025
Readout Electronics	1	3.872	3.872

The above reliability summary and calculations indicate where major effort should be expended to improve system reliability. It is apparent the major reliability offenders are the vacuum system, the suspension electronics, and the readout system (both pickoffs and electronics). Redundancy or simplification in these three areas could greatly improve the reliability of the SDMEG ARS.

SECTION V
SDMEG MODIFICATIONS

READOUT IMPROVEMENT

The study program reported in this document indicates that the miniature electrostatic gyro's current design can satisfy the spacecraft strapped-down attitude reference system requirements with exception of the accuracy of vehicle body rate outputs. To provide the necessary accuracy in the vehicle body rate outputs it would be desirable to investigate the possibility of reducing the noise on the gyro readout. The first step would be to identify the exact noise source; the second step would be to modify the gyro design to eliminate the noise source or attenuate its effect at the gyro output. Until the noise sources are identified, it will be difficult to predict the gyro modification necessary to reduce the noise effect. However, it will no doubt involve the rotor pattern and/or the optical pickoffs.

In establishing a noise level goal to use in improving gyro readout noise, the gyro readout noise level is assumed acceptable when it causes an RMS noise level on the system rate output equal to the lowest vehicle rate it is desired to detect. It will also be assumed that the lowest vehicle rate to be detected is 0.001 degree per second and that the rate output is obtained by differentiation of the gyro output. In addition, the noise on the gyro readout will be considered "white" with an effective bandwidth of ±5 cps.

From these assumptions and the relationship

$$\Phi o(\omega) = |G(\omega)|^2 \Phi i(\omega)$$

where

$\Phi i(\omega)$ = Power spectral density of input

$\Phi o(\omega)$ = Power spectral density of output

$G(\omega)$ = Fourier transform of system impulse response

it can be shown (see Section "Vehicle Body Rate from the End Axis Rotor Pattern") that the noise on the system rate output is related to the noise on the gyro readout by the following relationship

$$\overline{n^2} = \frac{3\pi \overline{R_n^2}}{\omega_B^3}$$

where

$\overline{n^2}$ = Average square of noise on gyro readout in degrees

$\overline{R_n^2}$ = Average square of noise on rate output in degrees per second

ω_B = Effective bandwidth of the noise in radians per second

Substituting

$$\overline{R_n^2} = (0.001)^2$$

$$\omega_B = 2\pi 5$$

in the above expression

$$\overline{n^2} = 0.35 \times 10^{-9} (\text{deg})^2$$

or

$$n = 0.067 \text{ arc-second RMS}$$

This is to say that the RMS level of noise on the gyro readout should be reduced to 0.067 are-second if vehicle body rates of the order of 0.001 degree per second are to be detected.

SHAPING ELECTRONICS

In addition to the modifications for alleviating the noise problem on the ARS rate output, there are several other desirable system modifications.

One rather simple modification is addition of a third set of readout shaping electronics. The gyro has three optical pickoffs arranged so the optical axes of the pickoffs form an orthogonal triad. The cosine rotor pattern used with the three pickoffs does not cover the entire surface of the rotor. It covers only enough of the rotor surface so that two of the pickoffs are active at any one time. With this situation it was originally believed that two sets of shaping electronics would be supplied for the two active pickoffs. This would be a satisfactory arrangement if there is sufficient time to switch the shaping electronics between the pickoffs as they pass in and out of the rotor pattern range. The study results indicated that for either/or both high vehicle body rates and high ARS output data rates there was not enough time for the switching function. It is faster to read all three pickoffs and take the data into the computer, even though one readout is erroneous.

The computer can then make the decision as to which readout to ignore with considerable saving in time. Addition of a third set of shaping electronics was assumed in arriving at system size and weight estimates. The shaping electronics add about four to five ounces and two to three cubic inches to the system.

ADJUSTMENT FOR INITIAL ALIGNMENT

Another useful modification is a means of adjusting the orientation of the magnetic axis of the gyro damping coils relative to the vehicle. This permits fine adjustment of the initial alignment of the gyro spin vectors relative to each other and to the vehicle coordinates. The damping coils will repeatedly align the gyro spin vector to the same case orientation with accuracy; but this case orientation must be aligned to coincide with the vehicle coordinates by adjusting the gyro position in the vehicle. However, without some means of adjusting the gyro position in its mountings, this is very difficult to do accurately. Another possible way to accomplish this alignment would be to adjust the orientation of the gyro spin coils relative to the case. Either arrangement will make it possible to adjust the initial alignment of the gyro.

MODIFICATIONS FOR SINGLE GYRO APPLICATION

The preliminary design of the landing capsule ARS revealed that system requirements can be readily satisfied with a single gyro if two modifications are made. Since the landing capsule application requires limited freedom in only two axes it is a natural application for a single electrostatic gyro, basically a two-axis sensor. To take advantage of this unique characteristic and provide the linear range required for the landing capsule it is necessary to place a "constant slope pattern" around the rotor equator and reduce the number of optical pickoffs from three to two. The pickoffs would be located on the case 90 degrees apart, both viewing the rotor pattern during system operation.

Since it is desirable to keep the landing capsule ARS as simple as possible, these modifications are in line with the design and will permit a relatively simple analog instrumentation of the associated readout system electronics.

SIMULTANEOUS PICKOFF READOUT

Although simultaneous readout of the gyro optical pickoffs is not necessary for the ARS concepts and conditions of this study, simultaneous readout will be desirable when high vehicle body rate exists or where the gyro outputs are used in navigation calculations. In the current readout system the pickoffs are read sequentially and the passage of time between readings contributes an error in determining the gyro spin vector if the vehicle has an angular velocity. Simultaneous reading of the pickoffs will eliminate this error and may permit the gyro readout to be synchronized with the system digital computer clock. This is a desirable feature since it greatly simplifies the gyro computer interface.

Since there is no proven way to obtain simultaneous readout of the gyro pickoffs, this would actually be a development effort rather than a simple modification of an existing gyro.

One approach to obtaining simultaneous readout of three orthogonal pickoffs requires measuring the rotor surface velocity at each pickoff. The velocity measurement will probably require the major development effort, but theoretically the velocity at the three pickoffs can be obtained simultaneously. There is a relationship between the three measured velocities, the rotor angular velocity and radius such that:

$$\vec{V}_1 = \vec{\omega} \times \vec{R}_1$$

$$\vec{V}_2 = \vec{\omega} \times \vec{R}_2 \qquad (102)$$

$$\vec{V}_3 = \vec{\omega} \times \vec{R}_3$$

$\vec{V}_1$, $\vec{V}_2$, $\vec{V}_3$ are the vector velocities of the rotor surface at the three pickoffs.

$\vec{R}_1$, $\vec{R}_2$, $\vec{R}_3$ are the position vectors relative to the center of the rotor of the three points of velocity measurement on the rotor surface.

$\vec{\omega} = \vec{\omega}_R - \vec{\omega}_C$ where $\vec{\omega}_R$ is the angular velocity of the rotor and $\vec{\omega}_C$ is the angular velocity of the gyro case.

From Equation (102)

$$|\vec{V}_1| = |\vec{\omega}|\,|\vec{R}_1| \sin\theta_1$$

$$|\vec{V}_2| = |\vec{\omega}|\,|\vec{R}_2| \sin\theta_2 \qquad (103)$$

$$|\vec{V}_3| = |\vec{\omega}|\,|\vec{R}_3| \sin\theta_3$$

where θ_1, θ_2, θ_3 are the angles between the pickoff axis and $\vec{\omega}$. If $\vec{\omega}_C$ has no component normal to ω_R, then θ_1, θ_2, θ_3 are the angles between the pickoff axes and the gyro spin vector. Since $\vec{R}_1$, $\vec{R}_2$, $\vec{R}_3$ are radius vectors of the rotor

$$|\vec{R}_1| = |\vec{R}_2| = |\vec{R}_3| = R$$

also let

$$V = |\vec{V}| \text{ and } \omega = |\vec{\omega}|$$

then

$$V_1 = \omega R \sin\theta_1$$

$$V_2 = \omega R \sin\theta_2 \qquad (104)$$

$$V_3 = \omega R \sin\theta_3$$

and from Equation (104) and considering that the pickoff axes are mutually orthogonal

$$\cos\theta_1 = \sqrt{\frac{-V_1^2 + V_2^2 + V_3^2}{V_1^2 + V_2^2 + V_3^2}}$$

$$\cos\theta_2 = \sqrt{\frac{V_1^2 - V_2^2 + V_3^2}{V_1^2 + V_2^2 + V_3^2}} \qquad (105)$$

$$\cos\theta_3 = \sqrt{\frac{V_1^2 + V_2^2 - V_3^2}{V_1^2 + V_2^2 + V_3^2}}$$

Equations (105) give the desired direction cosines of the gyro spin vector as functions of the three measured surface velocities.

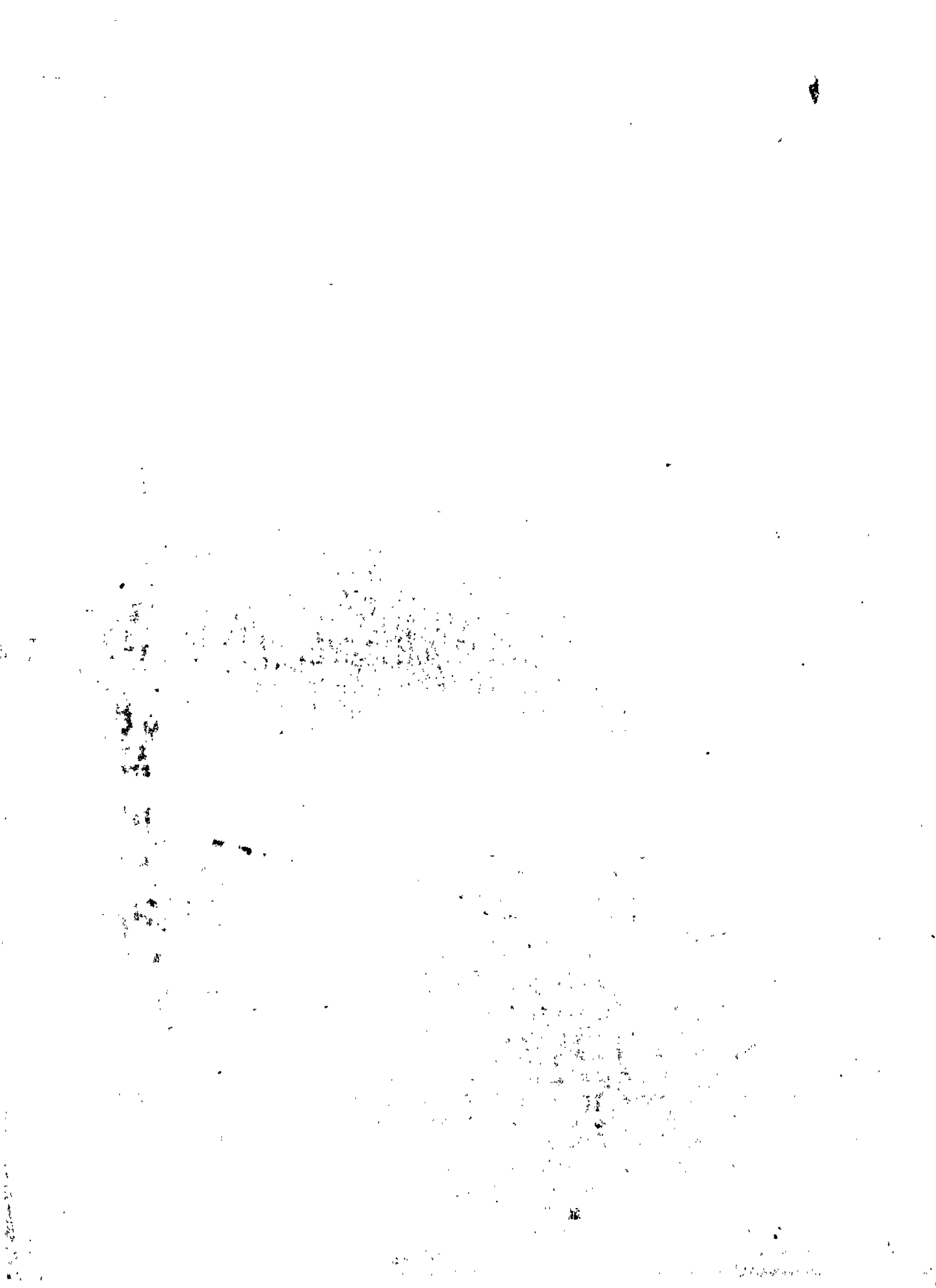

SECTION VI
RECOMMENDATIONS

INTRODUCTION

The end objective for the SDMEG is its application as an attitude sensor performing attitude control, guidance, and navigation functions. To reach this objective, certain component and system development and testing must be performed. This system study, which is being completed by this report, is one of many study and development tasks required before operational systems are in existence.

An attitude reference subsystem is an integral part of any control, guidance or navigation system. This study, an attitude reference system parameter study, defines the significant characteristics of this basic integral subsystem. Some of the results of this study identify areas, which together with the results of the component study effort, conducted concurrently, gives insight and confidence in required follow-on efforts. It is the intent of this section to identify and recommend continuing study and development work considered to be necessary to permit the development cycle to continue to the end objective of use of SDMEG's as an attitude reference for control, guidance, and navigation systems. A time table of the necessary events is shown in Figure 6-1.

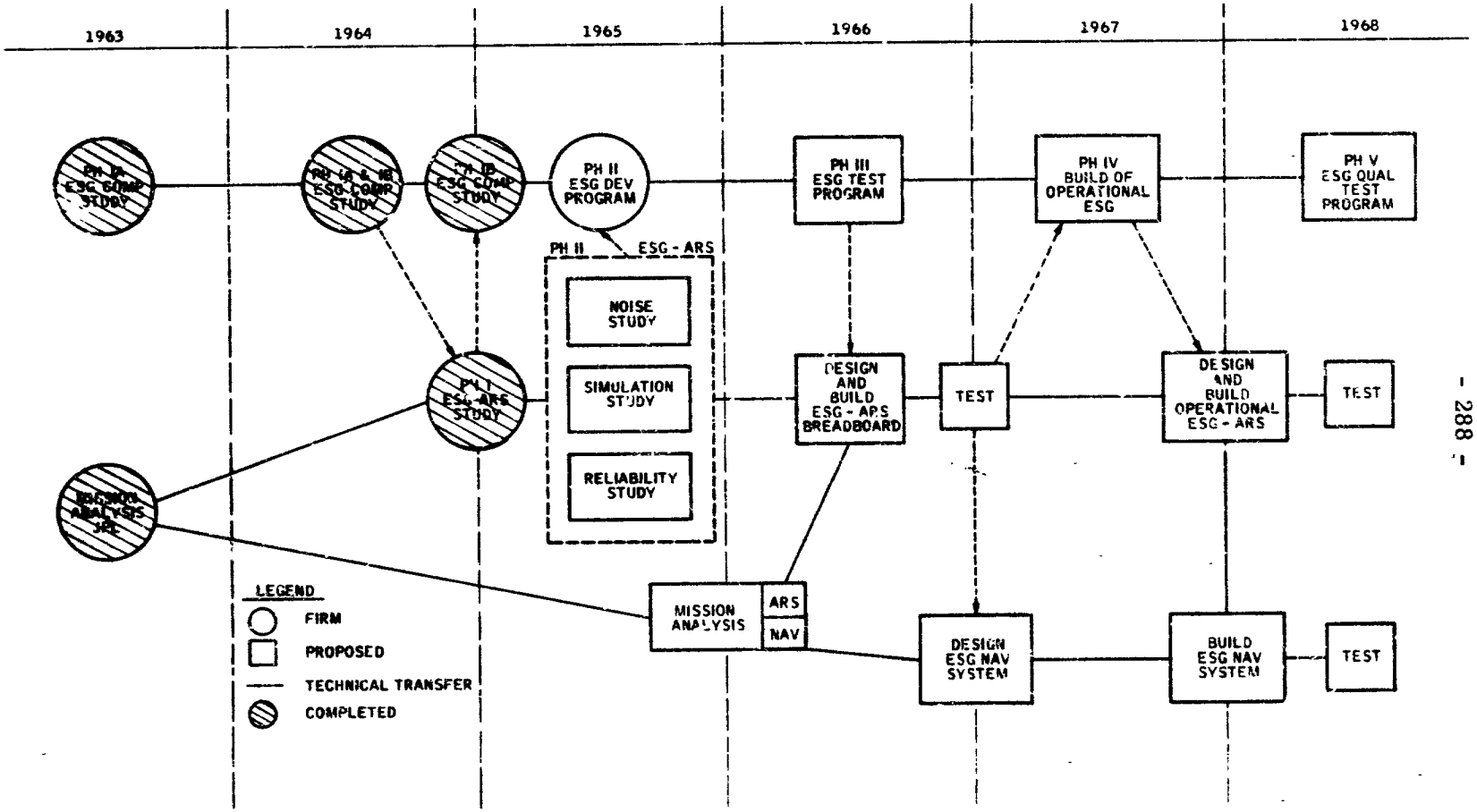

Figure 6-1. Over-all Program Plan

UMMARY

An eight-month ESG-ARS study has now been completed with the objective of obtaining information useful in making recommendations for utilization and integration of the SDMEG in spacecraft attitude reference systems. The study included two major tasks with the first task being a trade-off study of the parameters of an attitude reference system (ARS) which uses an SDMEG as a major component. Task II was the conceptual and preliminary design of an attitude reference system utilizing the SDMEG for a specific landing capsule mission. The more significant conclusions reached in this study are as follows:

1. An investigation of 12 different attitude reference system configurations with system pointing accuracies ranging from 0.04 to 0.07 degree revealed that over this accuracy range the system size and weight varied less than 10 percent. The study also revealed that the system size varied less than 10 percent between systems that had outputs of attitude error and vehicle body rate and systems that had only attitude error.

2. Accuracy to be expected does not require computation to compensate for gyro drift. The nominal 0.05 degree capability is assured for a minimum of one hour operation, which is considered adequate for any ΔV velocity or navigational sighting maneuver.

3. The noise present on the gyro readout from both the end axis pattern and the cosine pattern limits the usefulness of body rate signal derived from the gyro output.

4. It was concluded that precision gyro torquing did not simplify or increase the capability of the ARS concepts investigated and that a caging capability beyond that available in the damping coils of the current gyro design did not simplify the system design.

5. The preliminary design for the ARS concept investigated in the parameter study established the major characteristics of the digital controller. The controller is a general purpose serial/parallel machine with a 16-bit word. The arithmetic will be performed with 4 bits per bite. The bit rate will be 1.5 megacycles and the memory will be 1024 words. The controller will weigh about 12 pounds and occupy 388 cubic inches.

6. The preliminary design of the landing capsule ARS shows that all the requirements except the rate output accuracy may be satisfied with a system using a single ESG. The accuracy of the basic ESG is adequate for this application; however, the noise on the output does limit the accuracy of the derived rate output.

The development program on the sensor has just recently completed Phases IA and IB. Design feasibility has been shown for multi-mode suspension with a low-g suspension power of approximately seven watts. Design studies have determined a start-up-in-space automatic spin-up procedure with the sensor not suspended to withstand the 200-g shock launch environment. Studies have also indicated that the gyro can be designed to meet sterilization requirements and that performance can be maintained without temperature control. A breadboard sensor and suspension system have been fabricated and Phase II will consist of a test program on this assembly as well as the build and test of a second breadboard sensor and suspension system. Following Phase II will be a Phase III prototype design and test program. The sensor design will result in reduced size and weight with compliance to performance specifications demonstrated by a qualification test program. Phases IV and V will be the fabrication and qualification of operational sensors.

The design of the sensor is continuing on schedule and all milestones of the over-all plan to achieve operational sensors in 1968 are being met.

The next step in the development of SDMEG systems is a study consisting of three specific tasks:

1. A simulation study of the ARS to firmly establish the system concept and its parameters.

2. A simulation study to resolve the noise problem in deriving rate information.

3. A reliability study
   (This is a logical follow-on program since it gives maximum support to the gyro development program and also will resolve key problem areas in ARS system applications.)

The first task is a natural follow-on to the parameter study reported on in this document. In order to ensure that the basic system concept is sound, the system should be simulated and the simulation used to verify the concept and fix final system parameters. The third task is required in order to establish the relationship between redundancy and system reliability. This is a trade-off relationship that was not covered by the parameter study just completed. It is not known how system size and complexity might change under the reliability requirements of future spacecraft applications, and therefore it is important to carry out a study to obtain and have available for future use the trade-off information between size and reliability. The form of the study will be such as to produce the relationship between probability of mission success versus mission time for as many reliability models as possible. By generating sizing estimates for the models it will provide the desired trade-off data between reliability and system size and complexity.

Recognizing that these studies will more firmly demonstrate the feasibility of the strapped-down SDMEG Attitude Reference System as well as providing data that will be useful in the evaluation of future spacecraft applications, a recommended program has been formulated and is discussed in detail in the background portion of this section.

Supporting this program are two Honeywell programs which will provide direct inputs to the ARS digital computer simulation. The first program is a company study of preferred digital mechanization of various flight controllers. The output of this study will be the mechanization of the digital controller. Many of the potential design problems of the SDMEG Reference System will benefit from experience gained in the construction of the digital controller. The second supporting study is a specific program for the development of a digital controller for applications similar to the requirements of the AOSO program. The development of this digital controller also will support the ESG-ARS development program.

Following the ARS simulation and redundancy programs, further detailed mission studies are necessary prior to the preliminary design phase of either an ARS or Navigational System. These studies will play a major role in determining specific system requirements and early consideration of mission studies is recommended in order to meet the 1967-69 over-all program timing.

The mission studies will be particularly important in establishing the navigation system requirements. The SDMEG being developed for the ARS may also be used in a navigation system when combined with either an acceleration-measuring capability or with optical instrumentation for star and planet sightings.

The following items are system efforts that should be completed to derive maximum utilization from the SDMEG work that JPL has funded to date. Most of the following tasks are applicable to unmanned interplanetary missions; however, they are also related to manned space flights. The selection of the specific study tasks is dependent upon the contemplated end use of the equipment.

A. Mechanization of navigation and guidance systems oriented around the SDMEG Attitude Reference System

1. Determination of guidance requirements placed on ARS Digital Controller.

2. Studies conducted in the area of operational use of the SDMEG ARS for guidance.

3. Hardware oriented studies to develop technique for incorporative accelerometer-determined velocity information into SDMEG Attitude Reference System.

B. Analysis of SDMEG navigation and guidance systems

1. Simulation of an ESG system for a typical deep space mission to determine effects of quantization, computational error propagation, iteration rate and body rate on navigation operation.

2. Performance analysis of deep space mission to make trade-off studies between use of auxiliary updating equipment and long-term unaided system performance. This also includes the determination of critical system parameters for various flight regimes.

BACKGROUND

This section describes in detail the problems creating the need for the individual studies and the basic objectives of each study. The simulation and noise study is treated in a combined discussion because of the natural interface they have with each other.

SIMULATION AND NOISE STUDY

The need for the noise study arises from the desire to calculate the vehicle body rate from the ESG outputs. In the parameter study it was somewhat arbitrarily decided that the high accuracy ARS provide body rate information 100 times per second. To satisfy this requirement it is necessary to read or obtain new information from the gyro at each revolution of the rotor, and take differences between successive readings. Since each reading may have ±36 arc-seconds of noise, the difference between successive readings may be 72 arc-seconds and the time interval is the rotor period. The rotor period may be as short as 1/200 second.

Therefore, the indicated body rate may be as high as

$$72 \div \frac{1}{200} = 14,400 \text{ sec/sec} = 4 \text{ deg/sec}$$

Obviously an error in the computed vehicle body rate of 4 deg/sec is not acceptable. The solution to reducing the error in the calculated rate may be approached in two ways:

1. Devise filtering that will reduce the effect of the noise
2. Improve the readout so as to reduce the noise level

The system study will be concerned with the first solution while the component study will be concerned with the second solution.

Although filtering can be determined that will attenuate the effect of the noise, the filtering will also affect the phase of the rate signal and thus the stability of the attitude control loop. It is therefore necessary that a simulation of the control system be available to assist in the selection of suitable levels of filtering consistent with control stability.

It is anticipated that the filtering will be instrumented as part of the ARS digital computer. As such it may be an averaging type of filter that computes the average of a number of gyro readings and then makes use of the average value to calculate the attitude error and rate signals. An averaging filter will reduce the RMS noise by the square root of the number of samples or readings used in the average. It will also produce an effective phase shift that will increase with the number of readings included in the average. The control system simulation will permit the selection of a compromise between system stability and number of readings included in the average.

In addition to the averaging type filter the Z transform equivalent of high-pass, lead-lag, and other networks that promise to be useful in the stabilization of the control system in the presence of noise can be simulated as part of the ARS computer simulation. The control system simulation will allow a rapid and thorough evaluation of the usefulness of the various networks over a large range of the network parameters. The effort required to obtain the same information through the use of purely manual analysis would no doubt be excessive if indeed the information could be obtained by manual analysis.

In attacking the noise problem with the approach of improving the gyro pickoff system, readout data scatter can be traced to two major sources -- signal noise level and signal rise time. These errors can be controlled so that their effects upon readout position errors for an attitude reference system are insignificant. If, however, it is desired to derive vehicle rate information from the readout system, the presently encountered level of data scatter must be greatly reduced.

It is possible to significantly reduce the data scatter presently encountered in strapdown readout systems both by some redesign of the present components and circuits and by making trade-offs with existing readout operating parameters.

The existing pickoff preamplifier is considered state of the art in low noise amplifier design. Hence, reduction of the effect of signal noise must be accomplished by increasing the signal level and, consequently, the signal-to-noise ratio. The present pickoff sensor signal levels may be increased by increasing the light energy level at the pickoff field stop and/or by increasing the field stop size. The present pickoff design utilizes a lens and lamp to light the aperture. This light intensity can be increased by increasing the lamp filament temperature, hence reducing the operating life of the lamp and increasing the power consumption. The light intensity could also be raised by designing a more efficient light system which could gather the light from the lamp filament and focus it on the pickoff aperture.

Increasing the field stop size results in decreased data scatter even though the signal rise time is increased. (The signal level of the pickoffs increases as the square of the field stop diameter. This increase more than offsets the increased signal rise time which varies directly as the field stop diameter.)

It is possible to decrease the signal rise time of the present optical pickoffs by modifying the present preamplifiers. These preamplifiers exhibit a rise time of about three to five microseconds. It has been demonstrated that minor circuit modifications can reduce this to below one microsecond, which is compatible with present photosensors. As photosensor and transistor technology continue to improve, it is anticipated that significant improvements in both signal-to-noise ratios and signal rise times will be realized.

The simulation of the attitude control loop will also make it possible to verify the basic ARS concept. The concept for the parameter study was selected to minimize the data processing. In particular, it was selected to avoid matrix multiplications. In so doing the attitude error signal is not a linear function of attitude error and it would be appropriate to investigate the control system behavior for large error signals.

Figure 6-2 is a gross block diagram of the simulation of the attitude control system that would be used in the verification of the ARS concept. For this purpose the noise simulation would be omitted.

Figure 6-3 is a graphical representation of the calculations that would be included as part of the ARS computer simulation. In this figure $\hat{Q}_1$ and $\hat{Q}_2$ are commanded or desired positions of the gyro spin vectors in the vehicle coordinates. $\hat{S}_1$ and $\hat{S}_2$ are measured or observed gyro spin vectors in the same coordinate system. The signal $\vec{\Theta}$ obviously has a null when $\hat{S}_1 = \hat{Q}_1$ and $\hat{S}_2 = \hat{Q}_2$ and for small differences between the $\hat{S}$'s and $\hat{Q}$'s it can be expected that the system will control in a reasonable manner. However, for large differences in $\hat{S}$ and $\hat{Q}$ the performance is not so predictable. For example, if the vehicle is commanded to change its attitude by 180 degrees with respect to each of the gyro spin vectors, $\hat{Q}_1 = -\hat{S}_1$ and $\hat{Q}_2 = -\hat{S}_2$. With these values of $\hat{Q}$ and $\hat{S}$ the attitude error signal is zero. This is an unstable null and any small departure from it will result in an error signal of the proper sign to cause the system to drive to a stable null but the path or trajectory followed should be determined for attitude commands in the vicinity of the unstable null.

The simulation will also permit the investigation of the effect of the data controller parameters on the control system performance. For example, simulation of various data rates in the computer may result in a maximum data rate much less than the arbitrarily chosen 100/sec for the rate calculation.

Since it requires a minimum of two samples per cycle to determine a sinusoidal component in a signal, the sampling rate of 100/sec will permit the determination of sinusoidal components with frequencies up to 50 cycles per second. This is no doubt beyond the bandwidth of the control system. Since the control system bandwidth will probably be of the order of 5 cps, a bandwidth of 10 cps in the rate information should be adequate and therefore an iteration rate of 20/sec on the vehicle rate calculation would be satisfactory.

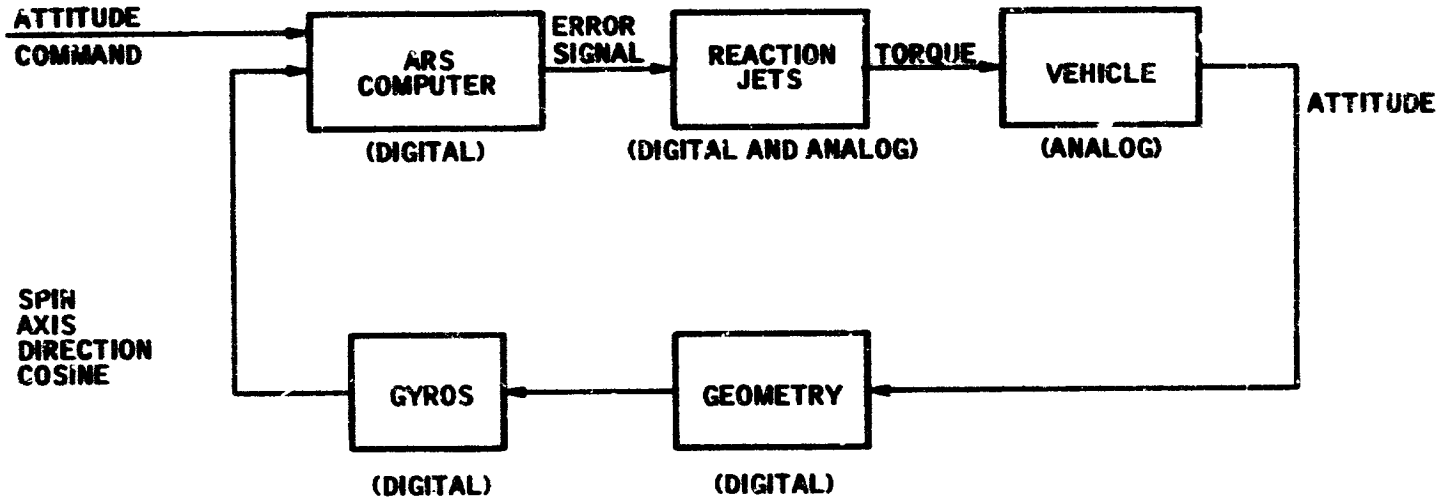

Figure 6-2. Blcck Diagram of Attitude Control System Simulation

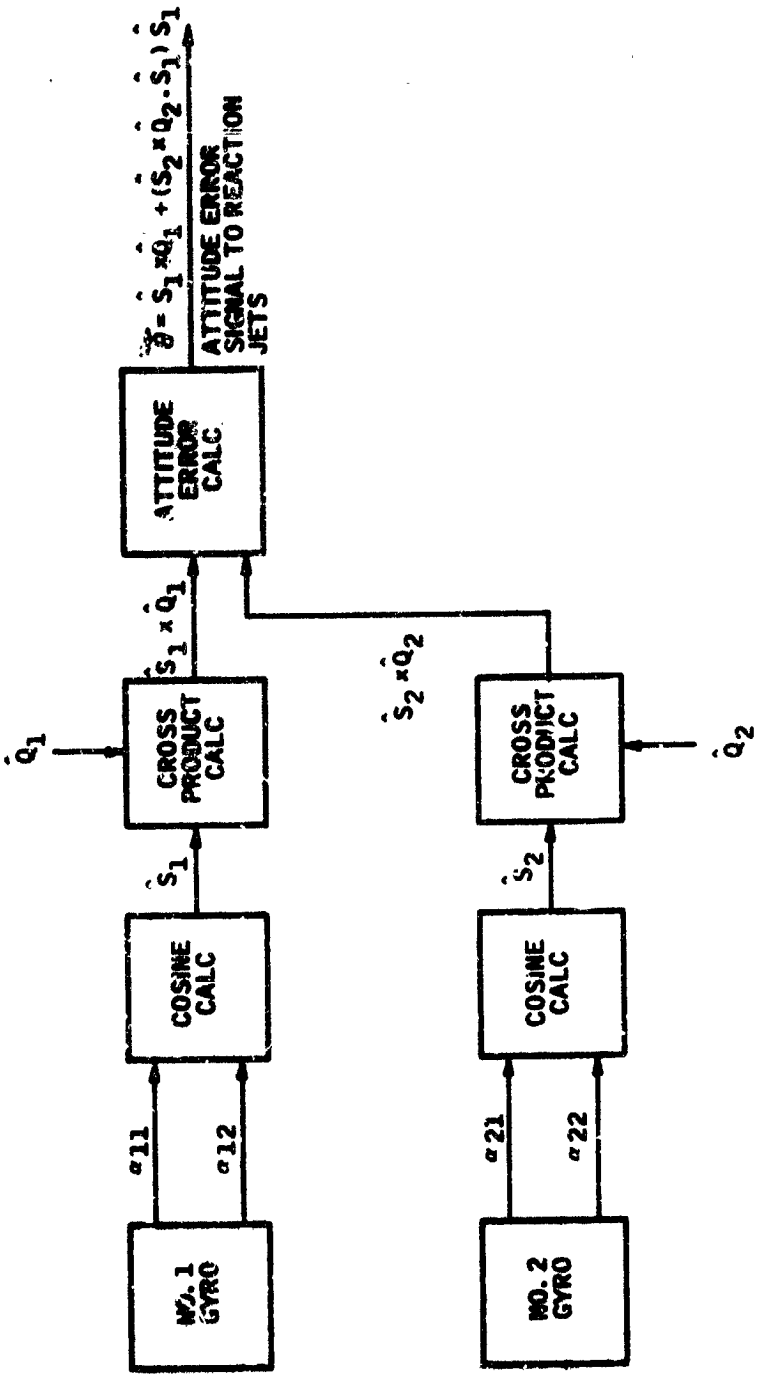

Figure 6-3. Flow Diagram of the Data Processing to Obtain the Attitude Error Signal

This reduction in the calculation iteration rate will permit an averaging of five gyro readings for each rate calculation. The result of this averaging is a reduction of the RMS value of any random noise on the gyro readout by a factor of $\sqrt{5}$.

Also, the reduction in the iteration rate for the vehicle rate calculation will result in fewer basic calculations per second in the digital controller. Therefore, the computer can be designed for a longer add time and possibly save some size in the controller. Currently the 100/sec iteration rate requires approximately 110,500 additions per second. A reduction in the iteration rate for the vehicle rate calculation to 20/sec will result in about 30,000 additions per second. Therefore, the add time can theoretically be 33 microseconds. A serial controller operating with a one megacycle clock and a 16-bit word could perform an addition in 16 microseconds. This would permit adequate time for the fetch and store operations as well as other computer bookkeeping. Also, the serial machine would be a simplification from the currently proposed serial/parallel machine. In addition to using the least amount of equipment the serial machine has some advantages in the event it becomes necessary to add redundancy to the machine for the purposes of reliability.

RELIABILITY STUDY

A reliability study is suggested since the parameter study considered a non-redundant system and conventional military specification parts in arriving at the reliability estimates. Reliability can be obtained by a number of approaches and the objective of the study would be to determine which approach requires the least expenditure in system size and complexity for various levels of reliability.

The attack on the problem would be to set up as many redundancy models for the SDMEG-ARS as possible and determine the reliability versus size, weight, cost, and power consumption for each. Models that could be examined are of the following basic types:

- Redundancy gyros
- Redundant computer
- Redundancy within the gyro
- Redundancy within the computer
- Redundant gyros and computer
- High reliability components in gyros and computer

In order to establish the preferred system redundancy, giving proper consideration to the various trade-off considerations involved, a state reliability analysis method will be employed. This analysis tool, which is a simple extension of basic probability theory, permits direct digital computer analysis of the most complex redundancy configurations. Using computerized state probability techniques, it is possible to determine the impact on the system caused by grossly changing the system redundancy mode, or by changing a single piece part failure rate. Whereas the present method of system reliability calculation requires considerable approximation and laborious hand calculation, state probabilities and figure of merit reliabilities, for all desired system configurations, are made available within minutes using the computerized model. This resultant ease and versatility enables total system trade-offs that previously have been prohibited because of the extreme amount of hand calculation time required, even for simple cases.

The system-redundancy analysis involves the use of probability state analysis techniques where the probability of the system under consideration being in some condition, state (failed, partially failed or operational, etc.), is expressible by a matrix differential equation:

$$\frac{d}{dt}\,\bar{P}(t) = \left[\Lambda^{T}\right]\bar{P}$$

where

$\bar{P}$ = a column state probability vector

$[\Lambda]$ = a stochastic matrix whose elements are comprised of the system failure rates

T = transpose

For example, given the following types of redundant systems:

A. Standby

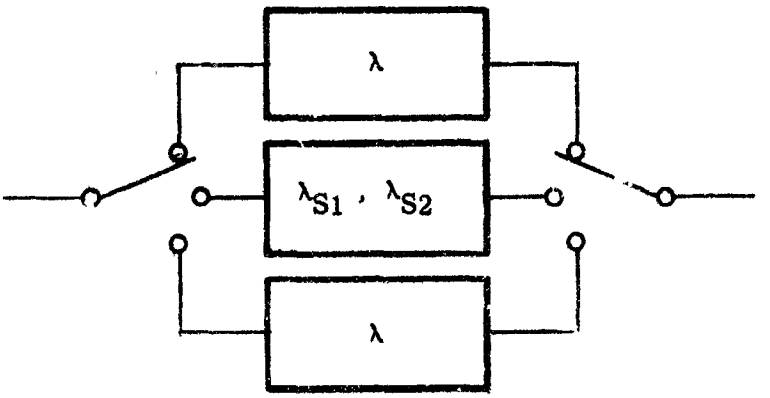

This configuration has four states of operation (simplified):

1. E_o - initial state of no failures
2. E_1 - switch failed and thus unable to switch to the standby element
3. E_2 - switch failed and in process switches to the standby element and is unable to switch back upon demand or primary element failed
4. E_3 - complete failure (neither system capable of continuing to operate

B. Parallel

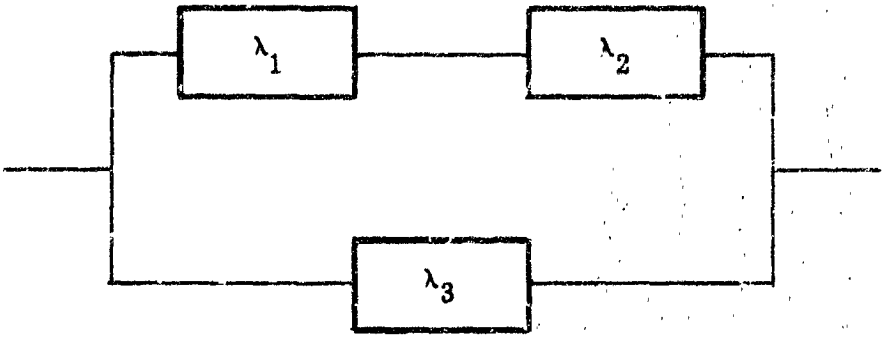

This configuration has four states of operation:

1. E_o - no failure
2. E_1 - upper channel failed, lower channel okay
3. E_2 - lower channel failed, upper channel okay
4. E_3 - total failure

C. Nonredundant

This configuration has two states of operation:

1. E_o - no failure
2. E_1 - total failure

D. Other Combinations of Elements Which Are Also Actuation Dependent

These would not cause any analysis difficulty. The probability of being in state E_1 at the end of t is

$$P_1(t + \Delta t) = P_1(t) + P_o(t)\,[\lambda \Delta t + 0(\Delta t)]$$

or

$$\frac{d\,P_1(t)}{dt} = P_o(t)\,\lambda$$

Similar equations can be obtained for states E_2 and E_3 as functions of the other states.

With this in mind, observing the state transition diagram, a transition matrix can be obtained directly:

		E_o	E_1	E_2	E_3 ← Upper Row
Left Column →	E_o	$-(\tau + \lambda_{S1} + \lambda_{S2})$	(λ_{S1})	$(\lambda + \lambda_{S2})$	0
	E_1	0	$-\lambda$	0	λ
	E_2	0	0	$-\lambda$	λ
	E_3	0	0	0	0

$= [\Lambda]$

Where the elements are the transition rates in going from the state indicated in the left column to that indicated in the upper row, inspection then reveals that the transpose of this transition matrix is the coefficient matrix of a first-order differential equation with the state probabilities as functions of time or:

$$\dot{P}(t) = \left[\Lambda^T\right] P(t)$$

From these schematics, the following transition diagrams are constructed:

For the redundant configuration (A), the following transition diagram is applicable:

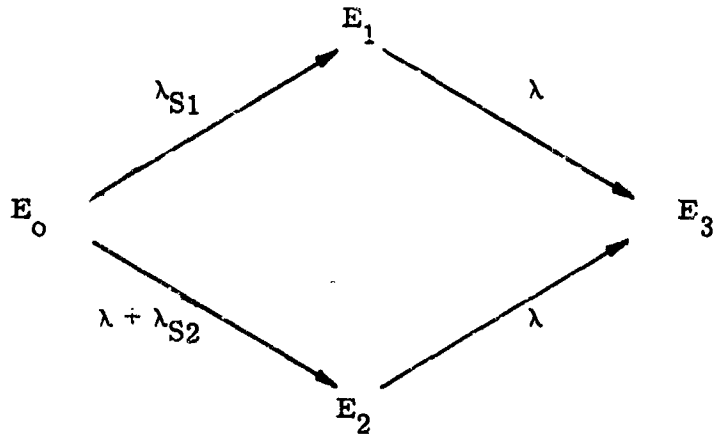

where:

λ = failure rate of the component

λ_{S1} = failure rate of switch yielding state E_1

λ_{S2} = failure rate of switch yielding state E_2

Using the basic laws of probability

(Probability of being in a particular state E at $t = t_o + \Delta t$) =

(Probability of being in the same state at $t = t_o$) x

(Probability of not changing state) +

(Probability of being in some other state at $t = t_o$) x

(The probability of making transition to E during time interval Δt)

Thus, the probability of being in E_o at $(t + \Delta t)$

$$P_o(t + \Delta t) = P_o(t) [1 - (\lambda + \lambda_{S1} + \lambda_{S2}) \Delta t + 0(\Delta t)]$$

or, passing to the limit:

$$\frac{d P_o(t)}{dt} = - (\lambda + \lambda_{S1} + \lambda_{S2}) P_o(t)$$

It is well known that the probability of system success is equal to the product of the individual subsystem success probabilities. Thus:

$$P_{success} = \prod_{i=1}^{N} [1 - P_i(fail)]$$

where

N = number of subsystems

$P_i(fail)$ = probability of subsystem failure

The above first-order differential equation is easily solved for extremely complex redundancy schemes using analog or digital computer techniques.

The ease of obtaining the system reliability assessments using this approach suggests it as a valuable design tool. In addition to generating relative reliability data, relative system design merit data such as cost, size, switching requirements, etc., can be obtained by solving the differential equation with constraints imposed on the various variables and relative costs associated with them.

An important concluding observation is that the proposed reliability study will be very broad. As indicated, its basic form will be such that one can interpret the best model (from those considered) versus time. This makes the study applicable for many future missions having large variations in mission time.

SUPPORTING PROGRAMS

There are two programs currently in progress in the Space Flight Systems Group at Honeywell that will directly benefit the proposed studies. The first of these programs is a study with the objective of establishing a basic digital controller configuration that could be used for numerous spacecraft control applications. The following programs were reviewed for the purpose of determining if they would benefit from a digital mechanization of the flight controller and if so what type of digital controller could satisfy the requirements of all. The programs were:

- AOSO
- LPTV
- VOYAGER
- APOLLO
- MOL
- LOP
- Aircraft Autopilots
- Boost Vehicle Autopilots

In all cases the indications are that a digital controller using a serial arithmetic unit with a 16-bit word or less and one to two megacycle bit rate will satisfy the requirements of all the programs. It appears that the input/output to the controller would require some modification or tailoring for each application in order to effect a proper interface with other equipment. However, the basic controller consisting of arithmetic unit, memory and control unit, would remain the same for all applications.

It is anticipated that the inputs to the controller would be derived from optical sensors, inertial sensors, thermal sensors, communications system, and actuator feedbacks. The controller will operate on these inputs to perform

various logic functions, signal conditioning and signal compensation and will provide outputs to actuators, sensors communication system, mode switching and possibly other subsystems.

In this program a configuration will be selected for the controller that promises to satisfy the greatest number of space flight control requirements, and it will be carried through logical design and simulation on a large computer.

The second program will extend the first in that it will take the logic design generated in the first program and will fabricate and test a breadboard of the controller. The breadboard will have the capability of performing mode control, power switching, signal compensation and other functions that the study shows to be desirable in addition to the data processing necessary for direct control and stabilization of the vehicle. Part of the breadboard test will be to include the controller in a control loop with a simulated vehicle. Also, the second program will make a study of reliability in the controller for the purpose of establishing tentative levels of redundancy for the various controller components. The emergence and acceptance of microelectronic design techniques makes redundancy a much more attractive solution to the reliability problem than it once was.

It is anticipated that the information resulting from these programs would be directly useful in the design of a digital controller to be used with the strapped-down ESG's. For example, the components and circuits selected during the breadboard stage of these programs would no doubt be used in the ESG controller also, and it is quite likely that many decisions made on these programs would be valid for the ESG controller.

There are also several programs in progress at Honeywell's Aero Florida Division, the results of which will support the recommended follow-on effort. This division has the responsibility to design, develop, test and deliver the inertial guidance systems for the Centaur high-energy space vehicle. In addition to the platform and platform electronics, the guidance equipment includes the digital coupler, digital computer and signal conditioner.

Also, Honeywell-Florida currently has a contract with the Air Force Research and Technology Division for the design, build, and laboratory testing of a gimbaled ESG navigation system. Coordination with this program has and will continue to benefit the SD-ESG component development and ARS system programs.

PRELIMINARY WORK STATEMENT FOR FOLLOW-ON EFFORT

The recommended tasks as discussed in detail above can be reduced to a set of discrete work statements. These tasks logically fall into two over-all groupings and are detailed below, along with time-phasing in Figure 6-4.

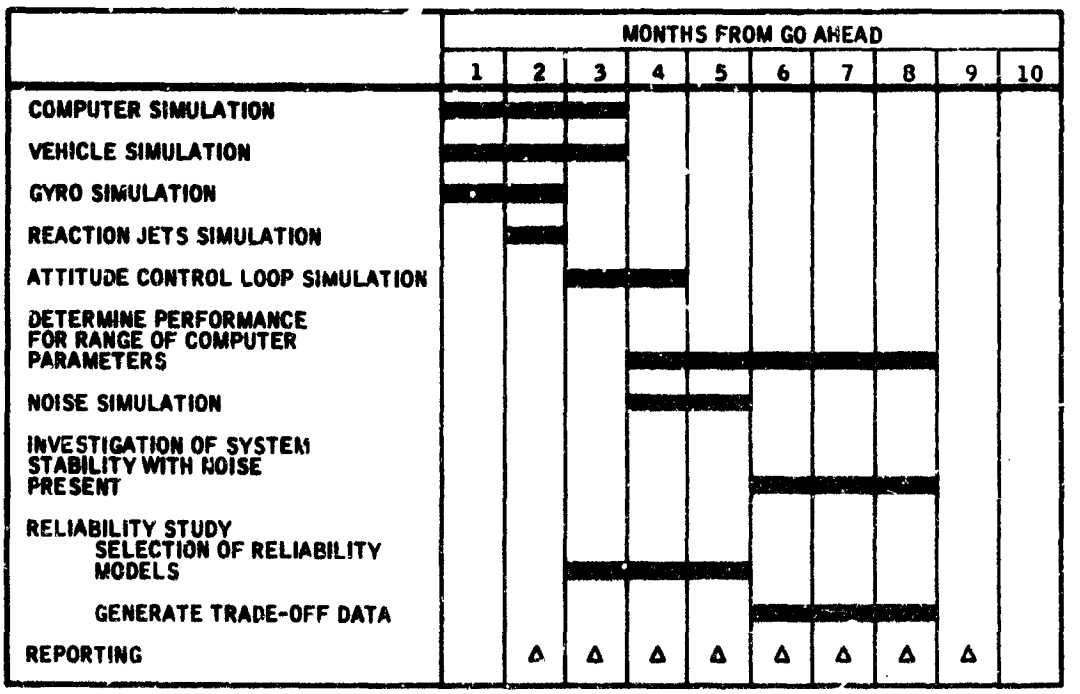

Figure 6-4. Preliminary Schedule

TASK I - SIMULATION AND NOISE STUDY

1. Simulate the ARS computer defined in the parameter study of JPL Contract No. 950915.

   a. Write a program to simulate the ARS computer on the digital computer of the hybrid computer installation.

   b. Conduct checkout of the simulation.

2. Simulate the selected space vehicle.

   a. Select the equations of motion, including bending modes, if any, and coefficients typical of an intraplanetary vehicle.

   b. Program the selected equations on the analog computer.

   c. Conduct checkout of the simulation.

3. Simulate the gyro output for input to ARS digital controller simulation.

   a. Derive the equations relating output of space vehicle simulation and gyro output pulses.

   b. Program the equations derived in (a) either analog or digital as necessary.

   c. Check out the simulation.

4. Simulate the dynamics of the reaction jets.

   a. Select a jet configuration and thrust level typical of the intraplanetary vehicle.

   b. Derive an analog or digital simulation as appropriate to operate with computer and vehicle simulations.

   c. Check out the simulation.

5. Simulate the attitude control loop.

   a. Interconnect the simulations of the vehicle, gyro controller and control jets.

   b. Verify the scaling throughout the simulations and check out the simulations.

6. Using the control system simulation investigate system performance.

   a. Determine system response to commands over the range of data rates on both attitude error and attitude rate.

   b. Determine effect on system operation of various controller accuracies (work length).

7. Simulate gyro readout noise.

   a. Write a program to generate pseudo random numbers with a distribution similar to the gyro readout noise.

   b. Insert the simulated noise in the control system simulation and determine the effect on system performance.

8. Investigate methods of obtaining control system stabilization in the presence of gyro readout noise.

   a. Include digital pseudo rate in the computer simulation and investigate the ability of this method to stabilize the system.

   b. Include a simple averaging filter in the computer simulation and determine the ability of the filter to stabilize the system.

   c. Investigate the effectiveness of digital filters of a lead-lag nature to effect stability in the control system.

TASK II - RELIABILITY STUDY

1. Select the reliability models.
2. Prepare computer programs.
3. Obtain reliability data from programs.
4. Summarize results (reliability versus system parameters)

APPENDIX A

DERIVATION OF EQUATIONS FOR CALCULATION OF THE THIRD SPIN AXIS DIRECTION COSINE

APPENDIX A

DERIVATION OF EQUATIONS FOR CALCULATION OF THE THIRD SPIN AXIS DIRECTION COSINE

INTRODUCTION

Since gyro readout can provide data from only two pickoffs at any one time, the direction cosine of the spin axis relative to the third pickoff must be computed from the direction cosines for the two active pickoffs and pickoff alignment data measured during gyro assembly and installation. The following discussion presents a derivation of the equations and relationship necessary to this calculation.

DEFINITIONS

For the purposes of this discussion, the gyro pickoff axes will be defined by the unit vectors $\hat{P}1$, $\hat{P}2$, $\hat{P}3$ which in general have a small departure from orthogonality.

The three direction cosines that locate the gyro spin axis relative to $\hat{P}1$, $\hat{P}2$, $\hat{P}3$ are defined by:

$$\alpha_1 = \hat{P}_1 \cdot \hat{S}$$

$$\alpha_2 = \hat{P}_2 \cdot \hat{S}$$

$$\alpha_3 = \hat{P}_3 \cdot \hat{S}$$

$\hat{S}$ is a unit vector along the gyro spin axis.

For this derivation, three orthogonal sets of reference frames are define in terms of the pickoff vectors $\hat{P}_1$, $\hat{P}_2$, $\hat{P}_3$.

The reference frames are defined as follows:

$$\hat{I}_1 = \hat{P}_1$$

$$\hat{J}_1 = \hat{P}_3 \times \hat{P}_1 / |\hat{P}_3 \times \hat{P}_1|$$

$$\hat{K}_1 = \hat{P}_1 \times (\hat{P}_2 \times \hat{P}_1) / |\hat{P}_3 \times \hat{P}_1| = \frac{\hat{P}_3 - \hat{P}_1 \cdot \hat{P}_3 \hat{P}_1}{|\hat{P}_3 \times \hat{P}_1|}$$

$$\hat{I}_2 = \hat{P}_2 \times (\hat{P}_1 \times \hat{P}_2) / |\hat{P}_1 \times \hat{P}_2| = \frac{\hat{P}_1 - \hat{P}_2 \cdot \hat{P}_1 \hat{P}_2}{|P_1 \times P_2|}$$

$$\hat{J}_2 = \hat{P}_2$$

$$\hat{K}_2 = \hat{P}_1 \times \hat{P}_2 / |\hat{P}_1 \times \hat{P}_2|$$

$$\hat{I}_3 = \hat{P}_2 \times \hat{P}_3 / |\hat{P}_2 \times \hat{P}_2|$$

$$\hat{J}_3 = \hat{P}_3 \times (\hat{P}_2 \times \hat{P}_3) / |(\hat{P}_2 \times \hat{P}_3| = \frac{\hat{P}_2 - \hat{P}_3 \cdot \hat{P}_2 \hat{P}_3}{|\hat{P}_2 \times \hat{P}_3|}$$

$$\hat{K}_3 = \hat{P}_3$$

The corresponding three matrices between the pickoff axes and the orthogonal reference frames are:

$$\begin{bmatrix} \hat{P}_1 \\ \hat{P}_2 \\ \hat{P}_3 \end{bmatrix} = \begin{bmatrix} 1 & 0 & 0 \\ \hat{P}_2 \cdot \hat{P}_1 & \dfrac{(\hat{P}_1 \hat{P}_2 \hat{P}_3)}{/\hat{P}_3 \times \hat{P}_1/} & \dfrac{\hat{P}_2 \cdot \hat{P}_3 - \hat{P}_1 \cdot \hat{P}_3 \hat{P}_1 \cdot \hat{P}_2}{/\hat{P}_3 \times \hat{P}_1/} \\ \hat{P}_3 \cdot \hat{P}_1 & 0 & \dfrac{1 - (\hat{P}_1 \cdot \hat{P}_3)^2}{/\hat{P}_3 \times \hat{P}_1/} \end{bmatrix} \begin{bmatrix} \hat{I}_1 \\ \hat{J}_1 \\ \hat{K}_1 \end{bmatrix} \equiv M_1 \begin{bmatrix} \hat{I}_1 \\ \hat{J}_1 \\ \hat{K}_1 \end{bmatrix}$$

$$\begin{bmatrix} \hat{P}_1 \\ \hat{P}_2 \\ \hat{P}_3 \end{bmatrix} = \begin{bmatrix} \dfrac{1 - (\hat{P}_1 \cdot \hat{P}_2)^2}{/\hat{P}_1 \times \hat{P}_2/} & \hat{P}_1 \cdot \hat{P}_2 & 0 \\ 0 & 1 & 0 \\ \dfrac{\hat{P}_1 \cdot \hat{P}_3 - \hat{P}_1 \cdot P_2 \hat{P}_2 \cdot \hat{P}_3}{/\hat{P}_1 \times \hat{P}_2/} & \hat{P}_3 \cdot \hat{P}_2 & \dfrac{(\hat{P}_1 \hat{P}_2 \hat{P}_3)}{/\hat{P}_1 \times \hat{P}_2/} \end{bmatrix} \begin{bmatrix} \hat{I}_2 \\ \hat{J}_2 \\ \hat{K}_2 \end{bmatrix} \equiv M_2 \begin{bmatrix} \hat{I}_2 \\ \hat{J}_2 \\ \hat{K}_2 \end{bmatrix}$$

$$\begin{bmatrix} \hat{P}_1 \\ \hat{P}_2 \\ \hat{P}_3 \end{bmatrix} = \begin{bmatrix} \dfrac{(\hat{P}_1 \hat{P}_2 \hat{P}_3)}{/\hat{P}_2 \times \hat{P}_3/} & \dfrac{\hat{P}_1 \cdot \hat{P}_2 - \hat{P}_2 \cdot \hat{P}_3 \hat{P}_1 \cdot \hat{P}_3}{/\hat{P}_2 \times \hat{P}_3/} & \hat{P}_1 \cdot \hat{P}_3 \\ 0 & \dfrac{1 - (\hat{P}_2 \cdot \hat{P}_3)^2}{/\hat{P}_2 \times \hat{P}_3/} & \hat{P}_2 \cdot \hat{P}_3 \\ 0 & 0 & 1 \end{bmatrix} \begin{bmatrix} \hat{I}_3 \\ \hat{J}_3 \\ \hat{K}_3 \end{bmatrix} \equiv M_3 \begin{bmatrix} \hat{I}_3 \\ \hat{J}_3 \\ \hat{K}_3 \end{bmatrix}$$

where $(\hat{P}_1 \hat{P}_2 \hat{P}_3) = \hat{P}_1 \cdot \hat{P}_2 \times \hat{P}_3$

All elements of matrices M_1, M_2 and M_3 may be determined from proper alignment measurements during gyro assembly and installation.

DERIVATION

The gyro spin axis may be expressed in the defined orthogonal reference frames as:

$$\hat{S} = (\hat{S} \cdot \hat{i}_n)\ \hat{i}_n + (\hat{S} \cdot \hat{j}_n)\ \hat{j}_n + (\hat{S} \cdot \hat{k}_n)\ \hat{k}_n \quad n = 1, 2, 3 \tag{A1}$$

and since $\hat{S}$ is a unit vector

$$(\hat{S} \cdot \hat{i}_n)^2 + (\hat{S} \cdot \hat{j}_n)^2 + (\hat{S} \cdot \hat{k}_n)^2 = 1 \tag{A2}$$

By inverting the matrices, M_1, M_2, M_3, ($\hat{i}_n$, $\hat{j}_n$, $\hat{k}_n$) may be expressed in terms of the pickoff axis $\hat{P}_1$, $\hat{P}_2$, $\hat{P}_3$.

The inverse of the matrix M can be found using the following formula:

$$ji^{th} \text{ element of inverse} = \frac{(-1)^{i+j} \left[\text{Minor of } ij^{th} \text{ element of M}\right]}{\left[\text{Determinant of M}\right]}$$

Consider matrix M_1 for the illustration of the matrix inversion procedure. If the inverted matrix M_1^{-1} is defined by the elements M_{ij}, then

$$M_{11} = \frac{(-1)^{i+j} \dfrac{(\hat{P}_1 \hat{P}_2 \hat{P}_3)\ 1 - (\hat{P}_1 \cdot \hat{P}_3)^2}{|\hat{P}_3 \times \hat{P}_1|^2}}{\dfrac{(\hat{P}_1 \hat{P}_2 \hat{P}_3)\ \left[1 - (\hat{P}_1 \cdot \hat{P}_3)^2\right]}{|\hat{P}_3 \times \hat{P}_1|^2}}$$

$$M_{21} = (-1)^{1+2} \frac{\left[\frac{\hat{P}_1 \cdot \hat{P}_2\left[1-(\hat{P}_1 \cdot \hat{P}_3)^2\right]}{|\hat{P}_3 \times \hat{P}_1|} - \frac{\hat{P}_3 \cdot \hat{P}_1\left[\hat{P}_2 \cdot \hat{P}_3 - \hat{P}_1 \cdot \hat{P}_3\, \hat{P}_1 \cdot \hat{P}_2\right]}{|\hat{P}_3 \times \hat{P}_1|}\right]}{\frac{(P_1 P_2 P_3)\left[1 - (\hat{P}_1 \cdot \hat{P}_2)^2\right]}{|\hat{P}_3 \times \hat{P}_1|^2}}$$

$$M_{21} = \frac{|\hat{P}_3 \times \hat{P}_1|\left[(\hat{P}_1 \cdot \hat{P}_3)(\hat{P}_2 \cdot \hat{P}_3) - (\hat{P}_1 \cdot \hat{P}_2)\right]}{|\hat{P}_1 \hat{P}_2 \hat{P}_3|\left[1-(\hat{P}_1 \cdot \hat{P}_3)^2\right]}$$

The other seven elements of the M_1^{-1} matrix can be derived in a similar fashion and are given in Equation A3. Equations A4 and A5 give the inverses of M_2 and M_3, respectively.

$$\begin{vmatrix} \hat{i}_1 \\ \hat{j}_1 \\ \hat{k}_1 \end{vmatrix} = \begin{vmatrix} 1 & 0 & 0 \\ \frac{|\hat{P}_3 \times \hat{P}_1|\ \hat{P}_1 \cdot \hat{P}_3)(\hat{P}_2 \cdot \hat{P}_3) - (\hat{P}_1 \cdot \hat{P}_2)}{(\hat{P}_1 \hat{P}_2 \hat{P}_3)\left[1-(\hat{P}_1 \cdot \hat{P}_3)^2\right]} & \frac{|\hat{P}_3 \times \hat{P}_1|}{(\hat{P}_1 \hat{P}_2 \hat{P}_3)} & \frac{|\hat{P}_3 \times \hat{P}_1|\left[(\hat{P}_1 \cdot \hat{P}_3)(\hat{P}_1 \cdot \hat{P}_2) - (\hat{P}_2 \cdot \hat{P}_3)\right]}{(\hat{P}_1 \hat{P}_2 \hat{P}_3)\left[1-(\hat{P}_1 \cdot \hat{P}_3)^2\right]} \\ \frac{|\hat{P}_3 \times \hat{P}_1|(\hat{P}_1 \cdot \hat{P}_3)}{\left[1-(\hat{P}_1 \cdot \hat{P}_3)^2\right]} & 0 & \frac{|\hat{P}_3 \times \hat{P}_1|}{\left[1-(\hat{P}_1 \cdot \hat{P}_3)^2\right]} \end{vmatrix} \begin{vmatrix} \hat{P}_1 \\ \hat{P}_2 \\ \hat{P}_3 \end{vmatrix} = M^{-1} \begin{vmatrix} \hat{P}_1 \\ \hat{P}_2 \\ \hat{P}_3 \end{vmatrix} \quad \text{(A3)}$$

$$\begin{vmatrix} \hat{i}_2 \\ \hat{j}_2 \\ \hat{k}_2 \end{vmatrix} = \begin{vmatrix} \dfrac{|\hat{P}_1 \times \hat{P}_2|}{\left[1 - (\hat{P}_1 \cdot \hat{P}_2)^2\right]} & -\dfrac{|\hat{P}_1 \times \hat{P}_2|\,(\hat{P}_1 \cdot \hat{P}_2)}{\left[1 - (\hat{P}_1 \cdot \hat{P}_2)^2\right]} & \\ 0 & 1 & 0 \\ \dfrac{|\hat{P}_1 \times \hat{P}_2|\left[(\hat{P}_1 \cdot \hat{P}_2\,(\hat{P}_2 \cdot \hat{P}_3) - (\hat{P}_1 \cdot \hat{P}_2)\right]}{(\hat{P}_1 \hat{P}_2 \hat{P}_3)\left[1 - (\hat{P}_1 \cdot \hat{P}_2)^2\right]} & \dfrac{|\hat{P}_1 \times \hat{P}_2|\left[(\hat{P}_1 \cdot \hat{P}_2)\,(\hat{P}_1 \cdot \hat{P}_3) - (\hat{P}_2 \cdot \hat{P}_3)\right]}{(\hat{P}_1 \hat{P}_2 \hat{P}_3)\left[1 - (\hat{P}_1 \cdot \hat{P}_2)^2\right]} & \dfrac{|\hat{P}_1 \cdot \hat{P}_2|}{(\hat{P}_1 \hat{P}_1 \hat{P}_3)} \end{vmatrix} \begin{vmatrix} \hat{P}_1 \\ \hat{P}_2 \\ \hat{P}_3 \end{vmatrix} = M_2^{-1} \begin{vmatrix} \hat{P}_1 \\ \hat{P}_2 \\ \hat{P}_3 \end{vmatrix} \qquad \text{(A4)}$$

$$\begin{vmatrix} \hat{i}_3 \\ \hat{j}_3 \\ \hat{k}_3 \end{vmatrix} = \begin{vmatrix} \dfrac{|\hat{P}_2 \times \hat{P}_3|}{(\hat{P}_1 \hat{P}_2 \hat{P}_3)} & \dfrac{|\hat{P}_2 \times \hat{P}_3|\left[(\hat{P}_2 \cdot \hat{P}_3)\,(\hat{P}_1 \cdot \hat{P}_3) - (\hat{P}_1 \cdot \hat{P}_2)\right]}{(\hat{P}_1 \hat{P}_2 \hat{P}_3)\left[1 - (\hat{P}_2 \cdot \hat{P}_3)^2\right]} & \dfrac{|\hat{P}_2 \times \hat{P}_3|\left[(\hat{P}_1 \cdot \hat{P}_2)\,(\hat{P}_2 \cdot \hat{P}_3) - (\hat{P}_1 \cdot \hat{P}_3)\right]}{(\hat{P}_1 \hat{P}_2 \hat{P}_3)\left[1 - (\hat{P}_2 \cdot \hat{P}_3)^2\right]} \\ 0 & \dfrac{|\hat{P}_2 \times \hat{P}_3|}{\left[1 - (\hat{P}_2 \cdot \hat{P}_3)^2\right]} & -\dfrac{|\hat{P}_2 \times \hat{P}_3|\,(\hat{P}_2 \cdot \hat{P}_3)}{\left[1 - (\hat{P}_2 \cdot \hat{P}_3)^2\right]} \\ 0 & 0 & 1 \end{vmatrix} \begin{vmatrix} \hat{P}_1 \\ \hat{P}_2 \\ \hat{P}_3 \end{vmatrix} = M_3^{-1} \begin{vmatrix} \hat{P}_1 \\ \hat{P}_2 \\ \hat{P}_3 \end{vmatrix} \qquad \text{(A5)}$$

To simplify the algebra, the elements of M_1^{-1}, M_2^{-1}, M_3^{-1} are redefined using the symbols A_n, B_n, C_n, D_n and E_n. The definitions are given in Equations A6, A7, and A8:

$$M_1^{-1} = \begin{bmatrix} 1 & 0 & 0 \\ B_1 & \sqrt{C_1} & D_1 \\ -A_1 & 0 & E_1 \end{bmatrix} \tag{A6}$$

$$M_2^{-1} = \begin{bmatrix} E_2 & -A_2 & 0 \\ 0 & 1 & 0 \\ D_2 & B_2 & \sqrt{C_2} \end{bmatrix} \tag{A7}$$

$$M_3^{-1} = \begin{bmatrix} \sqrt{C_3} & D_3 & B_3 \\ 0 & E_3 & -A_3 \\ 0 & 0 & 1 \end{bmatrix} \tag{A8}$$

Using the expressions for i, j, k, defined in Equations A3 and A6 in Equation A2, results in the following expressions:

$$1 = \left[\hat{P}_1 \cdot \hat{S}\right]^2 + \left[(\hat{P}_1 B_1 + \hat{P}_2\ C_1 + \hat{P}_3 D_1) \cdot S\right]^2 + \left[(-\hat{P}_1 A_1 + \hat{P}_3 E_1) \cdot \hat{S}\right]^2 \tag{A9}$$

Let

$$\hat{P}_1 \cdot \hat{S} = \alpha$$

$$\hat{P}_2 \cdot \hat{S} = \alpha_2$$

$$\hat{P}_3 \cdot \hat{S} = \alpha_3$$

Then

$$1 = \alpha_\beta^2 + \left[B_1\alpha_1 + C_1\alpha_2 + D_1\alpha_3\right]^2 + \left[E_1\alpha_3 - A_1\alpha_1\right]^2 \tag{A10}$$

solving for α_2,

$$\sqrt{C_1}\alpha_2 = -D_1\alpha_3 - B_1\alpha_1 \pm \sqrt{1 - \alpha_1^2 - \left[E_1\alpha_3 - A_1\alpha_1\right]^2} \tag{A11}$$

Similarly using A4, A5, and A7, A8 in Equation A2,

$$\sqrt{C_3}\alpha_1 = -D_3\alpha_2 - B_3\alpha_3 \pm \sqrt{1 - \alpha_3^2 - \left[E_3\alpha_2 - A_3\alpha_3\right]^2} \tag{A12}$$

$$\sqrt{C_2}\alpha_3 = -D_2\alpha_1 - B_2\alpha_2 \pm \sqrt{1 - \alpha_2^2 - \left[E_2\alpha_1 - A_2\alpha_2\right]^2} \tag{A13}$$

where

$$A_1 = \frac{/\hat{P}_3 \times \hat{P}_1 \; / \; \hat{P}_3 \cdot \hat{P}_1}{1 - (\hat{P}_1 \cdot \hat{P}_3)^2}$$

$$A_2 = \frac{/\hat{P}_1 \times \hat{P}_2 \; / \; (\hat{P}_1 \cdot \hat{P}_2)}{1 - (\hat{P}_2 \cdot \hat{P}_1)^2}$$

$$A_3 = \frac{/\hat{P}_2 \times \hat{P}_3 \; / \; (\hat{P}_2 \cdot \hat{P}_3)}{1 - (\hat{P}_2 \cdot \hat{P}_3)^2}$$

$$B_1 = \frac{/\hat{P}_3 \times \hat{P}_1 \; / (\hat{P}_1 \cdot \hat{P}_3 \; \hat{P}_2 \cdot \hat{P}_3 - \hat{P}_1 \cdot \hat{P}_2)}{(P_1 \; P_2 \; P_3) \quad 1 - (\hat{P}_1 \cdot \hat{P}_3)^2}$$

$$B_2 = \frac{/\hat{P}_1 \times \hat{P}_2 /(\hat{P}_1 \cdot \hat{P}_2\, \hat{P}_1 \cdot \hat{P}_3 - \hat{P}_3 \cdot \hat{P}_2)}{(P_1\, P_2\, P_3)\left[1 - (\hat{P}_1 \cdot \hat{P}_2)^2\right]}$$

$$B_3 = \frac{/\hat{P}_2 \times \hat{P}_3 / (\hat{P}_1 \cdot \hat{P}_2\, \hat{P}_2 \cdot \hat{P}_3 - \hat{P}_1 \cdot \hat{P}_3)}{(P_1\, P_2\, P_3)\left[1 - (\hat{P}_2 \cdot \hat{P}_3)^2\right]}$$

$$C_1 = \frac{/\hat{P}_3 \times \hat{P}_1/^2}{(P_1 P_2 P_3)^2}$$

$$C_2 = \frac{/\hat{P}_1 \times \hat{P}_2 /^2}{(P_1\, P_2\, P_3)}$$

$$C_3 = \frac{/\hat{P}_2 \times \hat{P}_3/^2}{(P_1\, P_2\, P_3)^2}$$

$$D_1 = \frac{/\hat{P}_3 \times \hat{P}_1 / (\hat{P}_1 \cdot \hat{P}_3\, \hat{P}_1 \cdot \hat{P}_2 - \hat{P}_2 \cdot \hat{P}_3)}{(P_1\, P_2\, P_3)\left[1 - (\hat{P}_1 \cdot \hat{P}_3)^2\right]}$$

$$D_2 = \frac{/\hat{P}_1 \times \hat{P}_2 / (\hat{P}_1 \cdot \hat{P}_2\, \hat{P}_2 \cdot \hat{P}_3 - \hat{P}_1 \cdot \hat{P}_3)}{(P_1\, P_2\, P_3)\left[1 - (P_1 \cdot P_2)^2\right]}$$

$$D_3 = \frac{/\hat{P}_2 \times \hat{P}_3 / (\hat{P}_2 \cdot \hat{P}_3\, \hat{P}_1 \cdot \hat{P}_3 - \hat{P}_1 \cdot \hat{P}_2)}{(P_1\, P_2\, P_3)\quad 1 - (P_2 \cdot P_3)^2}$$

$$E_1 = \frac{/\hat{P}_3 \times \hat{P}_1 /}{1 - (\hat{P}_1 \cdot \hat{P}_3)^2}$$

$$E_2 = \frac{/\hat{P}_1 \times \hat{P}_2 /}{/ - (\hat{P}_1 \cdot \hat{P}_2)^2}$$

$$E_3 = \frac{/\ddot{P}_2 \times \hat{P}_3 /}{1 - (P_2 \cdot P_3)^2}$$

Equations A11, A12 and A13 are the desired equations for the calculation of the third direction cosine. Equation A11 is used to calculate α in the event pickoffs 1 and 3 are providing gyro readout information. Equations A12 and A13 are used in a similar manner when the other pairs of pickoffs are providing readout data.

APPENDIX B

DERIVATION OF EQUATIONS FOR ATTITUDE ERROR AND BODY RATE

APPENDIX B

DERIVATION OF EQUATIONS FOR ATTITUDE ERROR AND BODY RATE

The following presents the derivation and discussion of the equations mechanized in the "Attitude Error Body Rate" section of the system computer.

ATTITUDE ERROR EQUATIONS

It is assumed that the stabilization and control system will be able to perform suitable reorientation and attitude hold maneuvers with an input signal that is not a linear function of the attitude error. It is also assumed that the input signal has its null coincident with the attitude error null. The assumption is also made that input signal and attitude error have the same sign everywhere.

It is also assumed that reorientation of the vehicle will be commanded by providing the attitude reference system with the six direction cosines that define the new desired position of the two gyro spin vectors in the vehicle body axis. In this derivation $\hat{Q}_1$ and $\hat{Q}_2$ are two unit vectors representing the commanded position of the gyro spin vectors in the vehicle body coordinates. $\hat{S}_1$ and $\hat{S}_2$ are two unit vectors representing the observed position of the spin vectors in body coordinates resulting from the gyro readout and the data processing of the "Cosine Computer" discussion.

The difference between the commanded and observed vectors is:

$$\bar{\Delta S}_1 = \hat{S}_1 - \hat{Q}_1$$

$$\bar{\Delta S}_2 = \hat{S}_2 - \hat{Q}_2$$

These differences may be related to attitude error, θ by

$$\overline{\Delta S}_1 = \overline{\theta} \times \hat{S}_1$$
$$\overline{\Delta S}_2 = \overline{\theta} \times \hat{S}_2$$

$\overline{\theta}$ is a unique rotation vector which will null simultaneously $\overline{\Delta S}_1$ and $\overline{\Delta S}_2$ if the vehicle is commanded to rotate about this vector until the magnitude of θ is zero.

Equating the two expressions for $\overline{\Delta S}_1$ and $\overline{\Delta S}_2$

$$\overline{\theta} \times \hat{S}_1 = \hat{S}_1 - \hat{Q}_1 \tag{B1}$$

$$\overline{\theta} \times \hat{S}_2 = \hat{S}_2 - \hat{Q}_2 \tag{B2}$$

Cross $\hat{S}_1$ into (B1) and cross $\hat{S}_2$ into (B2)

$$\overline{\theta} = \hat{Q}_1 \times \hat{S}_1 + (\overline{\theta} \cdot \hat{S}_1)\, \hat{S}_1 \tag{B3}$$

$$\overline{\theta} = \hat{Q}_2 \times \hat{S}_2 + (\overline{\theta} \cdot \hat{S}_2)\, \hat{S}_2 \tag{B4}$$

Dot $\hat{S}_2$ into (B3) and $\hat{S}_1$ into (B4)

$$\overline{\theta} \cdot \hat{S}_2 = \hat{Q}_1 \times \hat{S}_1 \cdot \hat{S}_2 + (\overline{\theta} \cdot \hat{S}_1)\, \hat{S}_1 \cdot \hat{S}_2 \tag{B5}$$

$$\overline{\theta} \cdot \hat{S}_1 = \hat{Q}_2 \times \hat{S}_2 \cdot \hat{S}_1 + (\overline{\theta} \cdot \hat{S}_2)\, \hat{S}_2 \cdot \hat{S}_1 \tag{B6}$$

Solve for $(\overline{\theta} \cdot S_1)$

$$\overline{\theta} \cdot \hat{S}_1 = \frac{1}{/\hat{S}_1 \times \hat{S}_2/^2} \left\{ \hat{Q}_2 \times \hat{S}_2 \cdot \hat{S}_1 + \hat{Q}_1 \times \hat{S}_1 \cdot \hat{S}_2\, (\hat{S}_1 \cdot \hat{S}_2) \right\} \tag{B7}$$

Substitute (B7) into (B3)

$$\overline{\theta} = \hat{Q}_1 \times \hat{S}_1 + \frac{1}{/\hat{S}_1 \times \hat{S}_2/^2} \left\{ \hat{Q}_1 \cdot \hat{S}_1 \times \hat{S}_2\, (\hat{S}_1 \cdot \hat{S}_2) - \hat{Q}_2 \cdot \hat{S}_1 \times \hat{S}_2 \right\} \tag{B8}$$

Equation (B3) is the desired expression for the attitude error.

From this equation it can be concluded that the attitude error is a function of only commanded and observed positions of the spin vectors. Since the command is given in body coordinates and since the spin vectors are measured or observed in body coordinates, the attitude error computed from Equation (B8) with these inputs will also be in the body coordinates.

BODY RATE EQUATIONS

Assuming the gyro spin vectors are known in body coordinates as a function of time the body rates may be determined as follows:

The rate of change of the spin vectors in inertial space may be expressed as:

$$\left.\frac{d\hat{S}_1}{dt}\right|_I = \left.\frac{d\hat{S}_1}{dt}\right|_B + \bar{\omega} \times \hat{S}_1$$

$$\left.\frac{d\hat{S}_2}{dt}\right|_I = \left.\frac{d\hat{S}_2}{dt}\right|_B + \bar{\omega} \times \hat{S}_2$$

where

$\hat{S}_1$ and $\hat{S}_2$ = spin vectors

$\bar{\omega}$ = angular velocity vector of the body in inertial space

$\left.\frac{dS}{dt}\right|_I$ = rate of change of S relative to inertial space

$\left.\frac{dS}{dt}\right|_B$ = rate of change of S relative to body coordinates

Since the gyro spin vectors are fixed relative to inertial space

$$\left.\frac{d\hat{S}_1}{dt}\right|_I = \left.\frac{d\hat{S}_2}{dt}\right|_I = 0$$

and

$$\left.\frac{d\hat{S}_1}{dt}\right|_B = \dot{\overline{S}}_1 = \hat{S}_1 \times \overline{\omega} \tag{B9}$$

$$\left.\frac{d\hat{S}_2}{dt}\right|_B = \dot{\overline{S}}_2 = \hat{S}_2 \times \overline{\omega} \tag{B10}$$

Crossing $\hat{S}_1$ into (B9) and $\hat{S}_2$ into (B10)

$$\overline{\omega} = \dot{\overline{S}}_1 \times \hat{S}_1 + (\overline{\omega} \cdot \hat{S}_1)\hat{S}_1 \tag{B11}$$

$$\overline{\omega} = \dot{\overline{S}}_2 \times \hat{S}_2 + (\overline{\omega} \cdot \hat{S}_2)\hat{S}_2 \tag{B12}$$

dotting $\hat{S}_2$ into (B11) and $\hat{S}_1$ into (B12)

$$\overline{\omega} \cdot \hat{S}_2 = \dot{\overline{S}}_1 \times \hat{S}_1 \cdot \hat{S}_2 + (\overline{\omega} \cdot \hat{S}_1)\hat{S}_1 \cdot \hat{S}_2 \tag{B13}$$

$$\overline{\omega} \cdot \hat{S}_1 = \dot{\overline{S}}_2 \times \hat{S}_2 \cdot \hat{S}_1 + (\overline{\omega} \cdot \hat{S}_2)\hat{S}_2 \cdot \hat{S}_1 \tag{B14}$$

Solve for $\overline{\omega} \cdot \hat{S}_1$ and substitute in (B11)

Equation (B15) relates vehicle body rate to spin vector rate relative to the body.

In using the above equation to calculate $\overline{\omega}$, the body rate, the computer will approximate $\overline{\dot{S}_1}$ and $\overline{\dot{S}_2}$ by finite differences of readings of $\hat{S}_1$ and $\hat{S}_2$.

APPENDIX C
COORDINATE TRANSFORMATION BY "METHOD OF LEAST WORK"

APPENDIX C

COORDINATE TRANSFORMATION BY "METHOD OF LEAST WORK"

Presented here is a simplified method of obtaining the matrix elements of orthogonal transformations and of Euler rate to body rate transformations.

Consider a rotation of a coordinate system about the Z-axis.

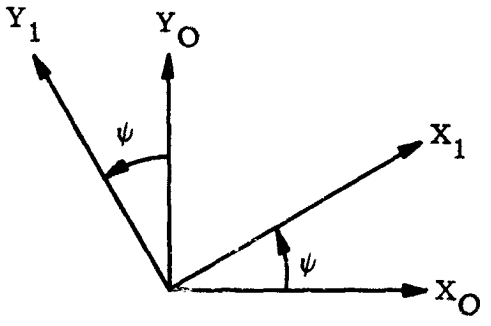

This can be expressed as a matrix transforming the vectors X_O, Y_O, Z_O into X_1, Y_1, and Z_1.

$$\begin{bmatrix} X_1 \\ Y_1 \\ Z_1 \end{bmatrix} = \begin{bmatrix} C\psi & X\psi & 0 \\ -S\psi & C\psi & 0 \\ 0 & 0 & 1 \end{bmatrix} \begin{bmatrix} X_O \\ Y_O \\ Z_O \end{bmatrix}$$

A figure representing a resolver can be drawn that will show this same transformation.

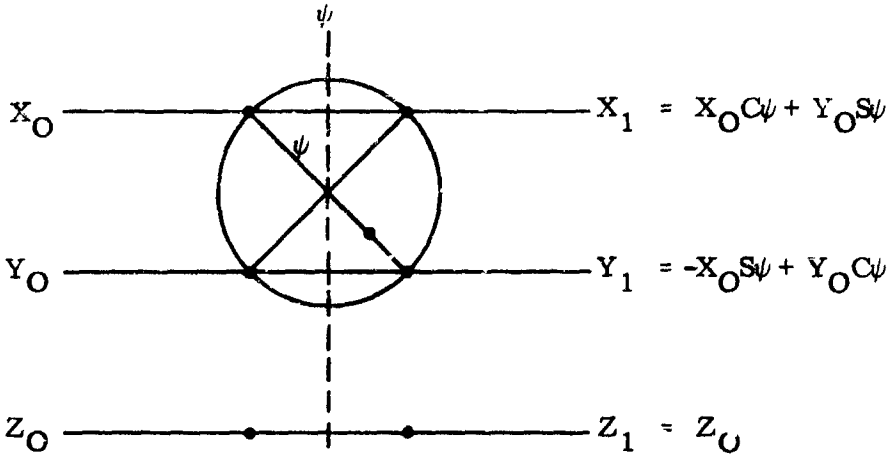

Following a signal through the resolver in a diagonal direction gives a sine function. A dot can indicate which sine function requires the negative sign. A signal going straight across is multiplied by the cosine.

A slightly modified picture is more useful.

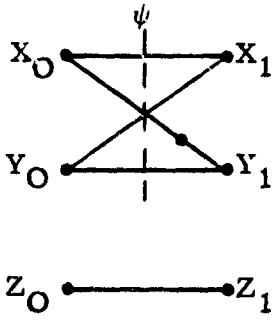

With this as the basic building block any number of additional rotations may be added.

Consider the transformation from inertial coordinates to body axis coordinates through the Euler angles ψ, θ, ϕ.

The first rotation is as pictured above. To this is added the blocks for rotation of θ about Y_1, and ϕ about X_2.

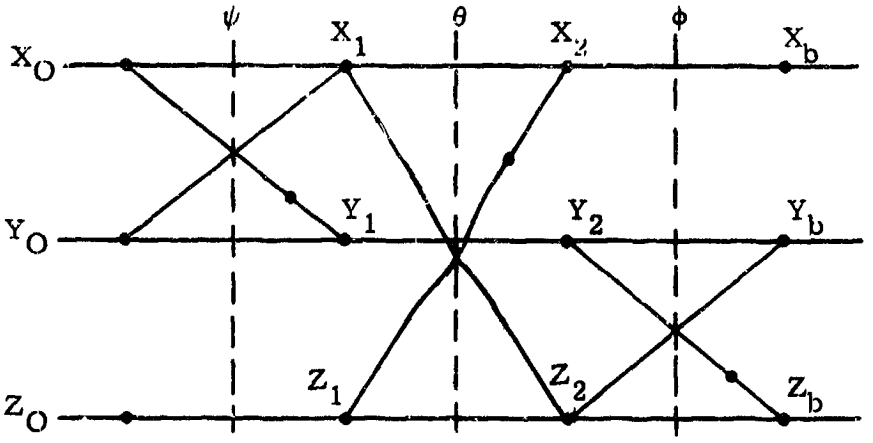

To transform a vector in the inertial system to the body axis system trace all possible paths from X_O, Y_O, Z_O to X_b, Y_b, and Z_b.

Thus the expression for X_b will in general contain X_O, Y_O and Z_O with appropriate coefficients. More than one path may be possible between two points. For example going from X_O to Z_b is possible by $C\psi\, S\theta C\phi$ and $(-S\psi)\,(1)\,(-S\phi)$.

Each element of the matrix can be written by inspection of the diagram.

$$\begin{bmatrix} X_b \\ Y_b \\ Z_b \end{bmatrix} = \begin{bmatrix} (C\psi\, C\theta) & & (-S\theta) \\ (-S\psi\, C\phi + C\psi\, S\theta S\phi) & (S\psi\, S\theta S\phi + C\psi C\phi) & (C\theta S\phi) \\ (S\psi S\phi + C\psi\, S\theta C\phi) & (S\psi S\theta\, C\phi - C\psi\, S\phi) & (C\theta C\phi) \end{bmatrix} \begin{bmatrix} X_O \\ Y_O \\ Z_O \end{bmatrix}$$

This inverse can be written by following all paths from X_b, Y_b, Z_b to X_O, Y_O, and Z_O.

$$\begin{bmatrix} X_O \\ Y_O \\ Z_O \end{bmatrix} = \begin{bmatrix} (C\theta C\psi) & (-C\phi\, S\psi + S\phi S\theta C\psi) & (C\phi\, S\theta S\psi - S\phi C\psi) \\ (C\theta S\psi) & (C\phi C\psi + S\phi S\theta S\psi) & (C\phi S\theta S\psi - S\phi C\psi) \\ (-S\theta) & (S\phi C\theta) & (C\phi C\theta) \end{bmatrix} \begin{bmatrix} X_b \\ Y_b \\ Z_b \end{bmatrix}$$

In this case (orthogonality) the inverse can be written immediately from the first matrix by interchanging rows and columns.

A special case of a non-orthogonal matrix is the transformation of Euler angle rates to body rates.

The original diagram can be modified to show these rate inputs.

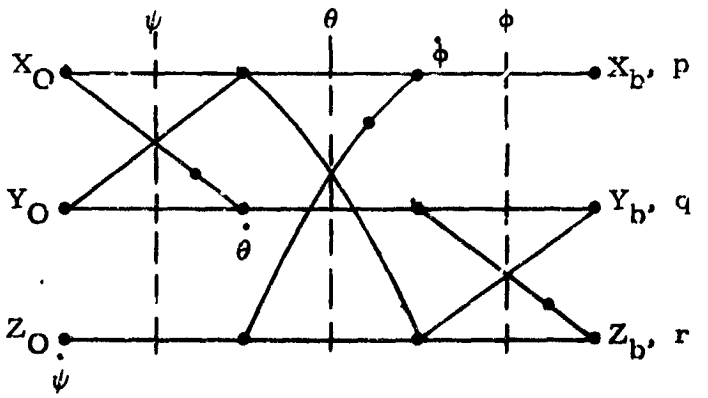

The transformation to body rates follows the same rules as the orthogonal transformation. Follow all possible paths from each of the Euler rates to the body coordinate system.

Thus:

$$\begin{bmatrix} p \\ q \\ r \end{bmatrix} = \begin{bmatrix} 1 & O & -S\theta \\ 0 & C\phi & C\theta S\phi \\ 0 & -S\phi & C\theta C\phi \end{bmatrix} \begin{bmatrix} \dot{\phi} \\ \dot{\theta} \\ \dot{\psi} \end{bmatrix}$$

The inverse of this non-orthogonal matrix is not so straight forward. Some rules can be stated that allow the inverse to be written by inspection.

The rules are:

(1) Cut the single line that connects two of the Euler rates (neglecting the lines that are unity). This will always be a sine function in the middle gimbal rotation.

(2) Divide (instead of multiplying) by the last function of the middle gimbal rotation before arriving at the desired Euler rate. It may be necessary to go through two functions of this middle gimbal rotation to complete the path. The example will clarify the rules.

$$\begin{bmatrix} \dot{\phi} \\ \dot{\theta} \\ \dot{\psi} \end{bmatrix} = \begin{bmatrix} 1 & \frac{S\phi S\theta}{C\theta} & \frac{C\phi S\theta}{C\theta} \\ 0 & C\phi & -S\phi \\ 0 & \frac{S\phi}{C\theta} & \frac{C\phi}{C\theta} \end{bmatrix} \begin{bmatrix} p \\ q \\ r \end{bmatrix}$$